NTNU
Norwegian University of
Science and Technology

Design of Airfoil for downwind wind turbine Rotor

Eivind Sæta

Master of Science in Energy and Environment
Submission date: June 2009
Supervisor: Per-Åge Krogstad, EPT

Norwegian University of Science and Technology
Department of Energy and Process Engineering

Problem Description

At the institute, there has been a significant amount of work done in developing an airfoil with very high lift-to-drag ratio. However, it has been developed for relatively low Reynolds numbers, and has a very dramatic stall. It is desirable to develop this profile further with regards to typical working conditions for offshore wind turbines. It is also necessary to change the profile stall characteristics so that it is more gradual, and hopefully to achieve this without significant reduction in efficiency.

The following questions should be considered in the project:

1 – The student is to study the work done previously at the institute.
2 - The theory of high lift-to-drag profiles is to be studied.
3 – The student will develop a new profile, either based on HOG-profile designed at the the department or from another geometry, where the main focus should be on high lift-to-drag ratio and stall characteristics.
4 – The properties of the developed profile should be tested with software such as Xfoil and/or Fluent.

Assignment given: 15. January 2009
Supervisor: Per-Åge Krogstad, EPT

Norwegian University
of Science and Technology
NTNU

Department of Energy
and Process Engineering

EPT-M-2009-68

MASTER THESIS

for

Stud.techn Eivind Sæta
Spring 2009

Design of airfoil for downwind wind turbine rotor t

Design av airfoil for nedstrøms plassert vindturbinrotor

Background and objective.

There is currently high research activities in the field of offshore wind turbines. This is in part due to the almost unlimited energy resources available outside the Norwegian coastline, but also due to public resistance towards land based wind turbines. Another important reason is that the oil industry present in the north sea is accountable for a large portion of the CO_2 emissions from Norway (ca. 26% in 2007; Ref. Fakta 2008: "Energi og vannressurser I Norge"). It would therefore be desirable to power these platforms with wind energy.

One of the challenges with floating wind turbines is that they do not have a fixed tower. It will therefore not be as easy to pitch the rotor into the wind at all times as for a land based wind turbine. Since an upstream rotor will always be unstable, while a downstream rotor will be stable, there is reason to investigate the possibilities for such a design for floating windmills at large ocean depths. In addition to stability, a downwind rotor will have the possibility of making the blades thinner, as bending due to strong wind loads will shift the blades away from the tower and thereby reduce the danger of a collision between blade and tower, as opposed to the upstream rotor case. Since the Reynolds number for the turbine blades will be very high, thinner blades could also allow for more efficient profiles.

Goal

At the institute, there has been a significant amount of work done in developing an airfoil with very high lift-to-drag ratio. However, it has been developed for relatively low Reynolds numbers, and has a very dramatic stall. It is desirable to develop this profile further with regards to typical working conditions for offshore wind turbines. It is also necessary to change the profile stall characteristics so that it is more gradual, and hopefully to achieve this without significant reduction in efficiency.

The following questions should be considered in the project work:

1 – The student is to study the work done previously at the department.
2 - The theory of high lift-to-drag profiles is to be studied.

3 – The student will develop a new profile, either based on the HOG-profile designed at the department or from another geometry, where the main focus should be on high lift-to-drag ratio and stall characteristics.

4 – The properties of the developed profile should be tested with software such as Xfoil and/or Fluent.

-- ” --

Within 14 days of receiving the written text on the diploma thesis, the candidate shall submit a research plan for his project to the department.

When the thesis is evaluated, emphasis is put on processing of the results, and that they are presented in tabular and/or graphic form in a clear manner, and that they are analyzed carefully.

The thesis should be formulated as a research report with summary both in English and Norwegian, conclusion, literature references, table of contents etc. During the preparation of the text, the candidate should make an effort to complete a well presented report. In order to ease the evaluation of the thesis, it is important that the cross references are correct. In the making of the report, strong emphasis should b e placed on both a thorough discussion of the results and an orderly presentation.
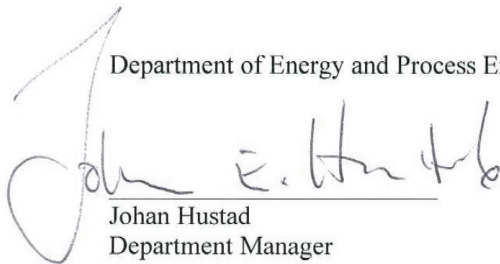
The candidate is requested to initiate and keep close contact with his/her specialist teacher and academic supervisor(s) throughout the working period. The candidate must follow the rules and regulations of NTNU as well as passive directions given by the Department of Energy and Process Engineering.

Pursuant to "Regulations concerning the supplementary provisions to the technology study program/Master of Science" at NTNU §20, the Department reserves the permission to utilize all the results for teaching and research purposes as well as in future publications.

<u>One – 1</u> complete original of the thesis shall be submitted to the authority that handed out the set subject. (A short summary including the author's name and the title of the thesis should also be submitted, for use as reference in journals (max. 1 page with double spacing)).

Two – 2 – copies of the thesis shall be submitted to the Department. Upon request, additional copies shall be submitted directly to research advisors/companies. A CD-ROM (Word format or corresponding) containing the thesis, and including the short summary, must also be submitted to the Department of Energy and Process Engineering

Department of Energy and Process Engineering, 12. January 2009

Johan Hustad
Department Manager

Academic Supervisor

Research Advisors:

Design of airfoil for downwind wind turbine rotor

Eivind Sæta

NTNU 2009

Summary

This thesis is on the design of an airfoil for a downwind wind turbine rotor with thin flexible wings, for offshore floating conditions. It has been suggested that such a system would to be lighter, simpler and allow for the use of more efficient airfoils.
There has been a significant amount of work done at NTNU to develop a "high-lift" airfoil. These are airfoils with very high lift-to-drag ratios. They operate very efficiently at their design angle, but tend to not work well over a range of angles and conditions, and have a sudden and dramatic stall characteristic. In this thesis, it is attempted to pick up the work done with the high-lift profiles at NTNU in the 1980's, and develop a new profile which has performance in the high-lift range, but with a much smoother stall and more stable characteristics, and to do so for the typical conditions expected for the suggested turbine.

A fictitious 5 MW version of the suggested turbine was created and analyzed with the blade element momentum method (BEM). This gave informative results about the conditions the new airfoil must operate in.

The high-lift technology and the earlier reports from NTNU were studied. Based on this knowledge and the numerical values from the BEM calculations, a serious of new airfoils were developed. By using the simulation programs Xfoil and Fluent (CFD), it was possible to modify and test a large number of airfoils and find the desired qualities.

It was possible to design airfoils that had performance in the high-lift range, while maintaining stable operation and having a soft stall, and also increase the lift coefficient to be able to design for lower angles of attack. The profiles created here appear to be suitable for wind turbines, and provide an impressive increase in performance compared to traditional airfoils.
Extra effort was put into making airfoils that were unaffected by roughness, air properties and Reynolds number, as stable performance in varying conditions are necessary for wind turbine blades. This was done by using adverse pressure gradients to control the point of transition.

A slow stall was achieved by letting the pressure recovery distribution gradually approach the local ideal Stratford distribution when moving back over the airfoil. This caused the flow separate at the back first, and then the separation would grow gradually forward with increasing angle of attack.
The inclusion of a separation ramp also worked very well together with the high-lift design, and allowed for an increased lift coefficient and more stable operation during the region of early stall.
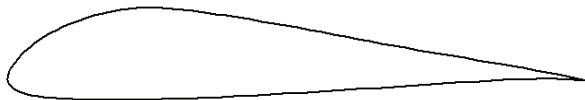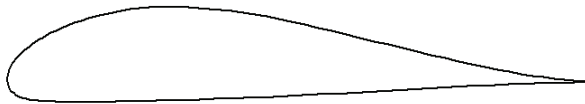

AR – profile

The most successful profile created appears to be the AR profile. It combines a diverged Stratford distribution with a separation ramp and a pressure spike at the nose to control

transition. It has a wider range, stalls later and softer, and has a much more stable performance with varying conditions compared to the original HOG profile from NTNU. At the design point, the maximum performance is reduced only 5.9 % compared to the HOG. For higher and lower angles of attack, and increased values of roughness and turbulence, the AR has an all round higher performance than the HOG. It appears to be usable for wind turbines, and would increase the maximum airfoil performance by up to 40 % compared to commonly used NACA profiles.

More good profiles were made, with varying thickness, stall and performance. Depending on the exact local requirements of an application, this report offers several interesting profiles to choose from. For instance, the D2 profile has round shape and over 16 % thickness, it has an even softer stall than the conventional wind turbine profiles, and would increase the maximum airfoil performance by up to ~34%. This profile would also be usable for upwind turbines.

D2 – profile

It was found that there is a big potential for manipulating the high-lift technology to give various shapes and performances. The usability of these profiles therefore appears to be wider than previously assumed.

Sammendrag

Denne hovedoppgaven omhandler design av airfoil for en nedstrøms vindturbin med tynne, fleksible vinger. For en flytende offshore vindmølle vil et slikt design kunne redusere vekt og gjøre systemet enklere, og samtidig tillate mer effektive vingeprofiler. Ved NTNU er det nedlagt en betydelig mengde arbeid for å designe et "high-lift" vingeprofil. Dette er vinger med svært høyt løft-til-motstands-forhold. Disse fungerer veldig bra rundt designområdet, men er vanligvis ikke veldig bra for andre forhold, og har en svært dramatisk og plutselig steilekarakteristikk.
I denne oppgaven forsøkes det derfor å gjenoppta arbeidet som ble gjort ved NTNU i 1980-årene, og å designe et nytt profil med ytelse som et "high-lift"-profil, men som steiler mye langsommere og er mer stabilt i varierende forhold, og å gjøre dette for de typiske forhold som er forventet for den foreslåtte turbinen.

En teoretisk 5 MW -versjon av den foreslåtte turbinen ble designet og testet ved hjelp av bladelementmetoden (BEM). Dette ga informative resultater om hvilke forhold den nye airfoilen vil møte.

"high-lift"-teorien, samt de tidligere rapportene fra NTNU, ble studert. Basert på dette og de numeriske verdiene fra BEM-kalkulasjonene, ble flere nye profiler utviklet. Ved å bruke simuleringsprogrammene Xfoil og Fluent (CFD), var det mulig å modifisere og teste et stort antall vingeprofiler, for å finne de ønskede kvalitetene.

Det er mulig å designe en airfoil som har ytelse i "high-lift"-regionen, men som har stabil operasjon for varierende Reynoldstall og har en myk steilekarakteristikk, og det lar seg også gjøre å øke løftekoeffisienten for å muliggjøre vingeoptimalisering ved lavere angrepsvinkler. Profilene som ble lagd i denne oppgaven ser ut til å ha karakteristikker som gjør at de kan brukes i vindturbiner, samtidig som de vil være en imponerende forbedring i forhold til de profilene som tradisjonelt brukes i vindturbiner.
Det ble satt ekstra fokus på å designe vinger som i stor grad var upåvirket av varierende Reynoldstall, ruhet og andre turbulensvariasjoner, siden vinger som skal brukes i vindturbiner er avhengige av stabil operasjon under varierende forhold. Dette ble gjort ved å bruke positive trykkgradienter for å kontrollere transisjonspunktet.

Myk steiling ble oppnådd ved å la fordelingen til trykkgjenvinningen gradvis nærme seg den lokalt optimale Stratford-fordelingen når man beveger seg bakover på vingeprofilet. Dette gjorde at det oppsto separasjon bakerst på vingen først, som så beveget seg sakte fremover ved økende angrepsvinkel. Det fungerte bra å inkludere en separasjonsrampe i "high-lift"-fordelingen. Dette gjorde at løftekoeffisienten ble økt, og overgangen til steileområdet ble forbedret.
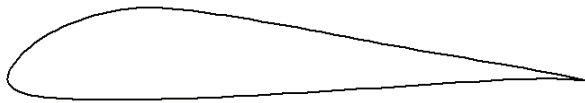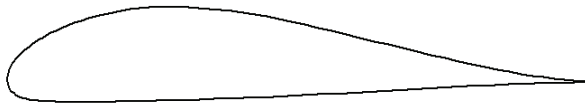

AR – profile

Det mest vellykkede profilet som ble laget ser ut til å være AR-profilet. Det kombinerer en divergert Stratfordfordeling med en separasjonsrampe, og en trykkoscillasjon ved

nesen for å tidlig introdusere en positiv trykkgradient som kontrollerer transisjonspunktet. Dette profilet har et bredere operasjonsområde, steiler saktere og mykere, og er langt mer stabil ved varierende forhold, sammenlignet med det originale HOG-profilet fra NTNU. Maksimal ytelse er kun redusert 5,9 % i forhold til HOG-profilet. Men for høyere og lavere angrepsvinkler, og for høyere verdier av ruhet og turbulens har AR profilet høyere ytelse, og totalt sett er det et langt bedre profil praktisk bruk. Det ser ut til å ha tilfredsstillende stabil og myk karakteristikk til å kunne brukes i vindturbiner, og vil i så fall øke airfoil-ytelsen med opptil ~40 % sammenlignet med standard NACA-profiler som er i bruk i dag.

Mange gode profiler ble laget med varierende ytelse, steiling og størrelse. Avhengig av de spesifikke lokale begrensningene som kreves, vil denne rapporten kunne tilby flere interessante profiler å velge mellom. For eksempel har D2-profilet en rund form og en tykkelse på over 16 %, og har en steilekarakteristikk som var enda mykere en de standardiserte profilene som ble brukt til sammenligning, men vil kunne øke ytelsen med opptil ~34 %. Dette profilet vil også trolig kunne være aktuelt for oppstrømsturbiner.

D2 – profile

Det viser seg å være et stort potensiale for å utvikle "high-lift"-teknologien til å gi forskjellig geometriske former og ytelser. Brukervennligheten til disse profilene ser derfor ut til å være større enn antatt.

Table of contents

List of symbols

a   axial induction factor

B   number of blades on turbine

c   chord length [m]

C_D coefficient of drag

C_L coefficient of lift

Cp   coefficient of pressure

Cp_{min} Minimum pressure coefficient over airfoil

Cp_{te} Trailing edge pressure

D   drag [N]

L   lift [N]

L/D   Lift-to-drag ratio

m   mass [kg]

p   pressure [Pa]

r   local radius [m]

R   full radius [m]

Re   Reynolds number

u   Flow speed in boundary layer [m/s]

U   Wind speed [m/s]

V   Local flow speed [m/s]

x   Length along equivalent Stratford plate

X   Length along airfoil chord

z   Height [m]

λ tip speed ratio

φ flow angle [deg]

α angle of attack [deg]

θ pitch angle [deg]

ω roational speed [s^{-1}]

η mechanical efficiency

ρ density [kg/m^3]

μ dynamic viscosity [kg/(m^2s)]

υ kinematic viscosity [m^2/s]

1 Introduction

This thesis is on the design of an airfoil for a downwind wind turbine rotor. The reason for the interest in this field is the emerging market for floating offshore wind turbines. In order to make these turbines economically competitive, it is needed to make them lighter, bigger and maintenance free. It has therefore been suggested to design a downwind offshore wind turbine, with relatively thin flexible wings. This system is believed to become lighter and simpler. It will also allow for the use of more efficient airfoils.

At the Norwegian University of Science and Technology (NTNU), there has been done a significant amount of work in trying to design a "high-lift" airfoil. These are airfoils with exceptionally high lift-to-drag ratios. Unfortunately, they also have very dramatic stall characteristics, and are therefore not usable for many applications, including wind turbines. The goal of this thesis is therefore to design a new airfoil which has the performance of a high-lift airfoil, but with a much softer stall, and to do so for the typical conditions expected for an offshore wind turbine. The point is to see if the high-lift technology can be incorporated into the thin-flexible-wing/downwind turbine concept.

In order to design the right airfoil, it is necessary to have a good understanding of what the rotor is trying to achieve, and what problems it faces. Sufficient study of turbine design theory and basic rotor calculations must therefore be conducted before starting the design process.

Chapter 2 will focus on the general reasons and consequences for going offshore and choosing the system suggested here, and how this changes to conditions for the rotor. Chapter 3 will study in depth the high-lift theory and general fluid mechanics involved. In chapter 4, a fictitious version of the suggested offshore wind turbine is designed using the blade element momentum method (BEM). The turbine is then analyzed for typical wind conditions, in order to get a good indication of the flow patterns along the turbine blades in operation. This will give a good indication of what conditions and requirements to design the new airfoil for. Finally, in chapter 5, the lengthy optimization process for finding a new airfoil begins. By starting with the high-lift profile developed at NTNU, and using the theory from chapter 3 and systematic experimentation, several attempts are made at creating airfoils with performance in the high-lift range, but with acceptable stall characteristics in order to be implemented on the suggested wind turbine.

The airfoils will be designed an analyzed by the aid of Xfoil and Fluent. The shear amount of information resulting from these simulations is so vast that only the most interesting results could be included in this rapport. Every airfoil discussed has its own section in the appendix with geometrical information, performance characteristics (C_L, C_D, and lift-to-drag ratio), and information about transition points and sensitivity to roughness. The information provided is sufficient for anyone to recreate the results for either verification or further optimization.

2 Downwind offshore wind turbine

There is currently a big interest in floating offshore wind turbines. The idea of harvesting the vast energy resources available at sea, out of sight of humans, is very tempting. The technology is not yet good enough to deliver a product that will be successful economically, but public and political pressure, EU guidelines (20-20-20), and the belief that the technology will be able to compete economically in the near future, causes the research and development of floating offshore wind turbines to move ahead rapidly. As this is being written (May 2009), the first prototype for StatoilHydro's HyWind program is being assembled outside Norway's south west coast.


Figure 2.1 – Hywind installation (Erik jørgensen/tu.no)

The advantages of going offshore are many. Wind turbines on land meet public resistance as they are perceived by many as ugly and visually disturbing. The flickering light effect they create can be annoying to people close by. They also make a certain amount of noise, which becomes a constant background noise for the local inhabitants. Another problem is that they kill a lot of birds who accidentally fly into the turbine blades[27]. Some claim that this problem is overrated as it is, for instance, no match for the amount of birds killed by flying into the windows of buildings every year. However, the problem is what kind of birds it kills. The turbines are usually placed in near coastal planes in western Norway, which are the nesting sites for precious birds such as sea eagles and Europe's biggest bird, the Eurasian eagle-owl (Hubro). These birds are not the kinds who are usually troubled by flying into windows [28]. All this, plus the general mark a wind park inevitably will make on the surrounding wilderness, makes it hard to get a governmental concession for building a wind park. When taking the turbines far out at sea, problems with esthetical and acoustic pollution, and the problems with surrounding wilderness and precious birds, goes away.

The biggest advantages are, however, in the technical arena. The wind offshore is more frequent and has a more uniform velocity profile. This, together with the vast spaces available at the open sea, provides an enormous potential for extracting energy.

Norway is already producing enough electricity for the home market, and the increase in electricity consumption has flattened out over the past years. Some critics therefore say there is no need for offshore wind energy [32]. There are, however, some major potential markets for this new energy. To the south of Norway, there is the European continent which is currently relying heavily on Russian gas transported through Ukraine, which has proven to be an unstable route of transportation. This, together with the EU's goal of 20% renewable energy by 2020, means that there is a huge potential for exporting the energy to the continent. Another point is that offshore oil installations account for approximately 26% of the CO_2 emissions from Norway. It would therefore be desirable to power these with offshore wind energy. A third point is of course the possibility of exporting the technology to other parts of the world. Other countries, such as Denmark, are far ahead when it comes to land based wind turbines. Norway has the potential for becoming the world leader in floating offshore wind turbines, thereby creating a new export market.
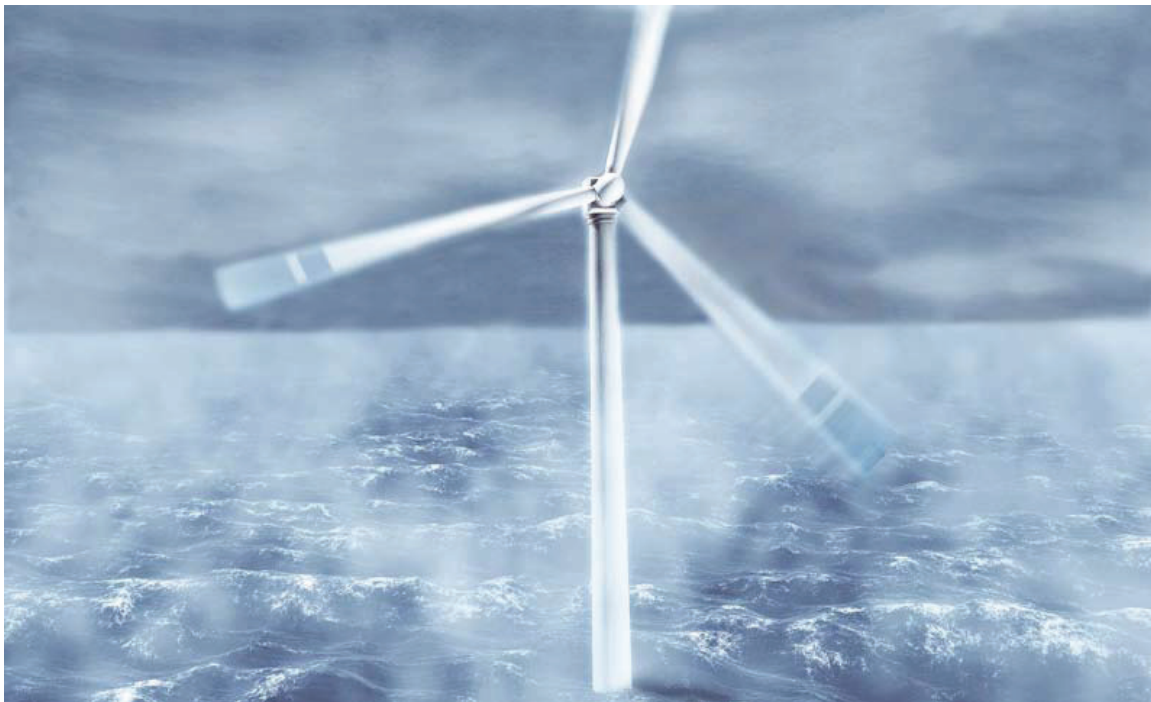

Figure 2.2 – Hywind illustration (StatoilHydro)

There are, however, some major difficulties in creating an offshore wind turbine. Installation, control and transport of electricity back to land are all costly and difficult projects, although the main problem is the inability to perform maintenance. In order for these turbines to be competitive economically, they have to be virtually maintenance free. The weakest link on wind turbines today is the gear box. A lot of work is therefore going into bypassing this problem. One promising technology is to use a directly driven generator, thereby eliminating the need for a gear box, while another concept uses a hydraulic gear box. This last concept, which is being developed by the Norwegian company Chapdrive, has the advantage of allowing for the generator to be located elsewhere than at the top of the turbine. This last point is very important. Lowering the

top weight reduces the need for a large subsea structure to keep the turbine floating stably, significantly reducing the size and cost of the total structure. The director of HyWind, Sjur Bratland, recently said that the two most important issues for realizing offshore wind power is making the turbines bigger and reducing the top weight[1].

Another way of reducing the top weight is to use thinner turbine blades, which is the technical area this report will focus on. Wings used on wind turbines today are relatively thick due to structural requirements. The wings will be subjected to extreme forces, and need to have a certain mechanical strength to cope, and to avoid bending. As mentioned above, one of the most important things in order to realize offshore wind power is that the turbines must become bigger, meaning the wings will get longer.
As blades are made ever longer, they will have an increasing tendency to bend backwards in strong winds. If a blade were to strike its own tower, the result would be disastrous. This has happened before, usually resulting in complete destruction of the windmill as both rotor blade and tower collapses [33].
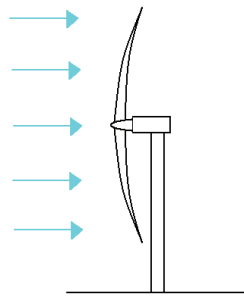
Figure 2.3 – Upwind wind turbine

If the rotor blades are going to get much bigger, the advantages of designing a downstream turbine starts to increase. For such a turbine, the rotor blades would tilt away from the tower in strong winds, eliminating this problem. This means that de structural requirements of the wing can be greatly reduced as is can be allowed to bend in strong gusts of wind. This creates the possibility of fitting a downwind rotor with relatively thin and flexible wings, which will both allow for longer wings and reduce top weight at the same time, thereby tackling two pressing issues at once.
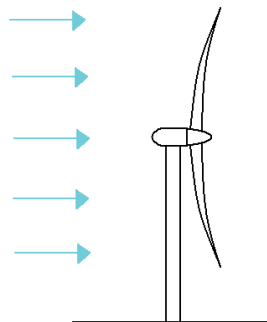

Figure 2.4 – Downwind wind turbine

Another problem for wind turbines is the extreme forces experienced in horizontal direction by strong gusts of wind. This puts huge requirements on the structure. With flexible downstream wings, the wings might automatically tilt back in gusts of winds, effectively reducing the area swept by the turbine, relieving it of the extreme forces.

Upstream wind turbines are unstable, and must always be turned towards the wind. This requires expensive control systems and a stable platform to stand on. When floating in water, the base of the turbine is not fixed, making things more challenging. This problem is also solved by a downwind turbine, as it would be auto corrective in terms of direction towards the wind. This eliminates the need for a major part of the control system, helping to make the turbine cheaper and reducing the likelihood of needed maintenance. In order to be truly stable, the wings have to be swept slightly backwards, to give the classic feather ball effect [3. chap 1]. If the wings are flexible, this swept design will probably come as a natural effect anyway.

In other words, the downwind concept offers some significant improvements which become more important as the turbines grow bigger and is out of reach for regular maintenance. They can, in theory, be lighter, bigger, auto corrective in terms of direction towards the wind, and semi corrective in terms of structural loads and power output during high gusts of wind. Although, there is also an obvious disadvantage; the reduced wind speed behind the tower.
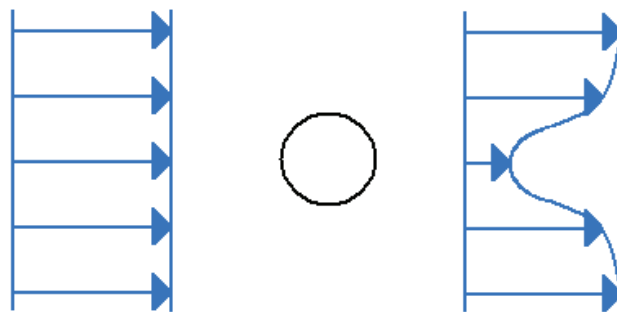
Figure 2.5 – Flow across tower

Every time a turbine blade passes behind the tower, it will encounter a portion of air that is moving slower than the surrounding air. This reduces the angle of attack, meaning there will be a sudden reduction in lift over the entire wing. This "kick" that will hit the wing every time it passes the tower, can in the long run cause structural fatigue. It also causes a slight discontinuity in the power produced by the turbine. Variation in wind speed is not a new problem. The turbine blade is already facing the natural turbulence in wind, plus the higher velocity at the top of the sweep area compared to the lower due to the shape of the velocity field. But this is of course something that is desirable to reduce as much as possible. Therefore, adding one more of source of variable wind speed is unfortunate.

Another Norwegian company called SWAY is trying to build a downwind offshore turbine, utilizing some of the advantages mentioned earlier. The turbine is floating freely and guides itself after the wind. It does, however, not use thin flexible wings as suggested in this rapport. But this turbine attempts to overcome the problem with reduced and unstable velocities behind the tower by shaping it aerodynamically.
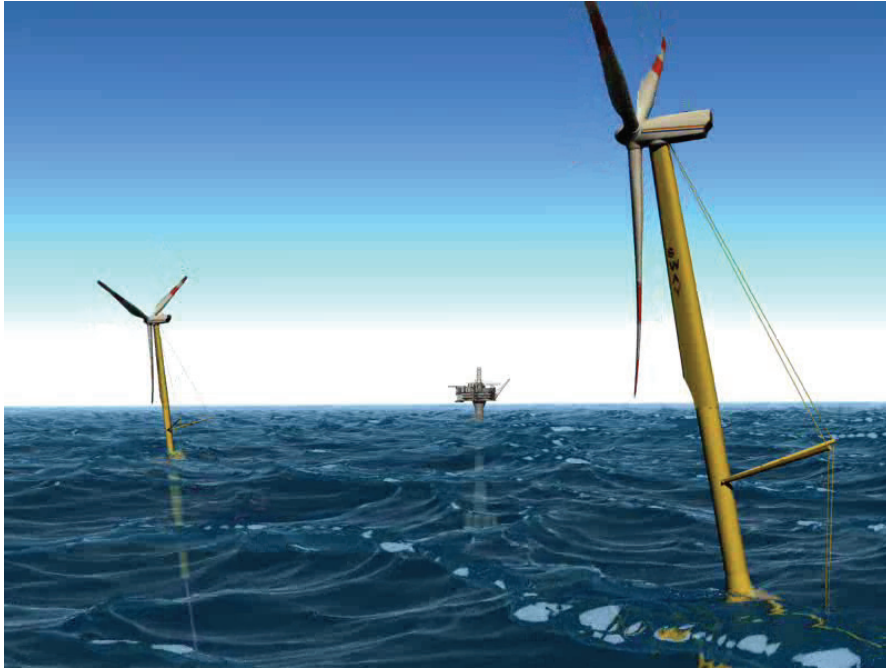
Figure 2.6 – Illustration of SWAY concept (SWAY)

It can be seen from figure 2.6, that the portion of the tower that is at the same height as the turbine, has been flattened out, to ensure a more smooth flow behind the tower.

The StatoilHydro HyWind concept is basically a wind turbine, identical to those used on land, put on top of a floating structure. This is simple, but the wind conditions, size, and the new floating environment might cause what is the best solution on land not be the best solution anymore. It is therefore needed to rethink the whole turbine system, taking the new conditions into account.

3 High lift theory

3.1 Introduction

The developments in this field started with an article by B.S. Stratford published in the Journal of fluid mechanics in 1959. He put forward a theory for designing a pressure distribution where the boundary layer is on the verge of separating during the entire pressure recovery phase. This meant that it was possible to find the fastest possible pressure recovery, thereby helping to optimize lift as well as making it theoretically possible to have zero viscous drag during the pressure recovery phase. This is the basic technology for high-lift airfoils. The work was continued, most notably by Liebeck, Lissaman and Strand, to develop ways to find the pressure distribution around an entire airfoil that would give the highest lift and lowest drag, and later use inverse design routines for designing an actual airfoil from this distribution. Airfoils developed with these methods perform extremely well at their respective design points, but tends to not work well over a range of conditions.

The potential for improvements using these methods are all regarding the top side of the airfoil. The bottom side of the airfoil is therefore largely ignored.
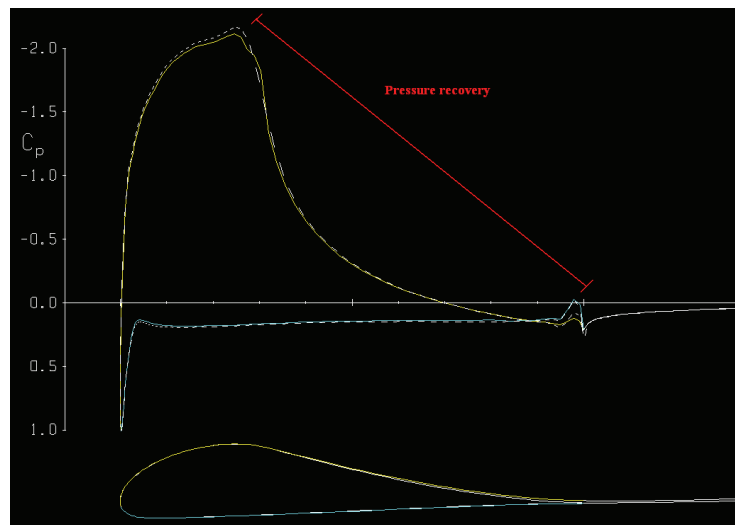
**Figure 3.1 –** Plot of pressure distribution from taken from Xfoil.

The term "high-lift" airfoil is somewhat misleading, as this theory is actually concerning airfoils with very high lift-to-drag ratios. It is therefore just as much a question of low drag as it is high lift. However, in the early days of this technology, there was much work done to design these airfoils to have high lift-to-drag ratios while at high lift coefficients, as it was hoped it could be used in vertical take off aircraft or man powered machines [8], which is probably a contributing factor to the name. Indeed, these wings were later to be used in man powered vehicles, as they were a realizing factor for the Gossamer Albatross, which flew over the English Channel by pedal power in 1979.

3.2 Boundary layers

3.2.1 Introduction

The conditions in the boundary layer are of extreme importance to an airfoil. The boundary layer growth, and the level of turbulence present in the layer, will drastically change the performance and behavior of an airfoil. They key to designing a good airfoil is therefore to understand boundary layers.

When a fluid flows over a solid surface, the tension generated will cause a boundary layer to build up close to the surface. This part of the flow will have a large velocity gradient, starting at zero close to the surface, and going up to free stream velocity further away from the surface.
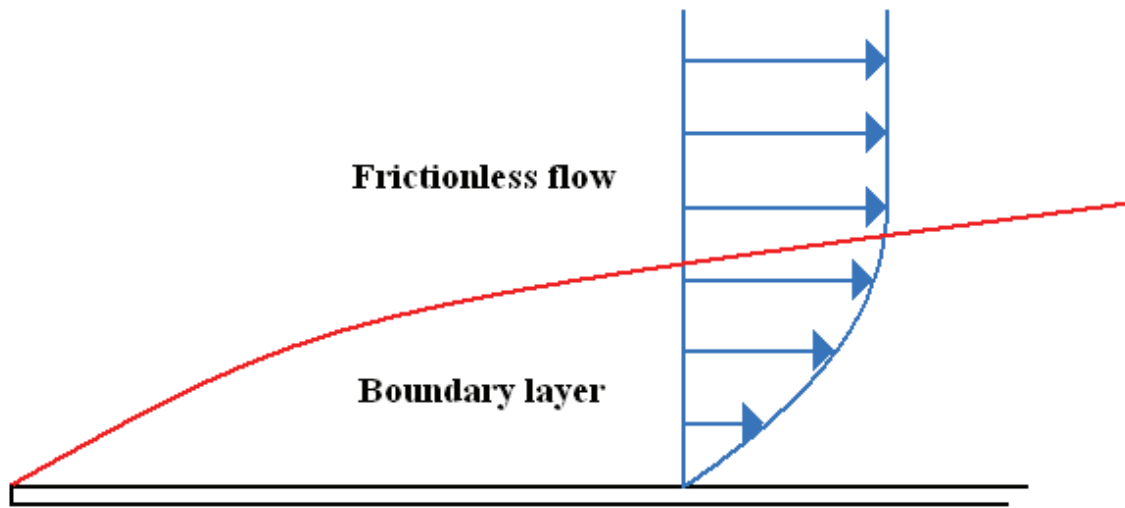
Figure 3.2 – Illustration of boundary layer

The general flow is divided into two areas; the boundary layer, which is ruled by viscous forces and has a significant velocity gradient, and the assumed to be frictionless flow further away. The limit that divides the two areas is usually defined as where the speed is 99% of the free stream flow.

The Reynolds number is a very important parameter when analyzing these kinds of flows, as the performance of airfoils can be very sensitive to the magnitude of this parameter, and especially to the location of the transition between laminar and turbulent flow:

$$\text{Re} = \frac{UL}{\nu}$$

For a two-dimensional, incompressible, stationary flow, the following equations apply:

3.1
$$u\frac{\partial u}{\partial x}+\upsilon\frac{\partial u}{\partial y}=-\frac{1}{\rho}\frac{\partial p}{\partial x}+\nu\left[\frac{\partial^2 u}{\partial x^2}+\frac{\partial^2 u}{\partial y^2}\right]$$

3.2
$$u\frac{\partial \upsilon}{\partial x}+\upsilon\frac{\partial \upsilon}{\partial y}=-\frac{1}{\rho}\frac{\partial p}{\partial y}+\nu\left[\frac{\partial^2 \upsilon}{\partial x^2}+\frac{\partial^2 \upsilon}{\partial y^2}\right]$$

If the following is assumed, the equations can be simplified:

$$Re \gg 1$$

$$\frac{\partial^2 u}{\partial x^2} \ll \frac{\partial^2 u}{\partial y^2}$$

This yields a simplified equation for the flow in the boundary layer:

3.3
$$u\frac{\partial u}{\partial x}+\upsilon\frac{\partial u}{\partial y}\simeq-\frac{1}{\rho}\frac{dp}{dx}+\nu\frac{\partial^2 u}{\partial y^2}$$

This equations are originally not meant for a curved surface, but they have been shown to work well as long as the radius of the curvature of the surface is large compared to the boundary layer thickness. Then "x" represents the arc along the surface, while "y" is everywhere normal to "x" [2. chap 7.3].

3.2.2 Separation and Stall
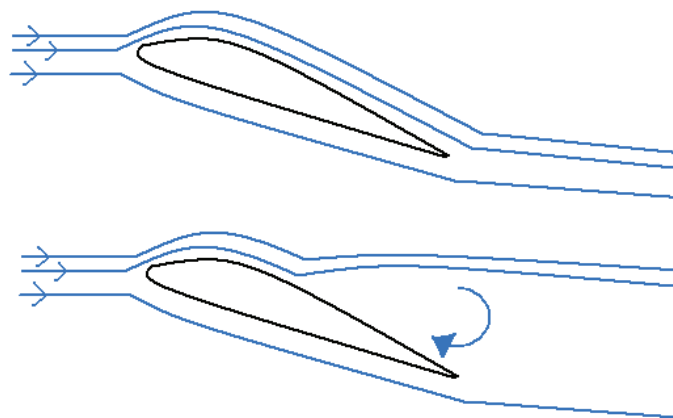
Figure 3.3 – Illustration of attached flow (upper) and separated flow (lower)

Separation is when the flow no longer manages to stay attached to the surface. When this happens, there will be a layer of reversed flow close to the surface, while the oncoming flow will be pushed away from the surface. In between the reversed and non-reversed flow, there will be an area of irregular flow. The area downstream of the separation point will have an almost uniform pressure, which will be nearly the same as the pressure at the separation point [19. chap 1.4]. The oncoming air flows over both the airfoil and the separation bubble, in effect flowing past a body of a completely different shape. This can reduce lift and increase drag dramatically. When a wing is being heavily affected by stagnation, and subsequent separation, it is said that the wing is in the stall area. This is usually visible as a shift in direction for the lift and drag curves of airfoils. If the progress of the separation occurs rapidly, the shift can be very sudden and dramatic.

As the air flows across the airfoil, it will be accelerated over the first part (negative pressure gradient), and it will be decelerated over the last part (positive pressure gradient). With a negative pressure gradient, separation is not a problem. With a positive, or adverse, pressure gradient, the risk of separation is big, as the air is flowing towards an increasing pressure. If the increase in pressure it faces is too big, the flow will get pushed away from the surface. The problem with separation is therefore mainly on upper surface at the back of the airfoil.
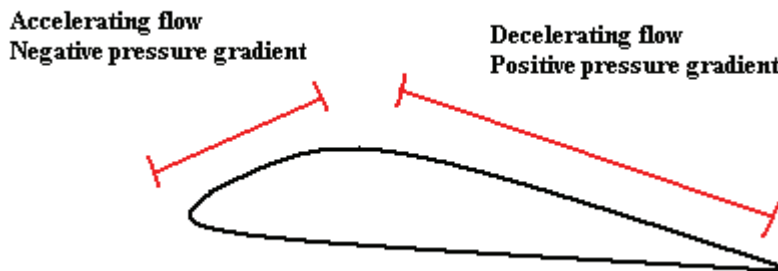
Figure 3.4 – General flow pattern over airfoil

It is therefore necessary to design the backside of the upper surface with great care to avoid separation, and it is this Stratford theory allows us to do, by defining the pressure distribution where the flow is on the verge of separating.

If simplifying equation 3.3 for conditions close to a solid plate (u = v = 0), the effect of the pressure gradient on the velocity field can be seen:

3.4
$$\left.\frac{\partial^2 u}{\partial y^2}\right|_{y=0} = \frac{1}{\mu}\frac{dp}{dx}$$

A negative pressure gradient, will give a continuous negative curvature of the velocity field. This is a stable boundary layer, without tendency to separation. If the pressure gradient is zero, the velocity field will not be curved close to the surface, but have a

negative curvature further out. For a positive pressure gradient, the velocity field will have a positive curvature close to the surface, switching to a negative curvature further out. This is an unstable boundary layer, and will separate if the pressure gradient gets too big [2. chap 7]. The three scenarios are illustrated here:
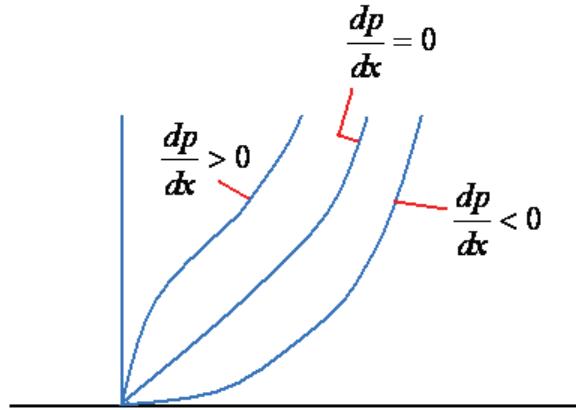
Figure 3.5 – Illustration of positive, zero, and negative pressure gradient on velocity field.

Separation means that the oncoming flow is pushed away from the surface by a layer of flow moving the opposite way. This means that the point where the flow is on the verge of separating can be defined as where the flow velocity close to the surface, u, is zero.
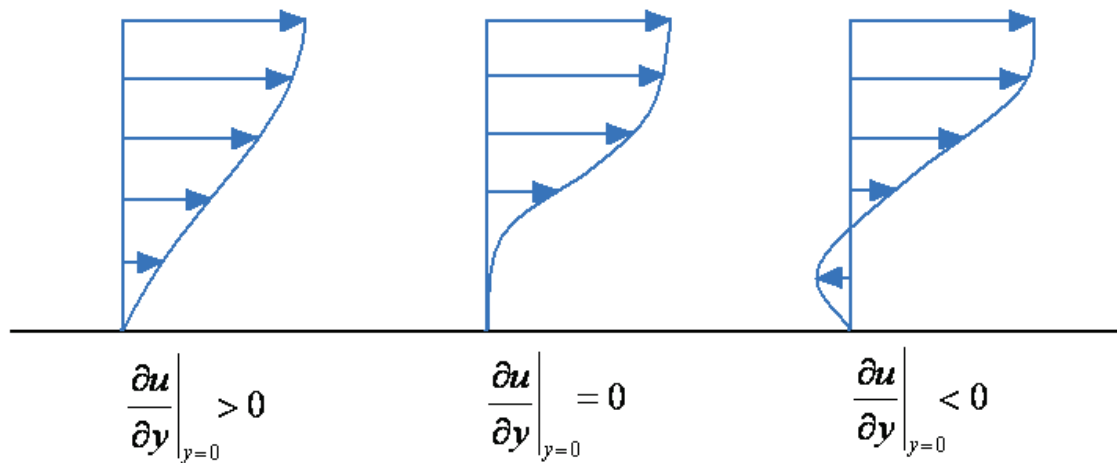

Figure 3.6 – Illustration of flow field for attached flow (left), on the verge of separating (middle), and separated flow (right)

3.2.3 Laminar vs. Turbulent flow

Airfoils are very sensitive to whether the flow is laminar or turbulent, as these two flow types possess very different qualities in terms of friction, boundary layer growth and tendency to separation. It is known from general fluid mechanics that the flow along a plate will usually start laminar, and then turn turbulent once the Reynolds number reaches

a critical value. For a big wing, this might mean that it will have laminar flow over the front, and then have the flow turn turbulent further back on the wing. This means there will be two types of flow present with very different qualities, and the transition point where the change occurs, will not be a fixed point. This is a very challenging factor when trying to design good airfoils.

In laminar flow, the streamlines will be smooth. The tension in the boundary layer comes from layers of fluid moving over each other, and the particles tend to stay in the same layer. In turbulent flow, the fluctuations cause the particles to get mixed and move through the layers. This causes the flow to be a more random mixture of particles of high and low kinetic energy, giving a much more uniform velocity profile [5. chap 2].
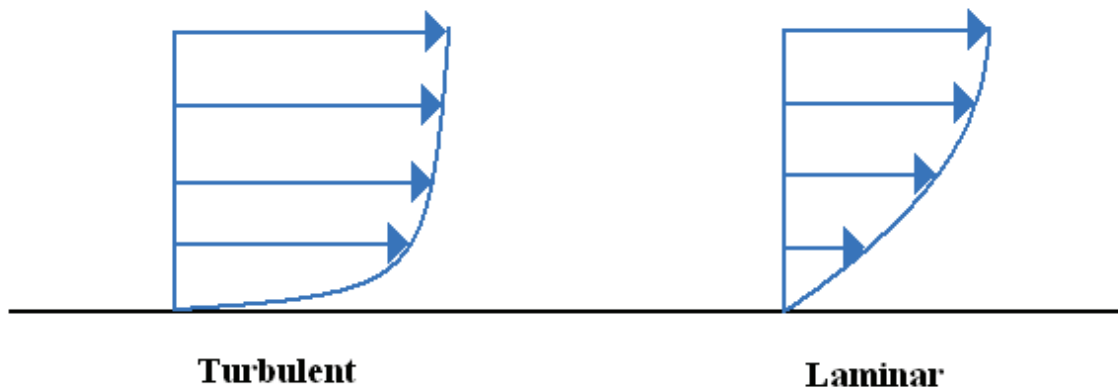

Turbulent   **Laminar**

Figure 3.7 – Illustration of the velocity fields of laminar and turbulent flow

Two of the most distinct differences in effect between laminar and turbulent flow is that turbulent flow has higher friction and lower tendency to separate. The reason for these qualities is clearly visible by looking at figure 3.7. It can be seen that turbulent flow has far higher velocity close to the surface compared to laminar flow. It is also known that separation occurs when the velocity at the surface drops below zero. Therefore, having a higher velocity close to the surface means it will take a higher pressure gradient to reduce the flows velocity to zero, thus the lower tendency to separate. This effect is clearly illustrated by comparing the velocity fields in figure 3.6 and 3.7.

This basic knowledge is used to improve performance in all sorts of applications, the most famous example being golf balls, which are dimpled to trigger turbulent flow, causing the flow to separate further back on the ball, thus resulting in less overall drag. Another example, from the world of evolutionary biology, is the humpback whales' flippers. This whale is known for extreme maneuverability and performing acrobatic maneuvers, and doing so with relatively small front flippers. The secret is that the leading edge of the flipper is covered with tubercles overgrown with barnacles, thus triggering the flow to go turbulent at the leading edge of the flipper. This allows the whale to do its tight turns without the flow separating over the flippers. Also, some types of fish, such as tuna and mackerel, have a set of distinct "finlets" along the upper and lower part of their

back body, and this is believed to help turn the flow turbulent before the flow hits the tale fin, contributing to the extreme thrust of these types of fish [12].
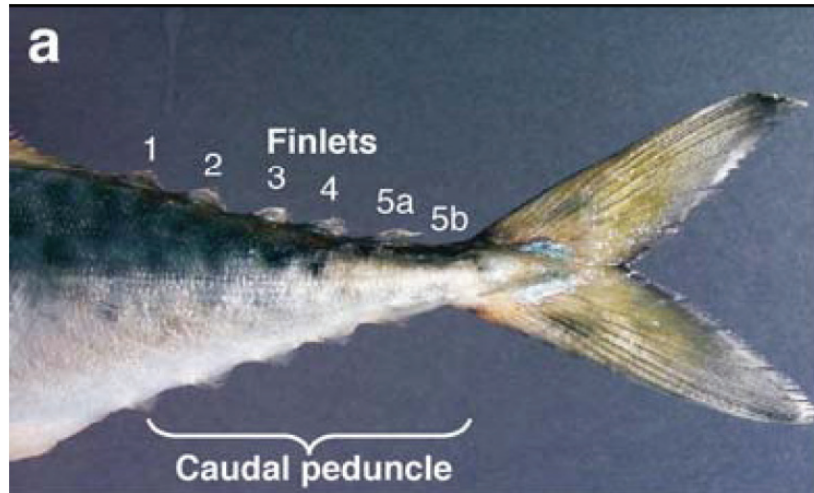
**Figure 3.8 –** Finlets on the back of mackerel, for inducing turbulent flow over the tail fin.

Figure 3.9 – Humpback whale showing its flippers, with front edges designed for inducing turbulence

3.2.4 Types of stall

There are mainly three ways in which a wing can stall:

a) Stall from the back of the wing. The separation starts from the back of the wing and gradually moves forward with increasing angle of attack. This is usually a mild type of stall, as it comes gradually.
b) Stall from the front of the wing. The separation starts as a bubble near the front of the wing. When the bubble bursts, it will cause a rapid change in the airflow over the wing, and is therefore a very dramatic stall.
c) Stall of thin wing. The separation starts as a long, stable bubble that gradually grows and eventually bursts.
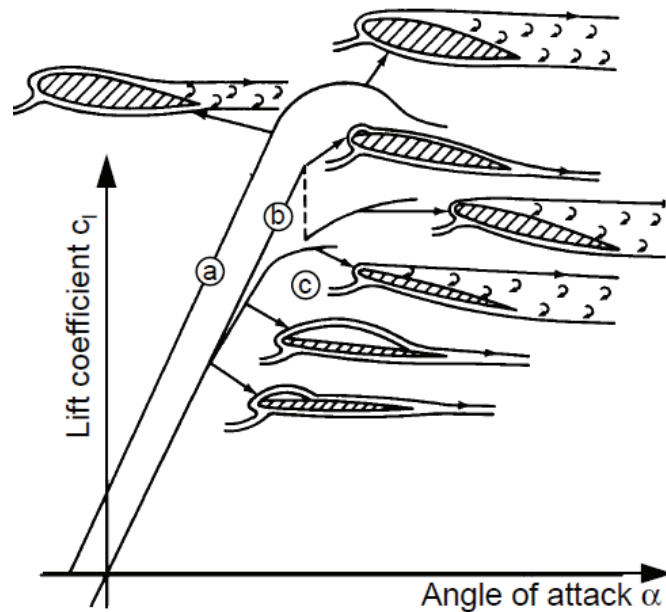
Figure 3.10 – Types of stall (taken from Seifert & Richert, 1998) [15]

3.3 Stratford theory

3.3.1 Introduction

This is a description of the method proposed by B.S. Stratford. The full workings and equations can be found in reference 6.

It is known that when a boundary layer is on the verge of separating, the velocity close to the surface is zero. The main idea behind Stratford's theory is therefore to design a pressure recovery where the velocity at the surface is always zero, thereby finding a distribution with zero viscous drag, and at the same time finding the fastest possible pressure recovery, helping to optimize lift. Stratford theory is only valid for pressure recoveries with turbulent boundary layers.

Figure 3.11 shows a standard topside pressure distribution (green). The first part of the graph shows the pressure drop over the front of the airfoil (reversed Y-axis). The pressure drops and stays low until the point labeled X_0, where the pressure recovery starts. The pressure has to be increased to equal the pressure on the bottom side of the airfoil by the time the flow reaches the trailing edge. It is the shape of this part Stratford theory concerns itself with. By stating that the velocity at the surface should be zero, the theory calculates what the corresponding local pressure gradient needs to be.

3.3.2 Equivalent length
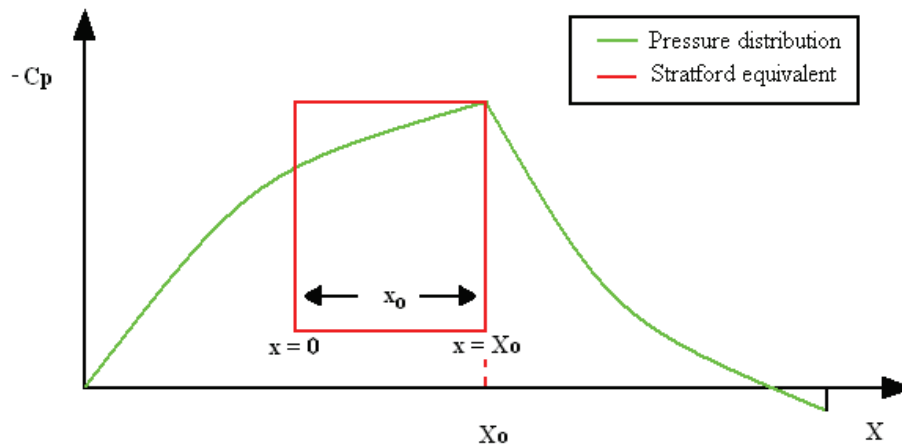
Figure 3.11 – Illustration of pressure distribution with equivalent Stratford plate

As we know from chapter 3.2, the necessary dp/dx to reduce the velocity at the surface to zero will be very dependant on the boundary layer and its level of turbulence. It is therefore vital to have an estimate for the conditions in the boundary layer when starting the calculations at X_0. Stratford suggests modeling the flow over the front of the airfoil as a phase of constant pressure over a flat plate. Since a negative pressure gradient inhibits boundary layer growth, the equivalent length along a flat plate will be much shorter. Stratford presents a set of equations for calculating the length of this fictitious plate,

illustrated in red in figure 3.12. Small x refers to lengths along the Stratford equivalent, while big X refers to length along the actual airfoil.

Stratford's simplified view of the case is therefore that the flow is first traveling through a phase of constant pressure, before a pressure gradient is suddenly applied at x_o.
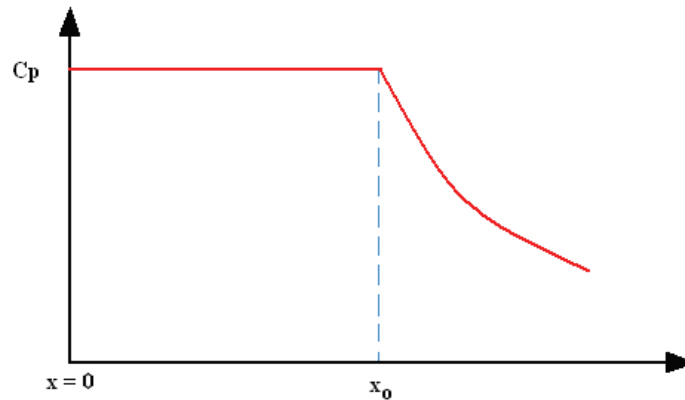
Figure 3.12 – Illustration Stratford's simplified view of the front of the airfoil

The designer must choose how low the pressure is to drop over the airfoil.
Since dynamic pressure is defined as:

$$P = \frac{1}{2}\rho V^2$$

where the density is assumed constant, the pressure can be expressed as a velocity, V. Stratford's equivalent plate model requires the stagnation point at the front of the airfoil to be close to $X = 0$, and a steadily increasing velocity towards Vo at Xo.

Stratford provides two equations for finding the distance, x_o, of the plate from the velocity change, one for assumed turbulent and one for assumed laminar flow.

3.5 (turbulent)
$$x_0 = \int_0^{X_0} \left[\frac{V}{V_0} \right]^3 dX$$

3.6 (laminar)
$$x_0 = 38.2(\mathrm{Re}_{x_0})^{-3/8} \left[\int_0^{X_0} \left(\frac{V}{V_0} \right)^5 d\left(\frac{X}{X_0} \right) \right]^{5/8} X_0$$

This value, x_o, will be a parameter that is put into the final equations.

3.3.3 Layers and calculation

In Stratford theory, the flow is divided into an inner and outer layer. These two layers will be calculated individually with different methods. The solutions are then matched to satisfy stream conditions [19. chap 1.5].

The basis for analysis of the outer layer is that the total pressure (static + dynamic pressure) is assumed constant along a streamline. The shear stress is assumed negligible. The increasing pressure will therefore only cause a loss of dynamic pressure for the outer layer.

For the inner layer, there is a transition from the conditions at the wall up until the start of the outer layer. At the wall, the pressure forces are balanced by viscous forces, while close to the outer layer, the pressure forces only reduce dynamic pressure. The losses close to the wall are modeled as flow along a flat plate.

The two solutions are then matched to have the same velocity and gradient values at the transition between the two layers. By including the condition that the tension at the wall has to be zero, the optimum solution can be found.
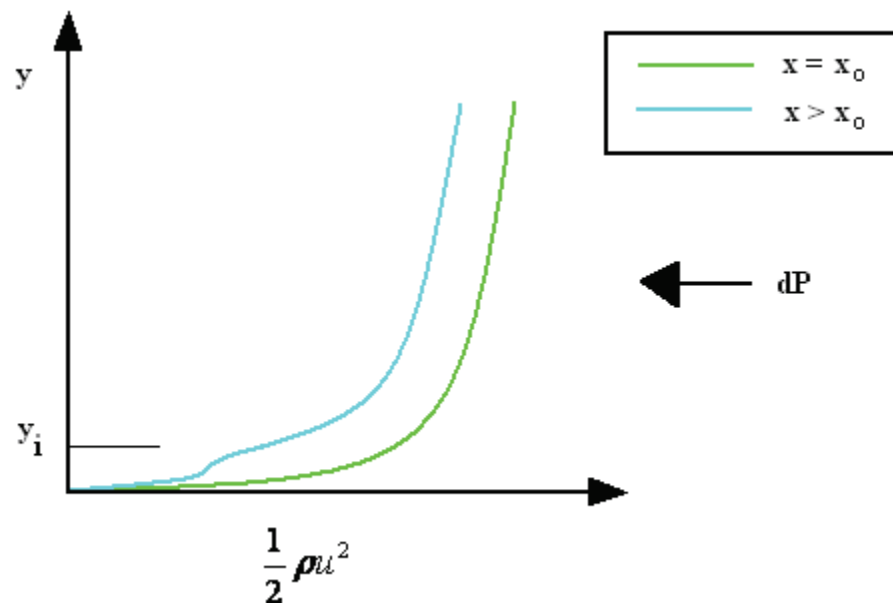
Figure 3.13 – Illustration of the velocity field at the start of the pressure recovery (green), and a bit further downstream (blue). It can be seen that the outer layer has only had a loss in dynamic pressure, while the inner layer has been deformed.

Starting from this design philosophy, Stratford uses both basic fluid mechanical equations and some new parameters that are determined experimentally, in order to find a solution. The detailed workings can be found in reference 6. In the end, Stratford reaches two fairly simple equations for finding the pressure coefficient at any point x downstream of x = x$_0$.

$$3.7 \quad \bar{C}p\left(x/x_0\right) = 0.49\left[\left(\mathrm{Re}_{x_0}\right)^{1/5}\left(\left(\frac{x}{x_0}\right)^{1/5}-1\right)\right]^{1/3}, \qquad \bar{C}p \le \frac{4}{7}$$

$$3.8 \quad \bar{C}p\left(x/x_0\right) = 1 - \frac{a}{\left[\left(\frac{x}{x_0}\right)+b\right]^{1/2}}, \qquad \bar{C}p > \frac{4}{7}$$

Where:

* $\bar{C}p$ is the reference pressure $\bar{C}p = \dfrac{P-P_0}{\frac{1}{2}\rho V_0^2}$

* a and b are constant chosen so that $\bar{C}p$ and $\dfrac{d\bar{C}p}{d\left(\dfrac{x}{x_0}\right)}$ match up at $\bar{C}p = \dfrac{4}{7}$

An optimization procedure based around equation 3.7 and 3.8 is therefore the basis for finding the shortest possible distance to regain the pressure between Cp$_{min}$ and Cp$_{te}$ (difference in pressure from minimum pressure to trailing edge pressure). These values must be chosen by the designer. The equations connecting $\bar{C}p$ and Cp are:

$$3.9 \quad Cp = \left(\frac{V}{V_0}\right)^2\left(\bar{C}p-1\right)+1$$

$$3.10 \quad \mathrm{Re}_{x_0} = \left(\frac{Cp_{te}-1}{\bar{C}p_{te}-1}\right)^{1/2}\frac{x_0}{c}\mathrm{Re}_\infty$$

Stratford developed his theory with a Reynolds number in the order of 10^6 in mind, and it is therefore most accurate in this region. Even so, the theory gives between $0 - 10\ \%$ too low results for the actual needed pressure. Stratford therefore comments that allowing a slightly faster pressure recovery than calculated will give the ideal result for an actual airfoil.

With this theory, there is not one universal optimum solution. The solution will depend on the conditions in the boundary layer, and the chosen Cp_{min} and Cp_{te}, and the optimum value of these factors will depend on the application. Finding the best solution will therefore be an iterative process.

The chosen trailing edge pressure, Cp_{te}, is of big significance for the final design. The velocity at the trailing edge has to be the same for both sides of the airfoil. By having a higher trailing edge velocity, there will be less pressure to recover, thereby making it possible to optimizing lift. However, a higher velocity at the trailing edge will make the back end of the wing very thin. As the thickness starts to move towards zero, it is clear that there are limits to how high the velocity at the trailing edge can be for a realistic wing. It will therefore be a structural limit to the trailing edge velocity. Liebeck gives an estimate for what are practical values [19. chap 2.6]:

$V_{te} / V_\infty = <0.8, 0.95>$

Which translates to:

$Cp_{te} = <0.0975 , 0.36>$

In this interval, the lower values of trailing edge pressure will give more lift, but might leave the wing structurally weak. Assumptions about Cp_{te}, Cp_{min}, the front of the wing and Reynolds number at x_o will give different results for the pressure recovery. A lot of iterative work is therefore needed to design a good wing.
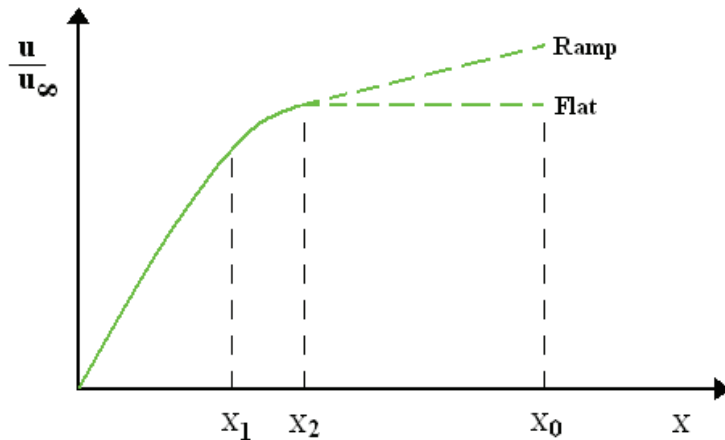
3.4 Front of airfoil

While Stratford theory only calculates the pressure recovery, other methods must be used to design the front of the airfoil. Robert Liebeck has written several papers on guidelines for designing the front of the airfoil when used in combination with Stratford recovery[7] [8] [9]. With regards to lift, it is preferable to have the pressure drop as quickly as possible. However, the way in which the air is accelerated will have an impact on the transition point, drag, boundary layer growth and probability of nose separation and much more.
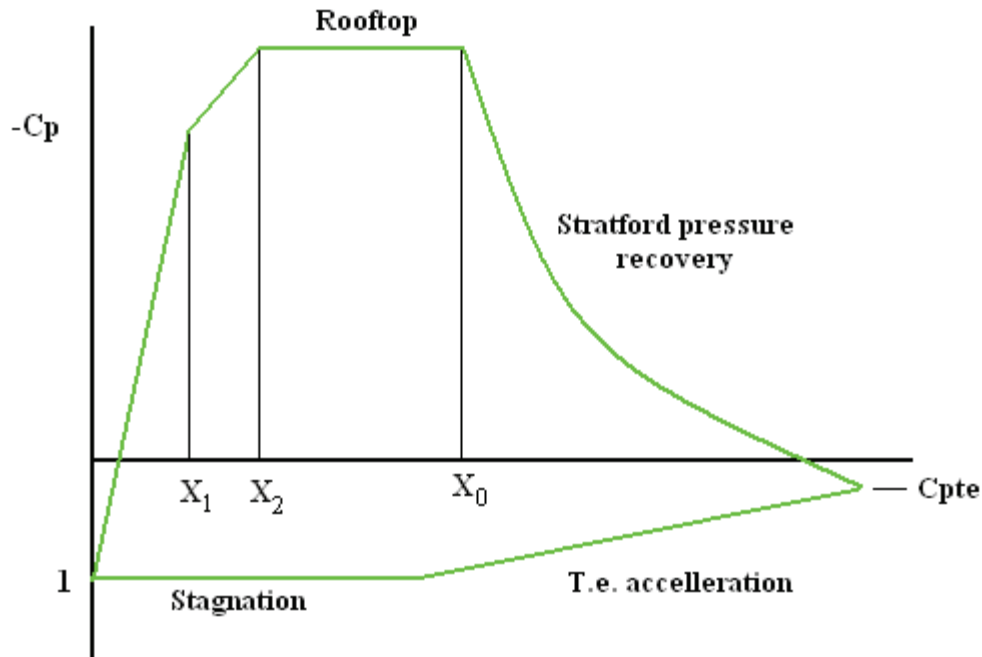
Figure 3.14 – Schematic view of total high-lift pressure distribution.

For high Reynolds numbers, or high angles of attack, the air will probably turn turbulent somewhere on the front part of the wing, before X_0. One of the factors influencing the location of the transition point between laminar and turbulent flow will be how the air is accelerated. A continuous negative pressure gradient inhibits boundary layer growth, and will make the flow turn turbulent later. Therefore, a more gradual drop in pressure towards X_0 will keep laminar flow longer. This will reduce drag, but also reduce lift as the area under the Cp-graph will be reduced. A quick pressure drop and a long flat rooftop will give a higher lift coefficient, but the drag and boundary layer growth will also be bigger. Another reason to avoid this design is that a too sudden pressure change can lead to nose separation. The curvature radius over the airfoil causes the pressure changes. If the pressure is to drop suddenly and be followed by a flat rooftop, there will be a very sudden change, which creates an area vulnerable to nose separation. This must of course be avoided, meaning that the path between X_1 and X_2 must be gradual and smooth [23. chap 2]. The leading edge must also be rounded in order to permit operation over a range of angles of attack.

The highest lift-to-drag ratios are achieved with a flat rooftop. A high-lift airfoil is therefore usually designed for having a flat rooftop at the design angle of attack, while more conservative airfoils, designed specifically for low drag, such as NREL airfoils, will have a ramp rooftop [16].

Figure 3.15 – distribution over front of airfoil

The pressure distribution will, of course, change with varying angle of attack, making the designed pressure distribution only occur at the design angle of attack. How the distribution change for other conditions must be carefully analyzed to ensure good performance over a wide range of angles. For a high-lift airfoil, the design will cause the rooftop of the pressure distribution to be tilted positively for low angles, have a flat rooftop for the design angle, and have a negatively tilted rooftop for high angles of attack.

3.5 Roughness

To which extent a wing has a non-smooth surface is referred to as "roughness". Bugs, salt, dirt, ice and other particles will inevitably be deposited on a wing. This means that the rate of roughness will vary. Roughness will help induce turbulence faster, meaning that with varying deposits on the wings, the transition point will move.

The exact location of the transition point will impact the performance significantly. The ideal is to have a laminar flow over the rooftop, and have the flow turn turbulent as the pressure recovery starts at X_0. In practice, the transition point will move with varying air properties, angles of attack, roughness on the surface, and several other factors. It must also be noted that for offshore wind turbines, which is the focus of this report, the Reynolds number will most likely be so big that it will difficult to keep the flow laminar long enough to reach X_0.

It is very important to a functional airfoil that it is insensitive to roughness [17]. It might therefore be useful to design the front of the airfoil so that the flow turns turbulent very early. That way, the flow over the rooftop will be turbulent anyway, thereby making the overall performance largely insensitive to roughness. This is not ideal for achieving high lift-to-drag ratios, but it might be necessary in order to get an airfoil that performs stably for a wide range of conditions, which will be needed for use in wind turbines.

3.6 NREL

Most airfoils used in windmills were originally developed for aircraft. The National Renewable Energy Laboratory (NREL) in the US has therefore developed a serious of airfoils designed specifically for wind turbines. Several reports are openly available on the design and performance of these airfoils [16]. The design philosophy behind the airfoils is only briefly explained. Insensitivity to roughness is presented as the most pressing issue. In addition, they stat as a "rule of thumb", it is favorable to have a continuous negative pressure gradient over the first 30% of the wing, and then have a concave pressure recovery in order to achieve low drag [17]. This matches the ideas presented by the high-lift theory.

3.7 Earlier works with high lift profiles at NTNU

In the early 1980's, there was a lot of research going on at NTNU regarding boundary layers. This research was mainly focused towards ships, and the boundary layers developing alongside the hull. It was discovered that the methods for estimating the boundary layers were inaccurate when the pressure gradients became large. They therefore wanted to find a pressure gradient they could do calculations on. This led to the interest in Stratford theory and high-lift wings.

A significant amount of research and investigations were done regarding high lift airfoils, culminating in the creation of the HOG-profile. This profile, and the reports leading up to its development, is the basis for the work done in this report.

As mentioned earlier, designing a high lift airfoil will be a lengthy process of making assumptions and iterating different solutions. Luckily, the old reports contain a lot of optimization work, where attempts have been made with various assumptions. This includes Stratford recoveries calculated for a range of Cp_{te} and Cp_{min} [19]. This gives a great overview of what would be ideal, and makes it a lot easier to know in which direction to take a design.

Computer codes were also written to optimize the front of the pressure distribution [23], and to use inverse theory to design an actual airfoil from the given distribution. Several designs were made, with the final HOG profile being the most successful.
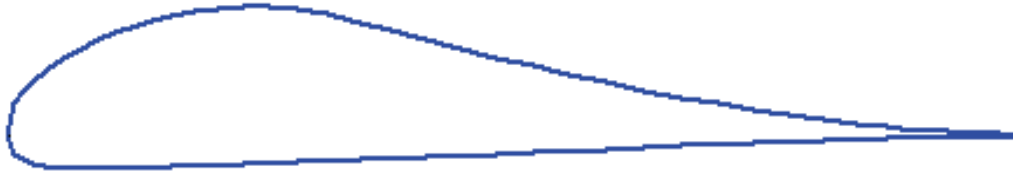
Figure 3.17 – HOG profile

This is a very good design, and the profile appears to have a very high lift-to-drag-ratio compared to standard airfoils. Although, as expected, it has a very dramatic stall characteristic, which makes it unsuitable for applications working under varying conditions.

Attempts were also made at making models and doing experimental tests. The results from this work are not very accurate. It turned out that the importance of the Reynolds number had been underestimated. The model was relatively small and the conditions in the wind tunnel were not suitable. Attempts at tripping the flow were not successful. It is now understood that the Reynolds number is of high importance to such airfoils.

In later years, the work at the university has focused more on the general and fundamental problems in fluid mechanics. But with the performance and weight of wings becoming of extreme importance for offshore wind power, this field is becoming interesting once more. In this rapport, it is therefore attempted to pick up the work done at this institute in the 80's, and see if it is possible to design a high lift profile without the dramatic stall, in order to make it suitable for wind turbines.

4 Design conditions

4.1 Introduction

In order to design a good airfoil, and understand to which extent the high lift theory can be implemented, it is vital to understand the main turbine design parameters and the conditions the wing will encounter. To get a clear view of how, and under what conditions, the profile must perform, we therefore design a theoretical turbine and analyze the flow over the wings.
Since we are interested in rather large offshore wind turbines, we must choose values that correspond well with such a design. The chosen values do not have to be anywhere near exact, but they should be "ball park" to provide a useful estimate.
It is therefore assumed that we want to build a 5 MW, 3-bladed wind turbine that is to be located in the North Sea outside Norway.

4.2 Scaling of turbine

The first issue to investigate is the wind conditions. The Norwegian meteorological institute has a vast database available online (www.met.no) with wind measurements from oil rigs in the North Sea. By comparing these values for several oil rigs over a wide range of years, it was clear that the most frequent wind speed was in the area of 8~9 m/s. By calculating the average of the most frequent wind speeds for a selection of 10 standard wind reports, the numerical value became 8.8 m/s. However, all these measurements were taken at an altitude of 10 meters. We must therefore use approximations to find out what the average wind speed is higher up.
The velocity profile of the wind will be much more uniform over sea than land, due to the smooth surface of the ocean, but there is still a significant increase in velocity with altitude.
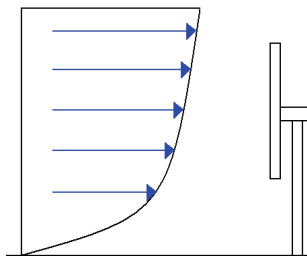
Figure 4.2.1 – Illustration of velocity field

There are many proposed methods for approximating a velocity field from a single measured value. It is here chosen to use the power law profile [3, chap 2.3.3.2].

$$4.1 \qquad U(z) = U(z_r)\left(\frac{z}{z_r}\right)^{\alpha}$$

Where U is wind speed, z is altitude, and denotation r indicates a reference value, i.e. the measured value. The important parameter in this model is the power law exponent, α. The value of this parameter changes with what kind of terrain the velocity field is assumed to travel over, and is highly variable. A rule-of-thumb value for this parameter is 1/7 (0.143), as first calculated by von Karman. The velocity field over water will be more uniform than over land, and it is therefore more correct to use a slightly lower value for α. According to refrence 4, when wind is calculated over open water, a more suitable value is 0.11.

To get a useful estimate of what speed to design for, we therefore calculate the wind speed at an altitude of 100 meters.

$$U(100) = 8.8 \left(\frac{100}{10} \right)^{0.11} = 11.34$$

According to this model, the most frequent wind speed at an altitude of 100 meters will be 11.34 m/s. In addition it must be remembered that the turbine will not be optimized for the most frequent wind speed, rather the value giving the highest overall power production, which is not the same, as the energy in the wind increases to the power of 3 with increasing velocity. It is therefore likely that the design velocity will be slightly higher than the most frequent velocity. The curved velocity field also means that the top of the turbine will see a much higher velocity than the bottom of the turbine. It is therefore not easy to pick an exact value, but based on the calculations done here, we assume a design wind speed of 12 m/s.

This value is not as critical as one might think, because a turbine is not optimized for a wind speed, but a tip speed ratio. The relationship between wind speed, rotational speed and radius is described by the tip speed ratio (TSR). This is an important parameter for turbines, and is given the symbol λ.

$$\lambda = \frac{\omega R}{U}$$

This means that even if the wind changes from the design conditions, optimum C_p can still be reached by regulating the rotation, ω, so that the design tip speed ratio is maintained. However, there will usually be limitations on what rotational speeds can be used due to the gear box and generator.

The next parameter to calculate is the radius of the turbine. The power output from a wind turbine can be estimated by the relation:

4.2
$$P = \frac{1}{2} \rho V_1^3 A C_p \eta$$

Where A is the sweep area of the turbine, Cp is the aerodynamic efficiency, and η is the mechanical/electrical efficiency [3. chap 3.2].

It is further assumed:

C_p = 0.4
η = 0.9
ρ = 1.2 kg/m^3

Since $A = \pi R^2$, it is possible to calculate the needed radius of the turbine:

$$5000000 = \frac{1}{2}1.2*12^3*\pi R^2 *0.4*0.9$$

This gives a radius of ~65 meters.

If assuming that the lowest sweep altitude for the turbine is at 10 meters altitude, the turbine will reach 140 meters above sea level. According to the power law profile, we well get a velocity field varying from ~8.8 m/s at 10 meters to ~11.8 m/s at 140 meters.
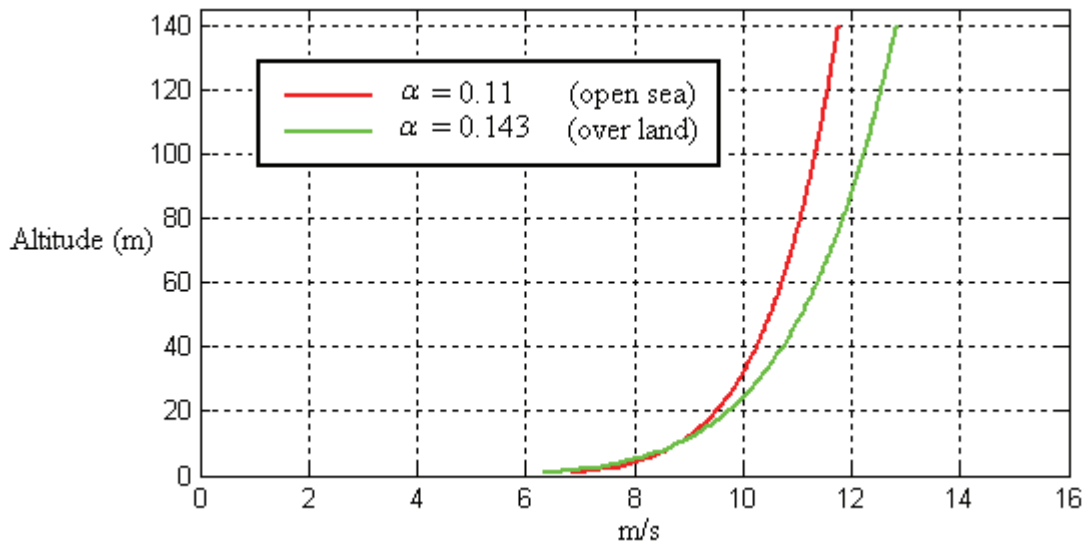
Figure 4.2.2 – Illustration of velocity field calculated for open sea (red) compared to calculation for over land (green)

Figure 4.2.2 shows that there is a lot to be gained by elevating the turbine, but this puts a lot of structural strain on the system. Only a thorough economical analysis can reveal at what altitude the best compromise between performance and cost of structure occurs. The more uniform velocity profile gives reason to believe that this could occur for a lower altitude for offshore wind turbines. But the design and cost of the subsea structure is completely different from the foundations on land, so there is no basis for drawing any conclusions regarding this. If it turns out to be less of a burden than assumed to elevate the turbine for offshore installations, it can be seen that there is a lot to gain by raising the lower sweep area up as far as to ~30 meters. This would give a much more uniform flow over the turbine, giving better performance, more power, and a more balanced loading on the system. However, elevations of this magnitude are unrealistic.

The chosen design tip speed ratio is a compromise between many structural and technical factors. Ideally, the efficiency of the turbine increases with increasing TSR. In practice, the drag on the wings starts decreasing the efficiency at high rotational speeds. The optimum TSR for a wind turbine is given by [3. chap 3.11]:

$$4.3 \qquad C_{p,max} = \left[\frac{16}{27}\right]\lambda\left[\lambda + \frac{1.32 + \left[\frac{\lambda-8}{20}\right]^2}{B^{(2/3)}}\right]^{-1} - \left[\frac{0.57\lambda^2}{\frac{C_L}{C_D}\left[\lambda + \frac{1}{2B}\right]}\right]$$

Where B is the number of blades on the turbine. This expression has been determined experimentally, and is accurate within 0.5% for TSRs between 4 to 20, lift on drag ratios from 25 to infinity, and 1-3 blades. The optimum solution is dependant on the lift-to-drag ratio and number of blades (which is assumed to be 3). If it is assumed that the high lift airfoil used will have a lift-to-drag ratio of approximately 150 (including roughness), the optimum TSR will be in the area of 9~10. The design value for L/D-ratio is not a sensitive parameter, as the chord length of the blades will be almost exclusively controlled by the chosen design C_L (the contribution from C_D is negligible). The ratio gives an idea about the optimum TSR, but the TSR will probably be limited by maximum allowable tip speed anyway, thereby giving the design L/D-ratio little significance.
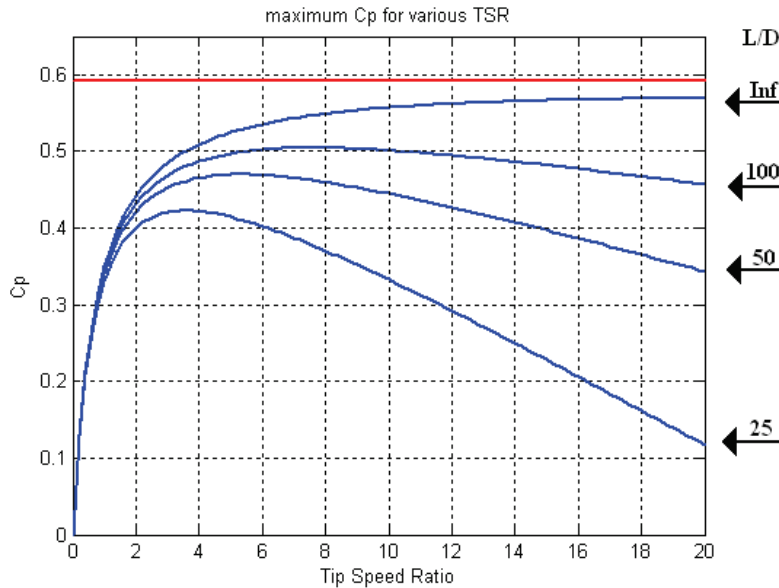
Figure 4.2.3 – Efficiency vs. TSR for varying L/D ratios, according to equation 4.3

On land, a limitation is that higher tip speed ratios make more noise, and some also claim that certain rotational speeds are more unpleasant to look at. These are not considered to be factors for offshore wind turbines, as they are not in the proximity of humans. Therefore, the only limitation set is that the tip speed should stay well below 100 m/s, in order to avoid compressible flow effects.

It is assumed that the airfoil used on the wings have a lift-on-drag-relationship of 150, with the following parameters at an assumed optimum angel of attack, 5°:

$C_L = 1.2$
$C_D = 0.008$

Using this information and a BEM-program created for an earlier project, a turbine design can be generated and tested (The full workings of the BEM-method can be found in reference 3).
Some quick tests revealed that a good value for TSR would be 7.5. At this value, the tip speed of the wing at standard operation would be 89 m/s, while at the same time staying near the optimum area as calculated by equation 4.3. Using these values, the following turbine could be created:
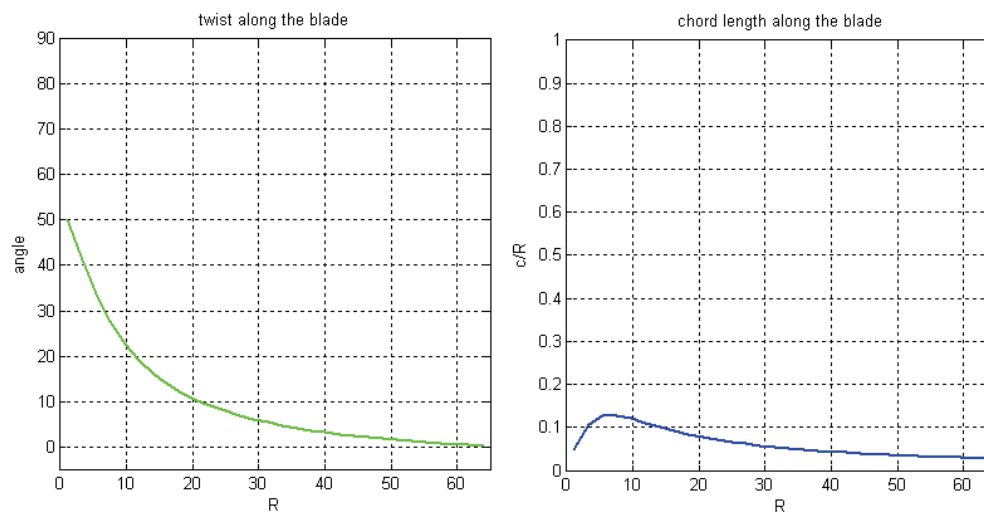

Figure 4.2.4 – Turbine blade dimensions

We now have a fictional offshore wind turbine of reasonable dimensions. Using the same program, the flow over the wings can be analyzed, giving a useful indication of what conditions to design the high-lift profile for.
It is assumed that we are dealing with a pitch controlled turbine, meaning that the wings will pitch with varying wind velocities to control its performance. The alternative is a stall controlled turbine, which uses wings with a very soft stall to control its performance [5. chap 7]. This is not viewed as a useful alternative in combination with high-lift profiles.

It is especially interesting to see what happens to the flow in variable wind conditions (turbulence), as it is important that the airfoil is working in its prime operational range and does not stall. For all the following calculations, the rotational speed and pitch is kept constant, while the wind speed varies. The calculations here are therefore simulating the wings pitched constantly for a wind velocity of 12 m/s.

4.3 Calculations of operational conditions
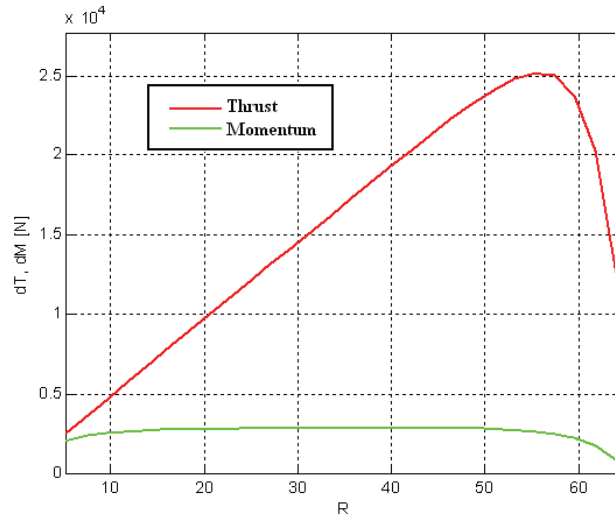
**Figure 4.3.1 –** Forces on turbine at design conditions.

Figure 4.3.1 shows the forces on the turbine at the design speed of 12 m/s. The momentum force needs to be multiplied with its local radius in order to get the force. It is therefore easy to see how the vast majority of the momentum and thrust forces are extracted far out on the blade (because they sweep a bigger area). This is why the outer part of the wing is much more interesting than the inner part. Also, the inner part of the wing is usually corrupted by structural requirements, causing it to be thicker, and is therefore unlikely to bee suitable for a thin high-lift profile anyway. The focus is therefore put mainly on the outer part of the wing. Figure 4.3.1 also shows clearly the tip loss caused by vortices. These losses can be reduced by using winglets. In order to perform efficiently, winglets are dependant on traveling at their specific design speed [29]. As shown in figure 4.3.2, the velocity at the tip will be remarkably stable, and the wings might therefore be suitable for winglets. But that is not the point of interest in this rapport.
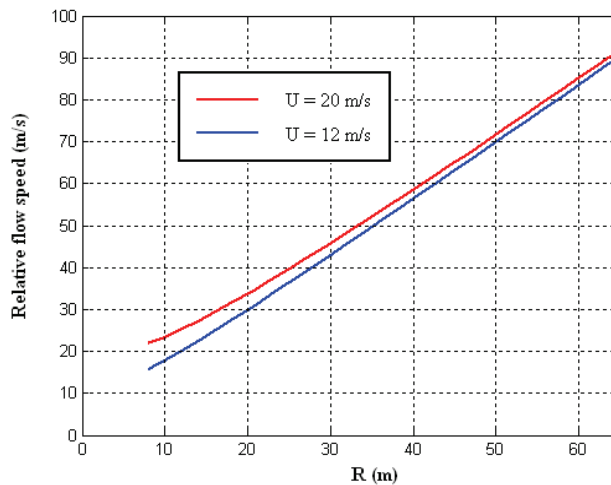
**Figure 4.3.2 –** Relative velocity over turbine blade

39

Fig 4.3.2 shows the velocity over the wing at different radii for wind velocities of 12 and 20 m/s. It can be seen that the velocity over the wing varies very little. This is because the major portion of this speed is made up by the rotational speed, and the incoming wind is therefore a relatively small contributor. This gives a relatively constant velocity, and should result in a very stable Reynolds number as well.

Since we know the relative velocity over the wing and the chord length, the Reynolds number can be calculated. As expected, figure 4.3.3 shows a Reynolds number that varies very little for a wide selection of wind speeds, especially for the outer regions. The magnitude of the Reynolds number is a very approximate value and we therefore only need to know a rough estimate. The value can be seen to be around ~1 x 10^7, and this is therefore chosen as the design Reynolds number.
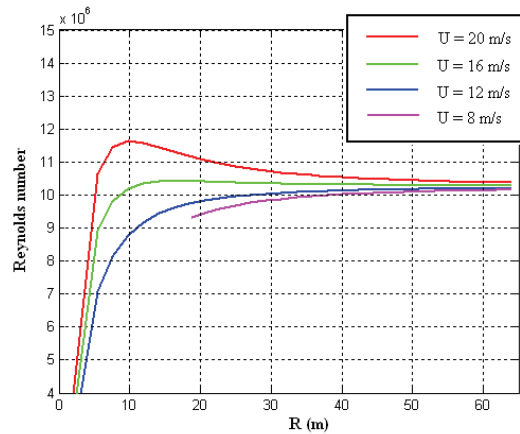
Figure 4.3.3 – Reynolds number across turbine blades. Kinematic viscosity is assumed to be 15.68e-6. Values go to zero for low radii due to hub modeling.

Since we are very interested in stall characteristics, it is important to have a view of how the angle of attack will vary along the wing in turbulent wind conditions. Figure 4.3.4 shows the angle of attack along the wing for a selection of wind speeds (pitch kept constant).
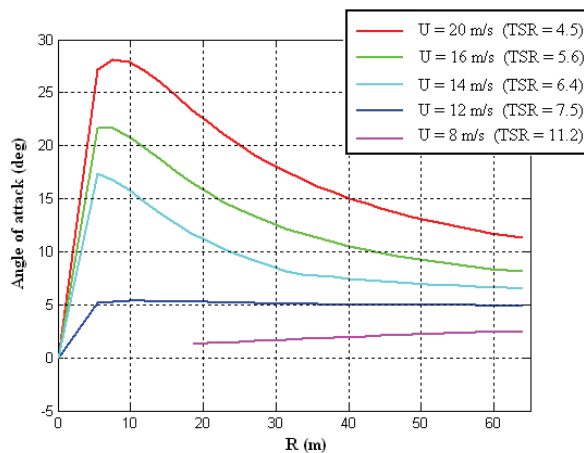
Figure 4.3.4 – Angles of attack across turbine blade for varying wind speeds (5º is design value)

A striking result is how vast the variations will be for low radii. This is a natural result of the enormous size of the turbine, causing the difference between the tip and root to be very big. It is clear that whatever airfoils are chosen for low radii, it has to be something with a very gentle stall, as separation will inevitably occur in gusts of wind. On the other hand, the force contributions from low radii are small compared to those further out on the wing. The performance at low radii is therefore not as critical, and can be allowed to have a more modest behavior. The inner area is not suitable for a high lift profile due to extreme variations in angle of attack, and, as mentioned earlier, it probably would also be impossible due to structural requirements. The focus is therefore put on the outer regions.

The average amount of turbulence in wind will vary from site to site, and must therefore be analyzed carefully in advance. The data from the North Sea does not contain such information, however, it is generally known that turbulence intensity in wind is usually in the range of 0.1-0.4 [3. chap 2.3.2.1]. Turbulence intensity is defined as:

4.4
$$TI = \frac{\sigma_U}{U}$$

Where σ_U is the standard deviation. In the "worst case scenario" of TI = 0.4, wind speed would then on average vary between 7.2 - 16.8 m/s (starting from the design speed of 12 m/s). Rare gusts of wind will of course exceed these values. It is the upper limit that is of concern, as this might lead to stall. According to figure 4.3.4, a jump from 12 to 16 m/s in wind speed would, at r = 40 m, lead to a change of ~6° in angle of attack. It is assumed that a high-lift profile is suitable for implementation for radii from 40 to 65 meters. For lower radii, the variations in angle of attack will be too big.

4.4 Chord length reduction

The induction factor, a, is value for how much the air is slowed down in horizontal direction over a wind turbine, and is defined as a = $(V_1 - V_2)/V_1$, where V_1 is the wind speed far upstream of the turbine, while V_2 is the velocity through the turbine sweep area. When taking out energy from the flow, the velocity will be reduced. When increasing the induction factor, a point will be reached where the reduction in velocity starts to decrease the efficiency of the turbine. The optimum point is at a = 1/3, which gives a maximum theoretical efficiency of 59.3% for wind turbines, also known as the Betz limit [5. chap 4]. This means that under ideal conditions, the wind turbine blades will be designed to result in an induction factor of 1/3, and that is the design parameter used to design the turbine in this chapter. However, as can be seen from figure 4.4.1 the thrust forces on the turbine rise much quicker with increasing induction factor compared to efficiency. Parts of turbine blades are therefore often designed to take out less than a = 1/3, in order to reduce thrust forces, while only having a minor loss in efficiency [34]. This will also reduce the cord length, and thereby the weight of the wings.
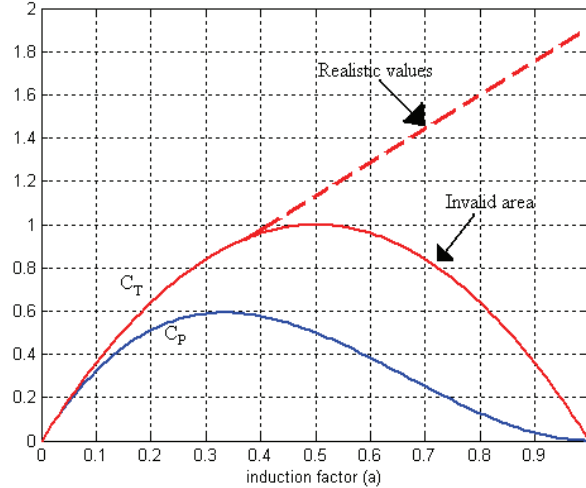
Figure 4.4.1 – Coefficients of thrust and power as a function of the induction factor, a.

Another way of loosing weight would be to reduce the chord length by designing for a higher lift coefficient, C_L.

Since the design induction factor dictates how much energy is supposed to be taken out of the flow, and the lift-to-drag ratio is large, the chord length will almost exclusively be given by the design lift coefficient. A higher lift coefficient must have a shorter chord length to keep lift constant, due to their inverse proportional relationship that can be seen from equation 4.5.

4.5

$$L = C_L \frac{1}{2} \rho V^2 c$$

One reason for not choosing a high lift coefficient is that it would mean that the design point of operation will be closer to the stall region. Also, the lift coefficient will be a structural compromise. As the design lift coefficient is increased, the force on the wing stays constant while the wing gets smaller. It is therefore obvious that there will be an optimum point of structural compromise between lift coefficient and chord length. For most wind turbines today, the design lift coefficient appears to be around 1.0~1.1 [34]. There is reason to believe that the thin flexible wing/downwind concept can handle higher design lift coefficients, as the wings would tilt back in strong winds, effectively reducing the sweep area of the turbine, and thereby relieving the wings of large forces. They will therefore not have to cope with forces of the same size as a conventional turbine. Until a detailed structural analysis of such wings is presented, we will not know how much it is useful increase the operational lift coefficient. It will not be a big change, as it is still important to operate at a safe distance from the stall region. It is therefore in this report assumed that it will be useful to design the wing with a lift coefficient up to C_L ~ 1.3.

The energy removed from the flow, which "a" is an indicator for, will be converted to lift and drag respectively. This means that when lowering drag, it becomes ideal to take out more lift. This means that a more efficient profile with low drag will actually result in a bigger ideal chord length, promoting an increase in weight. However, this increase is so small that it is negligible compared to the effect from the lift coefficient. Equation 4.6 gives the ideal chord length for a turbine blade at any local tip speed ratio [5. chap 8], and it can be seen that the parameter C_n decides how the airfoil affects chord length. Since a higher C_n will give smaller chord lengths, it is clear that a reduction in C_D will induce bigger chord lengths. Although the equations also illustrates how much more important the lift coefficient is compared to the drag coefficient. C_L is expected to be in the order of 150-200 times bigger than C_D. In addition, they are multiplied by their respective trigonometrical parameter. Since the flow angle, φ, is relatively low, it means that C_L will be multiplied by a factor close to 1, while C_D will be multiplied with something close to 0. This means that the contribution from the drag coefficient is almost negligible.

4.6
$$\frac{c(x)}{R} = \frac{8\pi a x \sin^2 \varphi}{(1-a)BC_n\lambda}$$

$$C_n = C_L \cos\varphi + C_D \sin\varphi$$
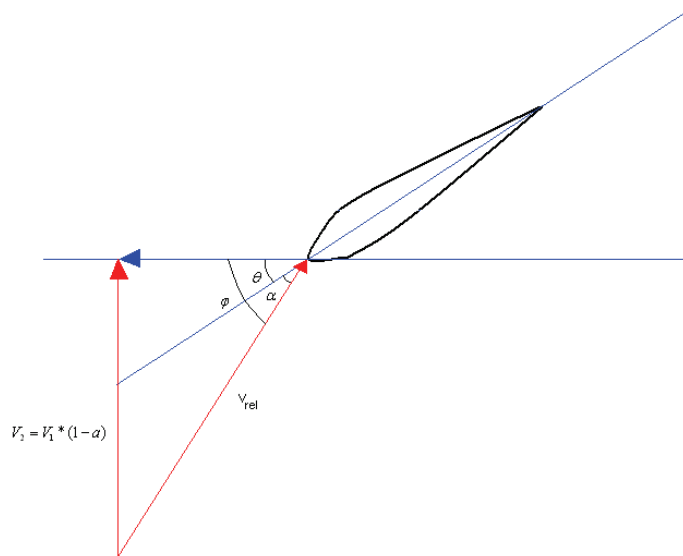
Figure 4.4.2 – Trigonometrical relations for flow angles.

5 New Design

5.1 Introduction

Based on the calculations in chapter 4, the design of a suitable airfoil can begin. The airfoil will be designed for a Reynolds number of 1×10^7, and the main focus will be on getting high lift-to-drag ratios and gentle stall characteristics.

The design process will be done with the aid of Xfoil and Fluent. Xfoil is a code written by MIT professor Mark Drela, and is freely available from the homepage of MIT (Massachusetts Institute of Technology). It is a two-dimensional panel code with coupled boundary layer codes for airfoil analysis. It incorporates inverse design theory, allowing an airfoil to be constructed from a given pressure distribution. This function is the basis for the work done in this chapter. By manipulating pressure distributions in Xfoil, and from that having new airfoils created and tested, it was possible to rapidly test and modify a large number of airfoils systematically.
Fluent is a commercial CFD software, which works by solving the Navier-Stokes equations over carefully gridded models. This is several orders of magnitude more time consuming and difficult compared to Xfoil. Therefore, Xfoil will be used as the primary tool for all testing and design, while Fluent will be used more modestly to confirm Xfoil predictions, and visualize flow where needed.

Stratford theory yields a profile where the entire backside of the airfoil is on the verge of separation. This is the reason for the very dramatic stall, as such a large portion of the profile is balancing close to the critical limit, causing the flow along the entire backside to separate almost at the same time. It will therefore be necessary to move the design somewhat away from a pure Stratford distribution, and make the pressure recovery slightly less dramatic. This is not as easy as it sounds. If one detail is changed, it affects the entire flow field, leaving any previous calculations for other parts of the airfoil outdated. Everything is connected, making it a very difficult iterative process, especially in the stall region where separated flow occurs. Separation will change the flow field around the entire wing, and continue to change with the magnitude of the separated area. Luckily, Xfoil makes it possible to modify pressure distributions, and then test their performance over several degrees very quickly, and is therefore an effective tool in optimising airfoil design.

Running CFD is difficult, and requires a lot of time and computer power. But it is very useful as it visualizes the flow, and gives very informative results. Running CFD with any sort of accuracy requires a lot of skills, and an in depth understanding of the various grids and simulation models available, and even so, programs such as fluent are notorious for giving too much drag [18]. It was therefore clear from the start that with the limited time, computer power and skills at hand, and the big number of airfoils to be tested, it was not realistic to produce CFD results with any numerical accuracy to be trustworthy. However, it is possible to set up reasonable grids and models, and thereby being able to use CFD as a visualisation tool, to better understand what is happening to the flow around the airfoil, as a general interpretation of the flow field will be presented.

Throughout this rapport, it will therefore be used numerical data only from Xfoil (unless mentioned otherwise), while images from CFD will be used to aid the understanding of the Xfoil results. While CFD is famous for giving too much boundary layer growth, drag and early separation, Xfoil probably gives too ideal results [18]. It is therefore important to analyse all results critically with this in mind, but the airfoils will be rated against each other with the same test methods, and should therefore still give good results for how good a particular airfoil is on a relative scale.

The design procedure for creating these airfoils was to modify and test the airfoils in Xfoil until a design was reached which appeared to be an improvement, then run a CFD simulation of this airfoil to visualize the flow. This would often give good indication of any potential problems, and where there was room for improvements. It was especially useful to see where and how the flow separated. The airfoil was then taken back into Xfoil and redesigned based on the new findings. This way, the design would loop between Xfoil and fluent, until a final design was reached. The airfoils presented in this rapport were all through this process many times, and in some cases took weeks to complete.

The Xfoil simulations were run with the viscous model set to Re = 1e7, and m = 0.19 (~62 m/s). In addition, it is important to be aware of the parameter Ncrit (critical amplification factor). This parameter says something about how easily any irregularities, such as roughness on surfaces, help induce turbulence. If the critical amplification factor is low, it means that irregularities will more easily induce turbulence. This factor is initially left at its default value, 9. All results presented here will be with this setting unless specified otherwise. However, all simulations are also run a second time with Nrit = 3, in order to have an indication of how sensitive the profile is to roughness, varying turbulence and change in the transition point. Both simulations are present in the appendix, and will be referred to throughout the discussion.

The Fluent simulations were run with models using a chord length of 2 meters, and a wind speed of 80 m/s (Re ~1e7, similar to conditions expected at r ~ 55 meters). It was solved with a K-omega SST model with transitional flows, with turbulence intensity set to 0.07 % and turbulence viscosity ratio set to 10.

The grid was made very dense close to the airfoil in order to model the boundary layers with sufficient accuracy, with a starting cell height of 1e-4. Further away from the airfoil, a standard triangular grid was used.
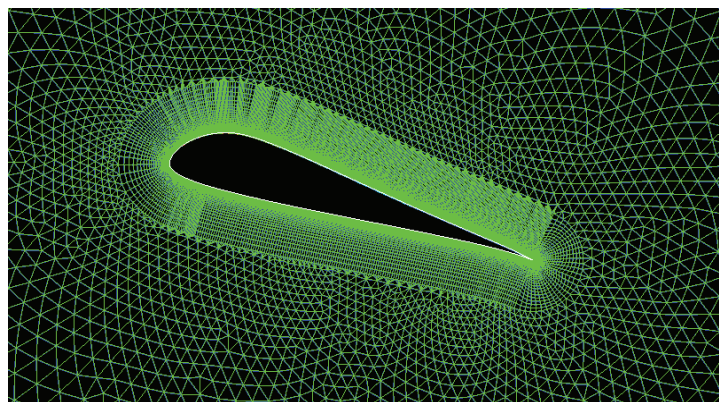
Figure 5.1 – Grid generated in Gambit for use in Fluent

In total, more than 100 modified profiles were made and tested. The most interesting of which are presented in this chapter. Each airfoil will be shown with a table that gives information about size and performance, and how much those factors differ from the HOG profile.
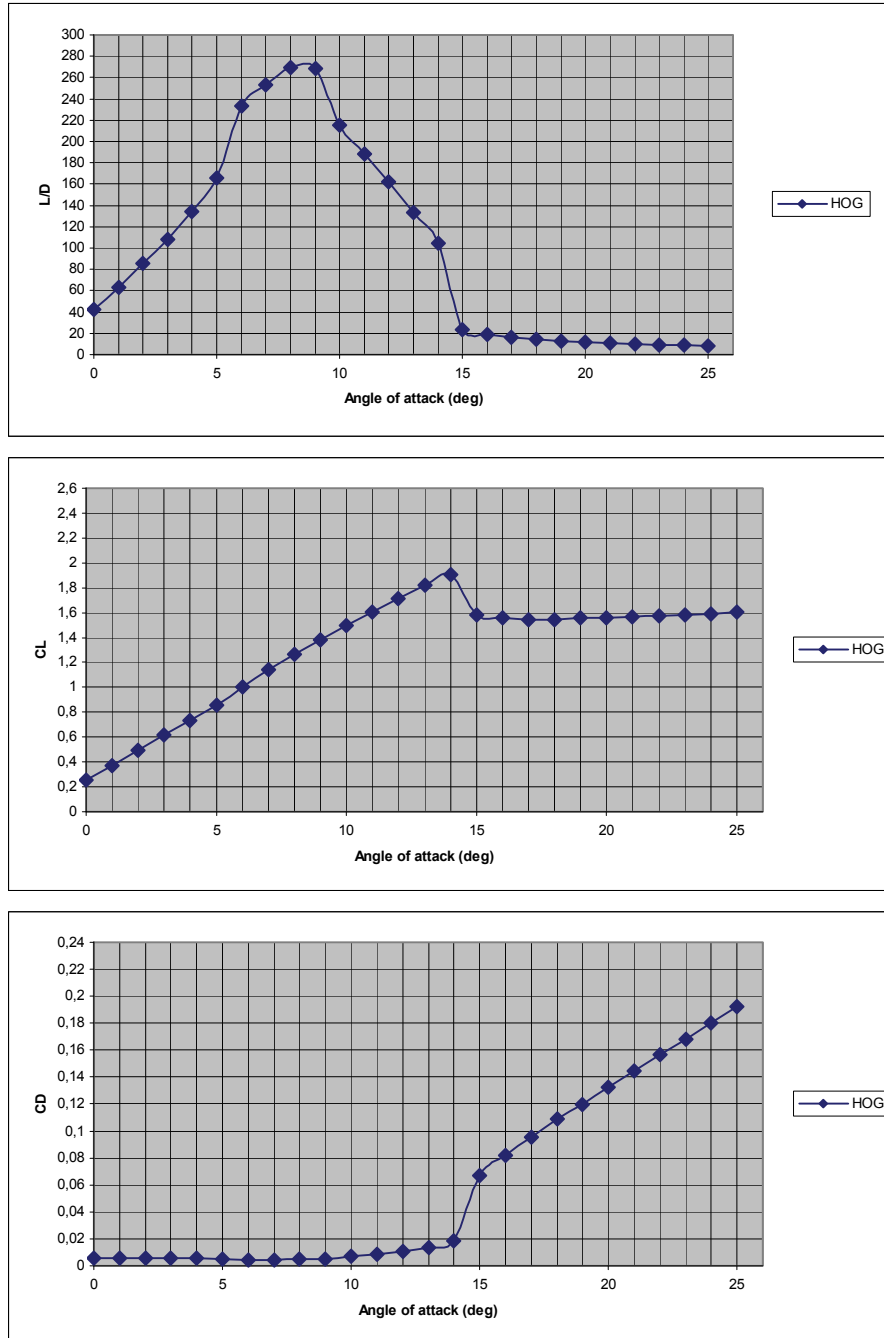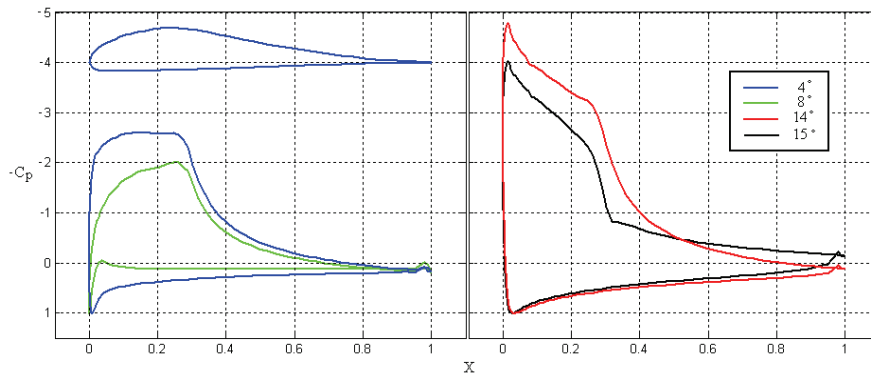
## *5.2 HOG-profile*

Figure 5.2.1 – HOG performance characteristics

The HOG profile is the high-lift airfoil developed at the institute, and is the basis for the work in this rapport. The profile delivers an extremely high lift-to-drag ratio over a few degrees (angles of attack), with the maximum point at 8° with L/D ~ 270. It then stalls dramatically between 14° and 15°.

Figure 5.2.2 – HOG pressure distributions

Figure 5.2.2 shows exactly what is expected. For the optimum angle of attack, 8º, there is a quick pressure rise, a long flat rooftop, before a Stratford pressure recovery. For lower angles of attack, 4º, the pressure rise is slower and the rooftop is tilted positively. For higher angles of attack, 14º, there is a sharp pressure increase before a negatively tilted rooftop.

The vast differences between the pressure distributions at 14º and 15º are clearly visible. At 14º, the pressure exactly manages to recover to the operational Cp_{te} without any sign of separation. At 15º, we see the sign of a large separation starting at X ~ 0.3, clearly visualized by the sharp corner on the pressure distribution. Upstream of the separation, the pressure over the head has fallen significantly, and downstream, the pressure is not sufficiently recovered, causing a higher Cp_{te}. This sudden and dramatic change in the flow is what causes the jump in the lift and drag curves. This process, the transition to separated flow, needs to be smoothed out and slowed down, in order to get a functional wing for the purpose of wind turbines.
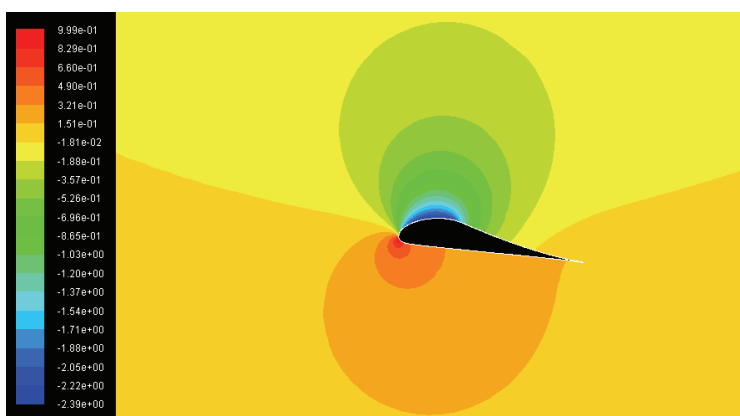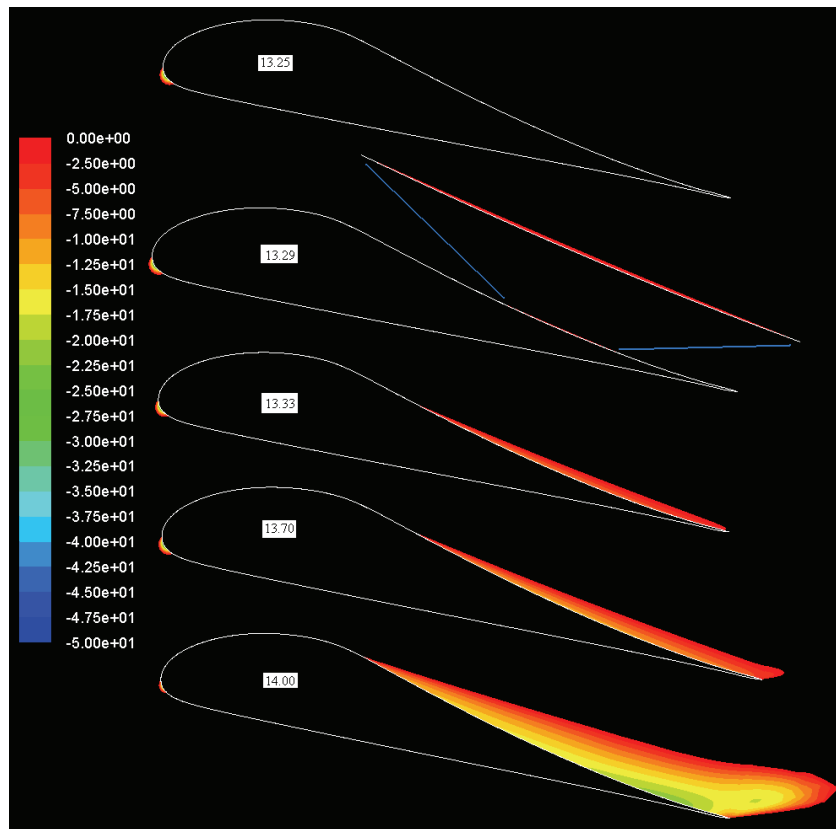

Figure 5.2.3 – CFD simulation showing Cp at α = 8º

In figure 5.2.1, the data is shown at an interval of one degree. However, a detailed run in Xfoil reviled that the vast majority of the change occurs between 14.0º and 14.1º. This suggests that the airfoil goes from no separation to full large scale separation in less than one tenth of a degree. A very dramatic stall indeed.

It was therefore very interesting to see if Fluent would confirm this, and if so, get a visualization of the flow when this occurs. Figure 5.2.4 shows CFD results for separated (reversed) flow for a selection of angles around the point of separation.

The results appear to confirm the Xfoil predictions. The first figure (13.25º) shows no sign of separation. The third figure, only 0.08º later, shows separated flow over more than half the wing. Indeed, also fluent predicts a dramatic change in under one tenth of a degree. The difference is that fluent calculates the occurrence of the separation about 0.7º ~0.8º degrees before Xfoil, but that is a very close match considering the difference in method.


Figure 5.2.4 – CFD simulation showing reversed flow (negative x-velocity) for angles around the point of separation.

The second figure above (13.29º) shows the separation starting as a bubble in the middle of the pressure recovery. It then grows rapidly towards both sides and bursts. This is a very bad form of stall, as we know from chapter 3.2.4.

The problem appears to be that the Stratford distribution has resulted in a wing where the pressure recovery is right below the value causing separation over the whole backside of the wing. This means that when gradually increasing the amount of pressure needed to be

recovered, the entire backside of the wing will separate almost at the same time, causing the flow to go from no separation to full separation in less than 0.08 degrees.
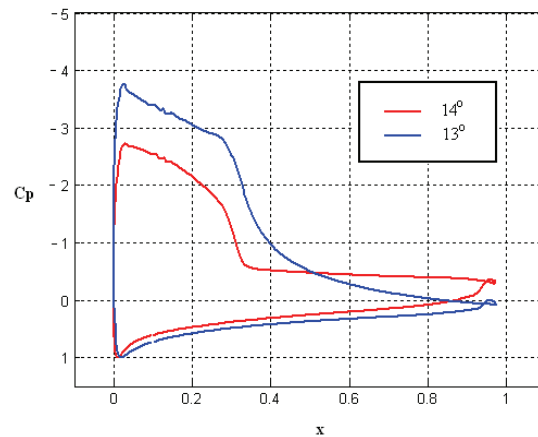
Figure 5.2.5 – CFD calculations of the pressure distributions before and after stall. It shows a similar pattern in change to Xfoil, illustrated in figure 5.2.2. The numerical values are not comparable, as the stall occurs earlier in Fluent.

It becomes clear that a wing using a pure Stratford recovery will not be reconcilable with a smooth stall. The basis for the Stratford pressure distribution is that the flow will be on the verge of separation over the whole backside of the wing. As theory predicts, and both Xfoil and Fluent confirms, this will cause a large portion of the wing to overstep its critical limit at the same time, resulting in a sudden destruction of the established flow field.

The plan is therefore to develop new airfoils which keep as much of the high lift capacity of the HOG profile as possible, but have a modified pressure recovery that lets the wing gradually overstep its critical limit causing separation. It is desirable to have a separations starting from the back of the wing, and slowly move forward. This is the least dramatic form of stall, and should be attainable by designing the pressure recovery so that the very back tip of the wing crosses its critical limit first. Then having the part of the pressure recovery overstepping its critical limit slowly move forward with increasing angles of attack.

In addition, it can be seen from appendix 10.1 that the HOG is extremely sensitive to roughness. The change to Ncrit = 3 causes the maximum L/D to drop 33% (L/D~182), and both this maximum point and the stall occurs 2º degrees earlier. This is dramatic, but expected, as it was designed to have, and has, a transition point at X_0, and will therefore be very sensitive to changes. This is another reason why this airfoil would not be suitable for use in a wind turbine. A reduction in performance is bad, but having the points of stall and maximum L/D shifting inwards with varying roughness is dramatic. The twist of the blade and system controlling pitch will be carefully designed to secure efficient operation and avoiding stall. Having these points move around with varying roughness and air turbulence can cause the wing to operate inefficiently and accidentally stalling. This is, of course, unacceptable.

5.3 NACA 4412

To keep things in perspective, it is useful to compare the high-lift profiles to a standard airfoil. It is chosen to use the NACA 4412 profile for this purpose, as it is a much used airfoil with soft stall characteristics.
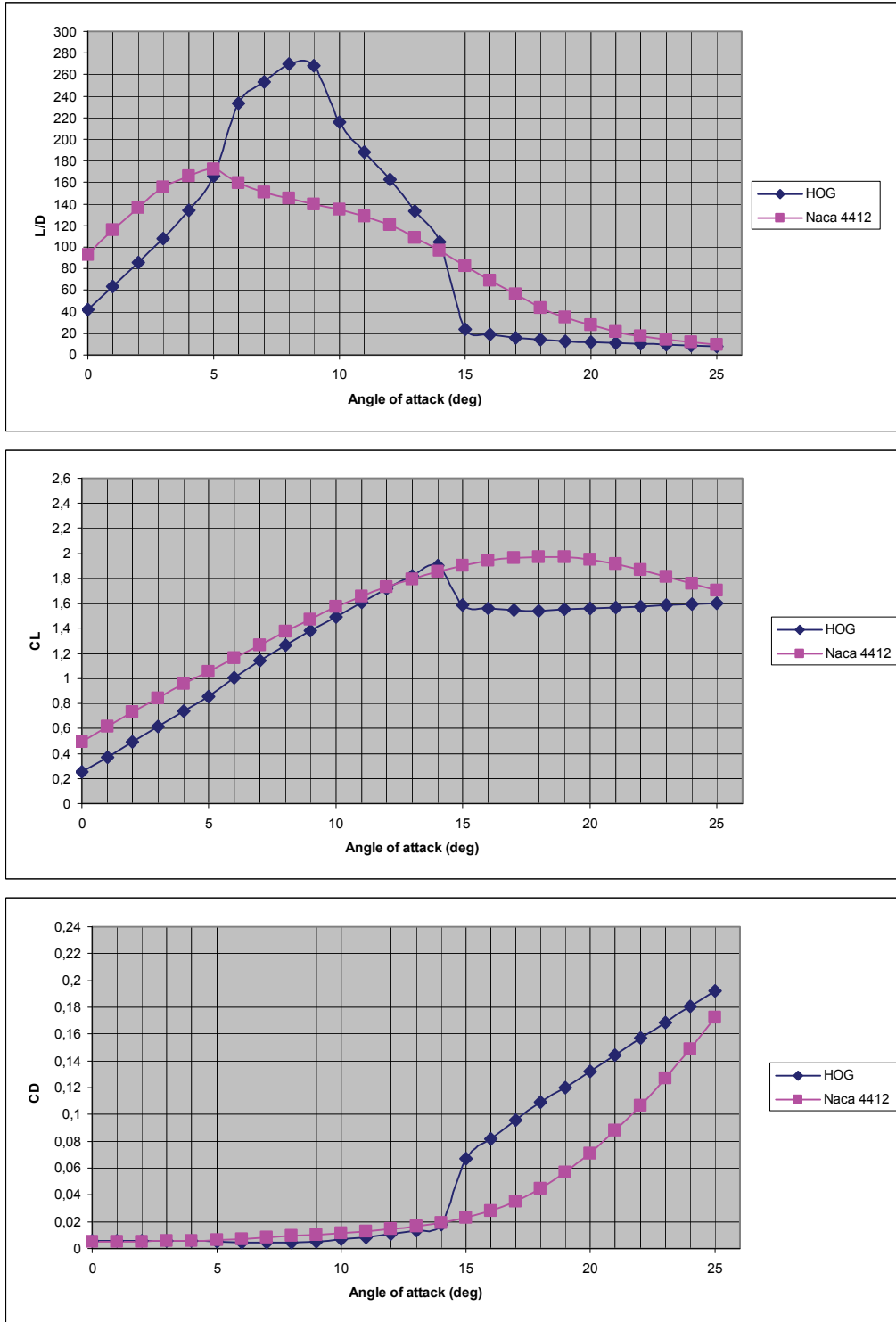
Figure 5.3.1 – NACA 4412 performance characteristics.

These two profiles have a very different performance. The Naca 4412 profile has a much more gradual and soft stall, free of any sudden changes. Its performance, however, is mediocre. It peaks at a L/D-ratio of ~172, compared to ~270 for the HOG profile. It does not have a concave pressure recovery shape, and, as expected, has high drag.
The pressure distributions of the Naca 4412 can be seen to rise suddenly, and then have an almost constant recovery from nose to tail. This will cause the two airfoils to have different boundary layer growth, making the maximum dp/dx at any given point different.
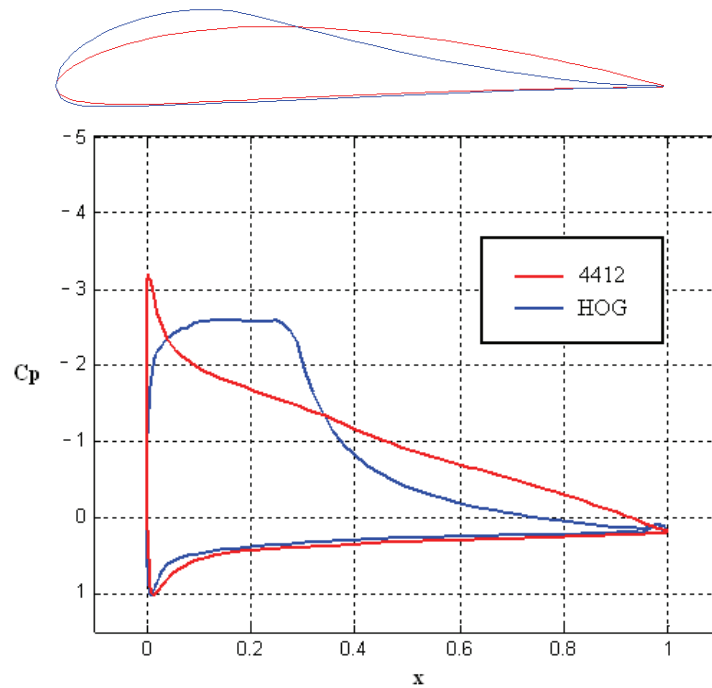
Figure 5.3.2 – illustration of shape and pressure distribution at α = 8º.

As the Stratford distribution clearly illustrates, an airfoil can tolerate less and less dp/dx as we move further back on the airfoil. An almost constant pressure recovery, such as the for the NACA 4412 , should therefore separate at the back first, and then the separation should move slowly forward with increasing angle of attack, since the critical limit will be overstepped gradually. This would explain the very gentle stall characteristics of this airfoil.

The performance of the Naca 4412 is comparable to most other airfoils used in wind turbines. For the purpose of this report, it is therefore used as a reference to find the characteristics and performance we are looking for. It can therefore be said that in order to be an improvement of significance, the L/D-ratio should be way higher than 170. At the same time, the L/D~270 performed by the HOG will probably be unattainable once moving away from a pure Stratford distribution. We are therefore looking for something in between, hopefully with a L/D-ratio in the 200+ region.

	L/D (n=9)	L/D (n=3)	Thickness (%)	Area (%)
Naca 4412	172 (5º)	138 (8º)	12.00	8.22
Modification	-36.3 %	-24.2 %	-22.8 %	+1.3 %

Table 5.3 – Naca 4412 compared to HOG

The first row in Table 5.3 shows performance and geometrical data for the NACA 4412, while the second row shows how much they differ from the HOG profile. It can be seen to have lower maximum thickness, but the total area is slightly increased. Both thickness and area are given as a percentage referenced to the chord length, meaning that a 1 meter long version of this wing would be 0.12 m thick and have a cross section area of 0.0822 m^2. The two first values are maximum L/D-ratio with Ncrit = 9 and Ncrit = 3 respectively. The number in brackets is the angle of attack at which this maximum point occurs.

Form looking in appendix 10.2, it is clear that this airfoil is a lot less sensitive to roughness than the HOG profile. The maximum point does move, but that is not very critical in this case as the L/D curve is very flat around this point, meaning that it will work well optimized for any angle in the area. However, the most important point is that the stall characteristic does not change at all. In fact, for α > 8, the performance is virtually identical for both Ncrit values. The reason can be seen in figure 5.3.3.
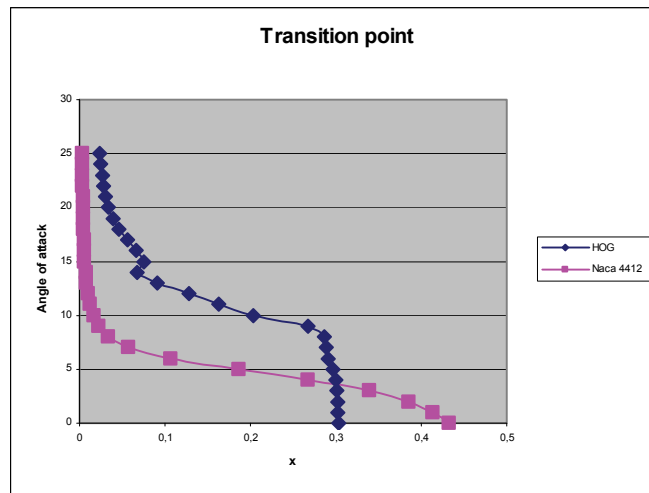
Figure 5.3.3 – Transition points Shown for Ncrit = 9.

The transition points for the Naca 4412 can be seen to mover forward on the airfoil very quickly with increasing angle of attack. From angles of attack α = 8°, the transition point is so close to the leading edge that it can not move much more. The flow will turn turbulent at the leading edge for α > 8°, regardless of roughness, thereby causing the patterns of performance to be almost identical for all levels of roughness at high angles of attack. Since the HOG does not have its transition point at the leading edge when entering the stall region, the stall characteristics are heavily influenced by roughness.
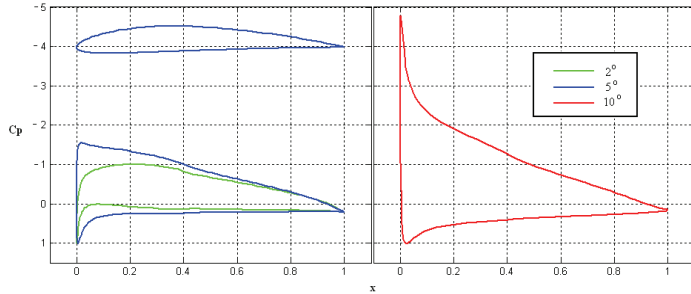
Figure 5.3.4 – NACA 4412 pressure distributions

From figure 5.3.4, it can be seen that for the design angle of attack, 5°, the pressure distribution has a quick rise and an almost constant pressure recovery from there. For higher angles of attack, there appears a pressure spike near the nose.
The reason the transition point moves to the leading edge so quickly for this airfoil, is that an adverse pressure gradient is applied almost immediately. This promotes the transition to turbulent flow. For higher angles of attack, the pressure spike causes a large adverse pressure gradient to appear near the front of the airfoil. This helps turn the flow turbulent very early, and it can be seen that the occurrence of the pressure spike coincides with the transition point reaching the leading edge. This way, pressure spikes are used to promote early transition in order to get stable performance [14].
The HOG's transition points only start moving forward for α > 8°. This is because up to that point, the rooftop is first tilted positively and later becomes flat, meaning that it will have a negative pressure gradient. For angles α > 8°, the rooftop is tilted negatively, meaning an adverse pressure gradient is applied almost immediately, causing the transition point to suddenly start moving forward.
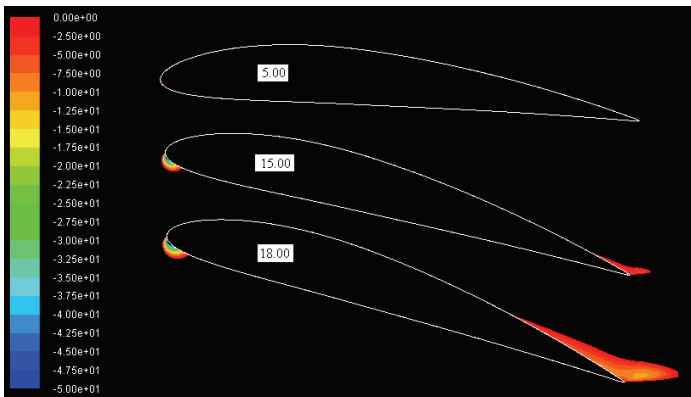
**Figure 5.3.3 –** CFD simulation showing reversed flow for the NACA 4412.

Fluent confirms the very soft stall predicted by Xfoil. The first sign of separation occurs at 15°, at the very back of the airfoil. The separation then moves very slowly forward. In the last picture in figure 5.3.3, it can be seen that an increase in angle of attack of 3° has only resulted in a modest increase in separation, compared to the very dramatic separation seen in the HOG profile in less than 0.1°.
It is clear that a constant pressure recovery allows the flow to separate at the back first, and move slowly forward.

5.4 A-profiles

5.4.1 A1

The first attempts at creating a new profile will start with the pressure distribution of the HOG profile, and then systematically smooth out its dramatic pressure recovery, and see how this affects the performance. Starting with the sudden drop at X~0.3, it is attempted to soften this to a more gradual transition in both directions, first for approximately X~ +/- 0.1, while keeping the rest constant. After a long optimisation process, the A1 profile was crated, which appears to be a very good design with the requested modification.
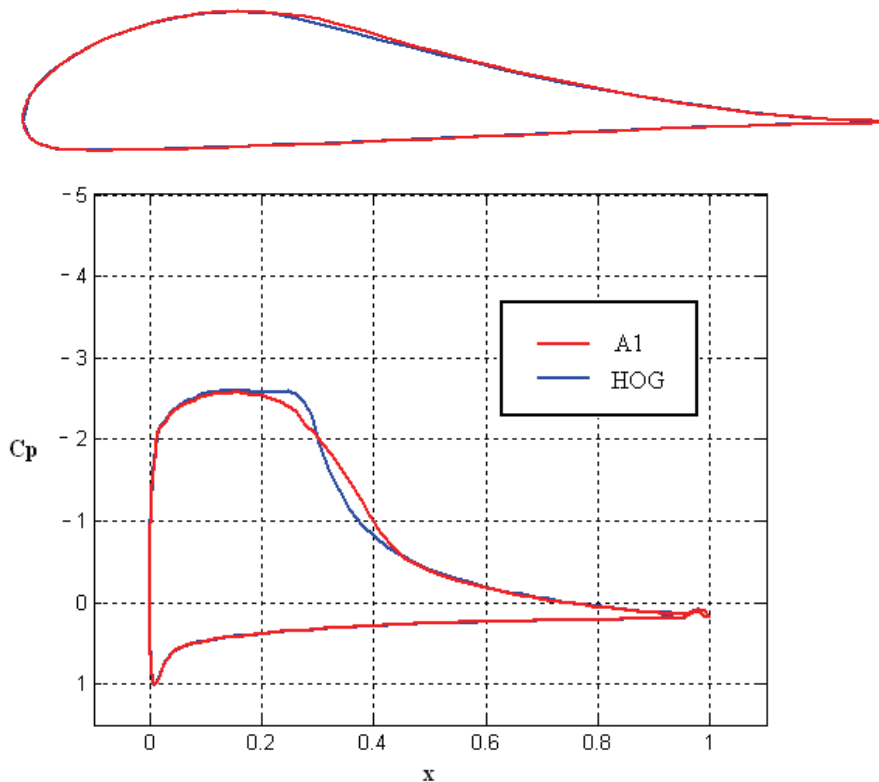
Figure 5.4.1 – illustration of shape and pressure distribution at $\alpha = 8°$.

The difference in the pressure distribution can be seen to result in a slight thickening of the geometry right behind the head of the profile. Other than that, the geometry is almost identical. The pressure distributions are very similar, except for the more gradual shape between x = [0.19, 0.43], causing about 25 % of the top side distribution to be modified.

As seen from figure 5.4.2, the stall has been smoothed out, while performance is only slightly reduced. It therefore appears to be a step in the right direction. However, a major reason for the softer stall is that it stalls 1° before the HOG, thereby having a smaller "drop" down to post stall conditions. That being said, the A1's post stall performance is slightly better than for the HOG.
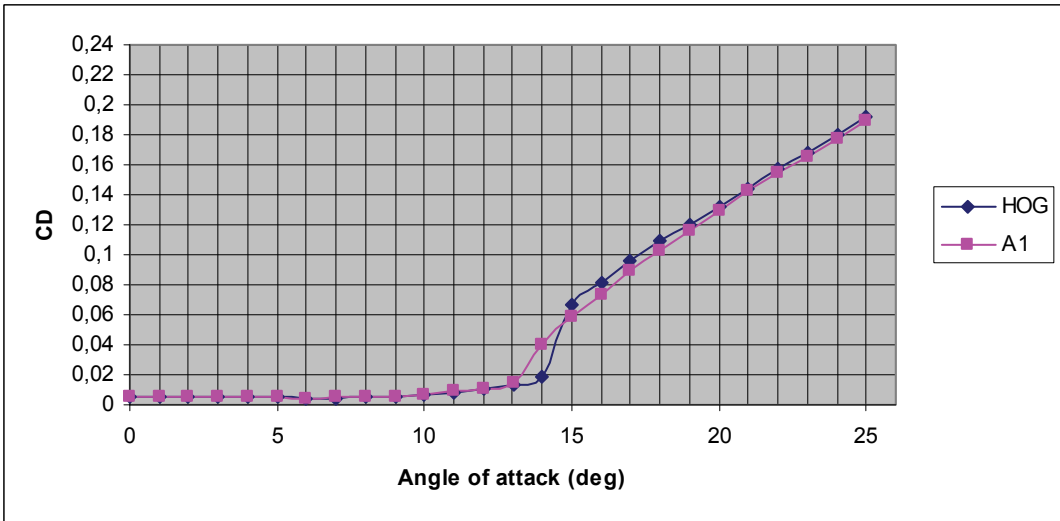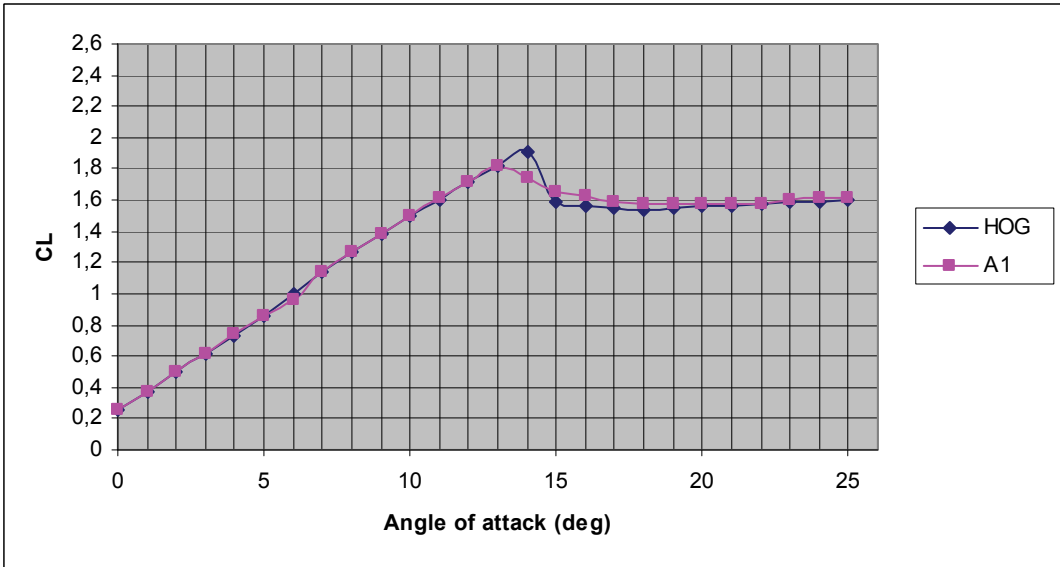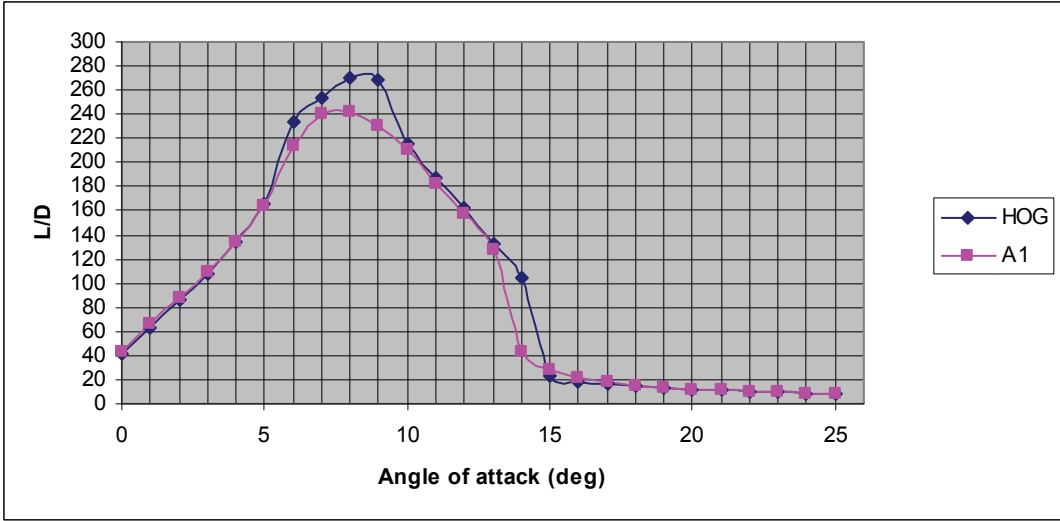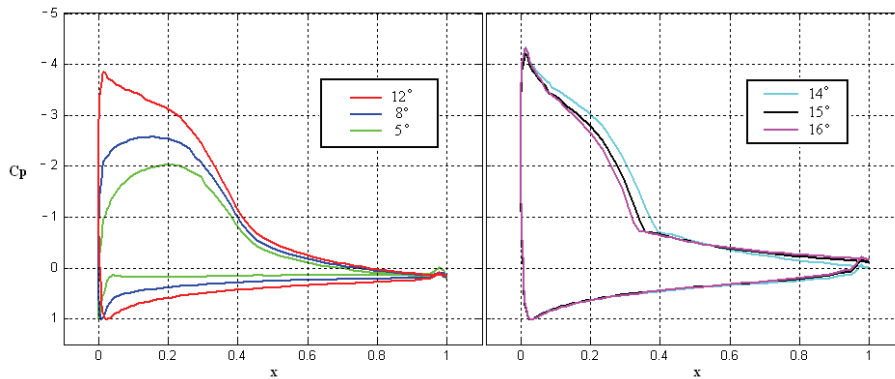
Figure 5.4.2 – A1 performance characteristics

Figure 5.4.3 – A1 pressure distributions

Separation now occurs 1° earlier, but only creeps up to X~0.4, compared to X~0.3 for the HOG. It then crawls slowly forward from there, resulting in the slightly softer stall.

	L/D (n=9)	L/D (n=3)	Thickness	Area
A1	243 (8°)	176 (8°)	15.62%	8.27%
Modification	-10.0 %	-3.6 %	-0.5 %	+2.0 %

Table 5.4.1 – A1 compared to HOG

In total, this new airfoil is not sufficient improvement. It stalls a bit slower, but earlier. The performance is still very good, with only the few peak degrees being slightly worse than the HOG. It is therefore reason to develop this modification further, to see if the stall can be made smoother before performance drops significantly. The next step is therefore to create a profile where the pressure distribution has an even larger modified interval.

5.4.2 A2

In this profile, the pressure distribution diverges from the HOG at the same point as for the A1, but does not reconnect until X ~ 0.7, causing the modified area to stretch over more than 50 % of the wing. This results in an airfoil where the head is slightly lowered and the back of the wing is lifted out, causing a less concave shape. This appears to give a very good performance and a much smoother stall. From figure 5.4.4, it can be seen that the performance is only slightly reduced for the few degrees of maximum performance. For higher angles of attack, it actually performs better. The peak area is flatter and the stall is much softer. This profile appears to have a lot of the qualities we are looking for.
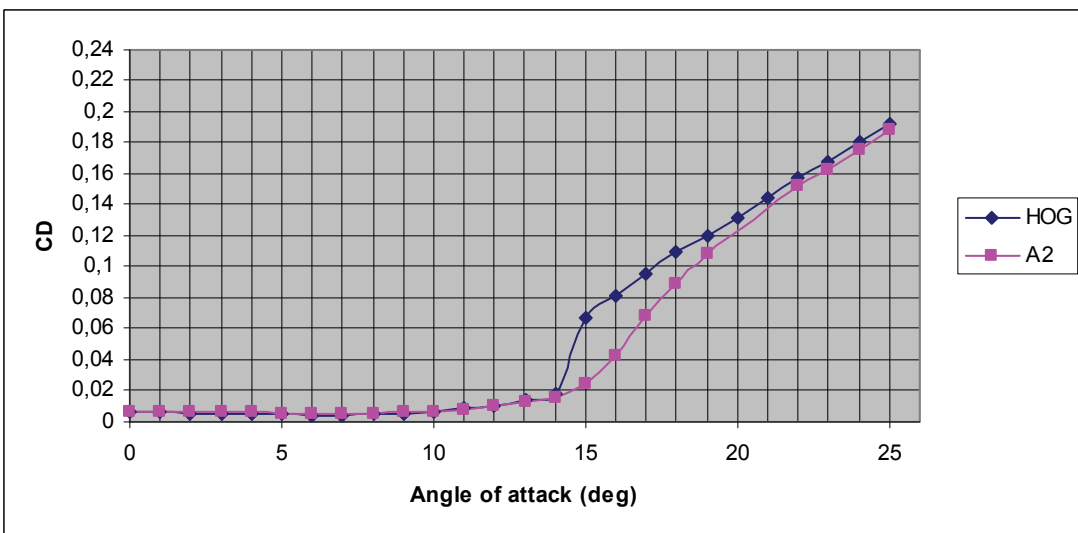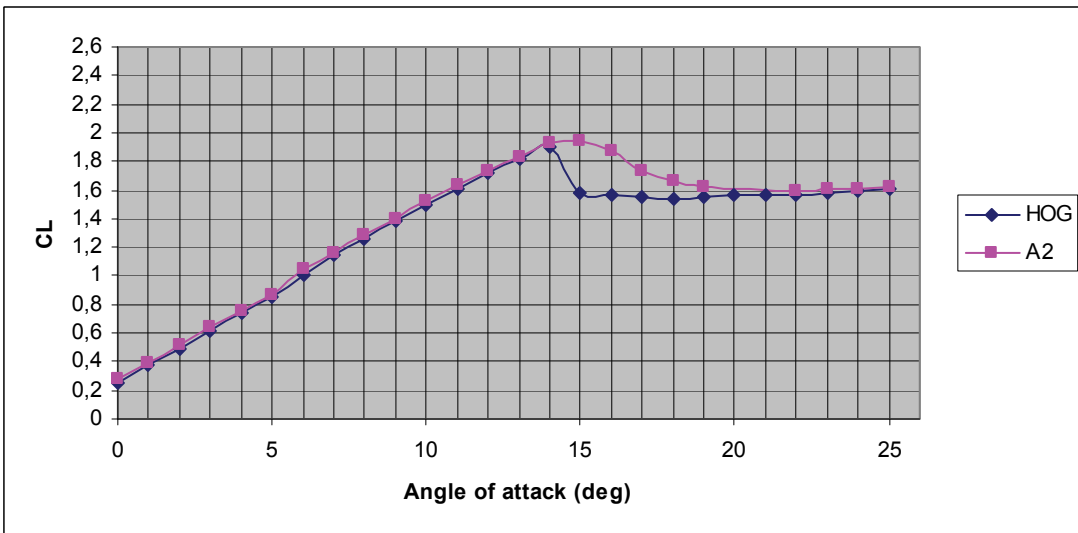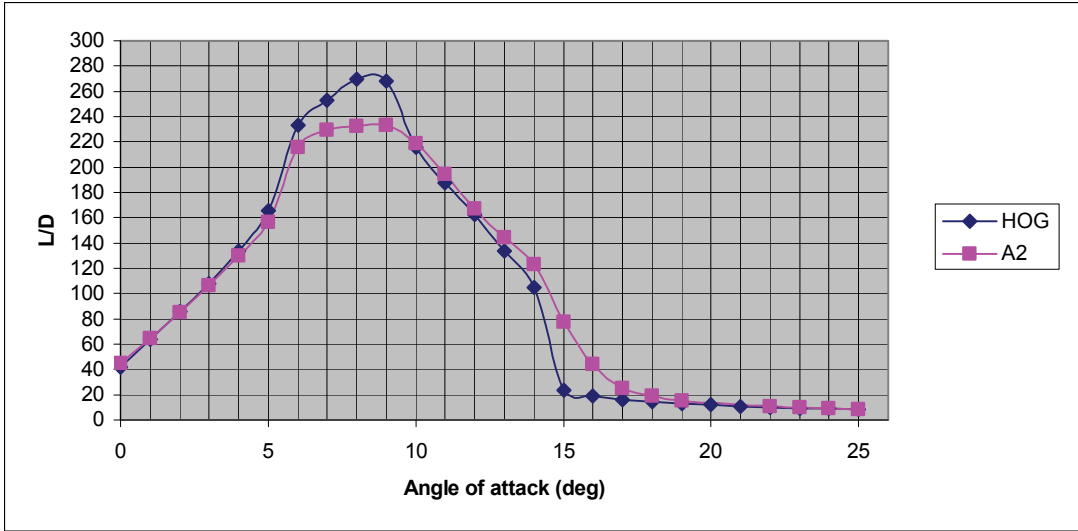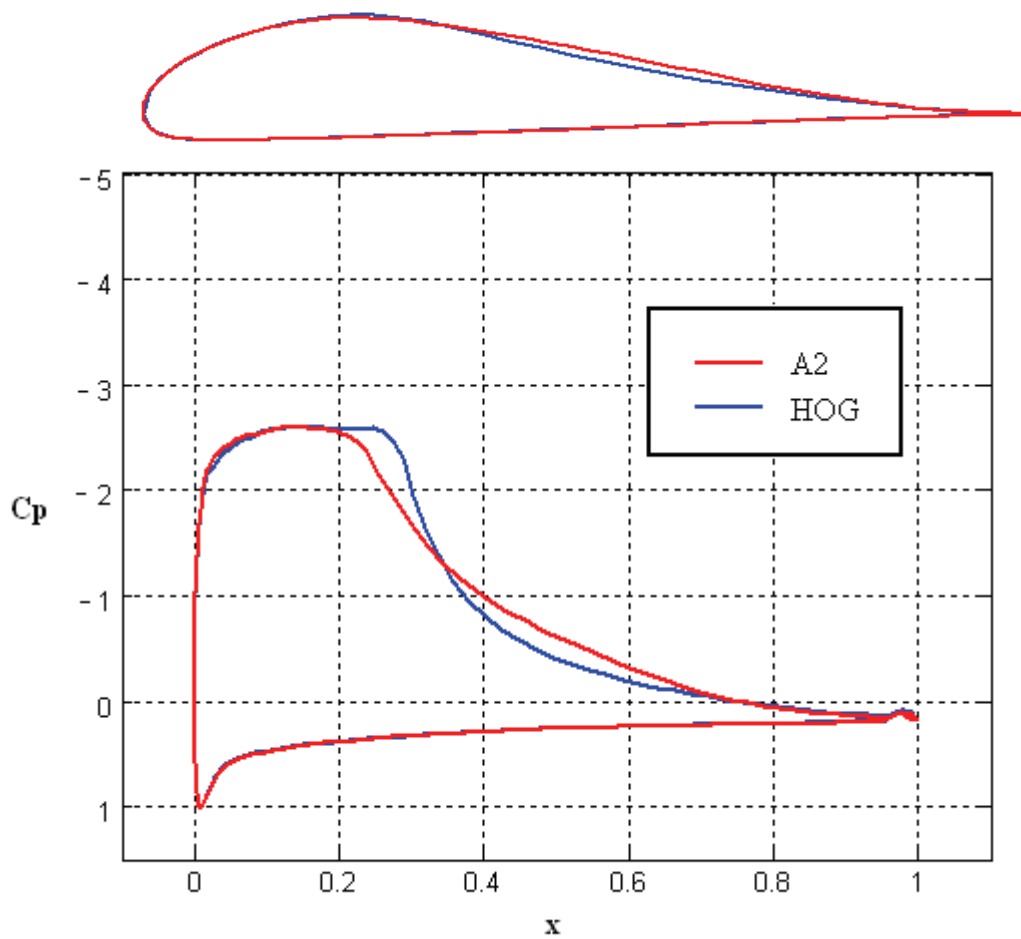
Figure 5.4.4 – A2 performance characteristics

Figure 5.4.5 – illustration of shape and pressure distribution at α = 8º.

	L/D (n=9)	L/D (n=3)	Thickness (%)	Area (%)
A2	233 (9º)	180 (7º)	15.40	8.50
Modification	-13.7 %	- 1.1 %	-1.4 %	+4.6 %

Table 5.4.2 – A2 compared to HOG

In addition to the good performance and smooth stall, the A2 is also less sensitive to roughness. While being a bit less efficient than the HOG at Ncrit = 9, their maximum performance is almost identical at Ncrit = 3. The stall does still shift inwards, but this is also reduced, and the two curves follow each other closely with the same general shape (appendix 10.4). This profile is a huge step in the right direction.
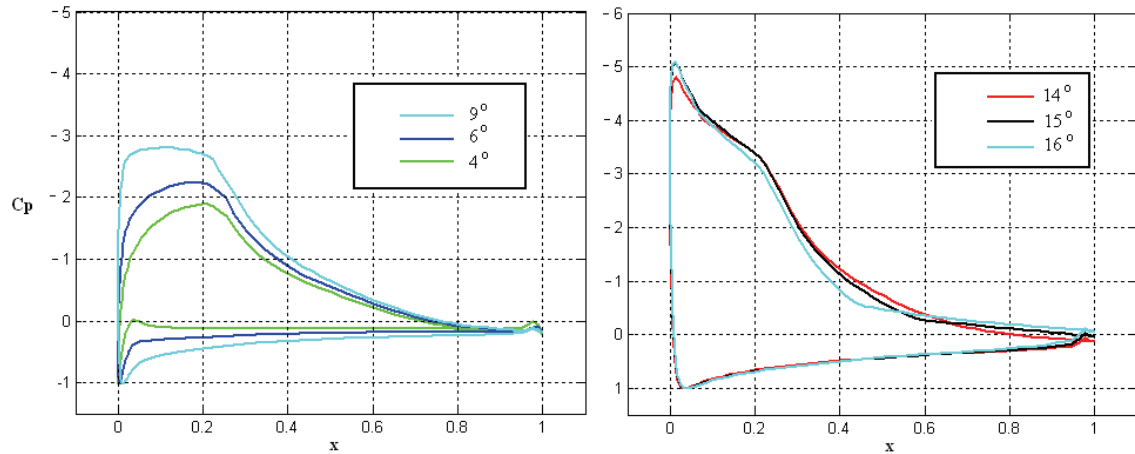
Figure 5.4.6 – A2 pressure distributions

The A2 has a maximum performance for α = 9°, which corresponds well to the flat rooftop seen in figure 5.4.6. To the right, it can be seen that separation creeps upwards very gradually from 14° to 16°, thereby giving the relatively smooth stall characteristics. Fluent confirms this, as it shows a gradual separation around the same angles of attack.
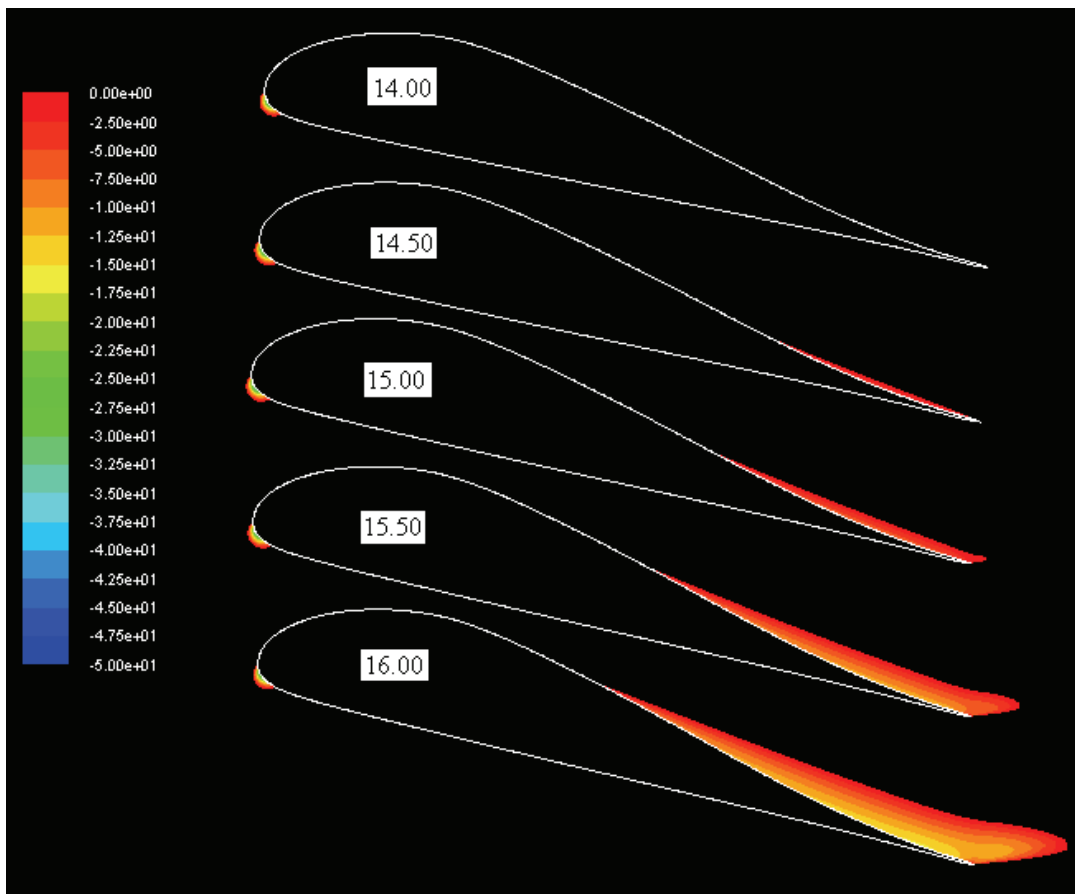

Figure 5.4.7 – CFD simulation showing reversed flow for A2 as separation occurs

5.4.3 A3

It is now interesting to use an even larger area of modified pressure distribution, to see if the trends continue. This work resulted in the A3 profile, which has a smoothed out distribution for x~ [0.1, 0.8], or roughly 70 % of the total top side distribution. This resulted in a profile where the backside of the wing has been made significantly thicker, reducing the concave shape even more.

	L/D (n=9)	L/D (n=3)	Thickness	Area
A3	232 (7º)	166 (9º)	16.09 %	9.12 %
Modification	- 14.1 %	- 8.8 %	+ 3.4 %	+12.4 %

Table 5.4.3 – A3 compared to HOG
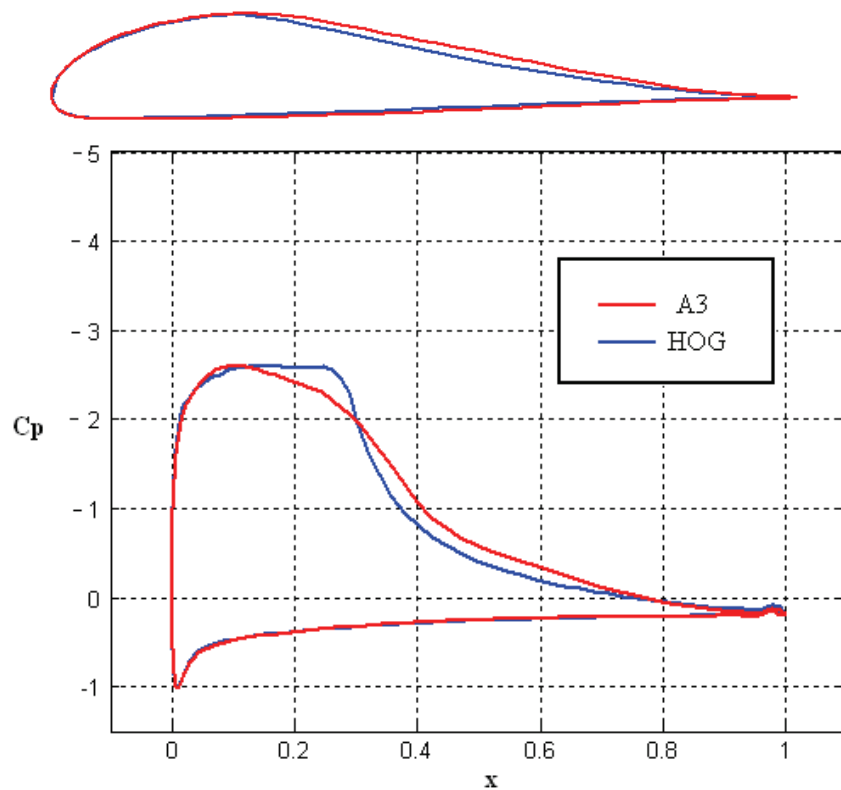
Figure 5.4.8 – illustration of shape and pressure distribution at α = 8º.

As seen in figure 5.4.9, this profile also appears to be very good. It has high performance and acceptable stall. If compared closely to the A2, it can be seen that it has roughly the same performance, and the post stall conditions are slightly better. However, it is thicker and more sensitive to roughness. In appendix 10.5, it can be seen that the stall is changed a bit more, and the maximum L/D point moves upwards. The performance is a bit lower in both cases. This is therefore believed to be a slightly less good profile compared to the A2.
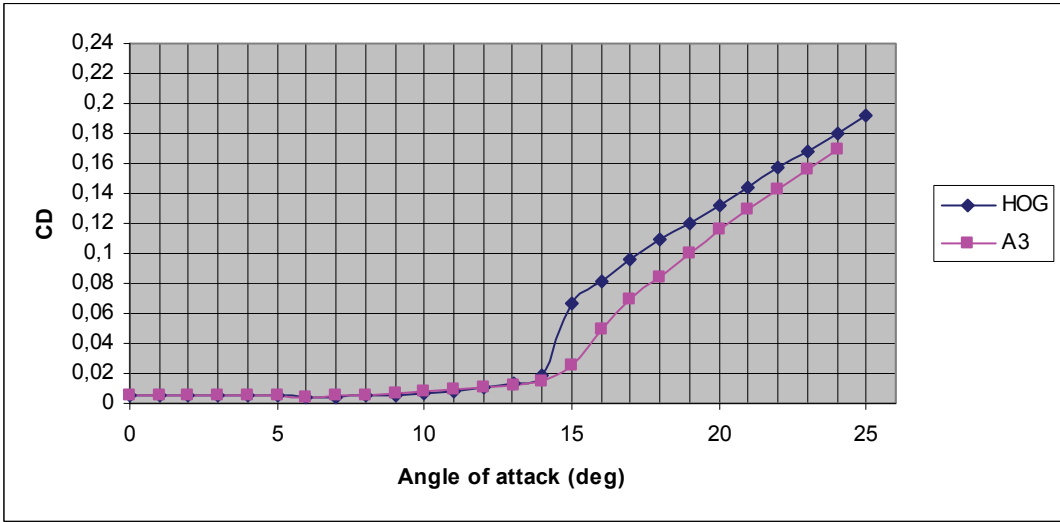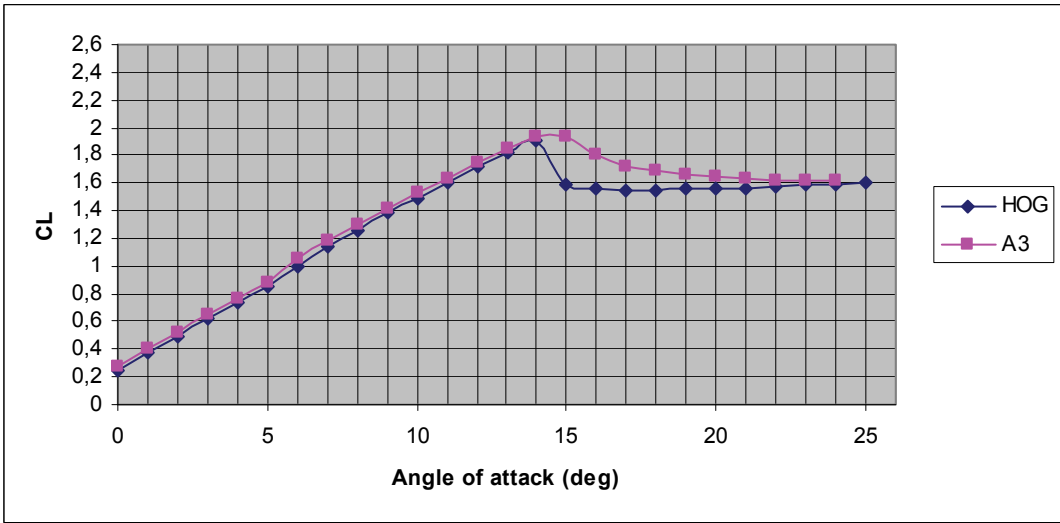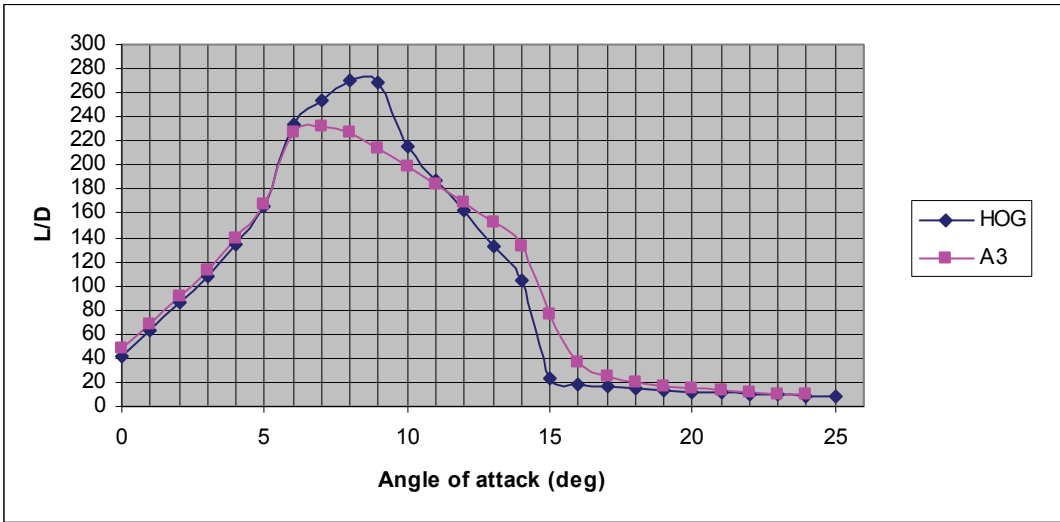
Figure 5.4.9 – A3 performance characteristics

5.5 B-profiles

So far, the only change has been to smooth out the HOG-distribution starting from the middle. This has given good results, but the stall is still not nearly as soft as the NACA 4412. The next step will be more experimental modification, in an attempt to make a hybrid of the HOG and the NACA 4412.

5.5.1 B1

The NACA 4412 has an almost constant pressure recovery. In trying to find a good way to merge the two distributions, the B1 was created. It has a quick pressure rise and a short rounded head (not present in the NACA 4412), but almost immediately starts recovering pressure. The pressure recovery is given a slightly concave shape (like the HOG), to lower drag. This is almost a 50/50 merger of the two distributions, and, remarkably, gives almost the result that was hoped for.
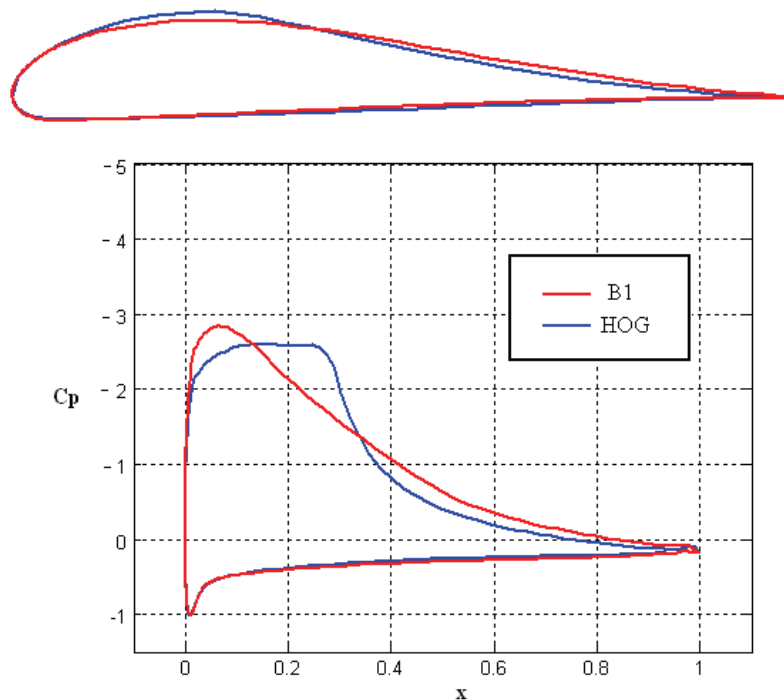
Figure 5.5.1 – illustration of shape and pressure distribution at α = 8º.

The stall has now become very gentle, and should be good enough for use in a wind turbine. The maximum performance, however, is only L/D~194. But to keep things in perspective, the NACA 4412 only reaches L/D~172.It must also be noticed that the profile keeps delivering high performance for a very wide range of angles. It has a performance of L/D >140 for 10º angles of attack. As can be seen in appendix 10.6, It also has low sensitivity roughness. The performance curves keep the same general shape, although the stall is shifted slightly inwards, but not a critical amount. The drop in performance is small, and the profile is also thinner. This is therefore definitely a design that should be paid attention to.
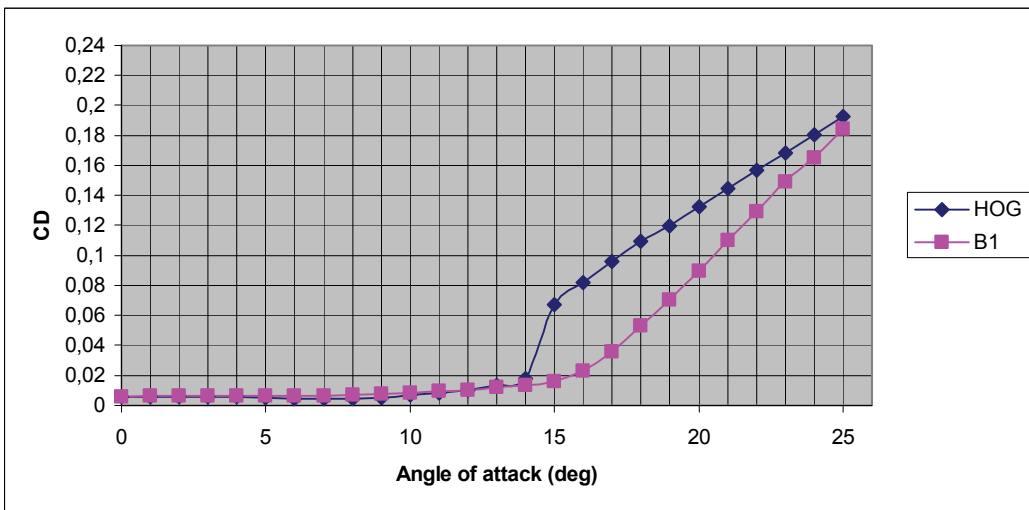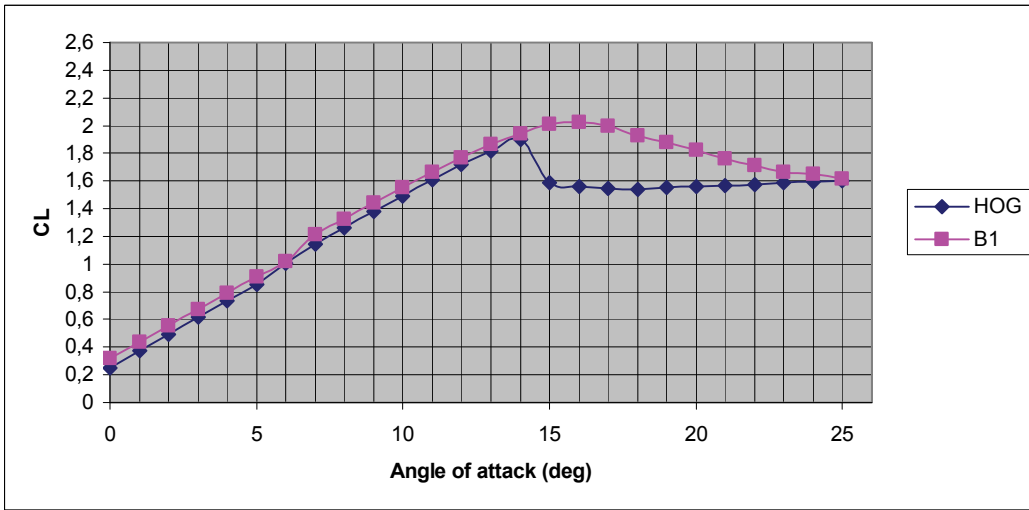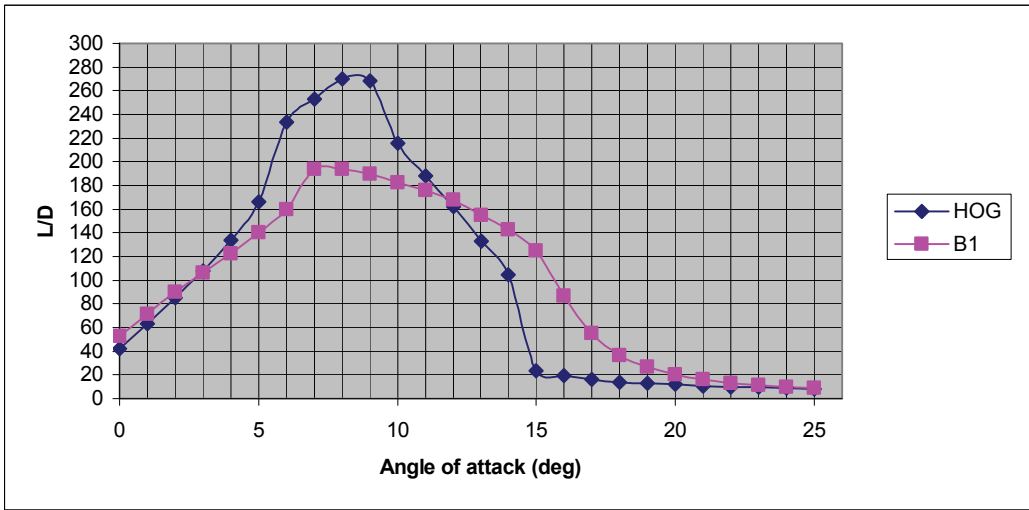
Figure 5.5.2 – B1 performance characteristics

	L/D (n=9)	L/D (n=3)	Thickness	Area
B1	194 (7º)	165 (8º)	14.05 %	8.09 %
Modification	- 28.1 %	- 7.7 %	- 9.7 %	-0.3 %

Table 5.5.1 – B1 compared to HOG

Table 5.5.1 shows that when roughness increases, its performance starts being in the same range as the HOG.
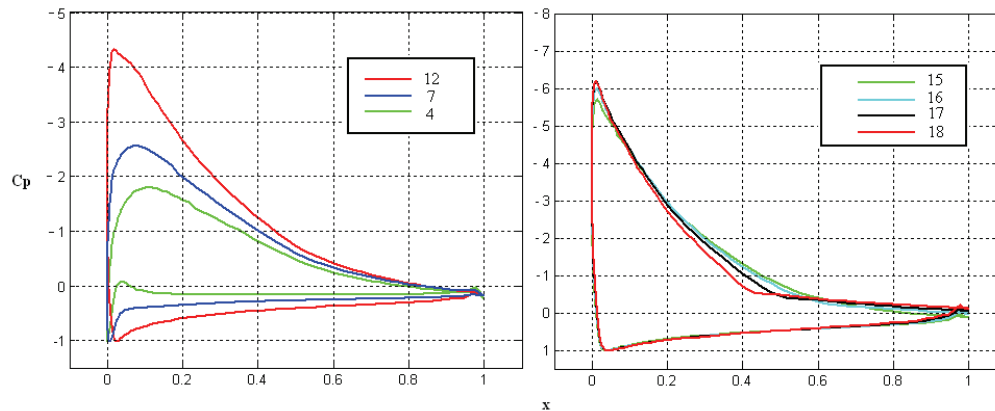
Figure 5.5.3 – B1 pressure distributions

From figure 5.5.3, it can be seen that the airfoil gives good pressure distributions for a wide array of angles. The pressure spike that appeared at the front of the Naca 4412 is gone, which is why it is a bit more sensitive to roughness, as the transition points will move forward later. For the stall region, there are no sudden changes and the separation progresses gradually. Fluent also calculates a gradual progression around the same angles of attack.

Figure 5.5.4 – B1, reversed flow, CFD simulation.

5.5.2 B2

The B2 profile resulted from a different tactic for connecting the qualities of the HOG and the NACA 4412. For the B2, the idea was to keep the classic "head" shape of the HOG distribution, but change the pressure recovery into a convex shape at the end, thereby making the back of the wing stall gradually, like the NACA 4412. In other words, let the front half be identical to the HOG and the aft half identical to the 4412.
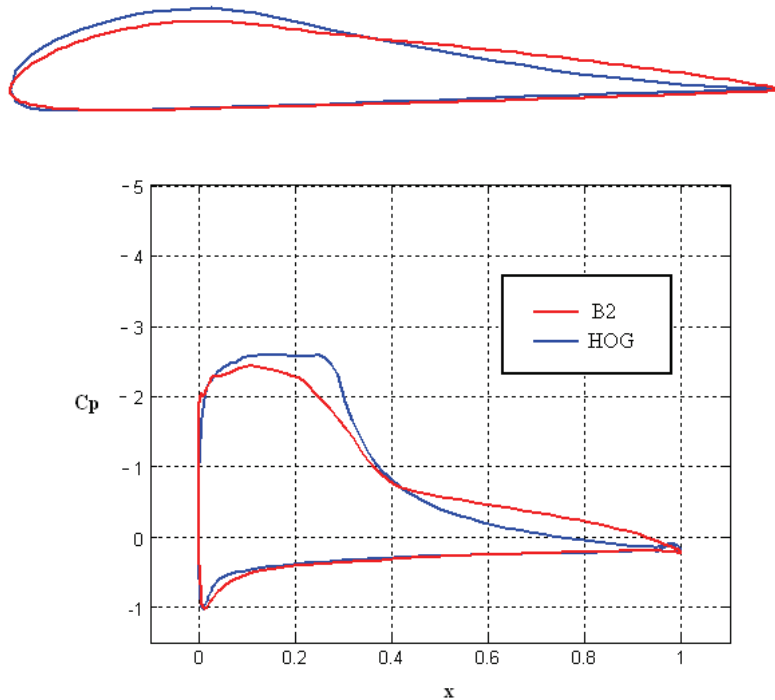
Figure 5.5.6 – illustration of shape and pressure distribution at α = 8º.

This oddly shaped profile, consisting of two convex curvatures, actually performs very well. This method for securing a slow stall from the back appears to work as planned, without reducing performance too much.

	L/D (n=9)	L/D (n=3)	Thickness (%)	Area (%)
B2	220 (7º)	179 (7º)	13.61	8.41
Modification	- 18.5 %	- 1.6 %	- 12.5 %	+ 3.7 %

Table 5.5.2 – B2 compared to HOG

It is a bit thinner than the HOG, and reaches L/D~220. Its best quality is that it has remarkably low sensitivity to roughness (appendix 10.7). The performance is reduced little compared to other profiles, and the maximum point and general shape of the L/D-curve stays the same. It can be seen to perform almost as good as the HOG for Ncrit = 3. The stall does not move or change magnitude at all. These are very good qualities for a profile meant for use in variable conditions.

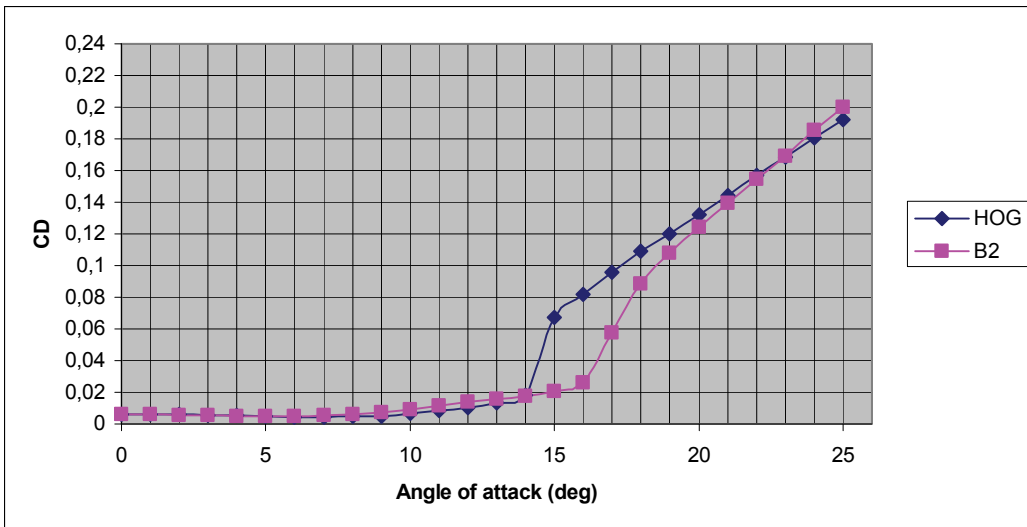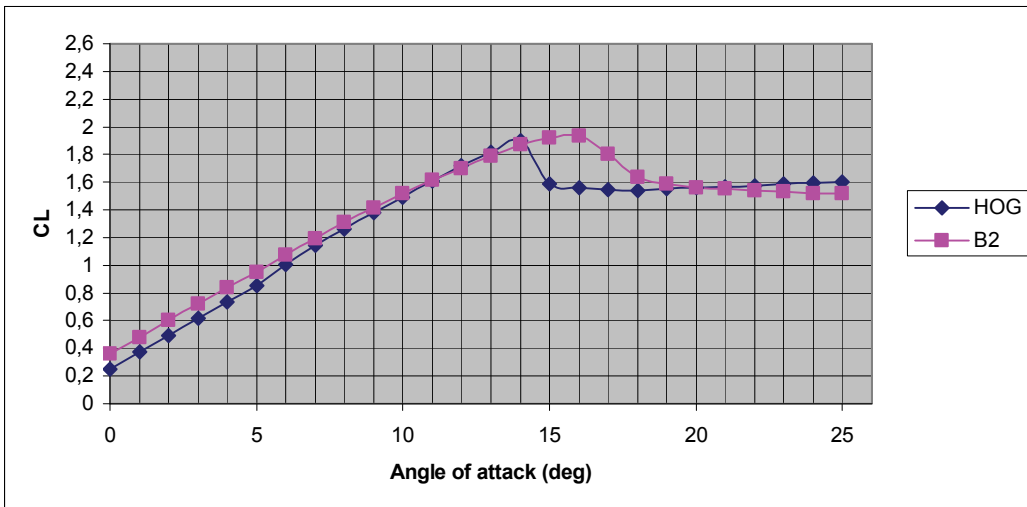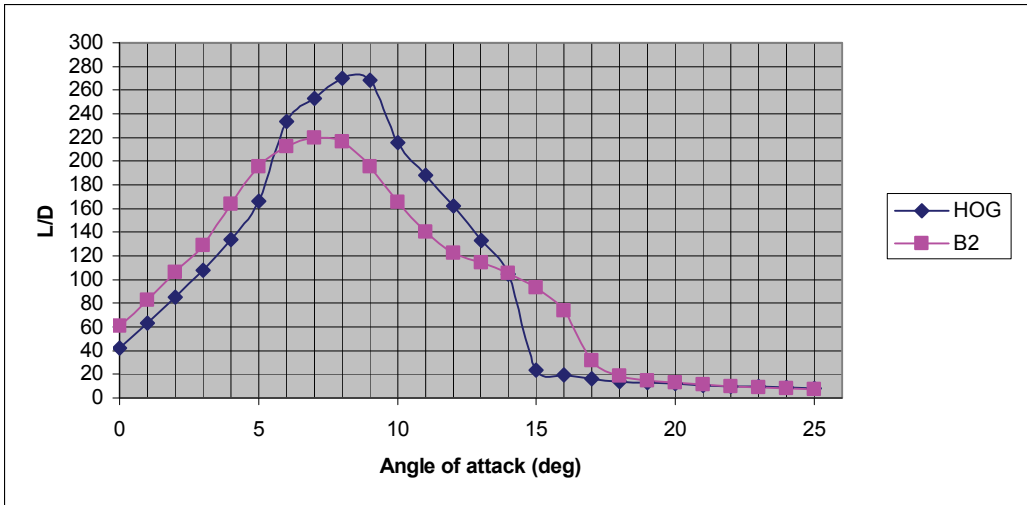**Figure 5.5.7** – B2 performance characteristics

Another positive trait in this airfoil is that it is relatively good for low angles of attack, which has been a missing quality in the earlier profiles. It also has a very rounded peak, with reasonably good performance extending to both sides.

From angles of attack 12° through 17°, the L/D-graph can be seen to bulge outwards in an unusual way. The reason for this can be seen in figure 5.5.8. By the time the angle of attack reaches 12º, the transition point has moved to the leading edge, and can not move much further. For low angles of attack, the moving transition point influences the variation in performance as the angle is increased. For angles of attack $\alpha > 12º$, the effect of the moving transition point is eliminated, causing a shift in how the airfoil is affected by increasing angles of attack. This is illustrated by the change in direction for the L/D-curve at 12º.
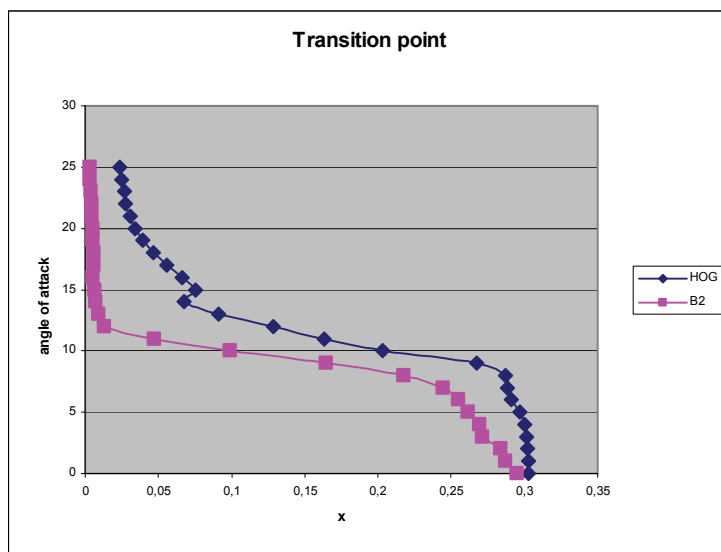
Figure 5.5.8 – Transition points, shown for Ncrit = 9.

This effect is also present in the NACA 4412, but the "bulge" in the L/D-curve is less obvious. Although, a weak bulge is clearly visible starting at ~8º in figure 5.3.1.

The CFD simulation of the B2 profile reveals the first sign of separation at $\alpha = 17°$, which is ~3.5° later than the HOG, and after this the separation grows gradually. The profile has an early peak performance and can therefore be optimized for lower angles of attack. Together, this means that the distance from the operating point to the dramatic increase in stall can be increased significantly. This wide safety margin, the good performance, the low thickness, and the low sensitivity to roughness means that this is a very interesting airfoil. The stall is not as soft as achieved in the B1, but the B2 has such a wide range, making it easier to avoid stall all together.
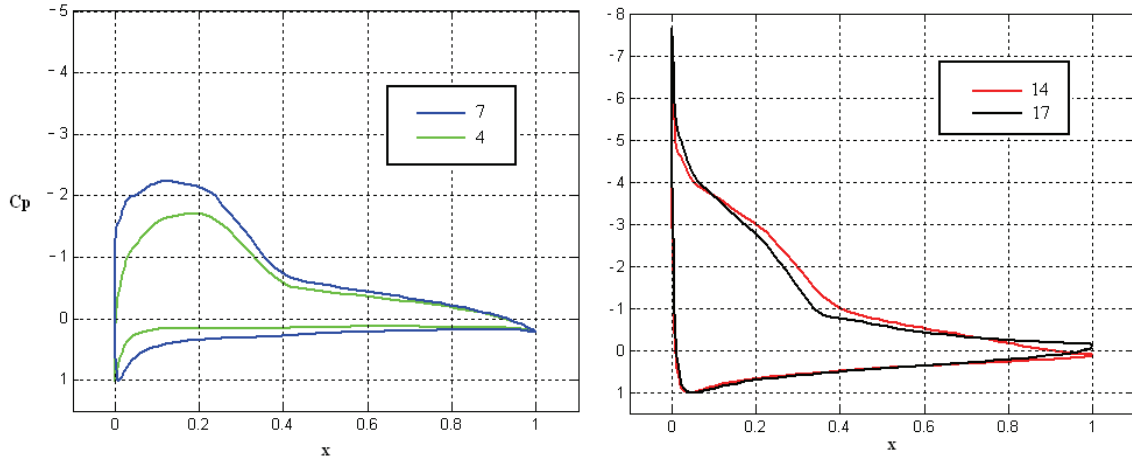
Figure 5.5.9 – B2 pressure distributions

The reason for the early transition, and the resulting stabile performance, is visible in figure 5.5.9. To the right, we see that the leading edge of this profile produces a pressure spike, like the NACA 4412, which promotes early transition.

The pressure distribution is affected very little by the separating flow. The changes are very gradual. Fluent predicts separation around the same angles of attack as Xfoil.
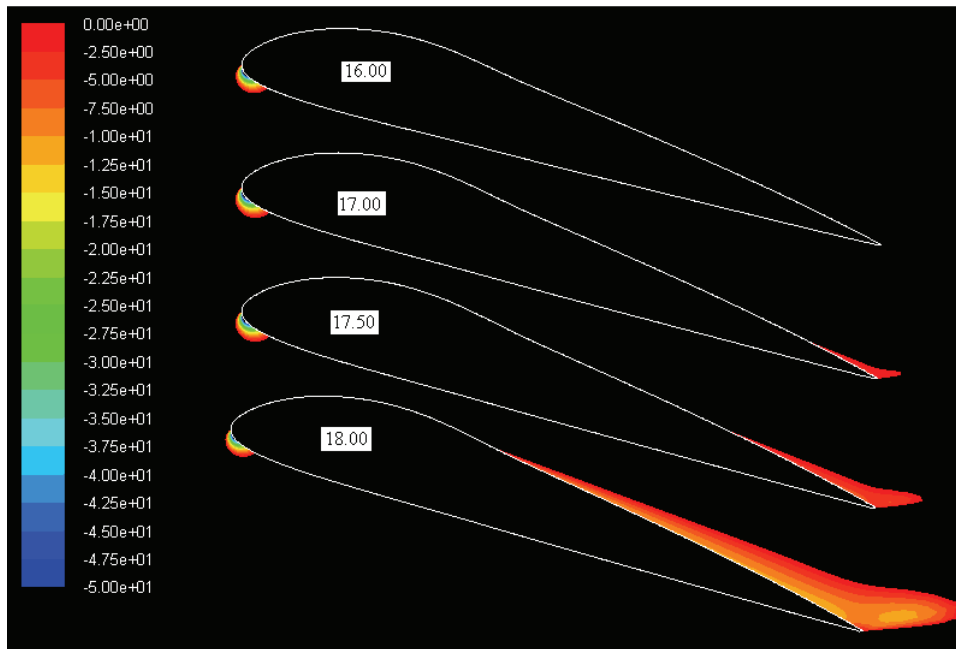
Figure 5.5.10 – CFD simulation of separated flow, B2

As seen in figure 5.5.10, separation does not occur until α = 17°, according to Fluent. Although, it can be seen from figure 5.5.7 that the lift and drag curves start bending a lot sooner. This is due to a growing stagnation behind the convex upper side of the trailing edge. This is not dangerous, and might in fact be helpful to provide a softer transition to the stall area and stabilize the turbine. The NACA 4412 has almost continuously curving

lift and drag curves, and uses this effect. The details of this phenomenon will be discussed in chapter 5.9.
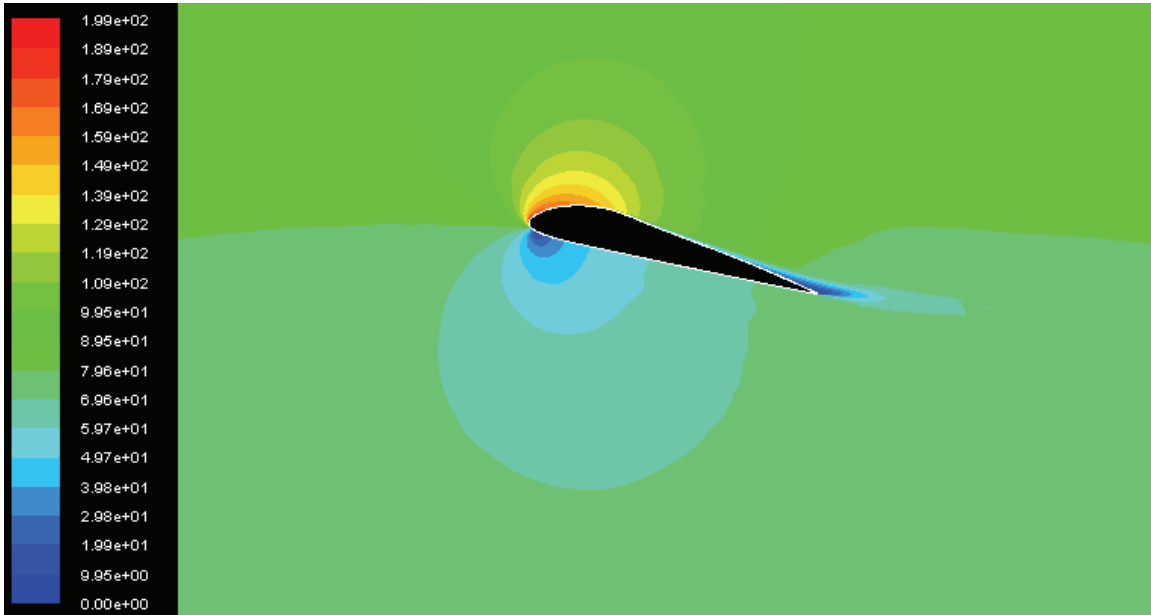
Figure 5.5.11 – CFD simulation, velocity at α = 14°. Stagnation is clearly visible around the upper trailing edge.
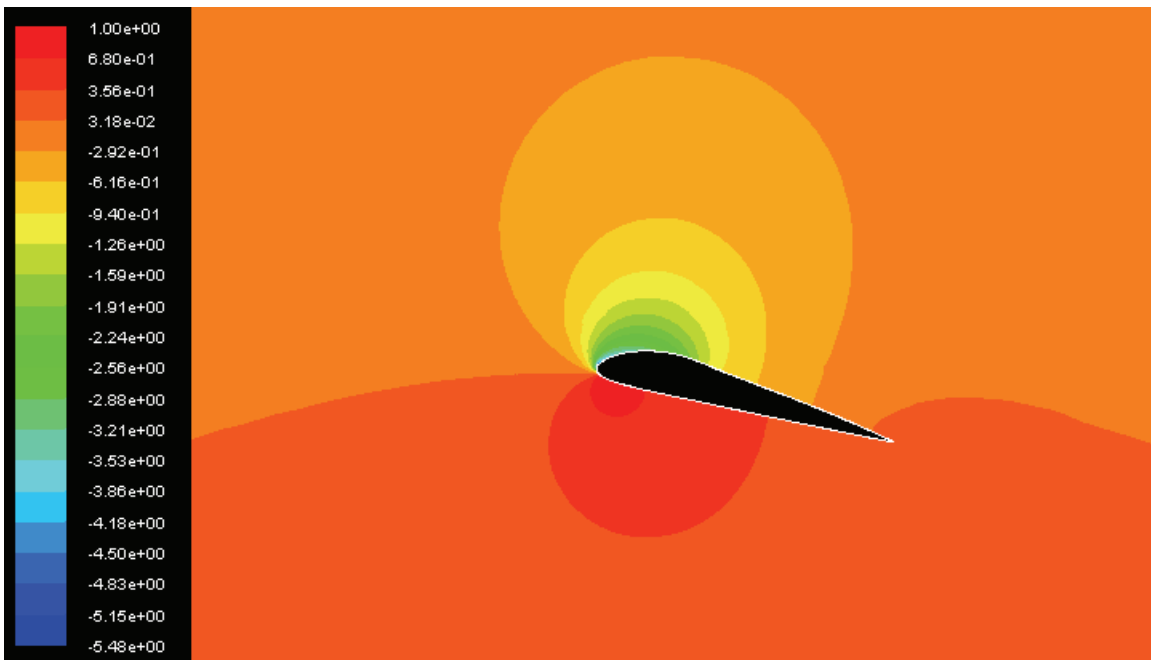
Figure 5.5.12 – CFD simulation, coefficient of pressure at α = 14°.

5.6 C-profiles

5.6.1 C-1

The work so far has given some interesting profiles, and it will now be attempted to develop some of them further. The B1 did not show extreme performance, but it showed a unique ability to keep good performance over a wide range. It was therefore interesting to modify the B1 further and make more extreme versions. This is the basis for the C-profiles. The first version, C-1, is given a much higher "head" compared to the B1. It is now basically the HOG distribution with the long flat rooftop traded for a higher and shorter pressure drop, starting pressure recovery sooner.
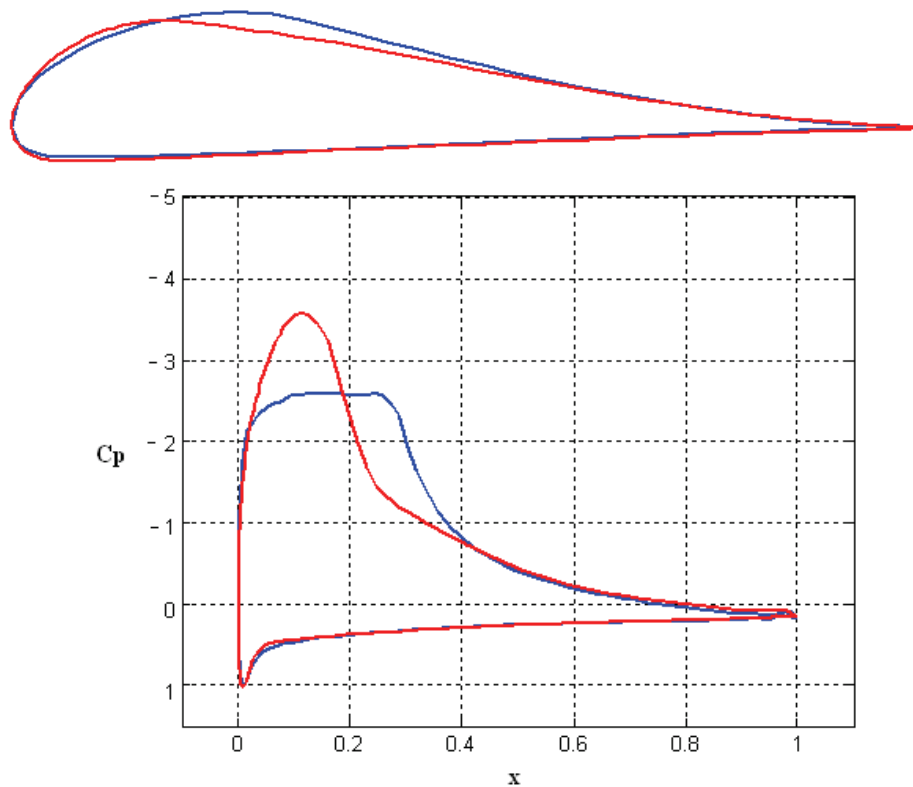
Figure 5.6.1 – illustration of shape and pressure distribution at α = 8º.

Indeed, the profile seems to develop further the B1's ability for stable performance, and good performance for high angles of attack. The C-1 stalls remarkably late, and is seen to provide useful operation up to α ~20º, before stalling very suddenly. It delivers a L/D-ratio between 200 and 220 for over 9º angles of attack, which is an extremely stable and good result.

This is very interesting, but this profile is probably not very usable in wind turbines. It is not good for low angles of attack, meaning it would have to be optimized for a relatively high angle of attack, and if it ever were to stall, the result would probably be dramatic. Although, the operational range is amazing, so in well controlled conditions, the profile is of big interest.
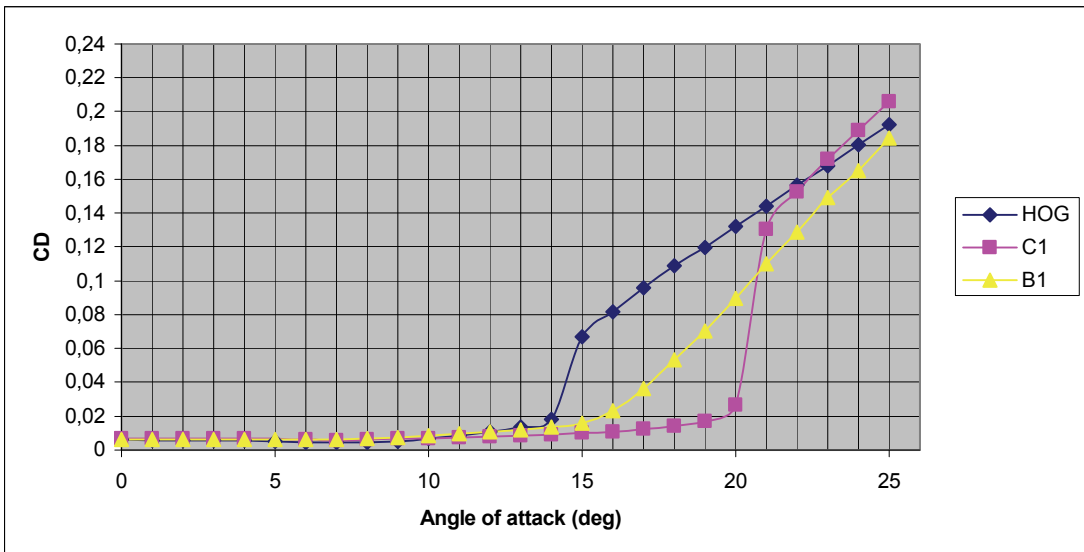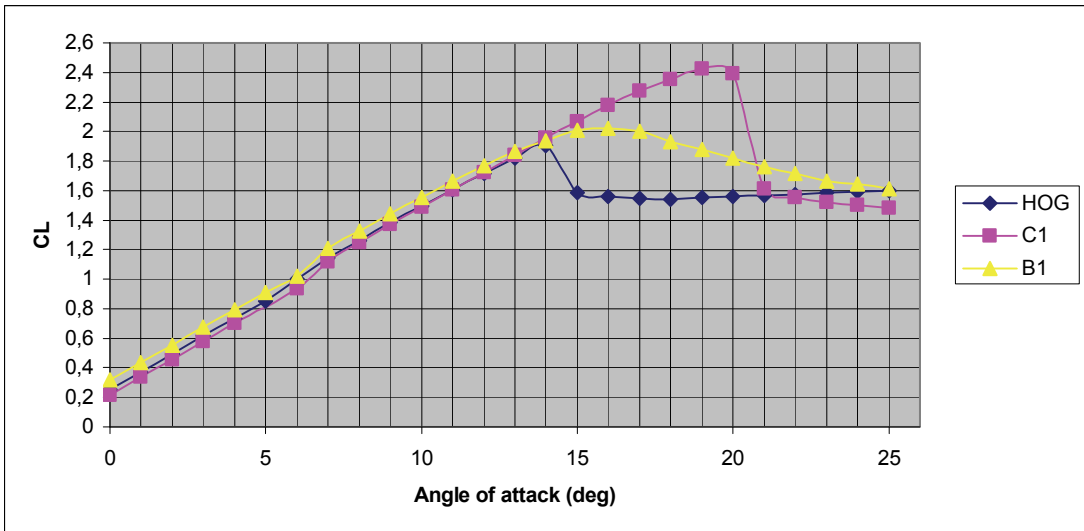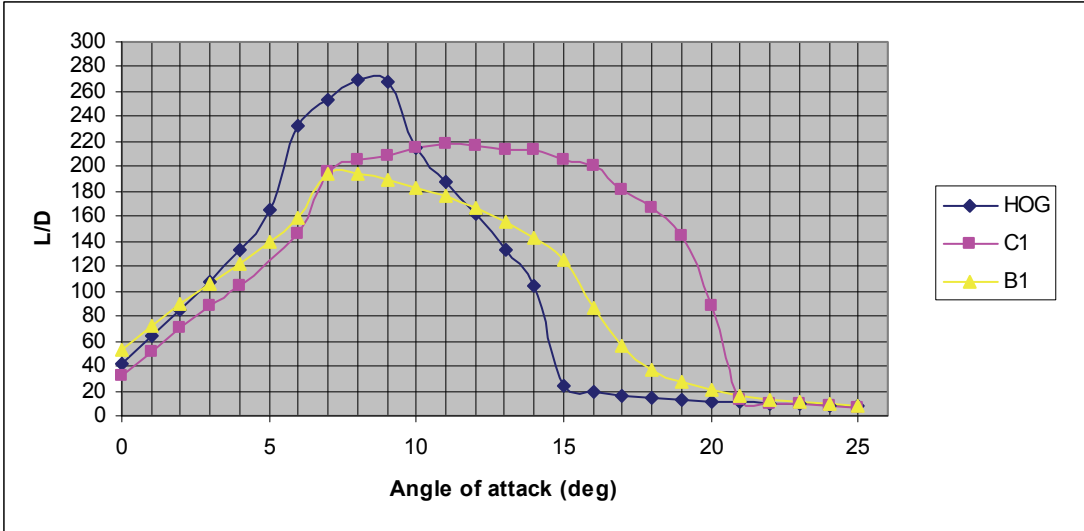
Figure 5.6.2 – C-1 performance characteristics

In terms of the early interest in high lift profiles in the previous decades, which was to get high performance at high lift coefficients [8], we here have a profile that delivers a L/D-ratio of 200 at a lift coefficient of 2.18, for α =16º.

	L/D (n=9)	L/D (n=3)	Thickness (%)	Area (%)
C-1	219 (11º)	198 (12º)	15.17	7.92
Modification	-18.9 %	+8.8 %	-2.5 %	-2.3 %

Table 5.6.1 – C-1 compared to HOG

These profiles also show a very good ability to be insensitive to roughness in terms of performance. The transition point is very stable for both angles and Ncrit values. This gives a profile which actually outperforms the HOG for Ncrit = 3. Even though it is insensitive to roughness in terms of performance, it is not when it comes to stall characteristics. The stall occurs ~3º earlier at Ncrit = 3, however, the stall is then slightly more gentle and curved, but still of unacceptable proportions (app. 10.8).
The reason for these behaviors is the short, but big, pressure drop at the front of the airfoil. This, in effect, works as an elongated pressure spike. The big adverse pressure gradient that occurs around X~0.2 triggers turbulent flow, making the transition to turbulent flow very stable around this point. Performance in the operational area is therefore largely unaffected by increasing roughness. However, for high angles of attack, the transition point will start moving forward over the previously laminar area. The location of this region of angles, where transition occurs before the big adverse pressure gradient, is of course heavily influenced by roughness on the front of the airfoil. This is what causes the highly variable point of stall.
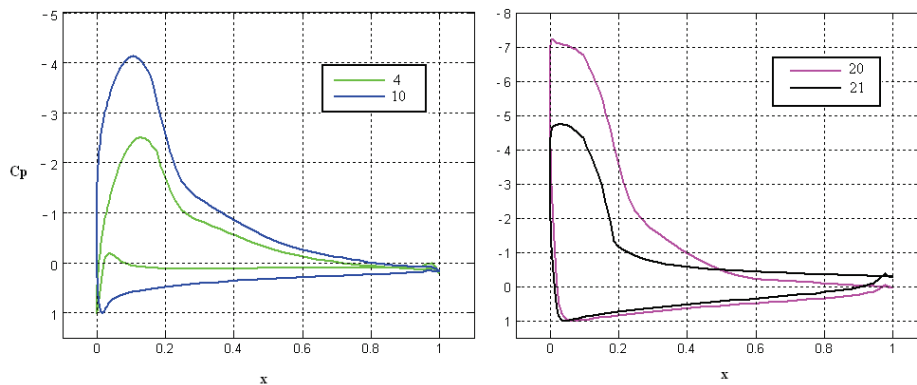
Figure 5.6.3 – C-1 pressure distributions

Fluent calculates the point of separation to occur around α~16º. This is a lot earlier than the original Xfoil calculation. However, Xfoil predicts a highly variable stall, which will occur earlier with increasing turbulence. The Fluent model is expected to generate more turbulence and boundary layer growth, and should therefore, according to Xfoil, be expected to stall earlier. This is therefore not a surprising result.

This profile shows a lot of interesting effects, but is too unstable and dramatic for use in wind turbines. In fact, such a wide operational range is not desirable. Since the energy

extracted from the wind increases with velocity to the power of 3, it is clear that a gust of wind will put extreme forces on the blade. It is therefore useful to have a lift coefficient that flattens out for higher angles of attack to help cope with the extreme forces. A wing with the C-1 profile would be subjected to colossal forces in a gust of wind, as the lift coefficient just keeps rising with increasing wind speed.
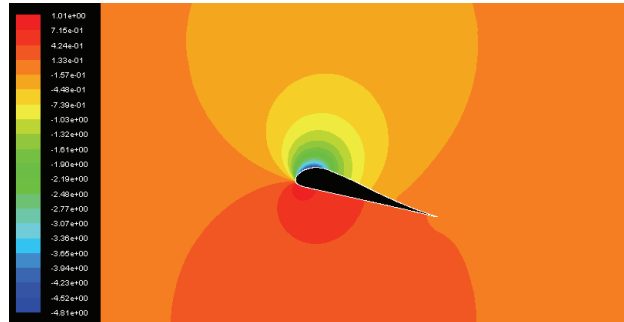
Figure 5.6.4 – CFD simulation, coefficient of pressure at α = 15°.

Even though the C-1 profile appears to be unsuitable for wind turbines, the unique effects it has are very interesting. The profile will therefore be developed further, in an attempt to keep the good effects, but get a more stable and usable profile.

5.6.2 C2

The first modification, in order to make a less dramatic profile, is to lower the pressure rise over the head slightly, and have a more continuous pressure recovery. The result is the C2.
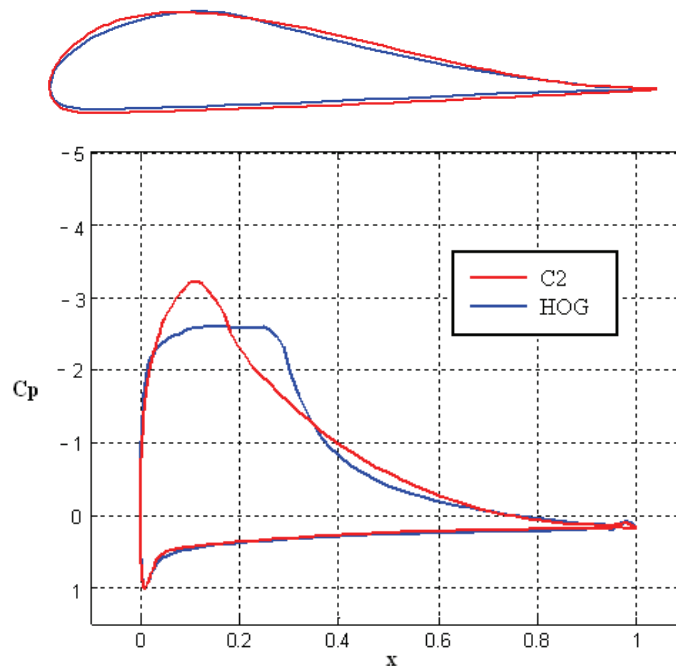
Figure 5.6.5 – illustration of shape and pressure distribution at α = 8°.
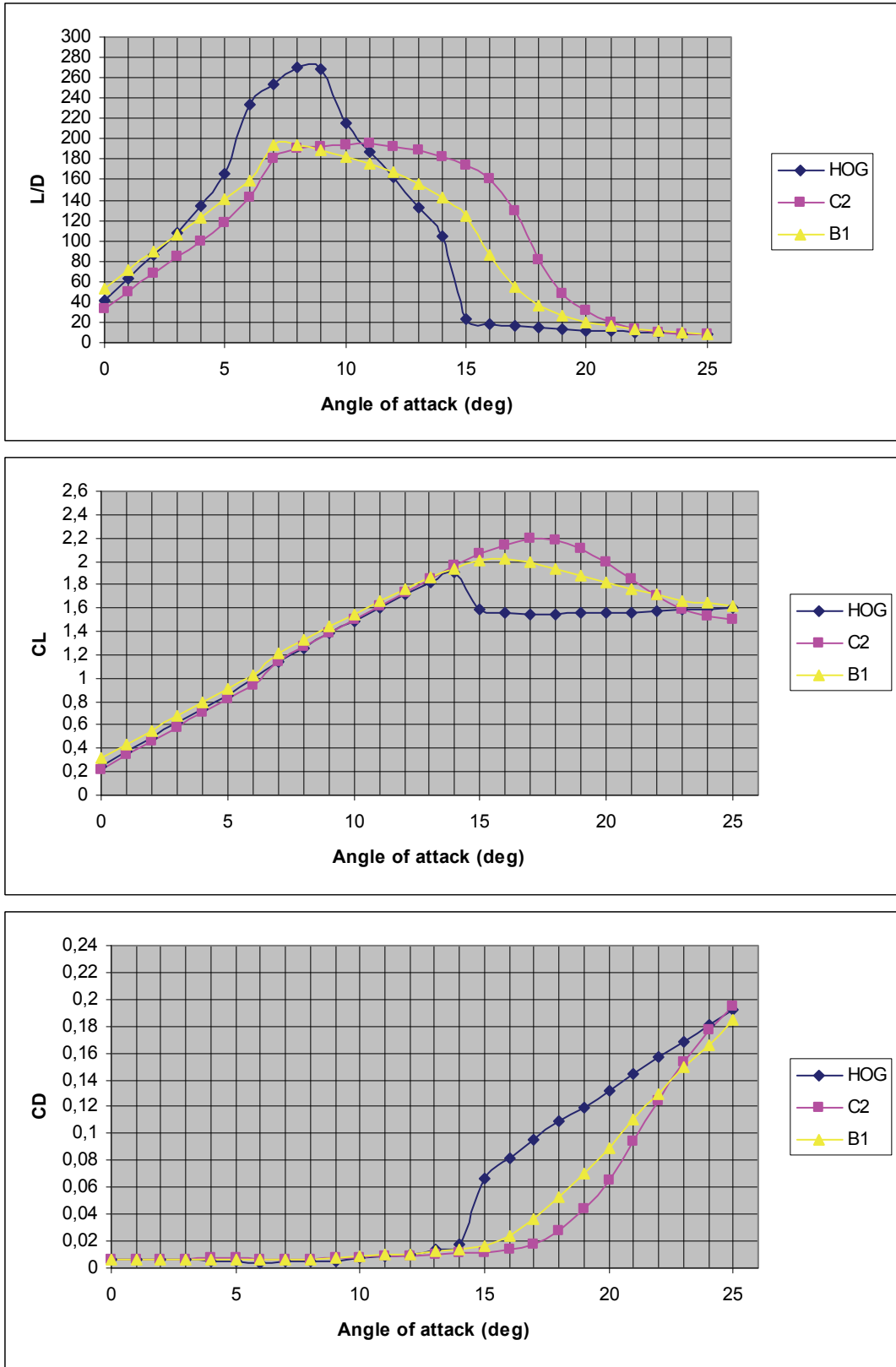
Figure 5.6.6 – C2 performance characteristics

	L/D (n=9)	L/D (n=3)	Thickness (%)	Area (%)
C2	196 (11º)	178 (10º)	16.10	9.13
Modification	-27.4 %	-2.2 %	+3.5 %	+12.5 %

Table 5.6.2 – C2 compared to HOG
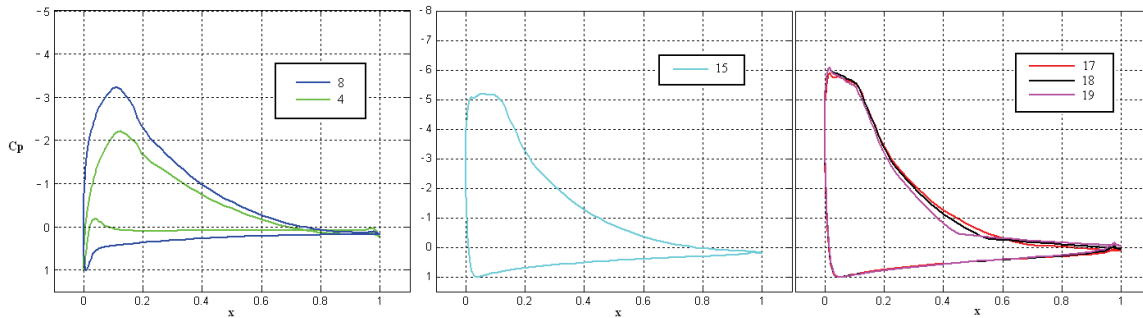
Figure 5.6.7 – C2 pressure distributions

This profile keeps the stable performance, but at a slightly lower lever. It keeps a L/D-ratio between 180 and 196 for 8º angles of attack. The stall occurs earlier, and is a lot softer. It also keeps the ability to be insensitive to roughness in terms of performance, almost matching the HOG for maximum L/D at Ncrit = 3. However, the stall still changes a lot, occurring almost ~3º degrees earlier (app. 10.9).

The profile is also a bit thicker. It is therefore attempted to make a third version which is supposed to be thinner, and have a more stable point of stall. The start of the pressure recovery was moved forward to let the stable transition point be closer to the leading edge.

5.6.3 C3
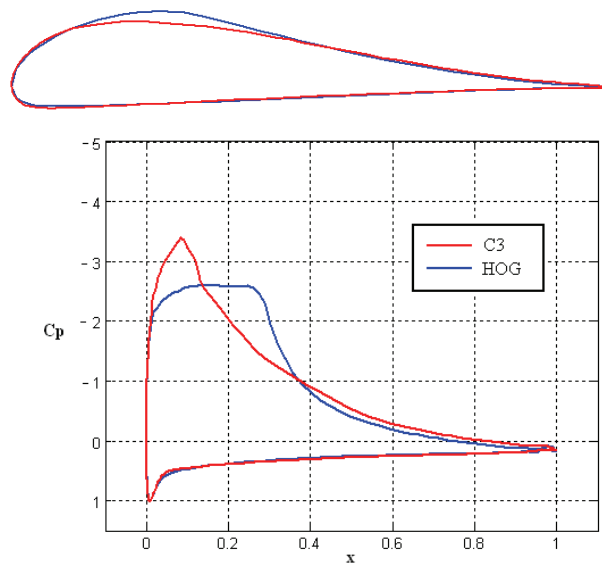
Figure 5.6.8 – illustration of shape and pressure distribution at $\alpha = 8º$.

	L/D (n=9)	L/D (n=3)	Thickness (%)	Area (%)
	184 (10º)	174 (10º)	14.01	7.83
Modification	-31.9 %	-4.4 %	-9.9 %	-3.5 %

Table 5.6.3 – C3 compared to HOG

This profile keeps the ability to have stable performance over many angles of attack, and the performance is remarkably little reduced by increasing roughness (app. 10.10). The transition point still makes a "jump" for high angles of attack, and causes the stall to still vary too much, even though it is noticeably less than for the C2.
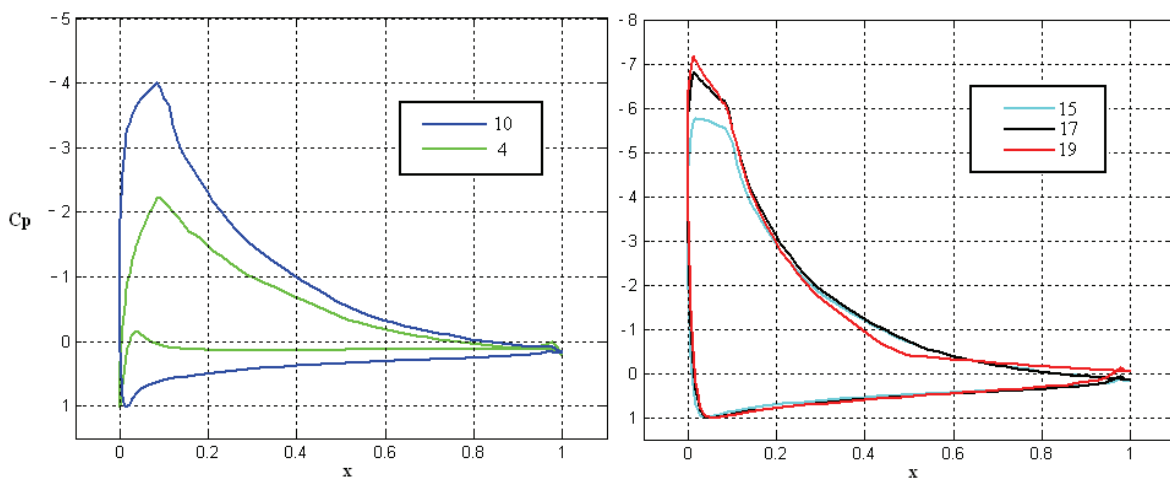
Figure 5.6.9 – C3 pressure distributions

The C-profiles are interesting, and have some very good qualities, but they do not appear to be right for wind turbines. They have too low performance for low angles of attack, and have a too variable stall. It is therefore decided to leave the C-design philosophy, and look for another way to modify the pressure distributions, to get good performance earlier, and a softer and more stable stall. It appears that the big pressure drop at the front of the C-profiles is what gives it the late peak in performance. Experimentation indicates that a lower pressure drop will give profiles that are better for lower angles of attack. This is the basis for the D-profiles.
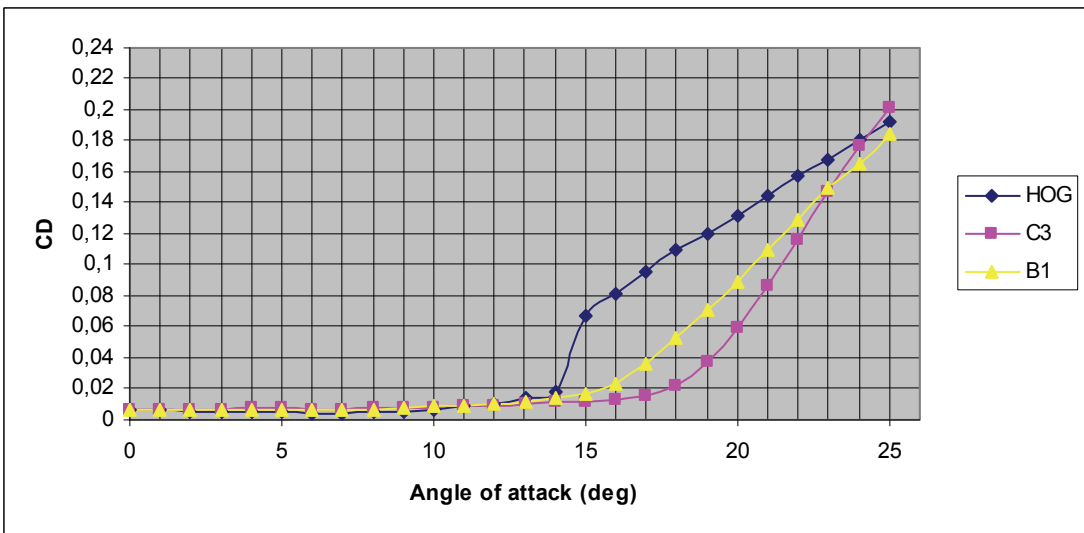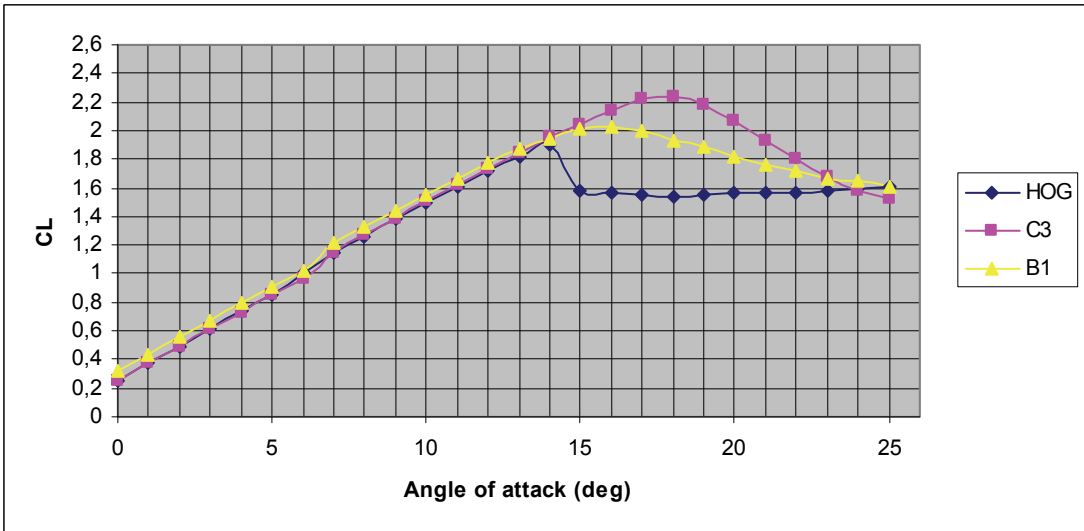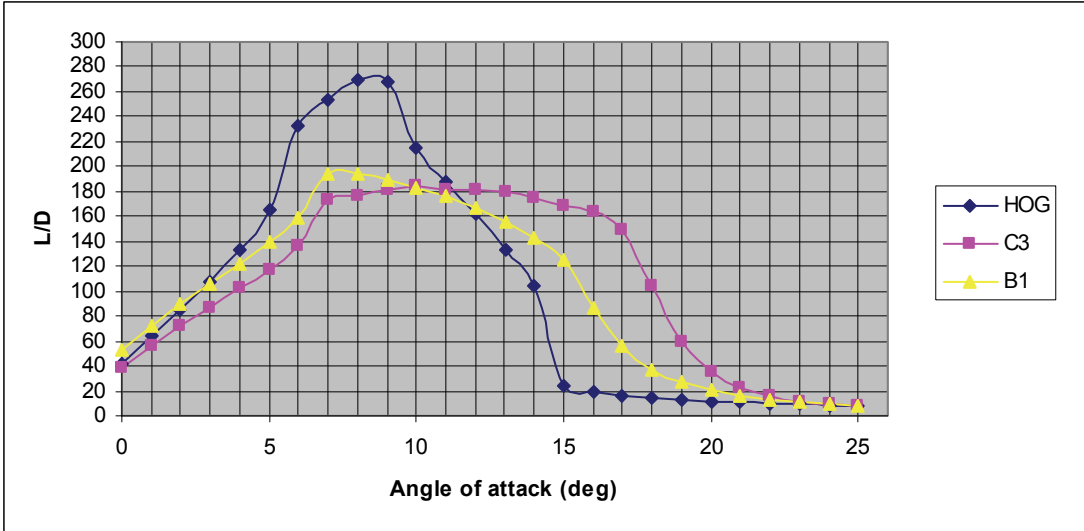
Figure 5.6.10 – C3 performance characteristics

5.7 D-profiles

5.7.1 D1

Going back to the B1 profile, the pressure drop over the nose is now lowered to the same magnitude as the HOG, thereby hopefully giving a profile similar to the B1, but with an earlier peak performance.
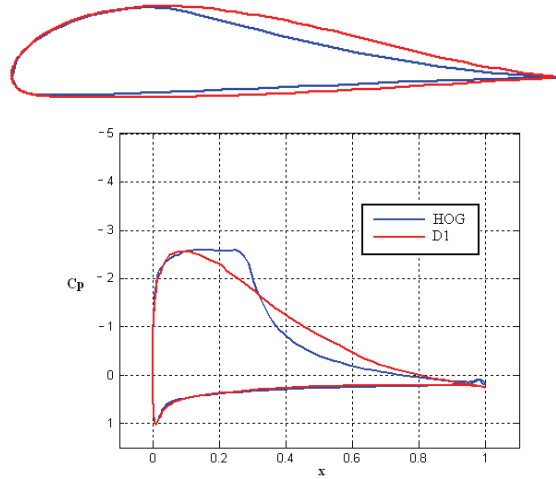
Figure 5.7.1 – illustration of shape and pressure distribution at $\alpha = 8°$.

	L/D (n=9)	L/D (n=3)	Thickness (%)	Area (%)
D1	197 (8°)	156 (9°)	16.56	10.17
Modification	-27.0 %	-14.3 %	+6.5 %	+25.5 %

Table 5.7.1 – D1 compared to HOG

This resulted in a relatively thick profile, but the effect in performance is what was hoped for. The new profile works better for low angles of attack, and has a rounded peak area. Also, the stall is now even softer. The profile is very insensitive to roughness both in terms of performance and stall (app. 10.11). The performance curve keeps the same general shape. The stall shifts slightly inwards about ~1° degree, roughly the same as the B1. The D1 therefore appears to be slightly better profile than the B1, although it is slightly bigger. The transition point is not near the leading edge, but moves slowly and varies little for various conditions.
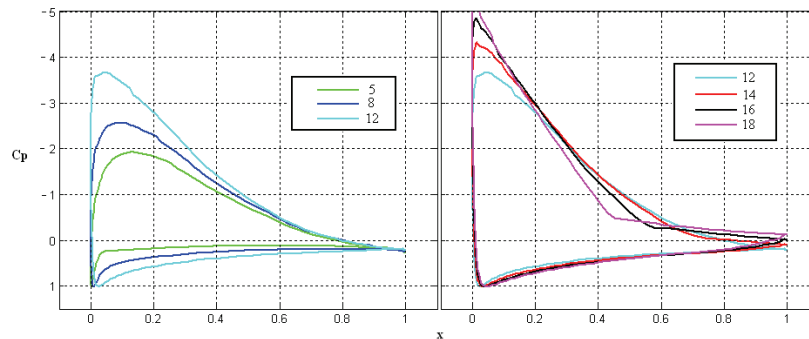
Figure 5.7.2 – D1 pressure distributions
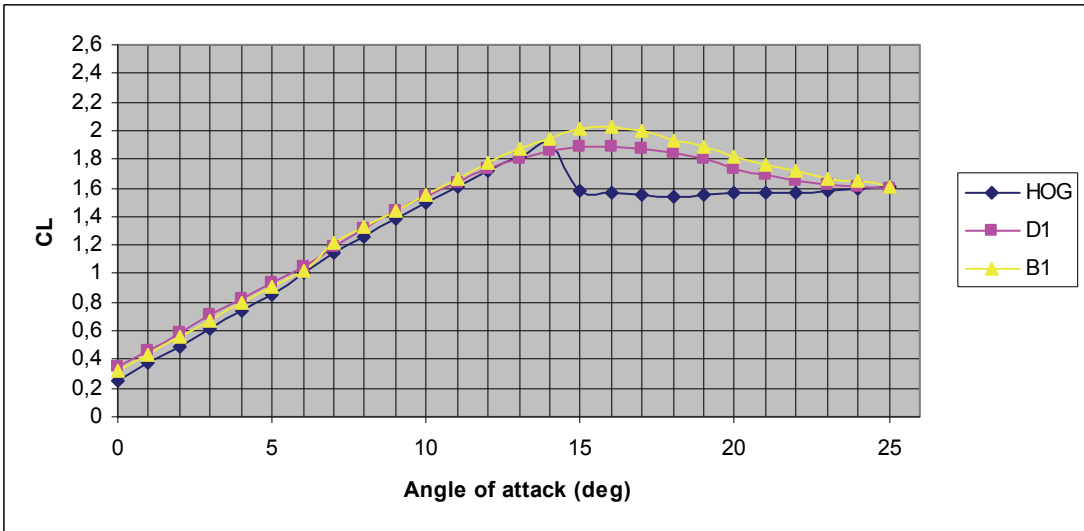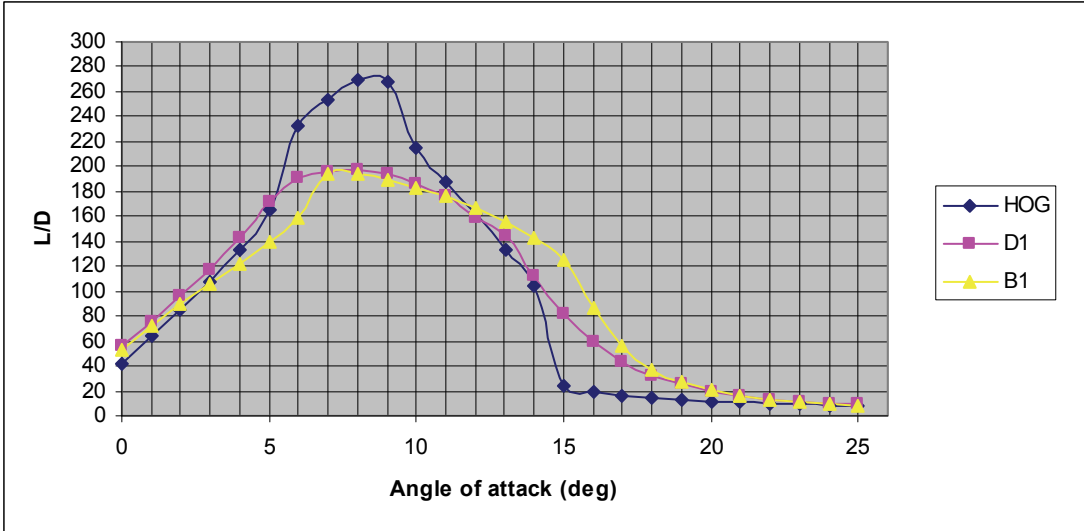
Figure 5.7.3 – D1 performance characteristics

5.7.2 D2

The D1 showed good qualities in terms of performance characteristics, but the maximum L/D-ratio of 197 is not of the magnitude that is ultimately hoped for. The design is therefore modified further to get higher maximum performance. The D2 profile has been given a slightly flat and elongated rooftop, transforming into a slightly concave pressure recovery.
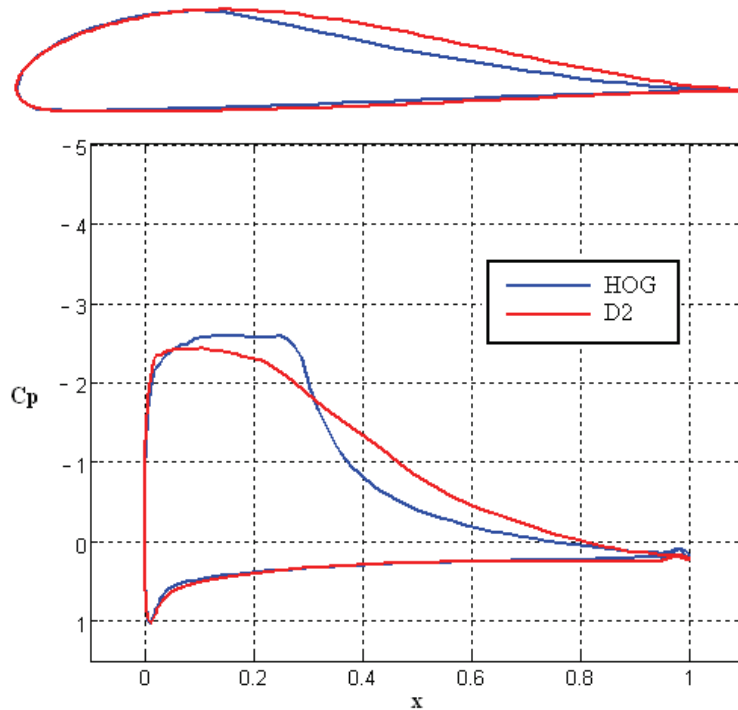
Figure 5.7.4 – illustration of shape and pressure distribution at α = 8º.

The D2 profile gives ideal performance. The stall is by far the softest in the profiles created, and it has a maximum performance of L/D~222, which is very good. It is also has low sensitivity to roughness regarding stall, with only a minimal shift inwards between the simulations (app. 10.12). The performance level is reduced a bit between the simulations, but the performance curve keeps the same general shape, and the profile should therefore be sufficiently stable for a wind turbine.

	L/D (n=9)	L/D (n=3)	Thickness (%)	Area (%)
D2	222 (7º)	154 (6º)	16.13	9.71
Modification	-17.8 %	-15.4 %	+3.7 %	+19.7 %

Table 5.7.2 – D2 compared to HOG
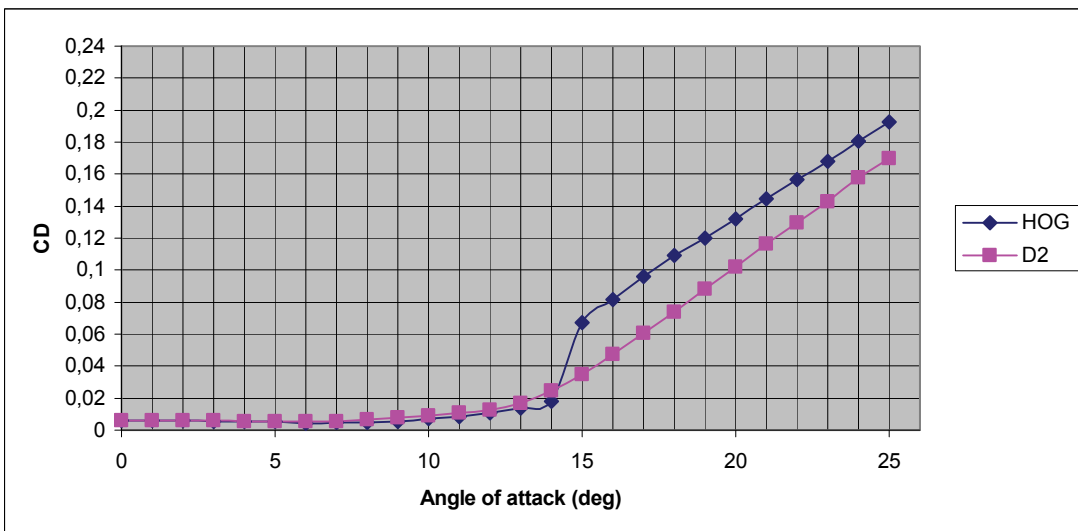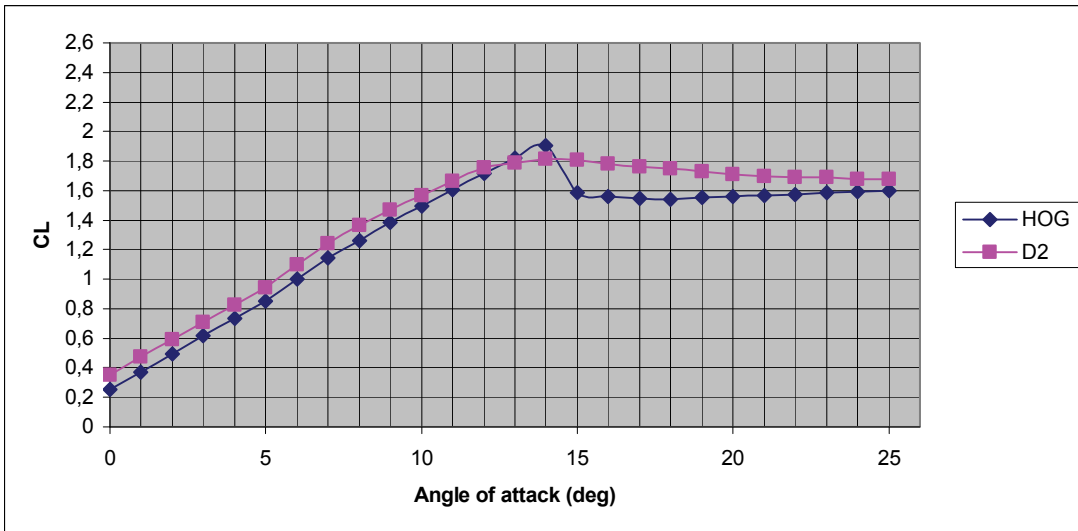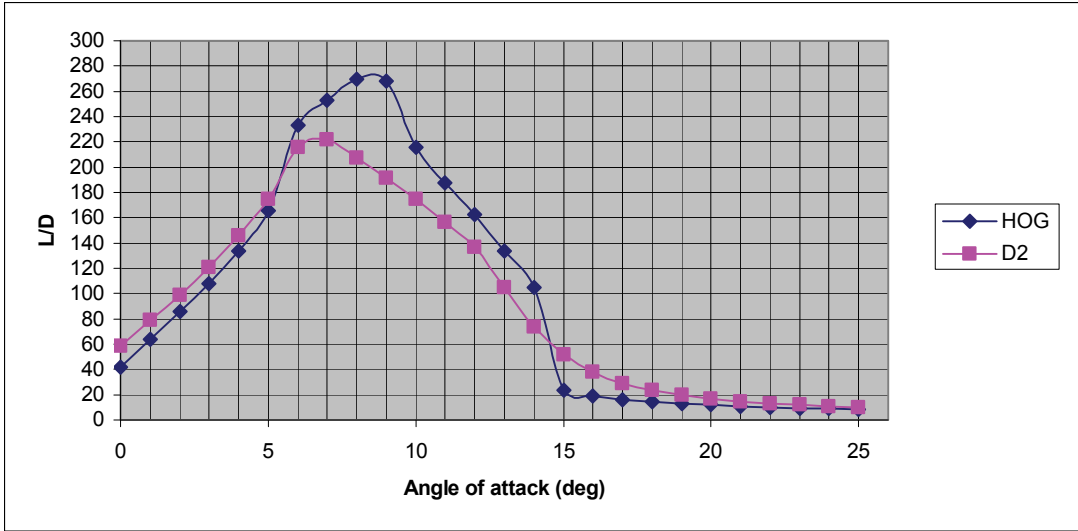
Figure 5.7.5 – D2 performance characteristics
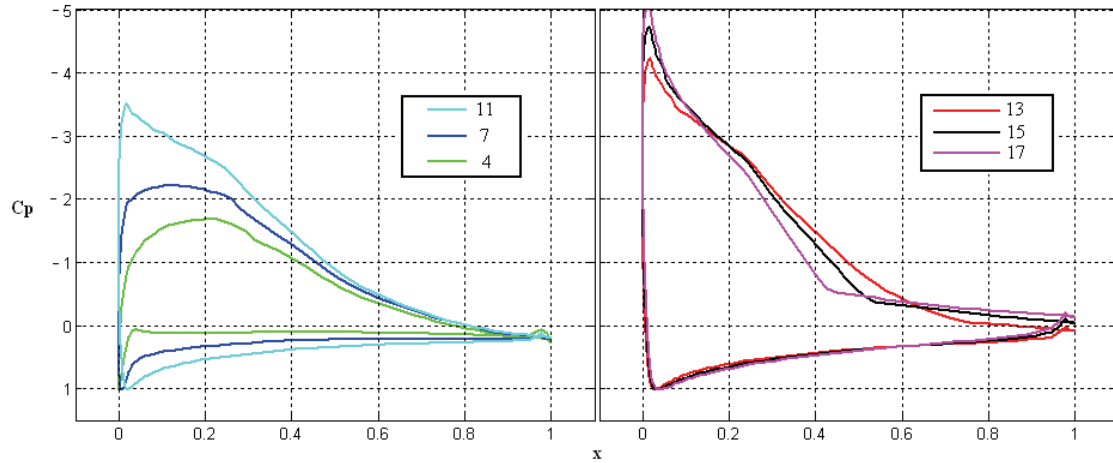
Figure 5.7.6 – D2 pressure distributions

The right window in figure 5.7.6 shows the gradually a gradually increasing separation, and fluent confirms this trend in figure 5.7.7, with the first occurrence of separation at 14º. This profile would probably work very well in wind turbines. It has a stable and soft performance, while at the same time being extremely efficient in the maximum area. This is therefore a success with the criterion set out at the start of this project. There is, of course, still room for improvement. It could still be better for low angles of attack, it is a bit thick, and it could always be even less sensitive to roughness. Therefore, the experimentation continues.
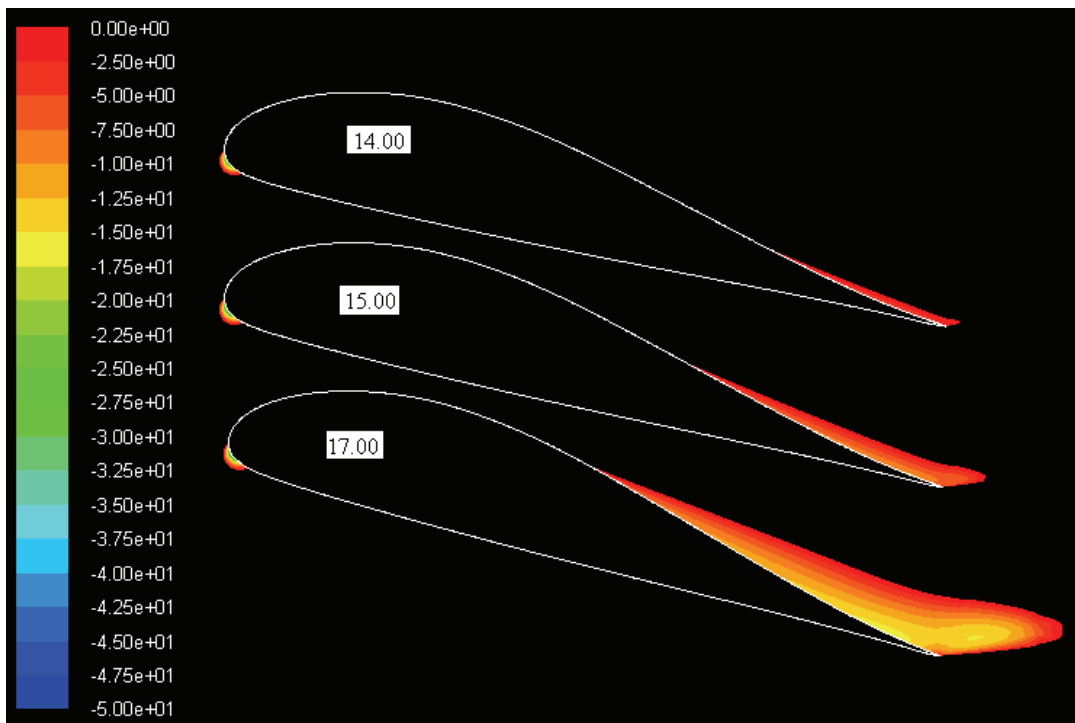
Figure 5.7.7 – D2, reversed flow, CFD simulation.
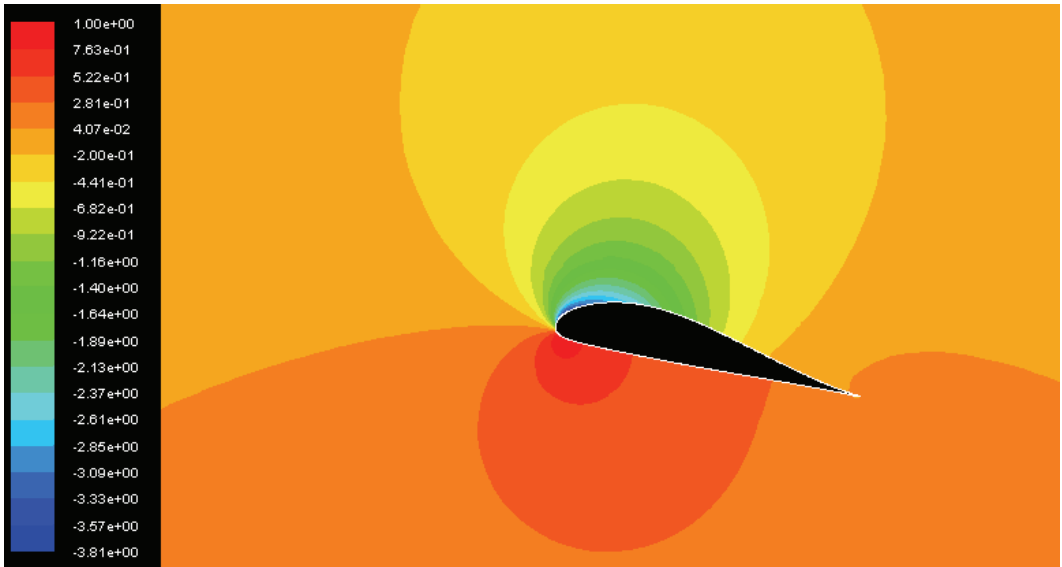
Figure 5.7.8 – D2, pressure coefficient at α = 13º.

In the next step of experimentation, it was decided to let the pressure drop peak later. This would give a slower, more gradual acceleration of the air, and should cause less boundary layer growth. This is the basis for the E-profiles.

5.8 E-profiles

5.8.1 E1
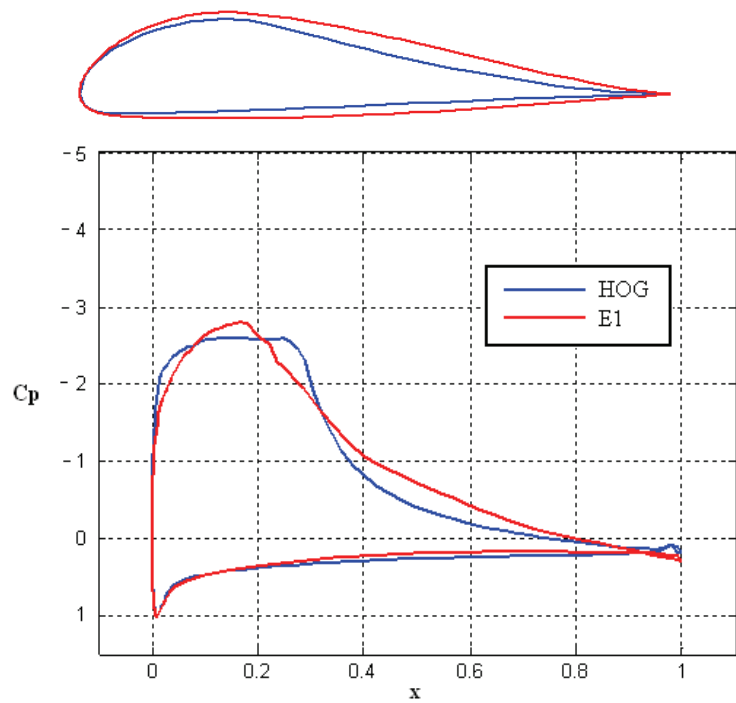
Figure 5.8.1 – illustration of shape and pressure distribution at α = 8º.

	L/D (n=9)	L/D (n=3)	Thickness (%)	Area (%)
E1	215 (10º)	194 (10º)	17.78	10.81
Modification	-20.4 %	+6.6 %	+14.4 %	+33.3 %

Table 5.8.1 – E1 compared to HOG

This pressure distribution resulted in a very thick profile. It can be seen to perform quite well, and having overall higher L/D-ratios than the B1, although with a bit sharper stall. It is very insensitive to roughness regarding performance, and can be seen from table 5.8.1 to outperform the HOG for Ncrit = 3.
Theory says that a continuous acceleration of air inhibits boundary layer growth and transition to turbulent flow. It was therefore expected that moving the "head" back, and having a slower pressure drop, would give transition points further back on the airfoil. This should improve performance. The transition is now stabile at the start of the adverse pressure gradient, as for the C-profiles. But as can be expected, the transition points start moving for high angles of attack, and give highly variable stall. The airfoil stalls ~3º earlier for Ncrit = 3 (app. 10.13).
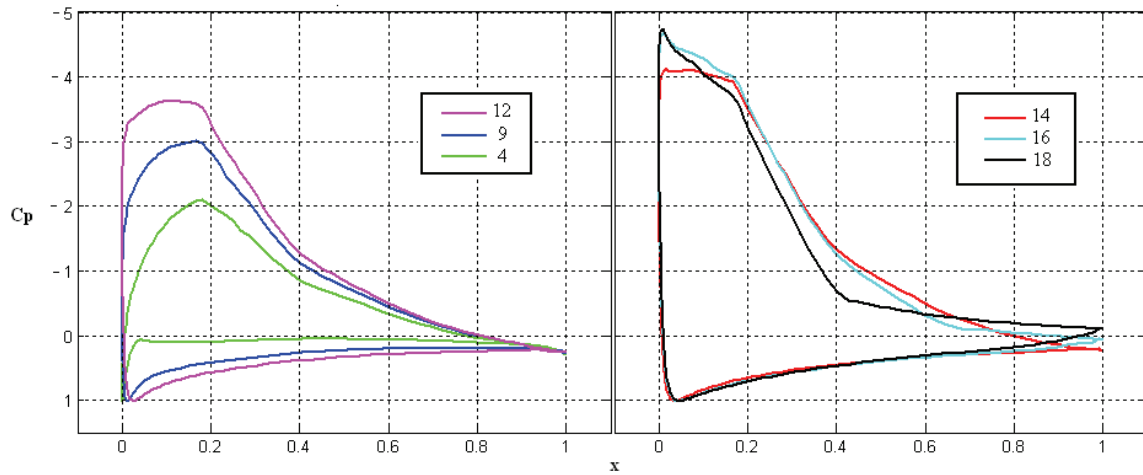
Figure 5.8.2 – E1 pressure distributions

This distribution gives good performance over a wide range, and the performance is little influenced by roughness. But it has a too variable stall, and is too thick. It also reaches its peak performance very late. This profile can therefore not compete with some of the better profiles made earlier. This design philosophy appears to be a step in the wrong direction for getting a stable airfoil.
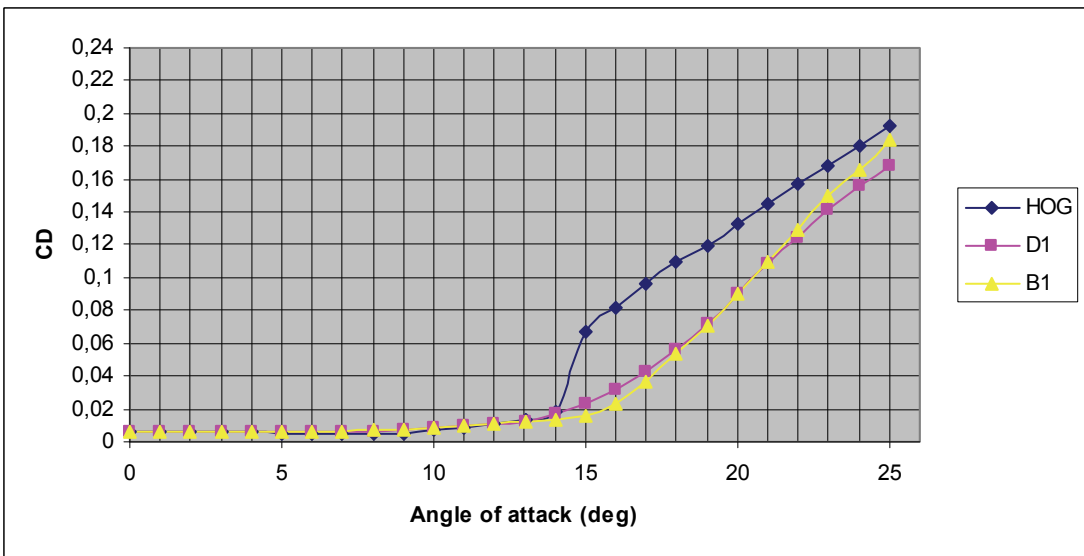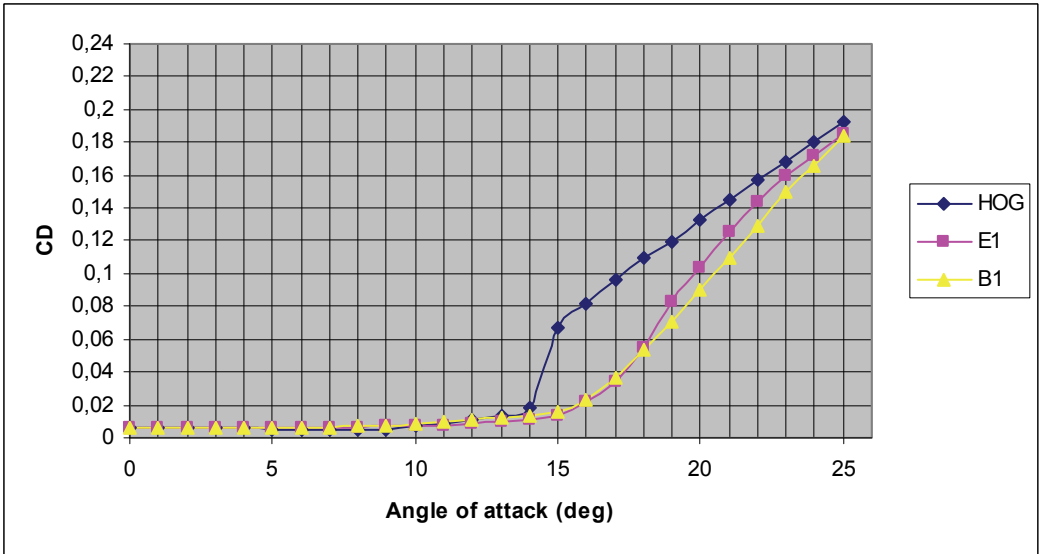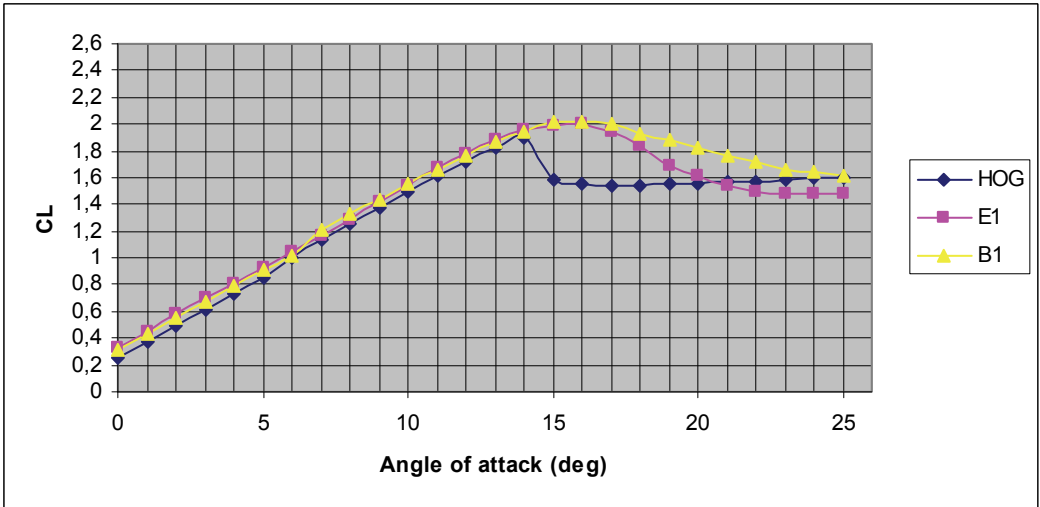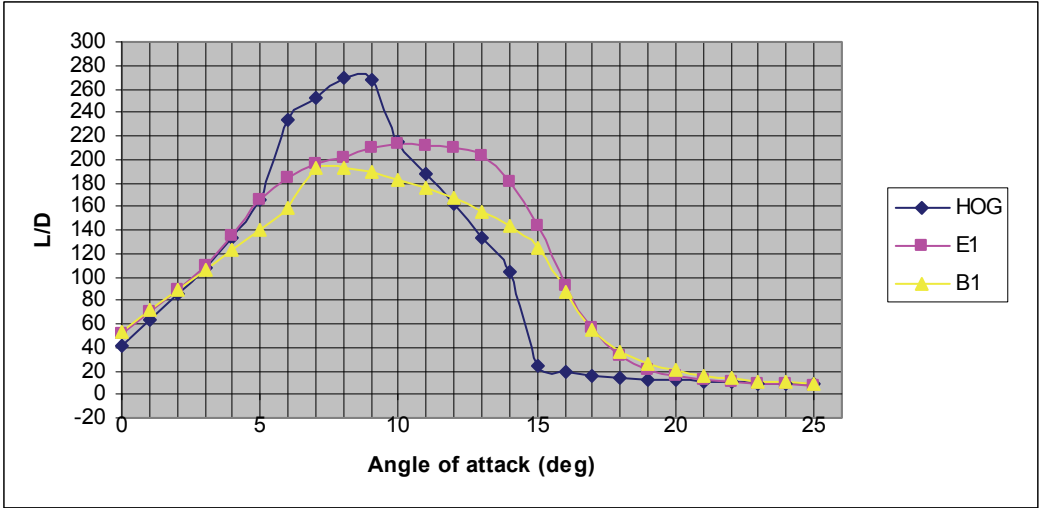
Figure 5.8.3 – E1 performance characteristics

5.8.2 E2

Another version, E2, was made which had a slightly bigger pressure drop. Again, we see the same effect as for the C-profiles. A bigger pressure drop makes the airfoil perform better for higher angles of attack, and less good for lower angles of attack. Comparing the two E-profiles in figure 5.8.6, shows that the E2 is almost identical in performance, only shifted slightly to the right. This is also what happened to the C-profiles when their pressure drop was increased. Besides that, the E2 still has the same positive and negative qualities as the E1. The transition points jump for high angles of attack, leaving it with a variable stall. While at the same time, it is almost unaffected by roughness in terms of performance level. It can be seen from table 5.8.2 that we for the first time have an airfoil with a L/D-ratio above 200 for Ncrit = 3.
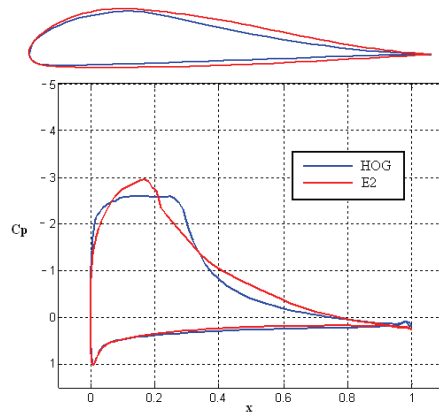
Figure 5.8.4 – illustration of shape and pressure distribution at α = 8º.

	L/D (n=9)	L/D (n=3)	Thickness (%)	Area (%)
	218 (12º)	203 (11º)	17.27	10.29
Modification	-19.3 %	+11.5 %	+11.0 %	+26.8 %

Table 5.8.2 – E2 compared to HOG

These airfoils have good qualities, but, in total, is not what we are looking for. They are too thick and the stall varies too much.
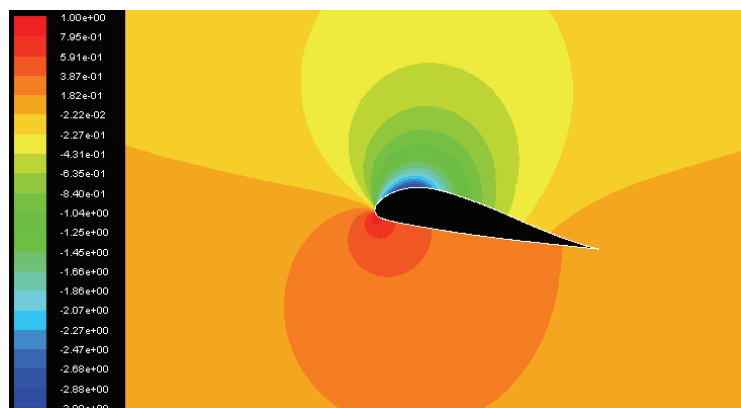
Figure 5.8.5 – CFD simulation, coefficient of pressure at α = 10º.
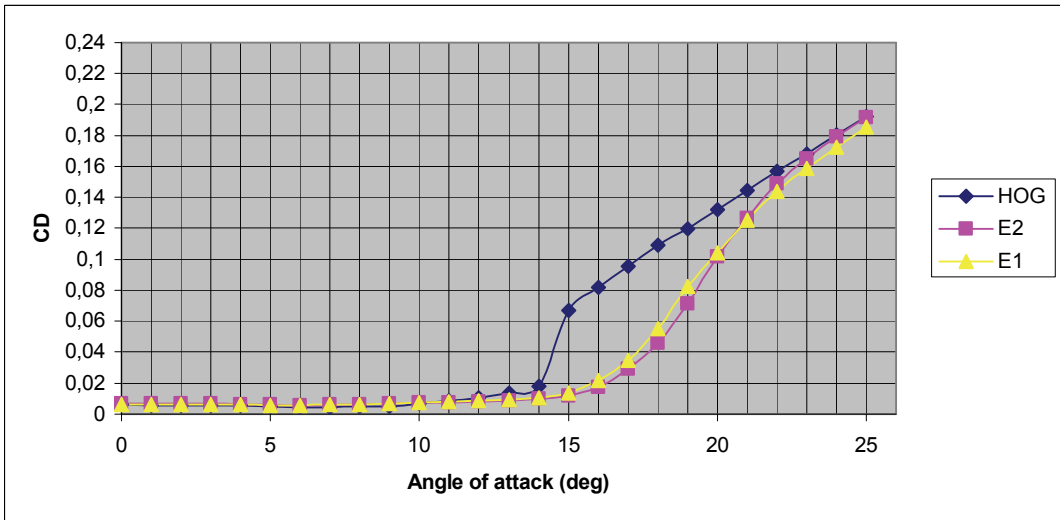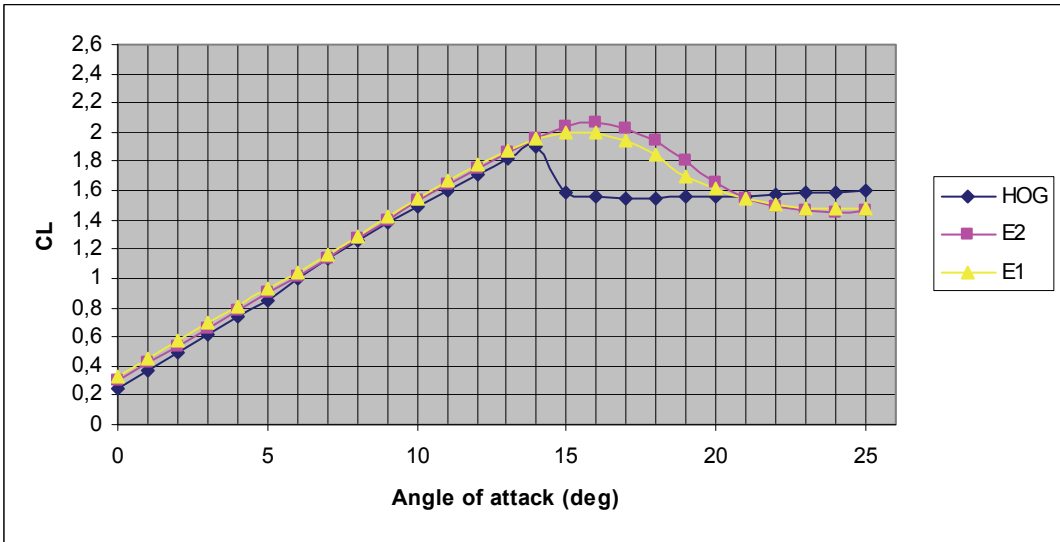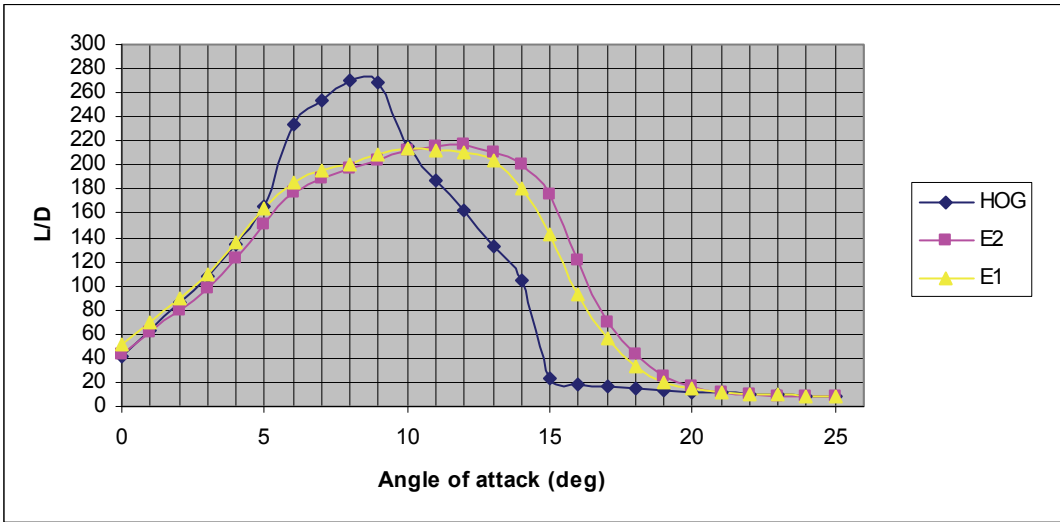
Figure 5.8.6 – E2 performance characteristics

5.9 NACA 63$_2$-415

We now have a good idea about how the pressure distributions can be manipulated to give the performance we want. It is now time to start focusing the work towards finding a final design. It is therefore useful to take a close look at the kind of profiles that are traditionally used at the outer parts of wind turbine blades, to get a better idea about how the airfoil should behave. According to several reports, a much used wind turbine tip profile is the NACA 63$_2$-415 [14][18]. It is almost identical to NREL airfoils designed for the same purpose, and we can therefore assume that this is a very well adapted design.
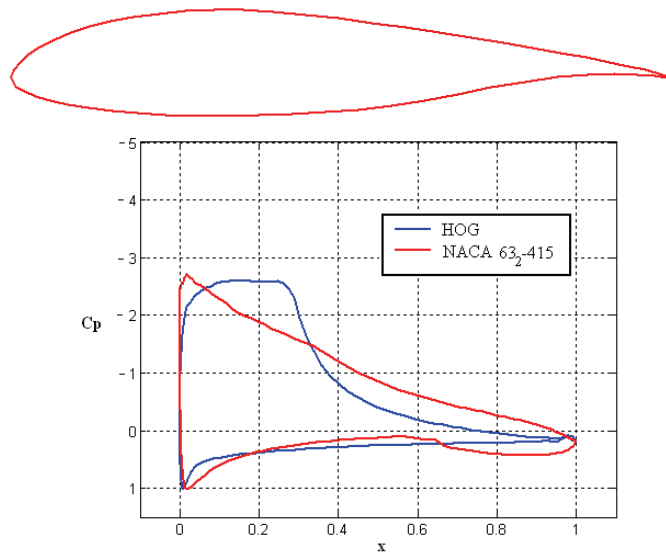
Figure 5.9.1 – illustration of shape and pressure distribution at α = 8º.

	L/D (n=9)	L/D (n=3)	Thickness (%)	Area (%)
NACA 63$_2$-415	165 (4º)	138 (5º)	15.97	9.91
Modification	-38.9 %	-24.2 %	+2.7 %	+22.2 %

Table 5.9 – NACA 63$_2$-415 compared to HOG

The performance level of this airfoil is only L/D~165, a lot lower than what we are aiming for in this project. However, it has the ideal characteristics in terms of stall and stability. It reaches peak performance very early, so it would be optimized for a low angle of attack. The stall is soft, and has a continuous, low curvature. The transition point moves rapidly to the leading edge. This gives identical stall characteristics for both levels of Ncrit, and identical level of performance for angles of attack above ~10º. Below that, performance is only slightly reduced. The pressure recovery can be seen to be an almost constant recovery from nose to tail, not unlike the Naca 4412.

The Lift and drag curves starts bending very early, and has a more continuous curvature the whole way, unlike the high lift airfoils which have a linear operational area, and then a relatively sudden stall. This constant curvature of the Naca 63$_2$-415 is due to the negatively tilted trailing edge. This is an important feature called a "separation ramp" [17].
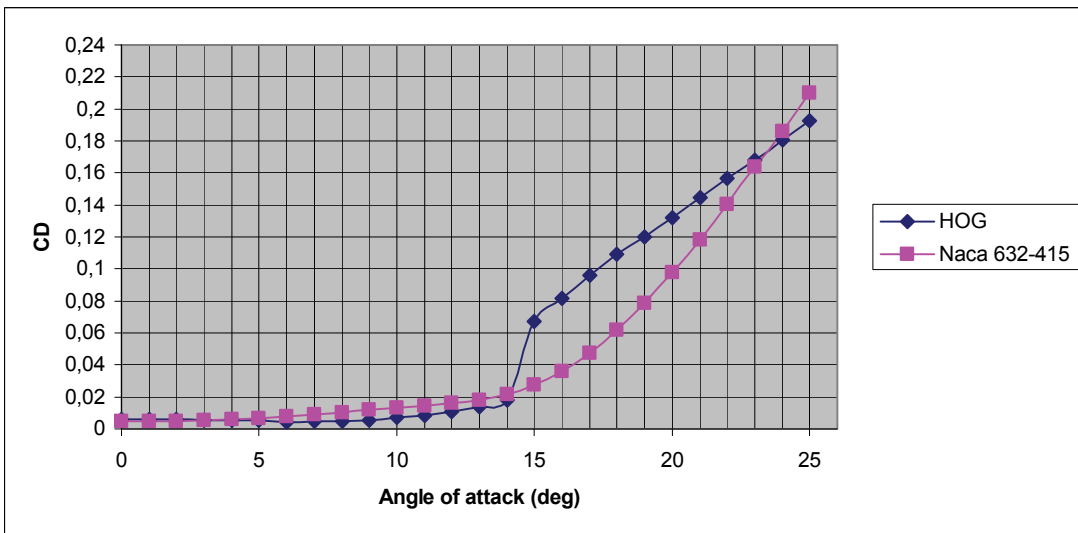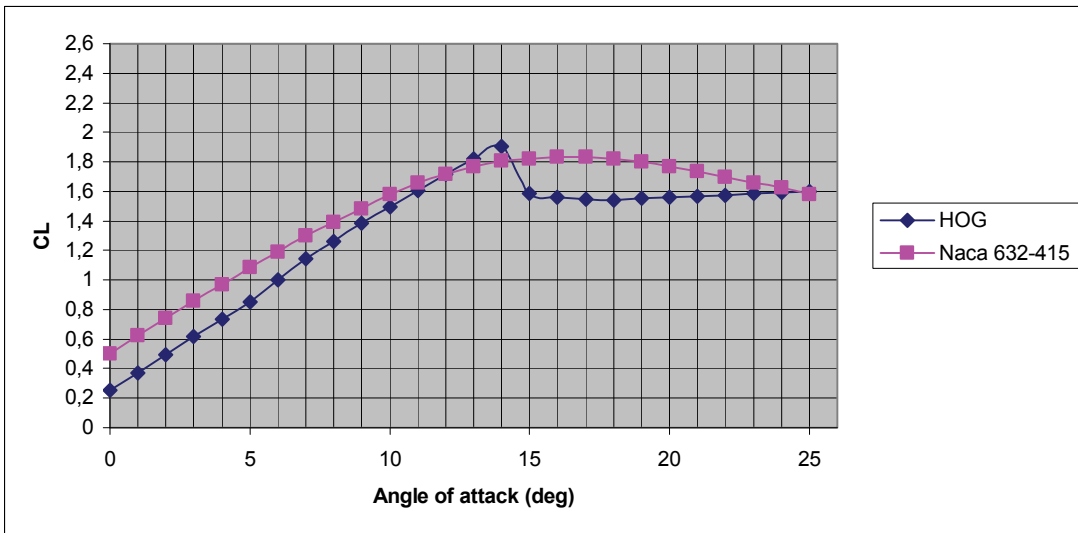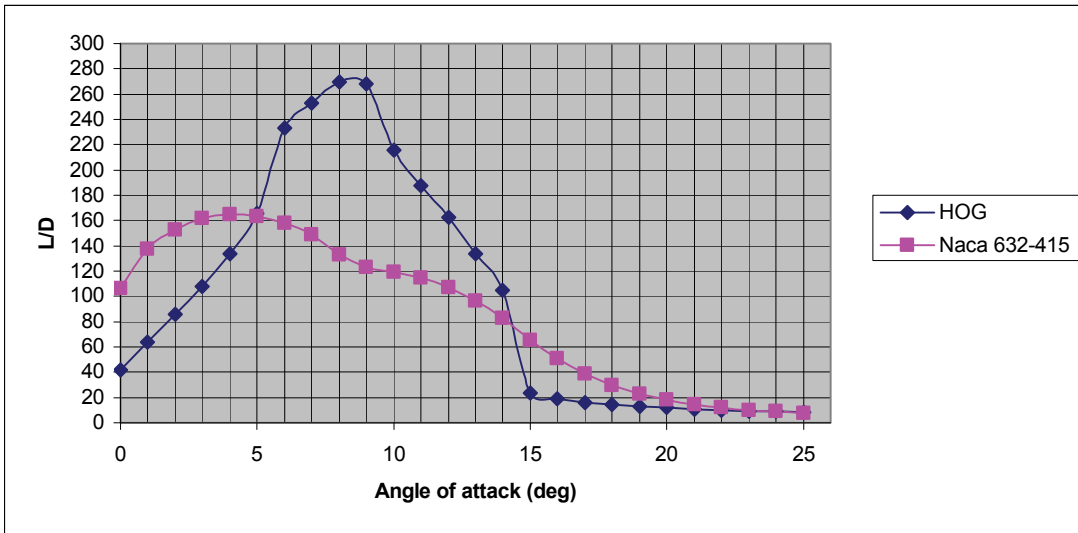
Figure 5.9.2 – NACA 63$_2$-415 performance characteristics

A separation ramp is tilt down on the upper trailing edge of airfoils. The ramp limits the effects of separating flow, thereby giving the profile a smoother stall. It does increase the drag slightly, and some loss in lift at high angles of attack, but the losses have proven negligible compared to the improved operation in the near stall area. Therefore, this feature is present here, and in almost every modern NREL-profile [16]. It can therefore be assumed to be of great benefit to wind turbine blades.
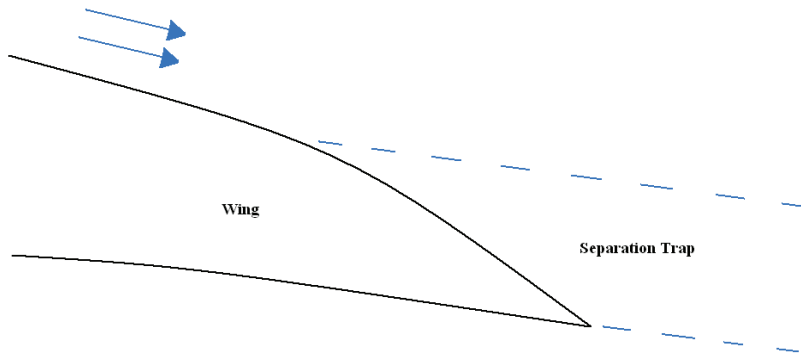
Figure 5.9.3 – Illustration of separation trap at trailing edge

The separation ramp works by having a relatively sharp "bend" that turns downwards at the back tip of the wings upper side. The design philosophy behind this feature is that it will allow separation to occur quite easily at the back tip, but it will be confined to the little space created by the ramp, meaning it will be locked in by the sharp bend. In other words, it is better to allow a little separation that can be controlled, rather than trying to avoid separation all together.

Stagnation will occur very early behind the separation trap. This will cause a "bubble" of stagnated flow to shape the trailing edge seen by the oncoming flow, in effect working as a "smart wing" which adapts its shape after varying conditions, thereby letting the pressure distribution adapt to the current situation. This is one of the reasons for this profiles' very gradual change in performance with increasing angles of attack. The lift and drag graphs can be seen to start bending very early. This is due to the stagnation reducing lift and increasing drag. This is not good for performance in this region, but it gives a very gradual transition to the stalled region, and therefore helps giving gentle characteristics.

An important thing to understand about separating flow is that there is no such thing as a stable separation. The separation point will oscillate back and forth, giving unstable lift and drag. This problem is what the separation trap is trying to compensate for. At the back, separation can occur quite easily, as the dp/dx-tolerance is at the lowest. But above the "sharp bend", the wing has an area which can tolerate a lot higher dp/dx. The separated flow will therefore not be able to move over the bend, thereby locking the separation in. The separation point will still oscillate back and forth, but it will be confined into the tiny ramp area, thereby not being able to cause significant trouble. In the end, the separation will move over the bend, but until then, the ramp helps provide stable operation for the early parts of separation. And even after moving over the bend,

the rest of the wing is designed so the separation will move forward very slowly, and therefore avoids any sudden change when the trap stops functioning.

It is very interesting to see how well the high-lift technology allows itself be combined with a separation ramp. The A and C profiles show extreme performance in lift and range respectively, but are troubled by to variable and dramatic stalls. It is therefore attempted to make versions of these profiles with a separation ramp. This will hopefully give more gradual and stable operation when approaching the stall area. Another good effect coming from the separation ramp is that the lift coefficient can be increased. Since the pressure is not supposed to be fully recovered when approaching the back tip, and rather have the quick jump to Cp_{te} over the separation ramp, this means that the whole pressure distribution can be "lifted up". This results in a generally lower pressure over the entire upper side of the airfoil, which will give higher lift.

5.10 AR
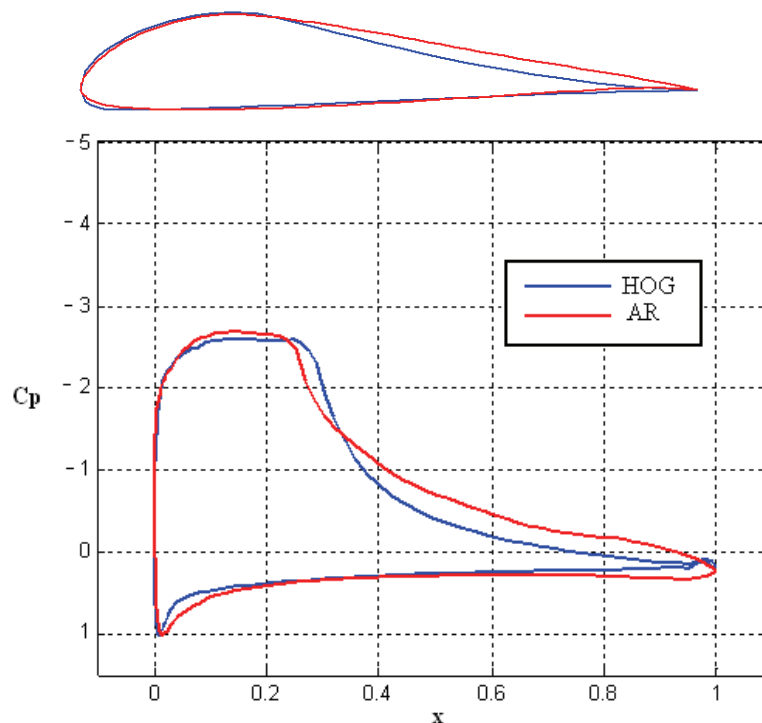
Figure 5.10.1 – illustration of shape and pressure distribution at α = 8°.

We know that having late transition to turbulent flow gives better performance, but more unstable characteristics. The compromise decided on, was therefore to design an airfoil which had a late transition point in the operational area, but as soon it moves above this region, the transition point should move rapidly forward, in order to get to the leading edge before entering the stall region. This will ensure constant stall characteristics. The modification attempted to achieve this was to change the leading edge slightly, so that a pressure spike would appear for angles of attack above the design region. The appearance

of this adverse pressure gradient would hopefully rapidly move transition forward, so the point of stall will not change with varying conditions.

	L/D (n=9)	L/D (n=3)	Thickness (%)	Area (%)
AR	254 (9º)	198 (7º)	15.59	9.03
Modification	-5.9 %	+8.8 %	+0.27 %	+11.4 %

Table 5.10 – AR compared to HOG

This new pressure distribution gives brilliant performance, and is probably the best profile created in this project. As expected, the lift coefficient is consistently higher, while drag stays in the same range as before. It has good performance for low angles of attack, which has been a missing quality in the earlier profiles, and it is also slightly better than the HOG for higher angles of attack. Performance is only marginally reduced for the peak performance range, with a maximum L/D ratio of 254, by far the highest of any of the soft stalling profiles in this report. This shows that the penalty you pay in drag for the separation ramp is low compared to the increase in lift. The stall is also of acceptable proportions, and it moves little with increasing roughness. Appendix 10.16 shows only a slight shift inwards. From figure 5.10.2, the attempted pressure spike is seen for $\alpha = 15º$. It helps the transition point move forward faster than for similar profiles, and it reaches the leading edge area at $\alpha\sim14º$. This causes the airfoil to have quite stable stall characteristics, with only a minimal shift between the simulations (app. 10.16). The performance area is, as expected, a bit reduced with roughness, but not much compared to other high-lift profiles. The L/D-curves have the same general shape, even though the Ncrit = 9 simulation peaks 2º degrees later due to an extended high performance area. However, since this airfoil has higher lift, it reaches a lift coefficient of 1.33 at angle of attack 7º. This means that it is probably unrealistic to have a higher design angle of attack than this. So the ideal design point will not change with roughness. At angle of attack 7º, the Ncrit = 9 simulation has a L/D-ratio of 232, which is still spectacular.
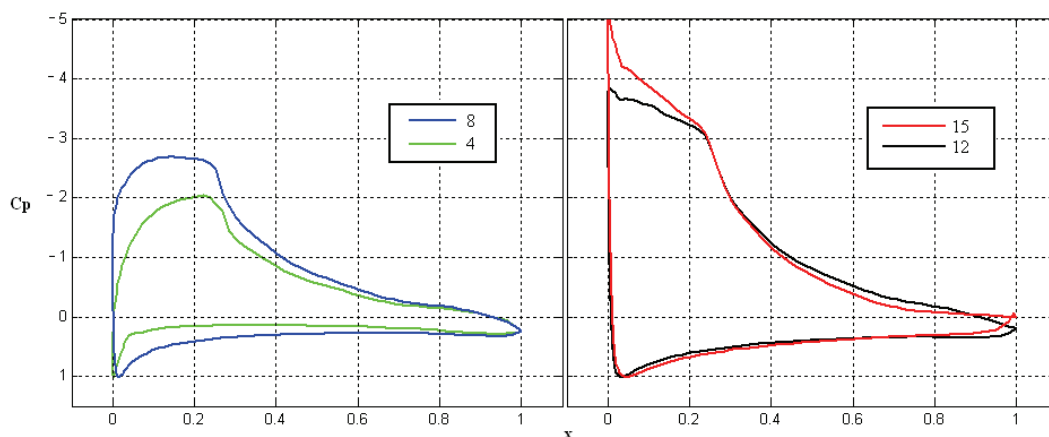
Figure 5.10.2 – AR pressure distribution. Notice the small pressure spike for high angles of attack (15º).
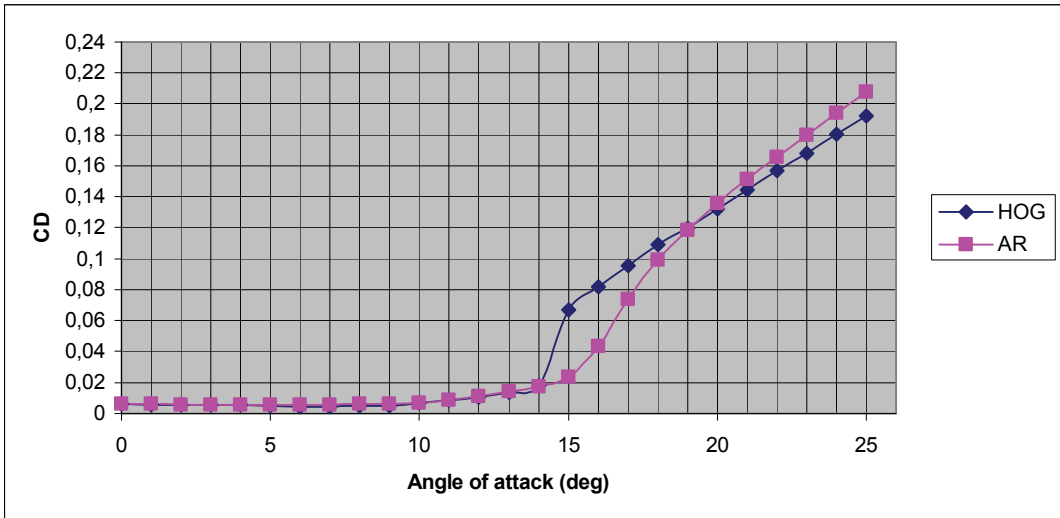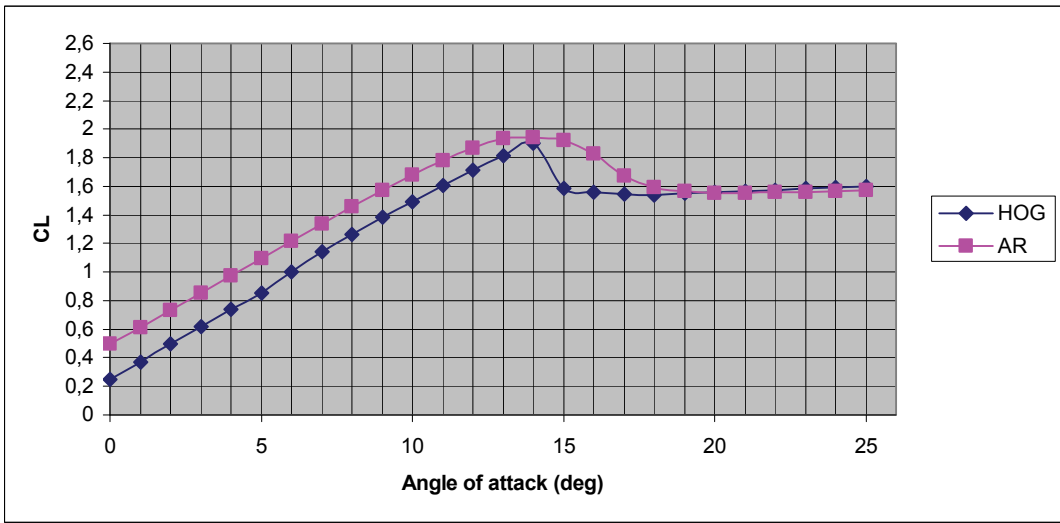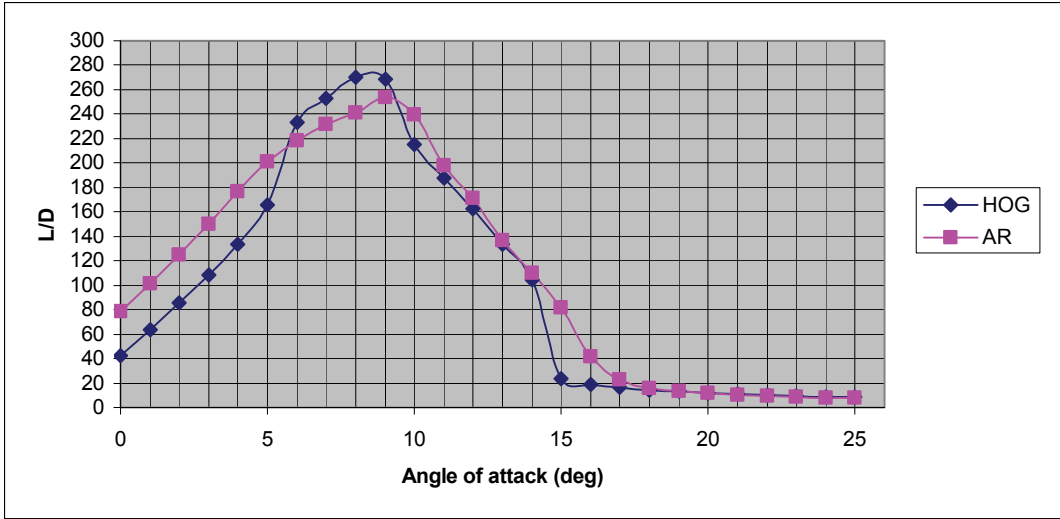
Figure 5.10.3 – AR performance characteristics

When comparing the Ncrit = 3 simulations, it is clear that the AR is an all round better profile compare to the HOG. It has better performance for every angle of attack, it stalls later and softer, and has more stable performance. It has a slightly thicker tail, but is in the same size range.
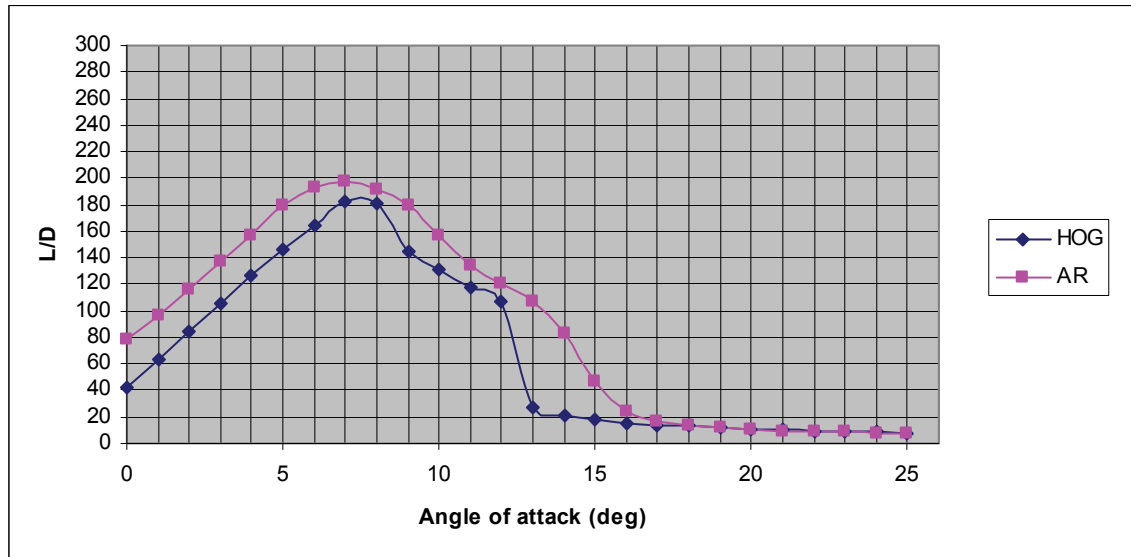
Figure 5.10.4 – L/D ratio. HOG vs AR at Ncrit = 3.

The AR appears to have soft and stable enough characteristics to be used in a wind turbine. In figure 5.10.5, Fluent is seen to confirm the gentle stall of this airfoil. If used at the suggested angel of attack, 7º, it will increase the L/D-ratio by 40.6 % compared to the standard profile, Naca 63_2-415, at its maximum angle, 4º.
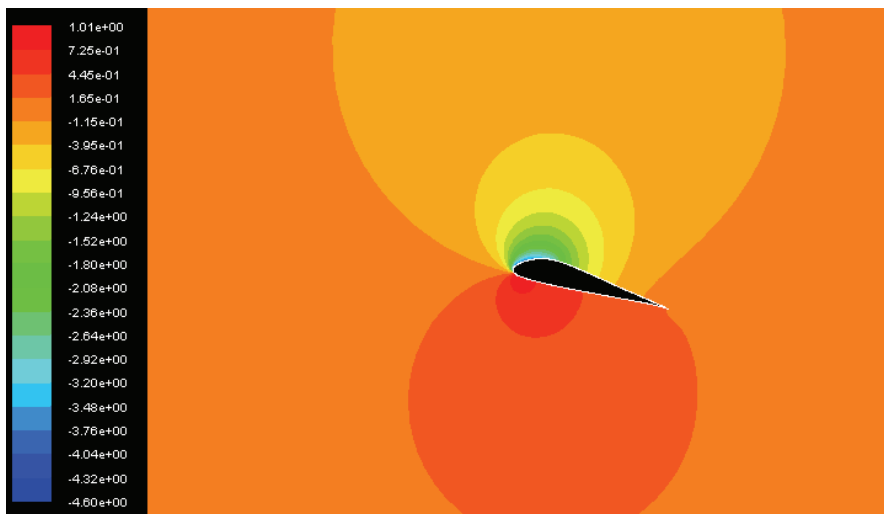
Figure 5.10.4 – CFD simulation, coefficient of pressure at $\alpha = 14º$.
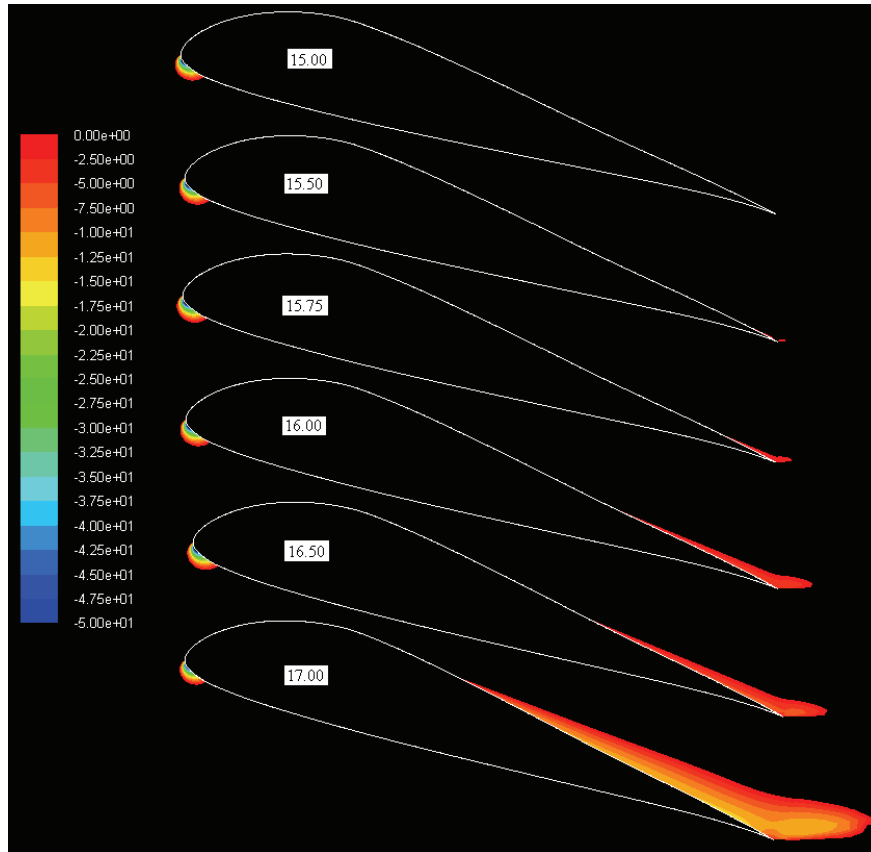
Figure 5.10.5 – CFD simulation, reversed flow.

As is characteristic for an airfoil using a separation ramp, its lift and drag curves will start
bending quite early. The AR profile is seen to have curved lift and drag curves above
~10º. Figure 5.10.5 clearly shows that this is not due to separation, as it occurs much
later. Rather, it is the effect of stagnation behind the separation ramp.

The inclusion of a separation ramp in an A-type distribution gave very good results. The
next step was to attempt the same for a C-type distribution. These had a remarkably
stable and long lasting performance, but were troubled with being bad for low angles of
attack and having a dramatic, variable stall.
This led to the CR profile, where the same modifications were made. The whole
distribution was lifted up, and a ramp was included at the back.

5.11 CR
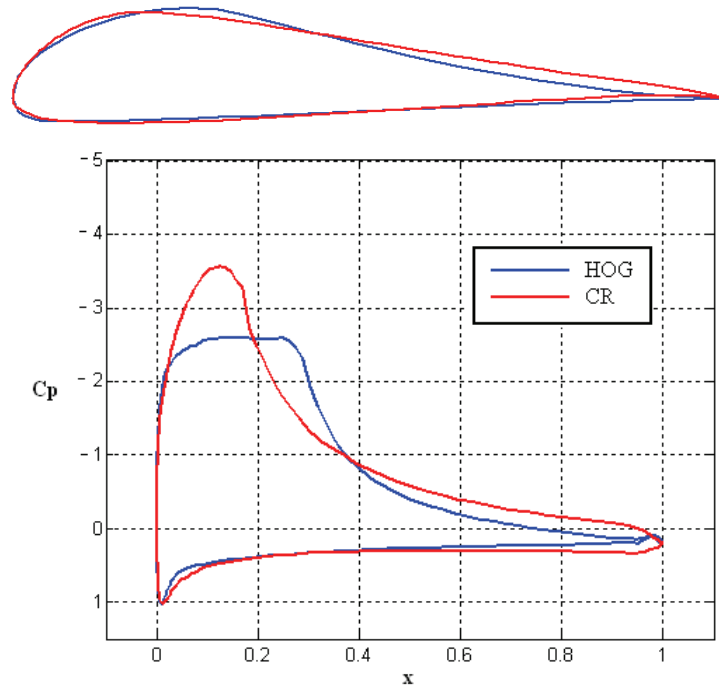
Figure 5.11.1 – illustration of shape and pressure distribution at α = 8º.

	L/D (n=9)	L/D (n=3)	Thickness (%)	Area (%)
CR	222 (12º)	209 (11º)	15.52	8.59
Modification	-17.8 %	+14.8 %	-0.27 %	+ 5.8 %

Table 5.11 – CR compared to HOG

The operational range is, again, very large, and the peak area gives performance ratios between 194 and 222 for 10º angles of attack. This time, it shows a much more rounded stall, and it is a lot better for low angles of attack. The modification appears to have worked as planned. The C profiles had a very small performance drop with increasing roughness, and this quality is preserved. This actually results in the highest L/D-ratio of all for Ncrit = 3 simulations so far, with L/D~209. This stability is not because the transition point is at the leading edge, rather it stays put at X~0.18, right at the start of the pressure recovery. As for the original C-profiles, the transition point leaps forward when approaching stall, and cases variable stall. The stall shifts in ~3º degrees between the two simulations (app. 10.17). Even so, the stall is still occurring quite late, and in an application that can be controlled from seeing angles of attack above ~15º, this profile would deliver very high performance over the whole range.
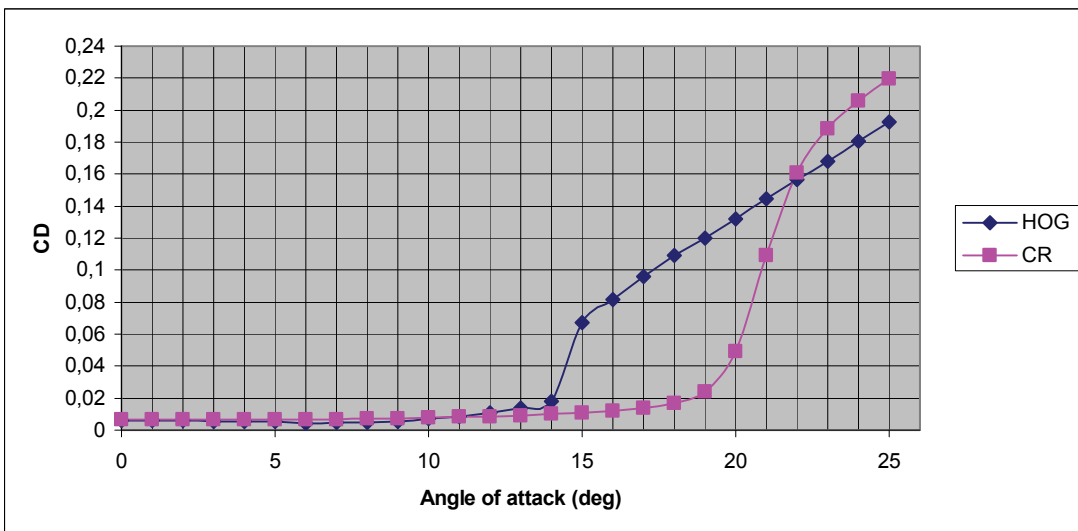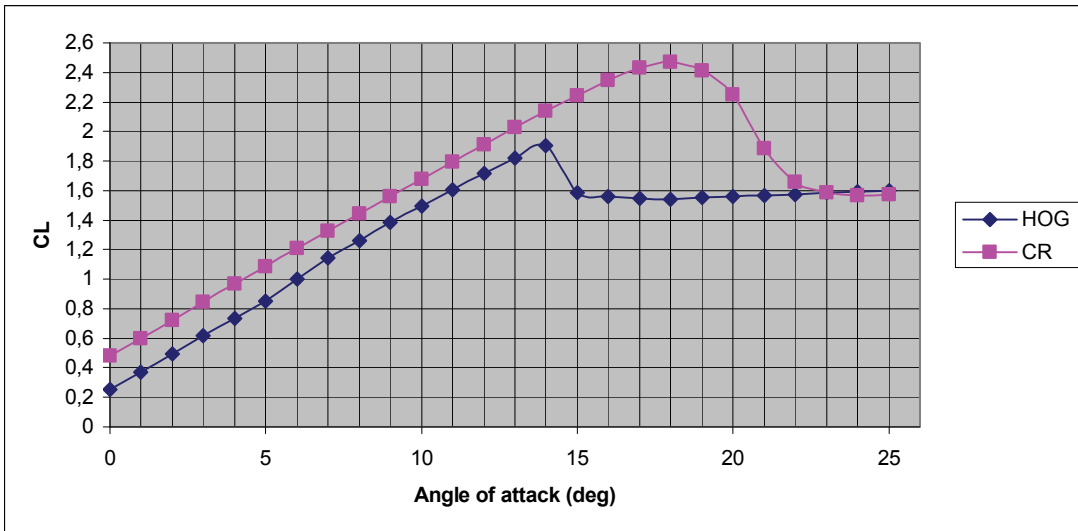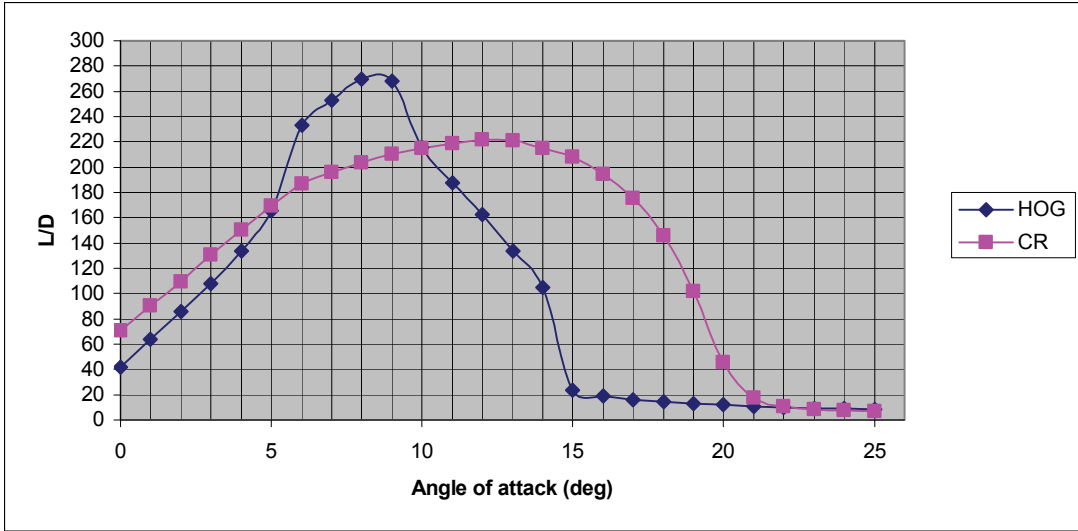
Figure 5.11.2 – CR performance characteristics

It must be remembered that it is probably not likely that a wing can be optimized for a lift coefficient higher than ~1.3 when used in a wind turbine. This means, in this case, that the design angle of attack can not be higher than ~7º. It is therefore unfortunate that the C-profiles have their peak performance for high angles of attack, and will not be able to utilize their quality sufficiently. For comparing both Ncrit simulations for the AR and CR, it is clear that a stable performance around $C_L = 1.3$ will work better with the AR profile, as it is better for low angles of attack, peaks earlier, and flattens out for higher angles of attack.
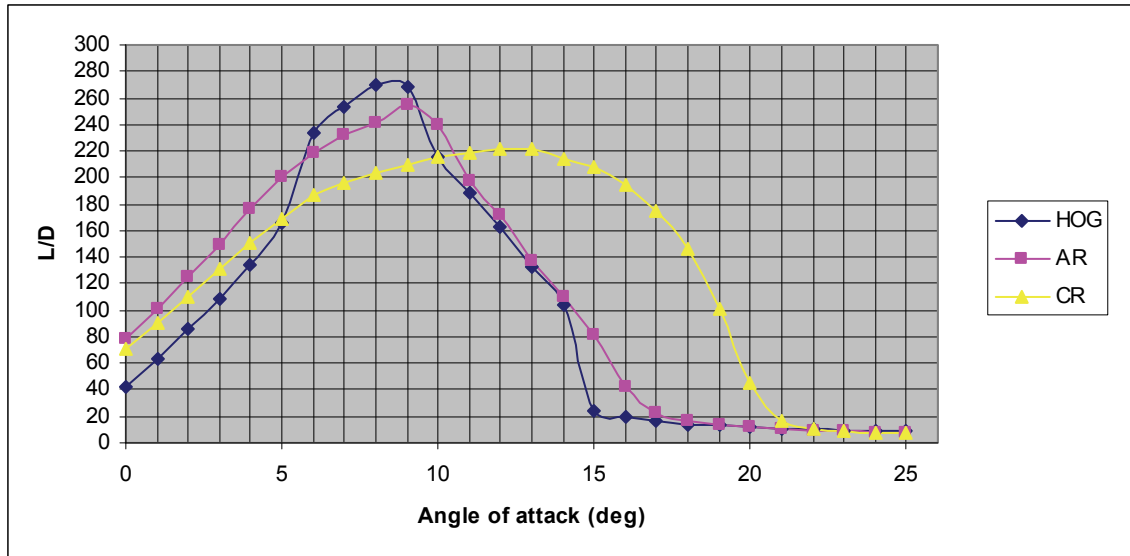
Figure 5.11.3 – L/D-ratio. CR vs AR vs HOG at Ncrit = 9.
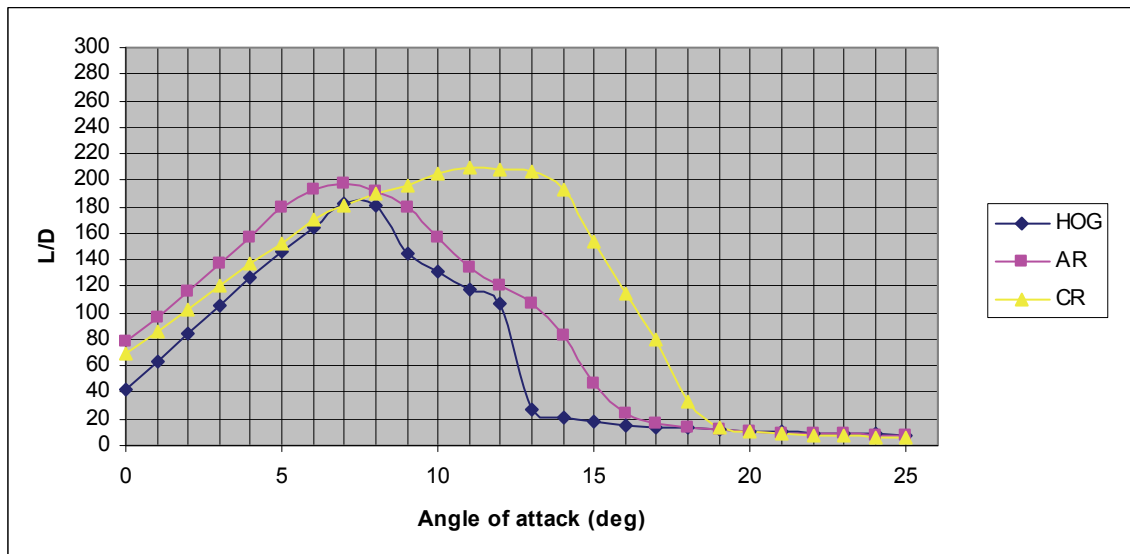
Figure 5.11.4 – L/D-ratio. CR vs AR vs HOG at Ncrit = 3.
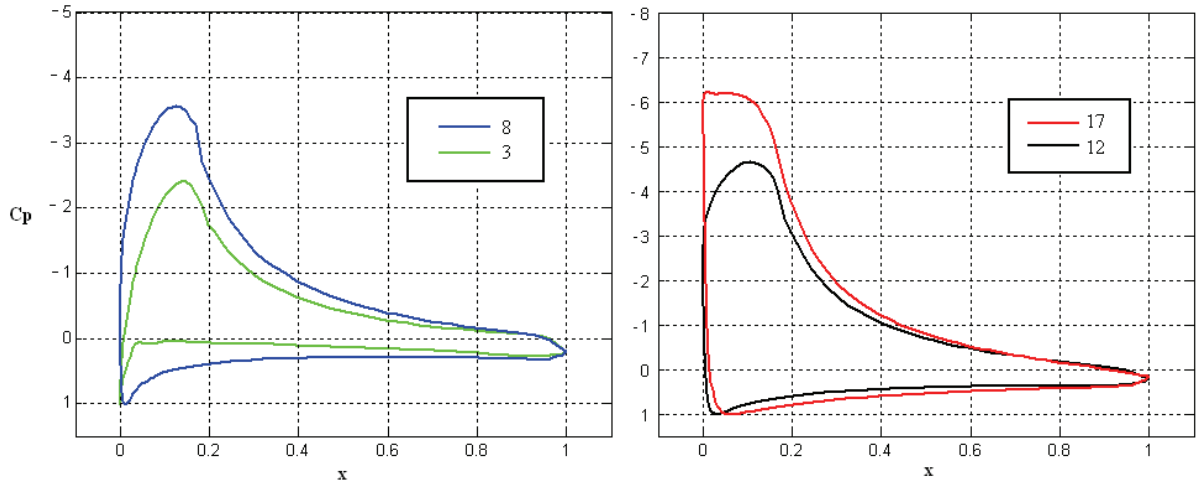
Figure 5.11.5 – CR pressure distributions

Figure 5.11.6 shows the rapid, but late separation. Not surprisingly, fluent predicts separation earlier than Xfoil. For the AR profile, fluent and Xfoil predicts separation at the same angle, as this profile has a much more stable stall point as boundary layer conditions change. This illustrates well the difference in stall stability.
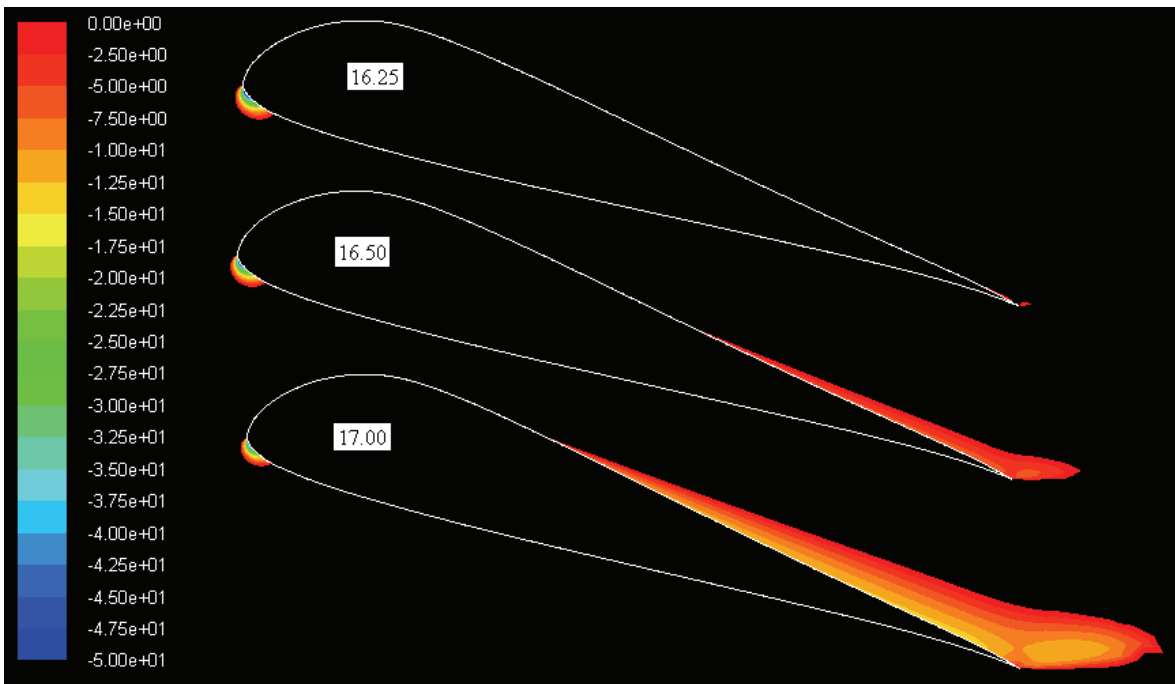
Figure 5.11.6 – CR profile, CFD simulations, reversed flow.

6 Further experimentation

6.1 Thinner profiles - TR

One of the reasons for this project was that it is needed to reduce the top weight of turbines, and thinner wings could accomplish this. The main work in this report has focused on getting better performance out of airfoils, but it was also interesting to see how much thinner it was possible to make the airfoil while keeping the same performance. It was therefore decided to modify the NACA 63_2-415, and see how thin it could be made while keeping its original performance. This resulted in the TR profile
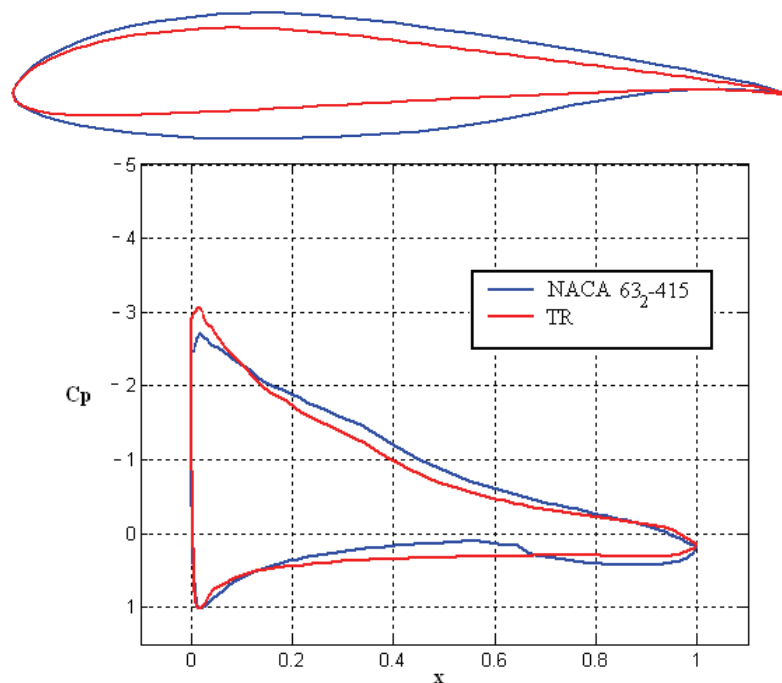
Figure 6.1.1 – illustration of shape and pressure distribution at α = 8º.

	L/D (n=9)	L/D (n=3)	Thickness (%)	Area (%)
TR	169 (6º)	135 (6º)	10.61	6.33
Modification (63_2-415)	+2.4 %	-2.2 %	-33.5 %	-36.2 %

Table 6.1 – TR compared to NACA 63_2-415

As can be seen from figure 6.1.2, the performance is very similar. They also have the same sensitivity to roughness and have similar transition points. The airfoils should therefore behave almost identically. The TR profile is 33.5 % thinner, and has 36.2% less cross sectional area. This would indicate a significant reduction in weight for a wing, while keeping almost identical performance for all conditions compared to the original NACA profile.

100
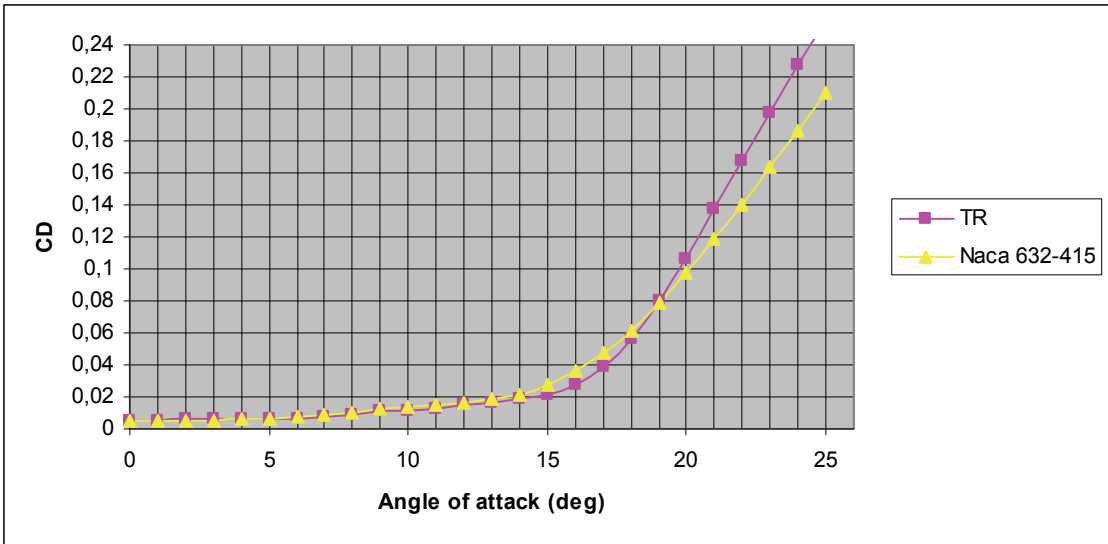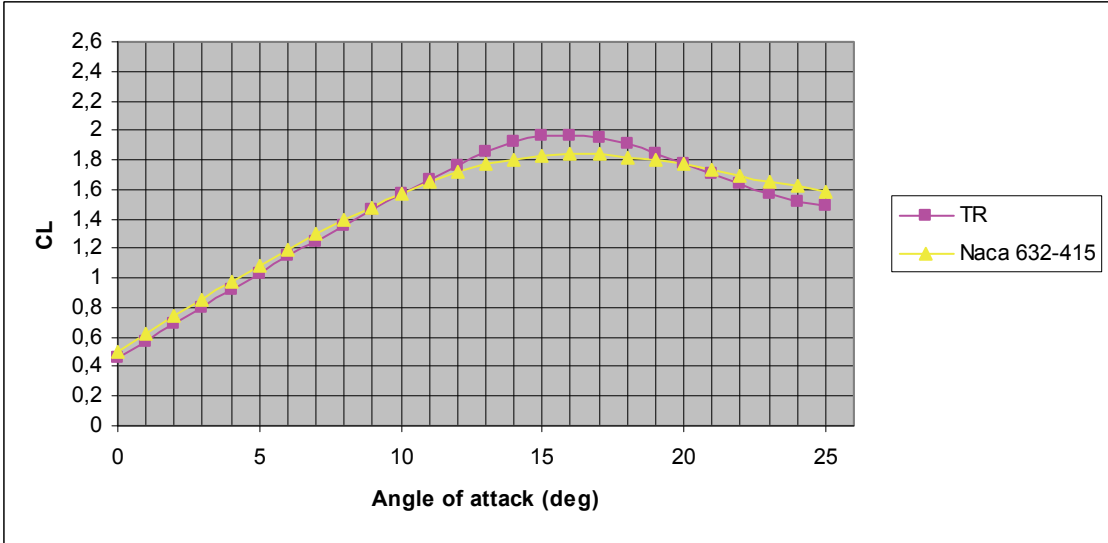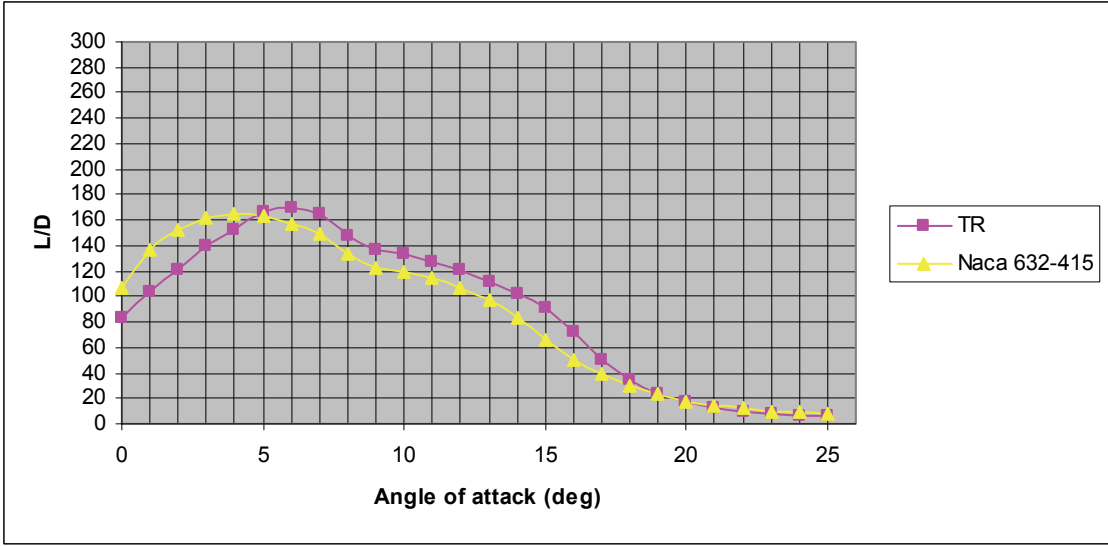
Figure 6.1.2 – TR performance characteristics

6.2 Improved high lift profiles

6.2.1 S1

In this project, it has been attempted to smoothen out the stall characteristics of the HOG profile. However, in order to investigate the high-lift technology closer, it was also interesting to ignore stall for a while, and see if it was possible to make a profile with an even higher L/D-ratio. The S profiles resulted from an attempt to beat the maximum performance of the HOG.

The S1 profile can be seen to have the general performance shape of the HOG, but has maximum performance area widened by 2º degrees, and it stalls 2º degrees later. Also, its maximum performance reaches L/D~ 273, marginally better than the L/D~270 of the HOG.
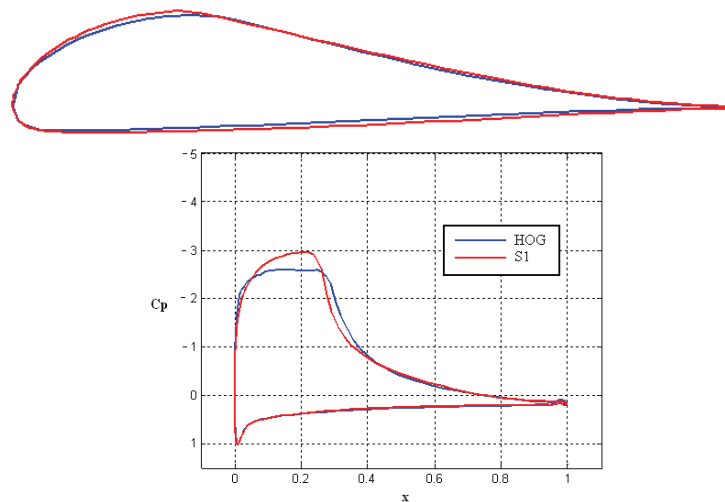
Figure 6.2.1 – illustration of shape and pressure distribution at α = 8º.

The S1 can be seen to be a better high-lift profile than the HOG, as it keeps higher performance longer, reaches a higher maximum performance, and stalls later. It is basically the HOG with 2º degrees extra operational area, and those 2º degrees have been added to the area of maximum performance. The design is optimized for α = 11º. This is the reason for the late peak. It still appears to have almost as good performance as the HOG for lower angles, thereby giving the increased high-lift area.

	L/D (n=9)	L/D (n=3)	Thickness (%)	Area (%)
	273 (11º)	231 (9º)	16.56	8.78
Modification	+1.1 %	+26.9 %	+6.5 %	+8.2 %

Table 6.2.1 – S1 compared to HOG

It is quite insensitive to roughness regarding performance, due to a stable stagnation point in the operational area, and reaches L/D~231 for the Ncrit = 3 simulation, which is remarkable. In comparison, the HOG preformed L/D~182 for the same simulation. The stall shifts 2º degrees in between the simulations in (app. 10.19), the same as the HOG.
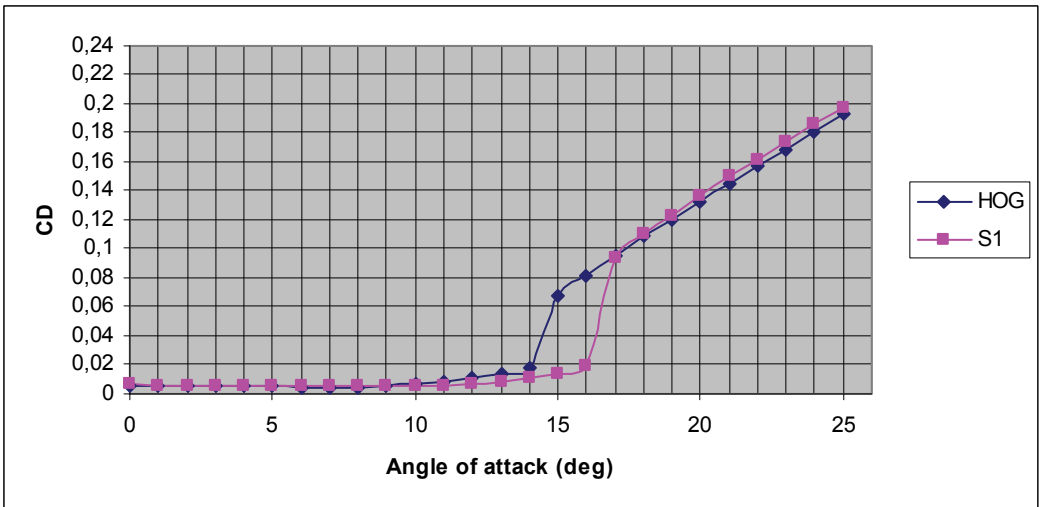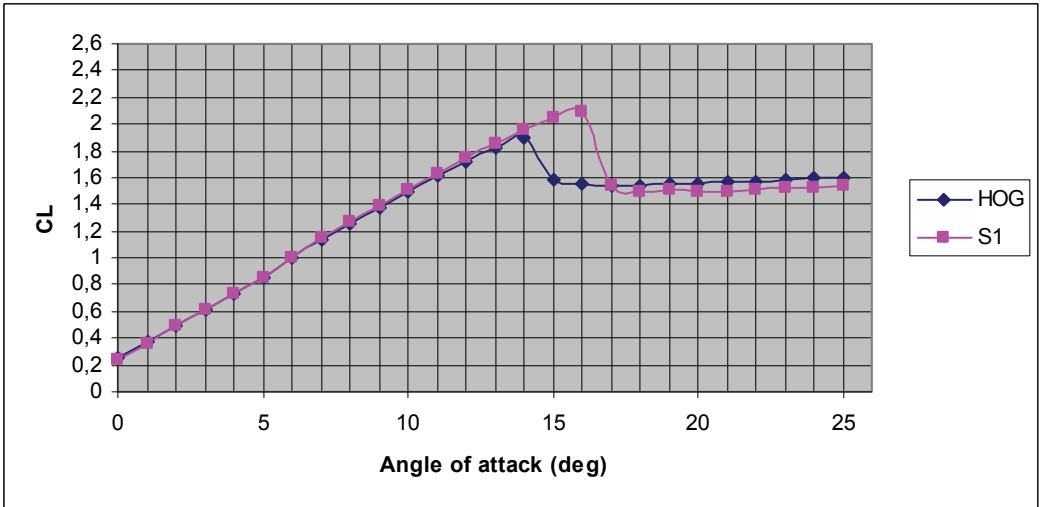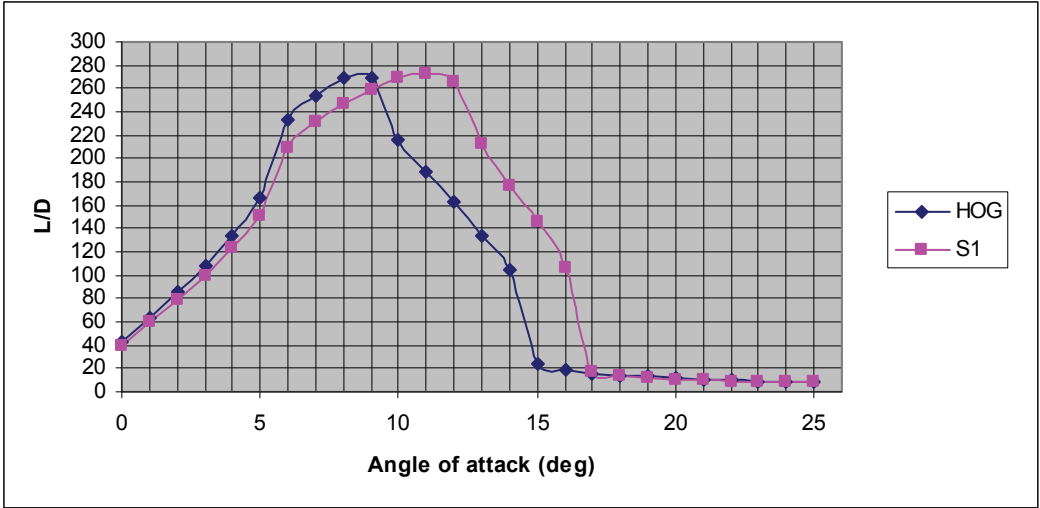
Figure 6.2.2 – S1 performance characteristics
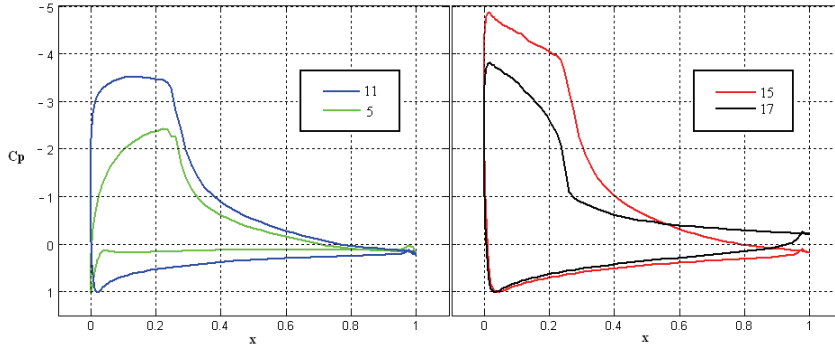
Figure 6.2.3 – S1 pressure distributions. Can be seen to be optimized with flat rooftop at α = 11º.

6.2.2 S2
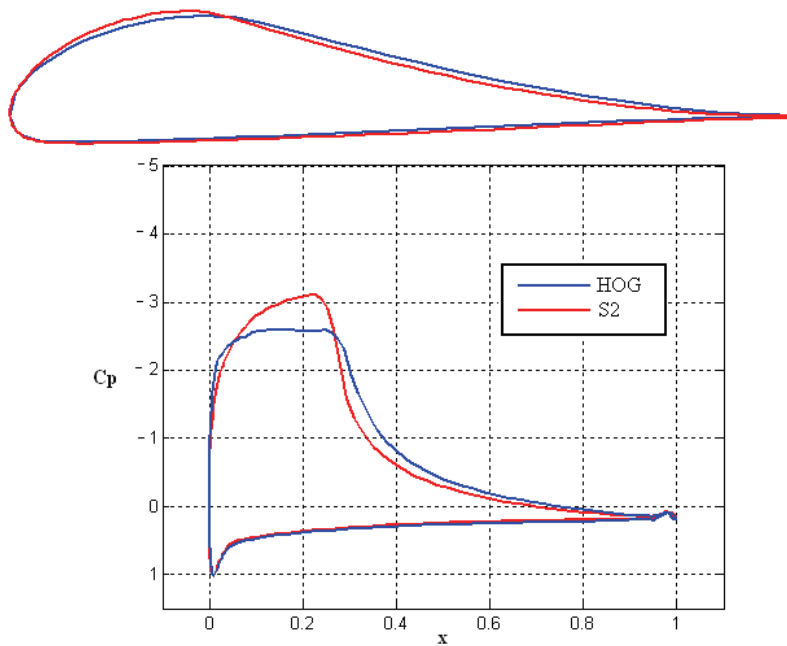
Figure 6.2.4 – illustration of shape and pressure distribution at α = 8º.

Another attempt, S2, was given an even higher pressure drop, and optimized for α = 12º. This resulted in a profile which behaves similar to the HOG and stalls at the same time, but keeps higher performance longer and reaches a higher maximum. The S2 reaches L/D~286, which is the highest value recorded in this project. It delivers an L/D ratio of over 250 for 6º angles of attack. As the S1, it is also insensitive to roughness regarding performance, and also sets a record for performance at Ncrit = 3 with L/D~253. The stall varies the same amount as for the other pure high-lift airfoils, and shifts in 2º degrees (app.10.20).
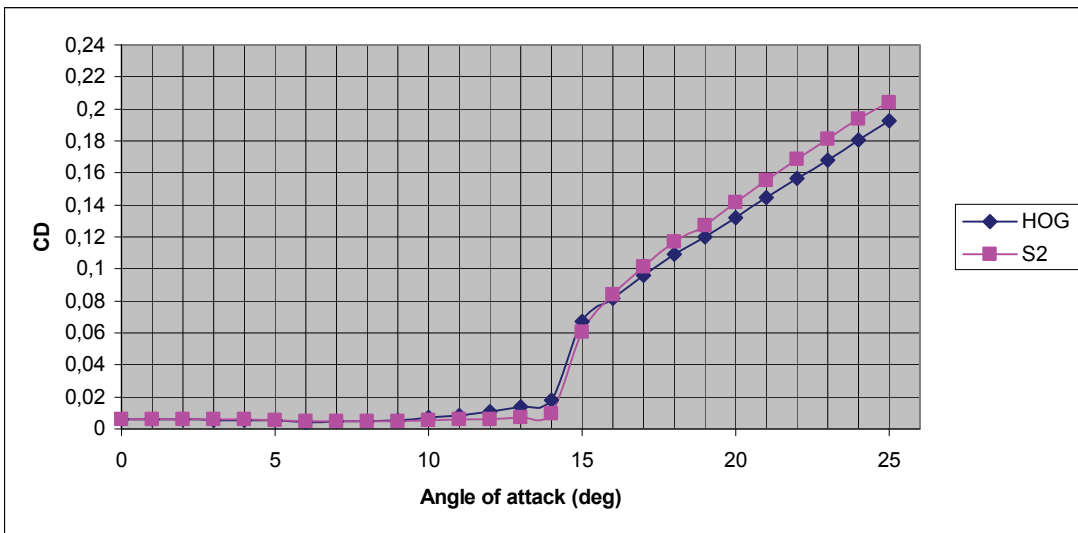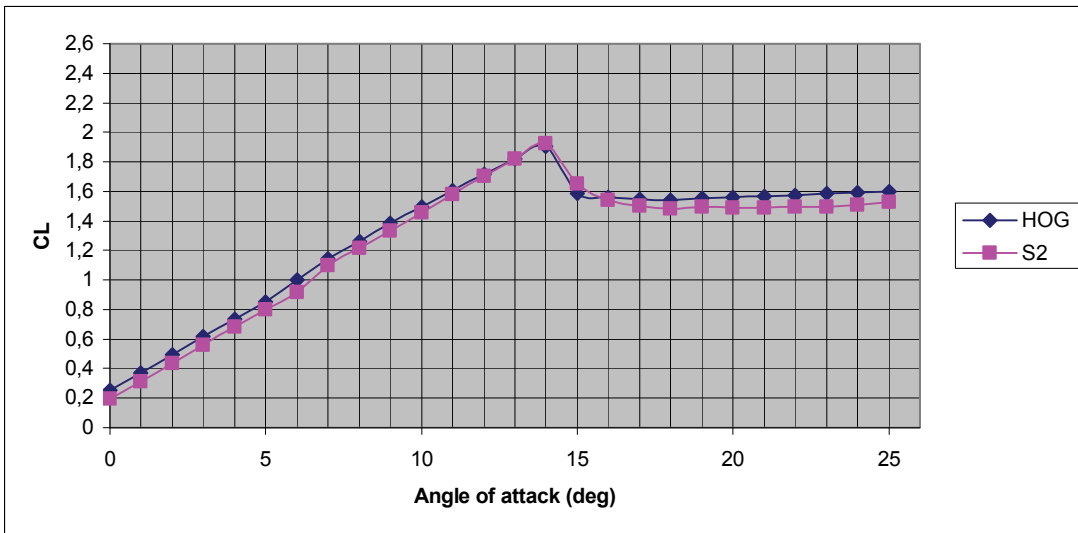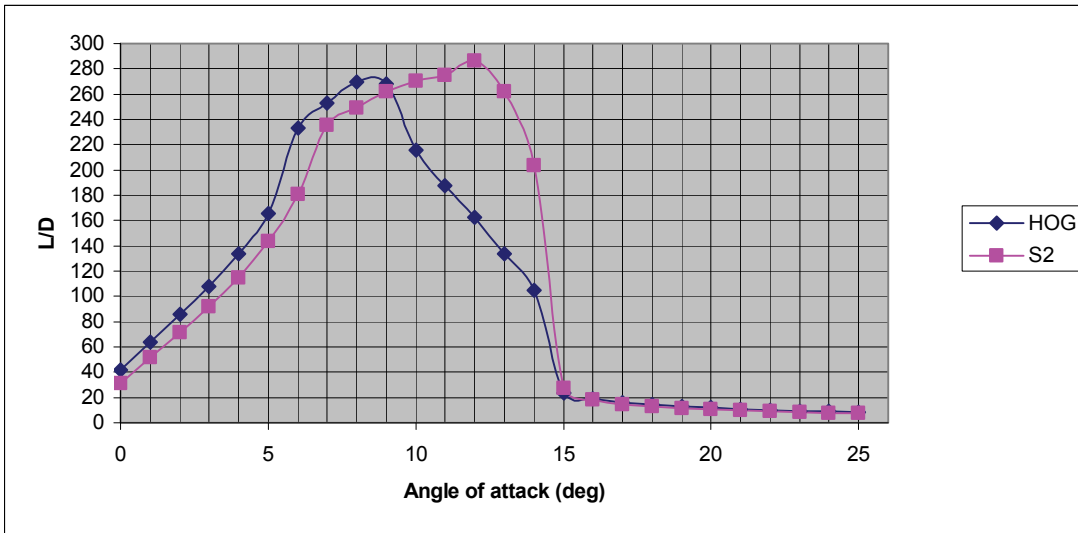
Figure 6.2.5 – S2 performance characteristics

	L/D (n=9)	L/D (n=3)	Thickness (%)	Area (%)
S2	286 (12º)	253 (9º)	16.45	8.14
Modification	+5.9 %	+39.0 %	+5.8 %	+0.4 %

Table 6.2.2 – S2 compared to HOG

This can also be said to be a better high-lift profile than the HOG, as it has the exact same stall characteristics, but has a L/D-performance which is higher, and maintains high performance for a wider range, and maintains performance much better with varying conditions.
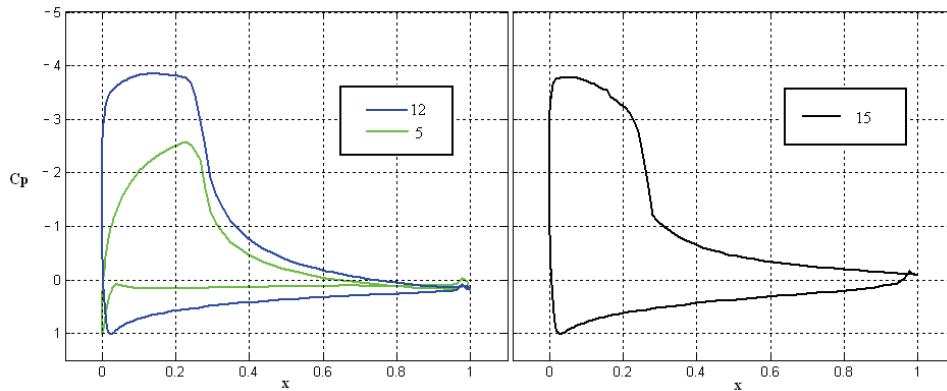
Figure 6.2.6 – S2 pressure distributions. Can be seen to be optimized with flat rooftop at α = 12º.

Figure 6.2.6 shows the pressure distributions of the S2, and it can be seen to be optimized for α = 12º, where the rooftop is flat. With increasing roughness, the maximum performance shifts inwards. From figure 6.2.7, it is clear that the S profiles maintain their performance much better than the HOG with increasing roughness, as they keep their transition points stable at the start of the pressure recovery for a wider range.
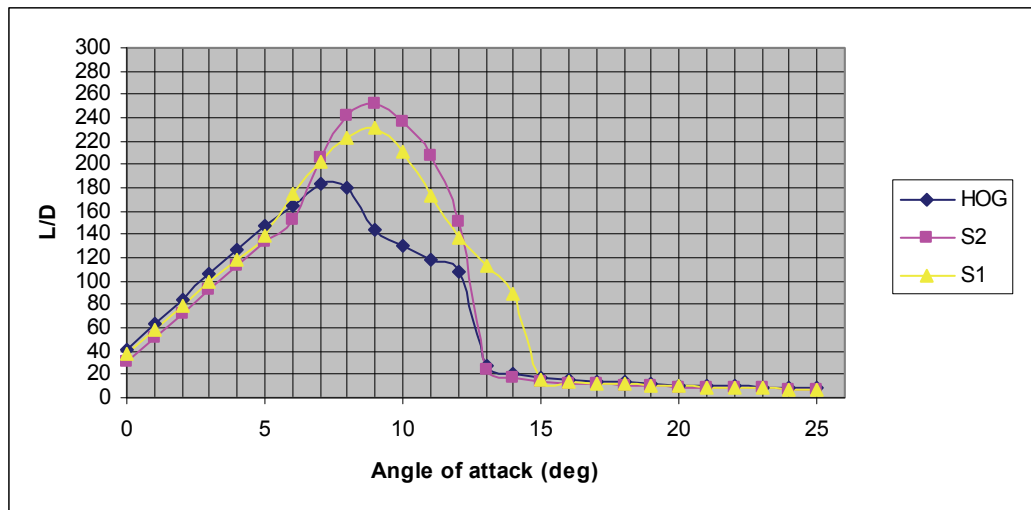
Figure 6.2.7 – L/D-ratio. S1 vs S2 vs HOG at Ncrit = 3.

7 Discussion

The work done in this report shows that there is a potential for implementing high-lift technology in wind turbines. It was possible to create profiles that had performance in the range of a pure high-lift profile, but appeared to stall softly and stably enough to be used in wind turbines. Exactly where the limit goes for what stall characteristics can be allowed in a wind turbine is not constant. It will vary with the over all system design, and where on the wing the airfoil is used. The most successful profiles created in this project have stalls that are gradual, slow, and without any sudden movements or extreme values. They therefore appear to be useful for wind turbines.

The profiles created appear to have significantly better performance than standard NACA and NREL airfoils. Several very good profiles were made of varying thicknesses, not only thin. This technology should therefore also be of interest for upwind turbines. For instance, the D2 profile was a very good airfoil with a thickness of 16.13 %, and it did not have a structurally weak tail. It was insensitive to roughness and had the softest stall of all profiles created in this project. This profile would be structurally usable for an upwind wind turbine, while delivering a maximum performance of L/D~222, which is 34.5% higher than the NACA 63_2-415 standard profile.
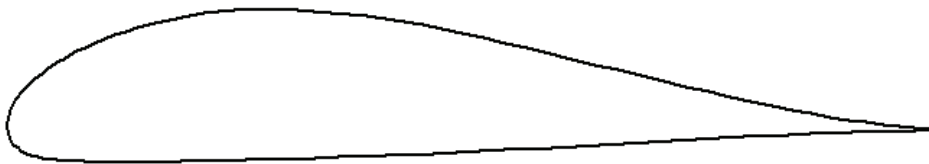
Figure 7.1 - D2 profile

Smoothing out the dramatic stall of the HOG profile was possible through redesigning the pressure recovery so that the very back tip of the wing separated first, and then have the separation gradually crawl forward. This was done by gradually approaching the local optimum Stratford distribution when moving back over the airfoil.

As discussed in chapter 4, it would be ideal to optimize turbine blades for slightly higher lift coefficients than what is currently used, in order to lower weight by having smaller chord lengths. The HOG profile has a very late rise in lift coefficient compared to the NACA and NREL profiles. In order to get a lift coefficient of 1.3, the HOG would have to be optimized for $\alpha = 8.5°$. This would place the operational point very close to the stall region. It was therefore desirable to find a way to have an earlier rising lift coefficient. The inclusion of a separation ramp at the back of the high-lift airfoils gave very positive effects. The transition to the stall area and operation during early stall was smoothed out, and resulted in a very docile stall. It also allowed the entire pressure distribution over the top side of the airfoil to be lifted up (lower pressure), giving a higher lift coefficient without significant increase in drag. This gave higher overall performance, including for

low angles of attack. The higher lift coefficients resulting from the inclusion of the separation ramp makes the profiles much more usable, and makes it possible to optimize turbine blades for high C_L.

It is important that an airfoil meant for use in wind turbines has stable performance and does not experience shifting stall characteristics with varying conditions.
It was found that the location of the transition point was very important in determining an airfoils performance. Since the transition to turbulent flow will vary with roughness on the wing, air turbulence and other air properties, this means that that the wing will have varying performance and behavior in varying conditions.
In order to secure stable performance, it is necessary to control the transition point as much as possible. Having the transition point at the leading edge is an effective way of doing this, as the transition will be unable to move any further. The application of an adverse pressure gradient quickly promotes the transition to turbulent flow, and can be used to control the transition point. The NACA airfoils used for comparison in this report are seen to apply an adverse pressure gradient almost immediately. In addition, for high angles of attack, they use a "pressure spike" which gives of a rather large adverse pressure gradient almost at the front of the airfoil. This secures transition close to the leading edge, and very stable performance.

A reason for the very high performance of the high-lift airfoils is that they have a late transition point. Laminar flow over the front secures low friction and minimum boundary layer growth. The flow then turns turbulent as it hits the adverse pressure gradient at the start of the pressure recovery. Therefore, when using the high-lift design in the operational range, it is not useful to have the transition at the leading edge. However, it is viewed as very important to have constant stall characteristics. In the final design, it was therefore attempted to modify the leading edge to have a pressure spike appear for high angles of attack only. This would allow the wing to have late transition and maximum performance at the operational range, and then have the transition point move rapidly forward for higher angles of attack, and reaching the leading edge before entering the stall region. This would secure constant stall characteristics, and as a side effect helped cause a more gradual transition to the stall area.

The Xfoil simulations were run two times with the critical amplification factor at 3 and 9 respectively, in an attempt to simulate varying roughness and air properties. The differences between these simulations give a good indication about how stabile the airfoil would be as conditions change. These simulations illustrate clearly the importance of controlling the transition points. The airfoils which had a moving transition point when entering the stall region (not reached the leading edge), had a highly variable stall occurrence.
Fluent does to some degree confirm the stability of an airfoil, as it usually predicted separation at the same angle as Xfoil for the airfoils with the transition point at the leading edge, while it often predicted separation a lot earlier for the airfoils with a moving transition point. This meant that the airfoils Xfoil predicted to have a varying stall were also the ones who showed the biggest difference between Fluent and Xfoil simulations, thereby showing that these profiles indeed were more unstable. This

indirectly proves Xfoil's prediction that these airfoils would be unstable in the stall region. It also shows that the airfoils Xfoil predicts to be stable, indeed perform similarly in other conditions, as the Fluent simulations have different turbulence modeling and boundary layer growth, but still gave the same result.

Parallel to this project, another student at NTNU, John Amund Karlsen, has done a project on comparing results from Xfoil/BEM, CFD and wind tunnel tests, to see how well they correspond [30]. The object being compared was a small wind turbine, R = 90 cm, standing in the wind tunnel at NTNU. He found that for this very small wind turbine, a critical amplification factor of 3 in Xfoil gave results that matched the tests. It is safe to assume that a large scale wind turbine, with a tip speed of ~90 m/s, would see more stable conditions, and be more useful to model with a higher value of Ncrit. At the same time, the default value for Ncrit in Xfoil, 9, was originally meant for testing aircraft wings. They would probably see higher speeds and encounter more stable air as they fly higher. It can therefore be assumed that this Ncrit value might be a bit too high for a wind turbine blade.

In total, we can feel safe that the value matching the actual conditions will be somewhere between 3 and 9. The two simulations run in Xfoil therefore represent the outer boundaries of expected performance. The actual performance should be somewhere in the middle. As long as the shift between the two simulations is small, the airfoil should therefore behave very stably in highly variable conditions, and is therefore assumed to be safe for use in wind turbines.

Even with the wide margin of error accounted for by the two Xfoil simulations and CFD, it must be remembered that these are relatively ideal 2D simulations. It will be necessary to do experimental tests in order to confirm that the adaptations work as prescribed in real conditions, and that there is no unforeseen problem with 3D effects or similar.

The enormous amount of information from each simulation done in this project is so vast, that it was impossible to include and discuss any more than the general characteristics. Still, the more detailed parameters were kept a close eye on to make sure that there are not any unwanted or surprising effects that do not show up in the results presented in this report. For instance, airfoils might have a highly variable aerodynamical moment, C_M. This can cause a structural challenge for the wing, especially for thin flexible wings. The airfoils presented here have very stable moment force, and should therefore not have any trouble with this. In fact, many of them have much lower and more stable C_M than the NACA-airfoils used for comparison. This might be yet another advantage of the high lift wings.

The increase in turbulence and boundary layer growth in the CFD simulations were also checked, to make sure that the models were behaving realistic. These phenomenons are extremely difficult to model, and no perfect model exists. CFD must therefore be run under detailed supervision, to make sure the models behave in a realistic way.
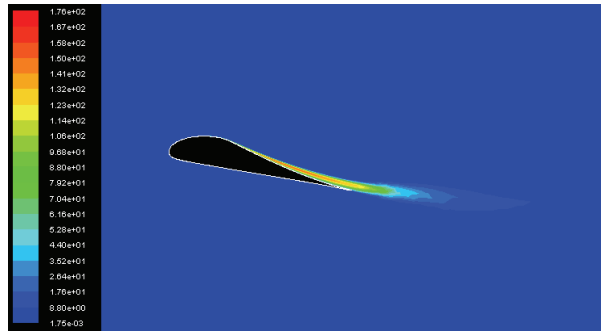
Figure 7.2 – CFD simulation of HOG profile at α = 12º. Showing turbulent kinetic energy, k.

The C profiles showed a unique ability to extend the region of high performance, and have a very late stall. They also had very stable L/D-performance with varying conditions, but a highly variable stall. The high performance area also occurred relatively late. The pressure distributions had very short, but big, pressure drop, followed by a slightly concave pressure recovery. The general shape is shown in figure 7.3.

They key to the performance characteristics of these airfoils is the short, but big, pressure drop. In terms of transition, it can almost be viewed as an elongated pressure spike. The shape will cause a large adverse pressure gradient to appear around X~0.2, which causes the transition point to be occur in this very short interval throughout the operational region. Since the transition is "locked" to this point on the airfoil, the performance is remarkably high and stable for a wide array of angles and conditions.
For very high angles of attack, the pressure rise at the front of the airfoil will become increasingly sudden, causing the tiny rooftop to become flatter and eventually tilted negatively. When getting close to this region, the transition point will start moving forward. The angle at which the transition point moves forward will vary heavily with roughness, causing the airfoils to be unstable in the stall region.
In effect, it has the operational stability of an airfoil with leading edge transition, but can still have a laminar rooftop. However, since the transition finally will jump forward, there will be a loss of stability at high angles.

High-lift profiles also have the transition point locked at the start of the pressure recovery up to the design angle. However, since they have a long flat rooftop at this angle, an increase in angle of attack will give a negatively tilted rooftop, meaning there will be an adverse pressure gradient over the front of the airfoil. This will make the transition point move forward for higher angles of attack. Since the C-profiles have such a short, rounded, rooftop, this problem is significantly delayed, and they manage to keep the transition point locked much longer. Hence the increased high performance range.
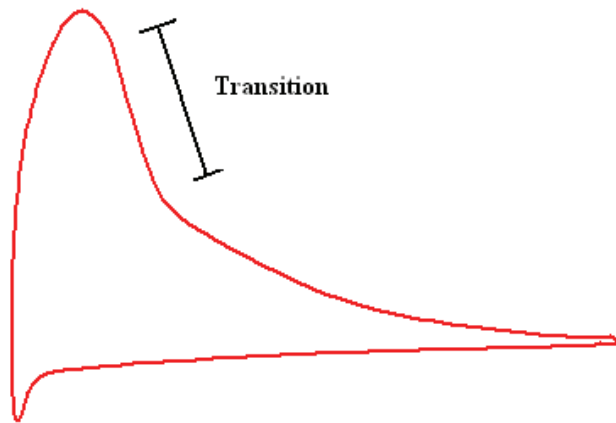
Figure 7.3 – Illustration of typical C-profile pressure distribution.

The C profiles also managed to keep the flow attached a lot longer, and in some cases did not show sign of separation before after α ~ 20º. This is again due in part to the transition point being locked in place up to very high angles. Once over the rooftop, the flow follows a slightly concave, but not dramatic, pressure recovery. This pressure recovery is not very close to the ideal Stratford recovery, and the flow therefore stays attached up to very high angles of attack. The airfoil still has a good lift coefficient due to the short, but big, pressure drop over the front.
This is not ideal with regards to lift, but makes it possible to keep the flow attached for very high angles.

It was found that with increasingly higher pressure drops, the high performance area shifted towards higher angles of attack. This was also found in the E airfoils. One explanation for this is that a bigger pressure drop means that the negative pressure gradient over the front will be bigger. Since a negative pressure gradient inhibits boundary layer growth, a bigger pressure drop will delay transition. This way, a bigger pressure drop will extend the range of angles with laminar rooftops.

The C profiles have very interesting effects, but are perhaps not what we are looking for. They are optimized for wide operational range, rather than maximizing the L/D-ratio. Still, their amazing ability to keep their high performance for varying conditions actually makes the CR profile set the record for highest L/D-ratio of for a Ncrit = 3 simulation amongst the soft stalling profiles, with L/D~209 (only beaten by the S-profiles, which are pure high-lift airfoils).
These profiles are very good as long as they never operate near the stall region. It is therefore unfortunate that they are bad for low angles of attack, and usually peak after α > 10º. This is not ideal for wind turbines, but in well controlled conditions, such as in a fan, they would probably be brilliant, as they could offer very high performance for a wide range of rotational speeds. The CR profile is by far the best of these profiles, with one of the highest and most stable performances of all, and one of longest operational ranges seen. It also has a relatively soft stall. It has a separation ramp, and therefore has an early rising lift coefficient. If the CR profile had been used in a wind turbine, the blade could have easily been optimized for α ~ 5º. This would have given more than 10º degree safety

margin up to the stall region, even for high roughness conditions. One could therefore argue that this profile would work quite well. The problem is that such a wide operational range is not desirable in standard wind turbines. In a strong gust of wind, the increase in absorbed energy is so massive that it is necessary to have a lift coefficient that flattens out for high angles of attack. It is better to enter a soft stall as this helps the wing minimize the thrust forces. This is why most airfoils designed for wind turbines have C_L graphs that start bending in not far above the design angle of attack.

It must be noted that what is said in the previous section only applies if the downwind concept works similar to an upwind concept, which it might not. There is currently no available information on the structural abilities of the suggested thin, flexible wings. So until then, this is all just speculation. But it if the wings can be design so that they tilt sufficiently back in strong winds, then this would probably fulfill the same role as the soft stall does for upwind turbines. If so, the turbine might work better in combination with airfoils with a wide operational range, thereby making the CR profile an interesting airfoil for wind energy after all.

Many of the other airfoils created had sufficient performance to be an improvement compared to standard wind turbine airfoils, while having sufficiently soft and stable stalls. The B1 and D1 would deliver soft and stable operation, while having noticeably higher lift-to-drag ratios.
The A2 is also a profile with very high performance, with L/D~233, but a bit more sensitive to roughness.
The B2 profile is also interesting, as it has high performance, with L/D~220, and the transition points move to the leading edge early, giving it very stable performance.

All the airfoils mention in the previous section are very good, and appear to be close to what we were looking for. However, they all have one problem. Their lift coefficients rise relatively late.
The AR profile, which combines an HOG-like pressure distribution with a separation ramp and a small pressure spike, is probably the best profile created in this project. It has an early rising lift coefficient, allowing a higher design C_L (or lower design angle of attack), and this corresponds with an early peak in maximum L/D. It has a soft stall that is sufficiently stable with roughness. Its maximum range is wide and gradual, and it gives the highest performance of all the usable airfoils, with L/D~254.
Therefore, the AR profile is the design that is chosen as the main result for this project.
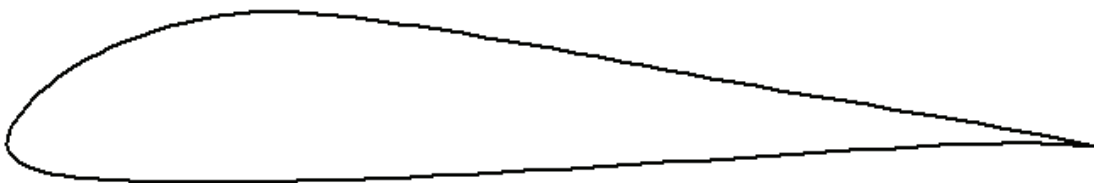
Figure 7.4 – AR profile

The AR profile uses a distribution similar in shape to a pure high-lift airfoil, and combines it with three important modifications:

-A separation ramp at the back, which allows higher lift coefficients and more gradual and stable operation when entering the stall region.

-A modified pressure recovery, which diverges gradually from the ideal Stratford solution when moving forward along the airfoil. This gives only slightly reduced performance while securing a gradual increase in separation.

-A pressure spike, which occurs at the front tip of the airfoil for high angles of attack to move the transition point close to the leading edge before entering the stall region. This will ensure that the airfoil will behave almost similarly in this region regardless of varying conditions.

Many high-lift airfoils have unpractical shape, often with a very thin tale. The AR profile appears structurally sound, with a thickness of 15.59% and a reasonably sized tale. It should therefore also be useful for implementation on the outer parts of upwind turbines.

In total, the AR appears to be the best profile, and should work well in the suggested downwind turbine system.
That being said, we currently know to little to be absolutely sure. There is not sufficient information about the structural nature of the suggested wings, or the level of turbulence in the wind it will encounter.
A structural analysis of the thin, flexible wings will give indications of what thickness the airfoils should be, and how big lift coefficients are possible. It will also show how the wings can bend back in high winds, and possibly be auto corrective for loading, perhaps making airfoils of other operational characteristics work better.
All this might change the criterion for the choice of airfoil, and the airfoil might have to be redesigned based on this information once it arrives.
If the structural analysis reveals that an even softer stall than that of the AR profile is needed, the best airfoil would be the D2, which still delivers brilliant performance while having the softest stall of all profiles in this report. It also has a slightly earlier rising lift coefficient than most other profiles, and is therefore an airfoil of big interest. Both the AR and D2 can be said to be the best profile, depending on which criteria is given the highest priority. It can therefore only be recommended to consider both of them for an application. The D2 is slightly thicker, and has a softer stall. One can therefore imagine using both of them, with the AR for large radii, and the D2 for lower radii.

The AR profile is a big success when referring to the original objective, which was to make a profile with performance in the same range as the HOG, but with a softer stall. The AR profile has a far softer stall, and only has a loss of maximum performance of 5.9 %. However, that is only in the maximum region of the ideal Ncrit = 9 simulation. For higher and lower angles, and for increased roughness conditions, the AR outperforms the HOG. The AR has also been given a much more stable stall, and a higher lift coefficient.

All in all, making it a much better profile for all practical uses. Still, there is of course room for improvement.

Several reports suggests methods for improving leading edge performance[14]. This is a field which was only briefly studied, as most of this project has focused on the pressure recovery and the subsequent stall characteristics. One of the leading edge improvements would be to design a better pressure spike. The one created for the AR does indeed get the transition points to move forward much more rapidly than for similar profiles, but it is not big enough and should ideally be made even more effective, in order to get the transition points all the way to the leading edge sooner. This will close the slight gap there is between the two Xfoil simulations in this area.

It must also be noted that the separation ramps at the back of the AR and CR profiles were designed by hand. A detailed study of separation ramps, and the optimization process around them, should make it possible to design better ramps than the ones used here.

A mathematical study of the magnitude of divergence between the ideal Stratford distribution and the one used, might make it possible develop an expression describing the relationship between the divergence from the ideal distribution and the paste at which the separation increases. If so, it would be possible to mathematically optimize the pressure distribution for a pre described gradual stall.

As mentioned before, experimental tests will be needed to confirm the qualities of the AR airfoil. The results from these might also suggest improvements.

Even if it were so that only conservative performance characteristics could be used, the creation of the TR profile showed that it is possible to maintain performance while reducing the thickness of the airfoil, making weight reduction possible if the structural demands on the wing can be reduced, such as in a downwind flexible wing concept.

Experimentation with the high-lift technology also reviled that it was possible to create better pure high-lift airfoils than the HOG. Both the S1 and S2 showed higher and longer lasting maximum performance. The key to their performance was that they were optimized for 11° and 12° degrees respectively. Even so, their performance rose nearly as early as the HOG, resulting in a wider maximum area. This therefore suggests that it is better to use high design angles for such airfoils. The S1 and S2 also maintain their performance much better with increasing roughness. This is because they accelerate the air faster over the front, and will have a negatively tilted rooftop all the way up to angles of attack ~11°/12°, and they also have a bit shorter rooftop. This combination keeps the transition point stable at the start of the pressure recovery for much longer, providing maximum operation for all simulations, while the HOG's transition point starts moving very early with increasing roughness.

Both the S1 and S2 would perform extremely well under controlled conditions, such as in a fan. The S2 performs L/D > 250 for 6° angles of attack. This would give the fan very high efficiency for several rotational speeds. Even with Ncrit = 3, the S2 reaches a maximum of L/D-ratio of over 253, more than what most other high-lift profiles can do at Ncrit = 9. This shows that there is also a big room for improvement for the pure high-lift technology.

When studying the experimental results in the earlier reports from NTNU, it appears that they consistently get better performance for a slightly higher angel of attack than the calculated optimum angle. If going back to Stratford's original paper from 1959, he makes a comment saying that his method will give 0-10 % too low result, meaning that the ideal pressure recovery in reality will be slightly faster. This seems to explain why they get better results for slightly higher angles of attack than designed for, as the pressure recovery will be "pushed" a bit beyond the ideal Stratford theory, and thereby be closer to actual ideal performance. This is probably one of the reasons why it was possible to create profiles that performed better than the theoretically ideal HOG profile.

As discussed briefly earlier, it would be ideal to design for slightly higher lift coefficients to get smaller chord lengths. By once again using the BEM program, and redoing the rotor blade design for $C_L = 1.3$ (original value was 1.2), it was found that for r = [40, 65] m, the average reduction in chord length was 7.7 %. For a $C_L = 1.4$, the reduction was 14.3%.

Another method suggested was to design for lower values of the induction factor, a, to get less thrust and lower chord lengths, with only a slight decrease in efficiency. It can be seen from figure 7.5 that around the ideal value of a = 1/3, the efficiency curve is flat, while the graph for coefficient of thrust has a significant gradient. This means that a small shift to lower values will yield a much bigger loss in thrust than efficiency.
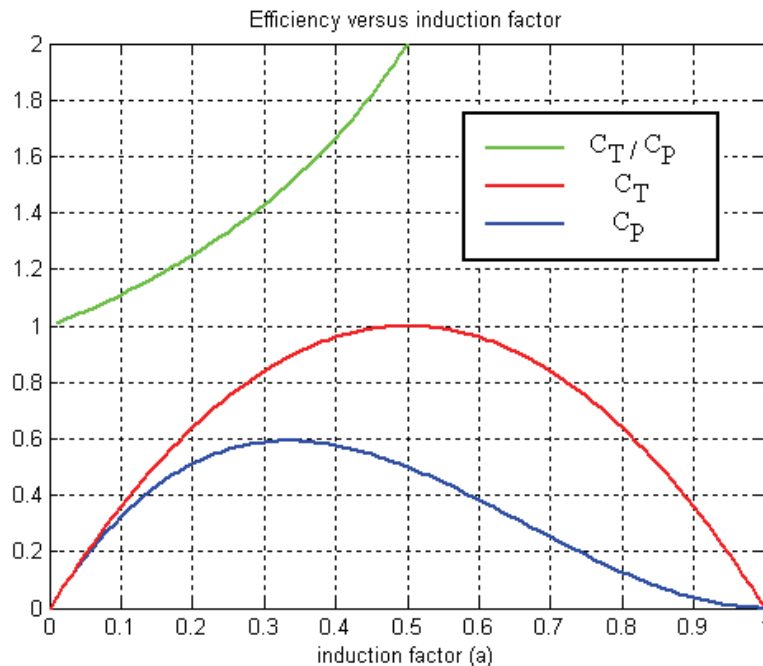
Figure 7.5 – Coefficients of performance and thrust vs induction factor, a.

If, for instance, the design induction factor is reduced from 0.33 to 0.20, the following changes occur:

	a = 0.33	a = 0.20	Reduction
Cp	0.5925	0.5120	13.6%
Ct	0.8844	0.6400	27.6%

Table 7.1 – Coefficients of efficiency and thrust with varying induction factor a.

This rather drastic change is seen to reduce thrust more than twice as much as efficiency. For a smaller change, the ratio will be even higher. Since we know from equation 4.6 that the ideal chord length is proportional to 1/(1-a), it is easy to see that this change would yield a 16.25 % reduction in chord length, thereby also reducing weight.

Only a thorough structural and economical analysis can reveal what design value the parameters should have. More thrust will raise the need for a stronger tower and bigger subsea structure.

In the quest for reducing top weight, the by far biggest step will come with the possible success of the hydraulic gear box, allowing the generator to be placed elsewhere than at the top. For a an offshore turbine, the generator can then even be placed below sea level in the subsea structure, and use its weight as ballast to stabilize the system. This would have a double effect, reducing the total size and cost of the system significantly.

Another thing that is needed to rethink once going offshore is the optimum number of blades. On land, the choice has fallen on the 3-bladed turbine for the vast majority of windmills. With top weight and cost being two very pressuring factors in the realization of offshore wind turbines, it is possible that a 2-bladed design would be better. This would again require a detailed structural and economical analysis to be able to answer, taking the new airfoils and conditions into account.

The high-lift airfoils are best for implementation on the outer parts of wings. This is where most energy is extracted, but the far outer parts are corrupted by tip losses and subsequent vortices. This can be improved by using winglets. They will reduce drag and improve lift, making the wing functional over the outer parts as well. Winglets must be carefully designed, and are dependant on a constant design speed to work efficiently. As seen in figure 4.3.2, the tip speed of these turbines will be remarkably stable, as most of the velocity comes from the turbines rotational speed. This will probably make these wings suitable for winglets. How this will work in combination with wings that are tilting back in strong winds is unknown, and would have to be investigated.

8 Conclusion

It is possible to flatten out the stall characteristics of a high lift airfoil without a big loss in performance. It is also possible at the same time to make the airfoil maintain its performance better for a wide range of angles and conditions. This allows for the creation of high-lift profiles with characteristics usable for wind turbines. It is possible to make soft stalling high-lift profiles that are not thin or structurally weak. This technology should therefore also be of interest for traditional upstream wind turbines.

The soft stall can be achieved by gradually approaching the local optimum Stratford distribution when moving back over the airfoil. This caused the flow to separate at the back first, and then have the separation grow gradually forward with increasing angle of attack.

The inclusion of a separation ramp works very well together with the high-lift design, and helps giving an even more gradual stall. This feature also allows for the lift coefficient to be a lot higher, making it possible to optimize the wing for a lower angle of attack or higher lift coefficient. This is an important improvement as wings using a standard high-lift profiles would have to be optimized for a rather high angle of attack.

The transition point is shown to be of big importance to the performance of airfoils. It is necessary for an airfoil meant for use in wind turbines that it has constant characteristics. This can be achieved by having the transition point near the leading edge, inhibiting any significant change with increasing roughness or air turbulence. The transition point should at least move to the leading edge before entering the stall region, as this will ensure constant stall characteristics for the airfoil. A pressure spike at the front of the airfoil can be used to achieve earlier transition, as it applies a significant adverse pressure gradient early, promoting transition.

9 References

[1] - Teknisk ukeblad, vol 8, 2009. Page 60.

[2] – Frank White, Fluid Mechanics, fifth edition. Mcgraw-Hill, 2003.

[3] – Wind energy explained, Manwell, McGowan, Rogers. Wiley, 2002.

[4] - Determining the power-law wind-profile exponent under near-neutral stability conditions at sea, Hsu, S.A., E.A. Meindl, and D.B. Gilhousen, 1994, J. Appl. Meteor., Vol. 33, pp. 757-765.

[5] – Aerodynamics of wind turbines, second edition, Martin o.l. Hansen. Earthscan, 2008.

[6] – B.S. Stratford, The prediction of separation of the turbulent boundary layer. Journal of Fluid Mechanics, vol 5, 1959.

[7] – Robert Liebeck, A class of airfoils designed for high lift in incompressible flow. Journal of aircraft, vol 10, NO 10, 1973, AIAA.

[8] – Robert Liebeck, optimization of airfoils for maximum lift. Journal of aircraft, vol 7, NO 5, 1970, AIAA

[9] – Robert Liebeck, Design of subsonic airfoils for high lift. Journal of aircraft, vol 15, NO 9, 1978, AIAA

[10] – T. Strand, Exact method for designing airfoils with given velocity distribution in incompressible flow. Journal of aircraft, vol 10, NO 11, 1973, AIAA.

[12] – Kristy Hanson, Effect of leading edge tubercles on airfoil performance. Ph.D thesis, university of Adelaide, Australia, Faculty of engineering, computer and mathematical sciences, 2007.

[13] – Dan Somers, Design and experimental results for a natural-laminar flow airfoil for general aviation applications. NASA TP-1861, Langley research centre, scientific and technical information branch, 1981.

[14] – Bak, Fuglsang, Modification of the NACA 63_2-415 leading edge for better aerodynamic performance (Wind energy department, Risø National Laboratory). Journal of solar energy engineering, vol 124, 2002.

[15] – Seifert, Reichert, A recipe to estimate aerodynamics and loads on iced rotor blades. Report from Deutsches Windenergie-Institut, Ebertstraße 96, D-26382 Wilhelmshaven, Germany.

[16] – www.nrel.gov (read march 2009)

[17] – Dan Somers, The s825 and s826 airfoils. NREL/SR-500-36344, 2005, www.nrel.gov

[18] - V. Parezanovic, B. Rasuo, M. Adzic, Design of airfoils for wind turbine blades. Report from University of Belgrade, Serbia.

Project reports from earlier work at NTNU:

[19] – Jørn Hanssen, Høy-effektive vingeprofil. 1984.

[20] – Gorm Jenssen, Trykkfordeling rundt vingeprofil med høy løftekoeffisient. 1987, spring.

[21] – Gorm Jenssen, Trykkfordeling rundt vingeprofil ved høy løftekoeffisient. 1987, fall.
(NB! This is not the same as refernce 20. Two reports exist with identical titles and written by the same writer, from spring and fall of 1987 respectively,

[22] – Asmund Huser, Grensesjiktfordeling på en vingeseksjon nær separasjon. 1987.

[23] – Asmund Huser, Programpakke for konstruksjon av optimal vinge ved forskjellige Reynoldstall. 1988.

[24] – Kaspersen, Kvandal, Vingeprofil med høyt loft/motstandsforhold. 1989.

[25] – Asmund Huser, Grensesjiktsforhold ved store trykkgradienter. 1987.

[26] – Gorm Jenssen, Bruk av inversprogram for konstruksjon av vinger. 1987.

---

[27] - http://www.usatoday.com/news/nation/2005-01-04-windmills-usat_x.htm (read may 2009)

[28] - http://www.nrk.no/nyheter/distrikt/nordland/1.6283974 (read may 2009)

[29] – Basic study of winglet effects on aerodynamics and aeronautics using large-eddy simulation, shimooka, iida, arakawa. University of Tokyo.

[30] – John Amund Karlsen, CFD modelling of a small wind turbine. 2009 master thesis, NTNU.

[31] – www.winddata.com (read February 2009)

[32] - http://www.tu.no/energi/article200175.ece (read february 2009)

[33] - http://1234.tv2.dk/article.php/id-10544486.html (read march 2009)

[34] – First hand information from Per-Egil Skåre, Dynacvec.

10 Appendix A (simulations)

10.1 HOG
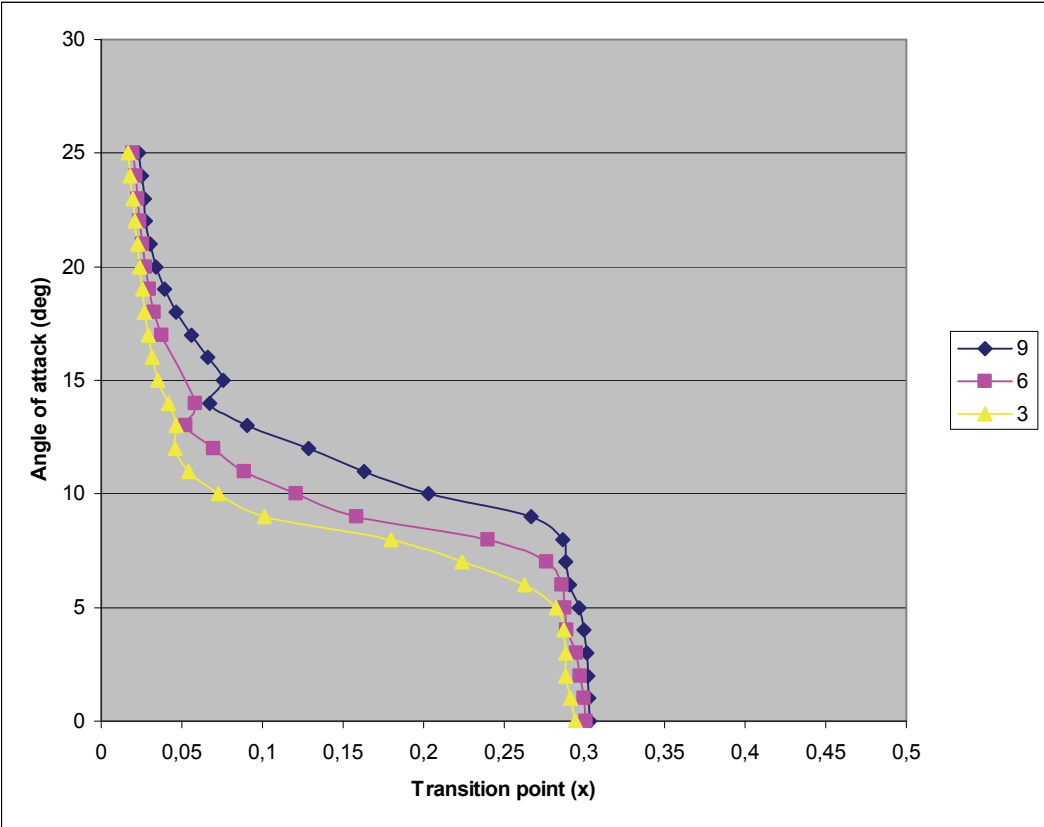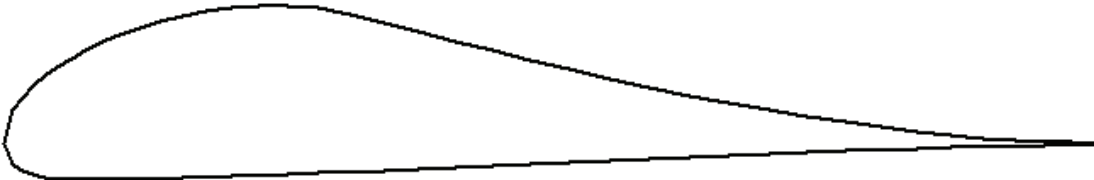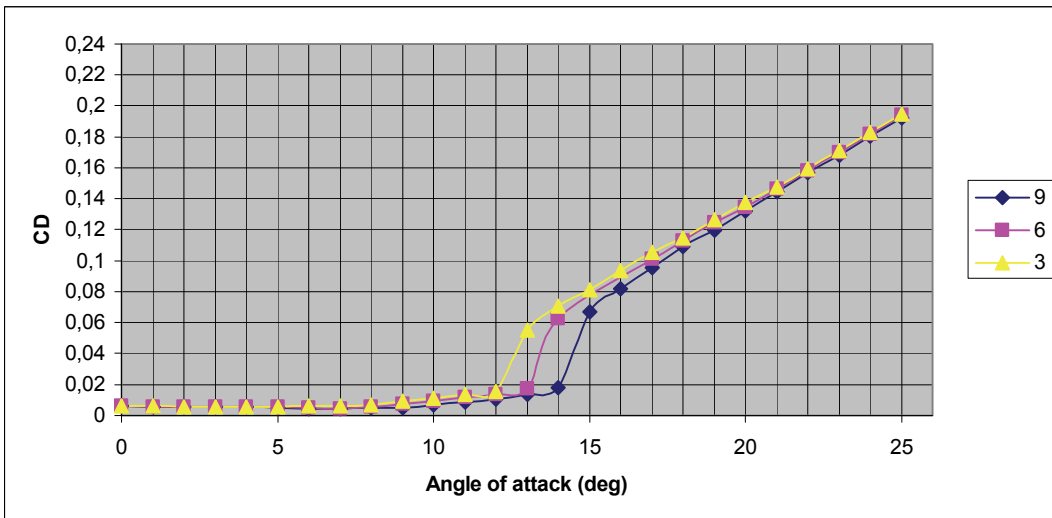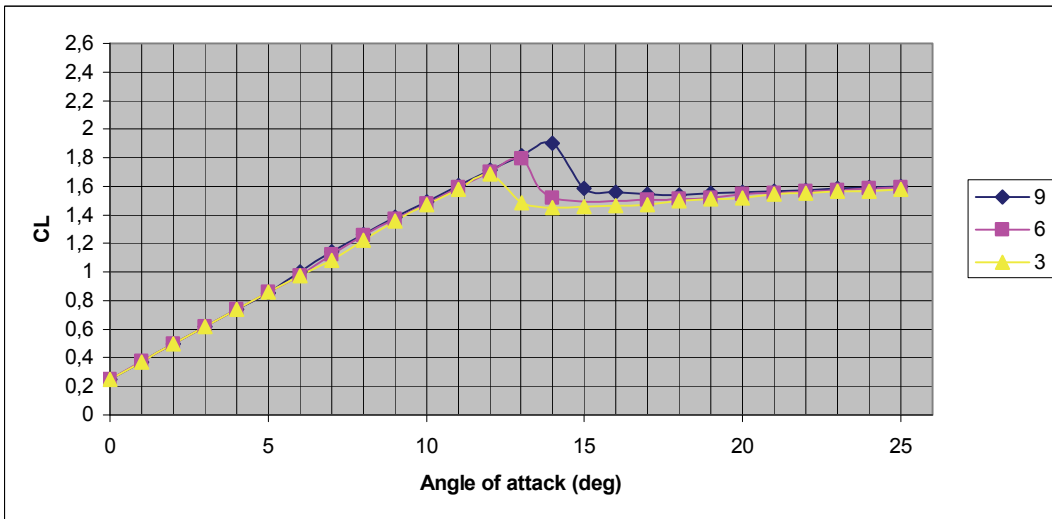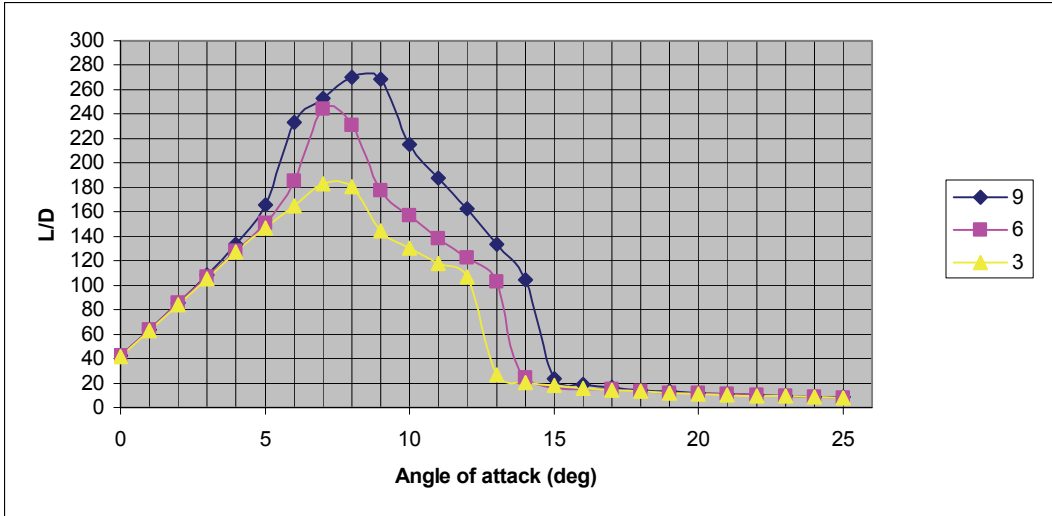
10.2 4412
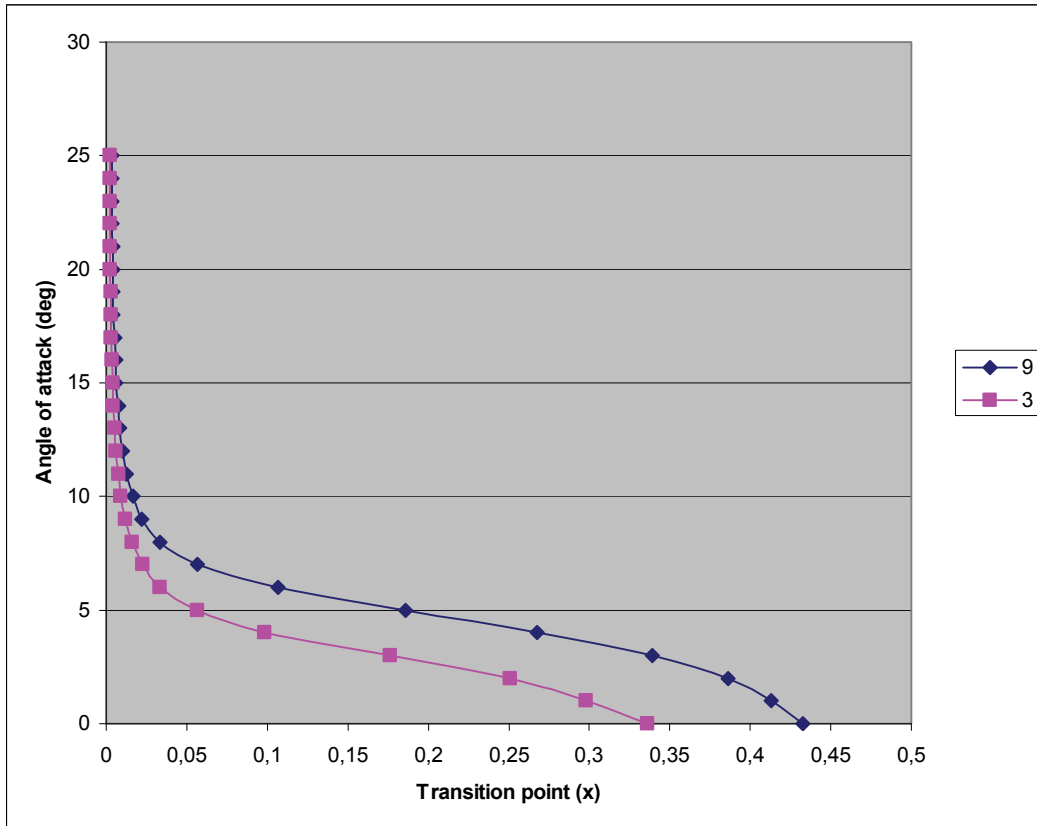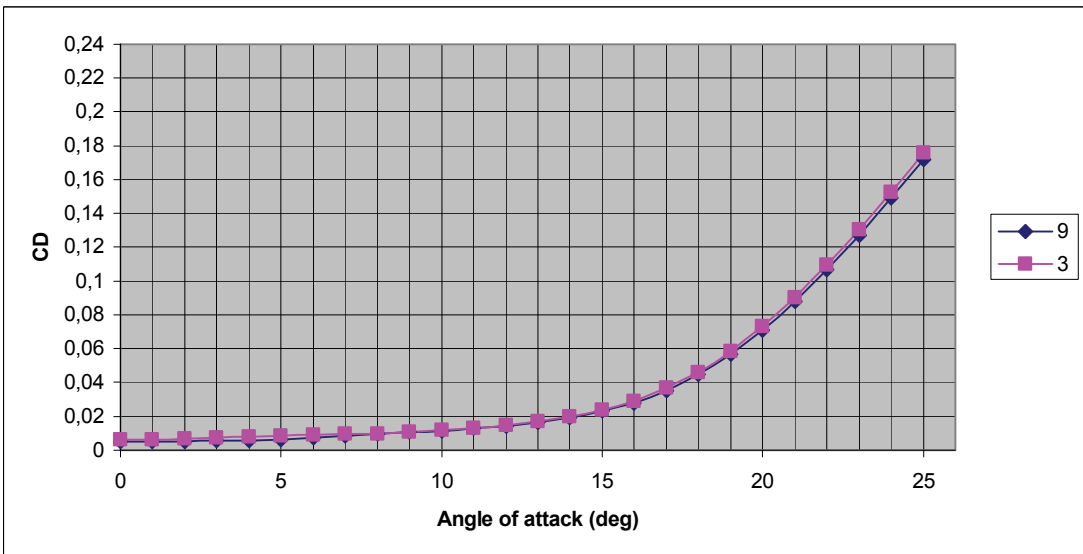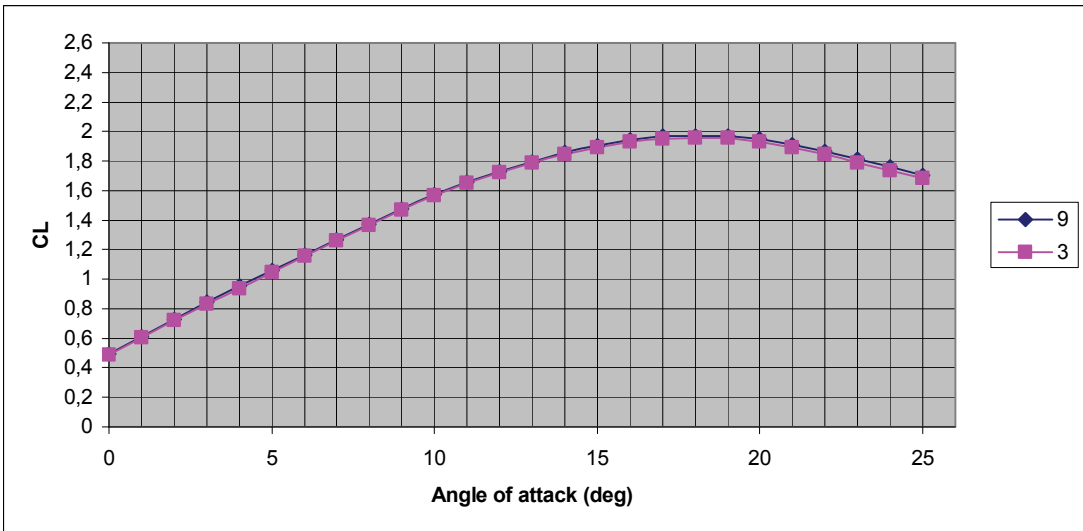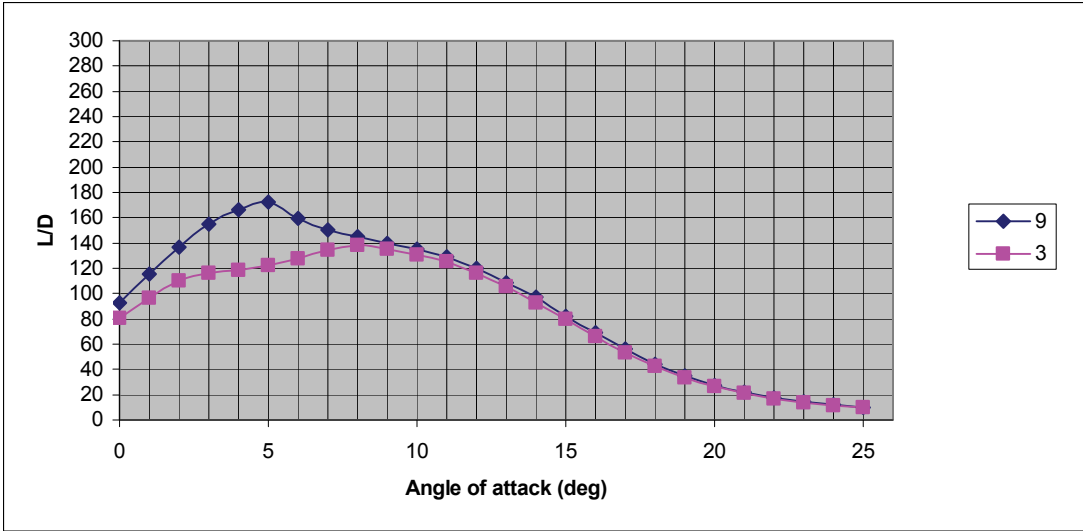
10.3 A1
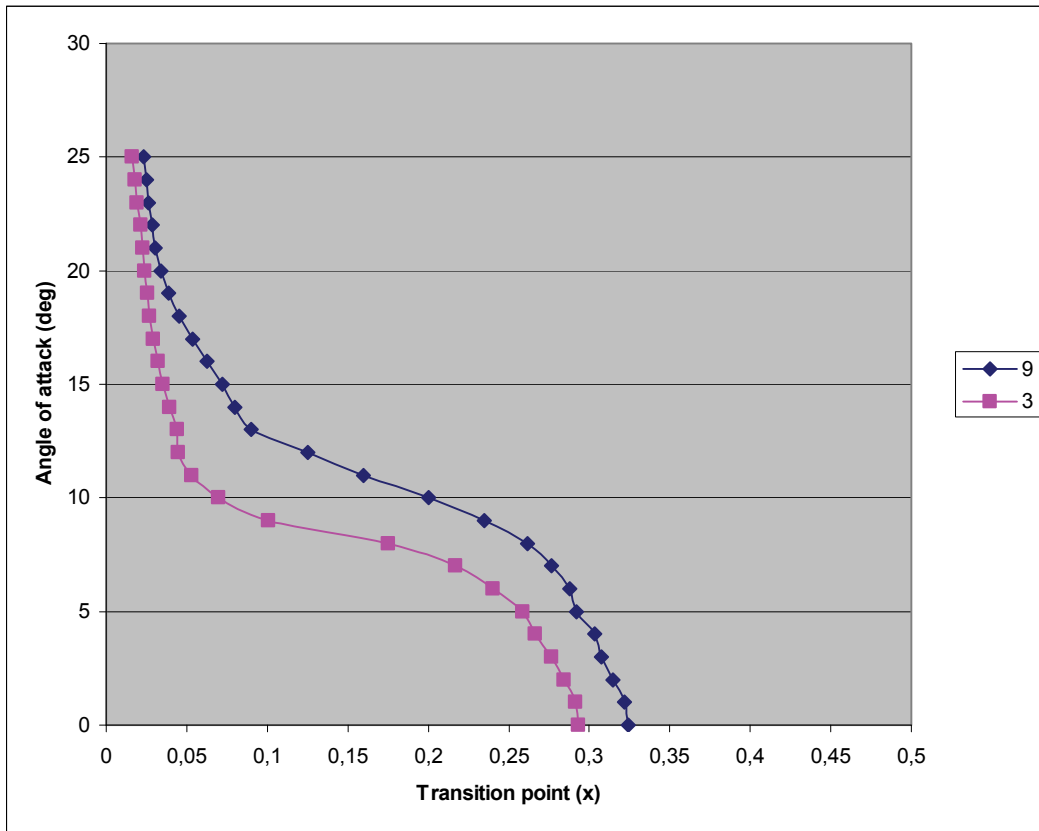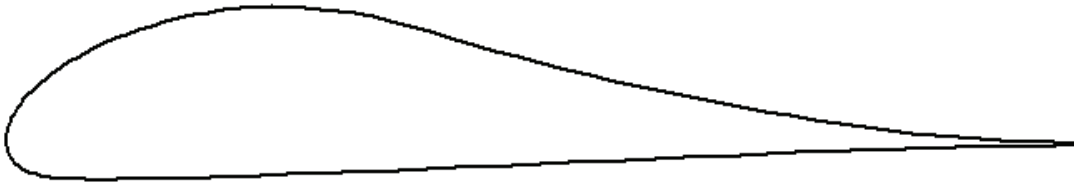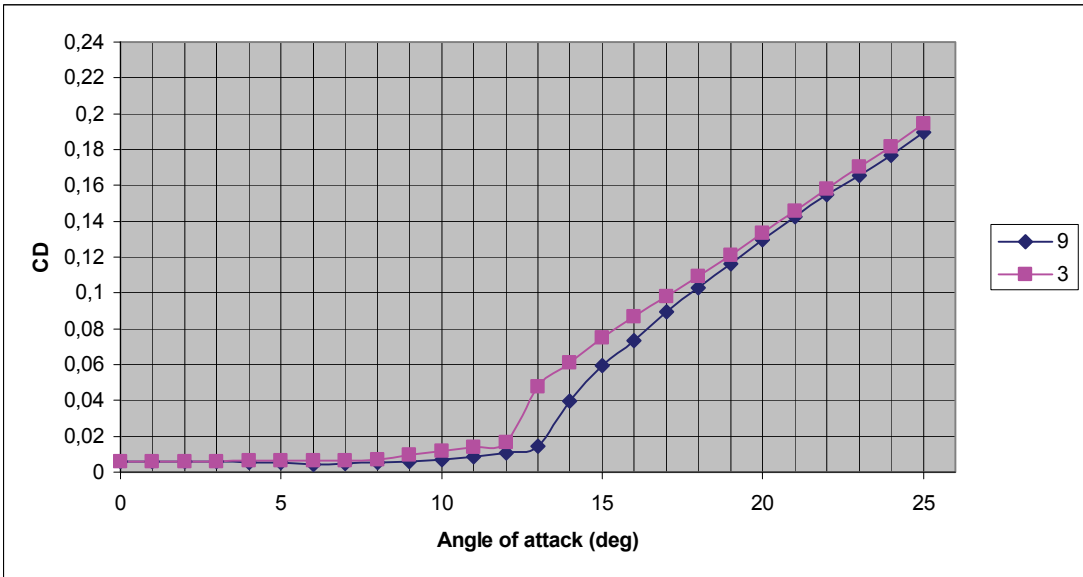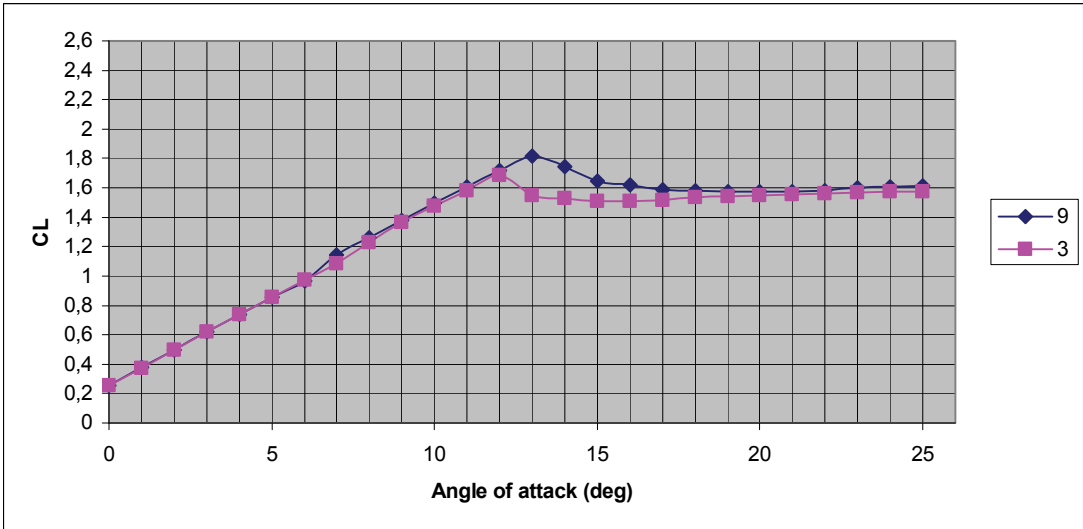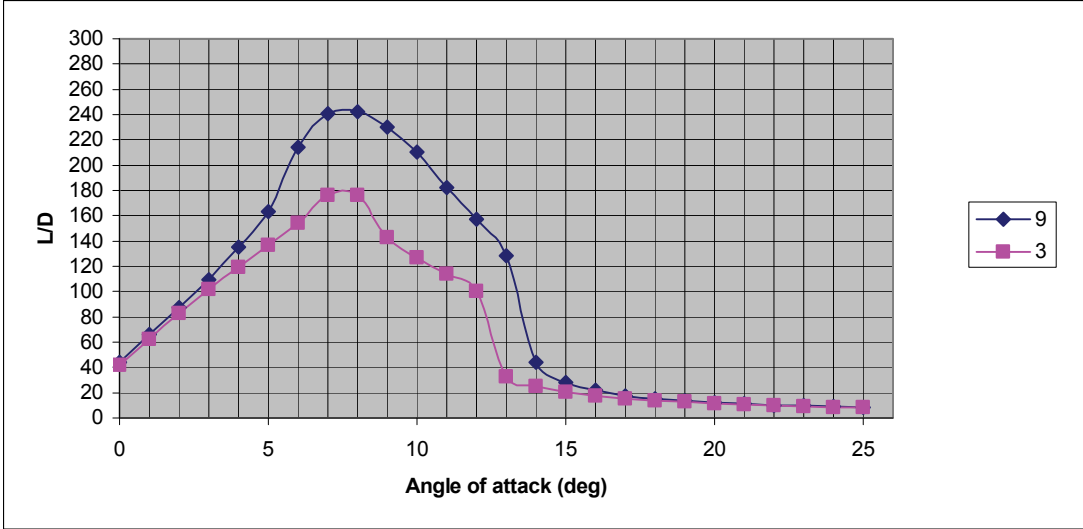
10.4 A2
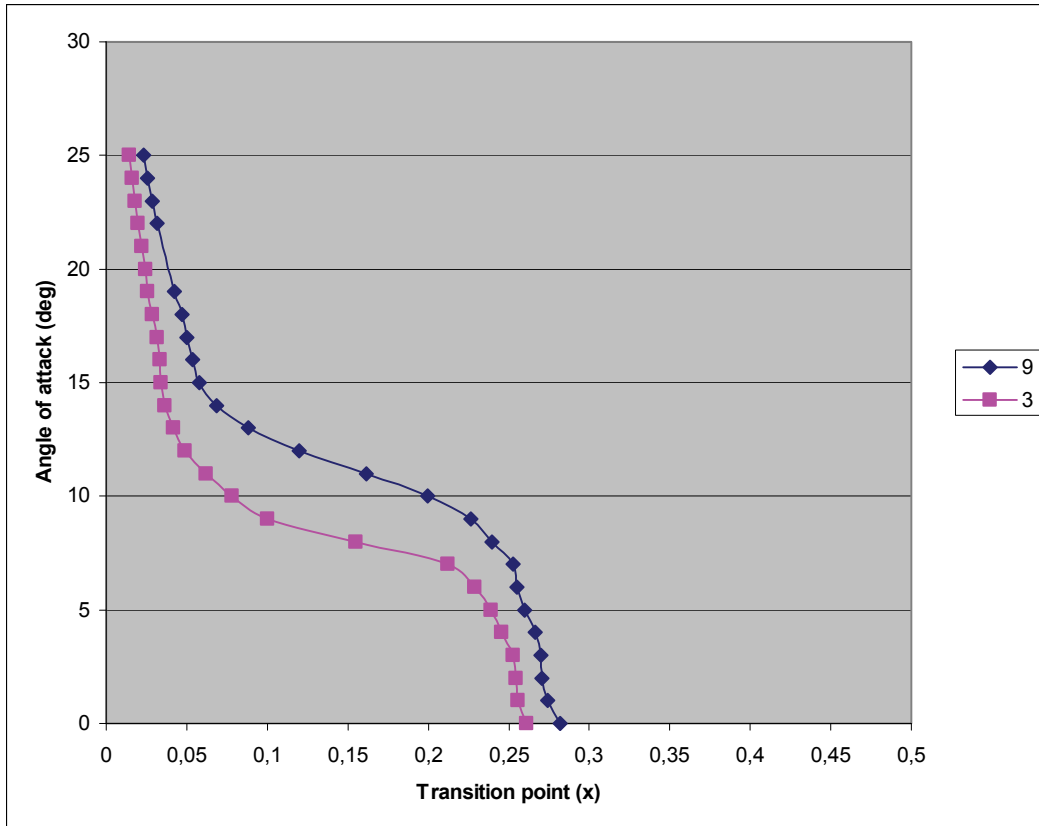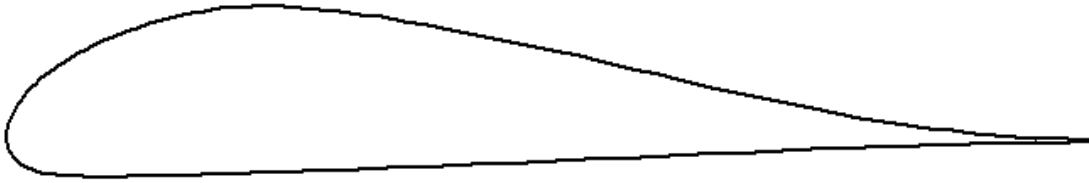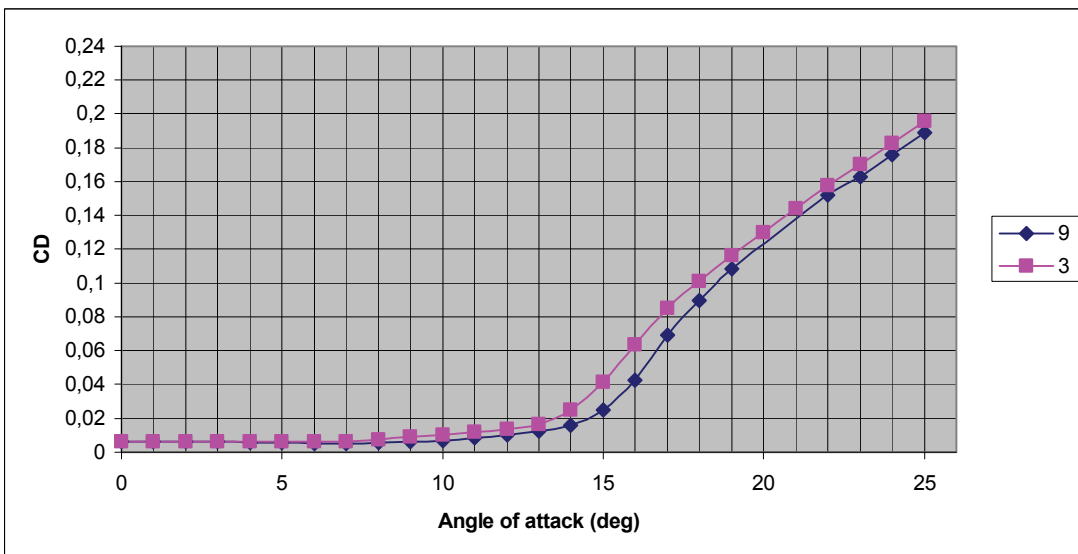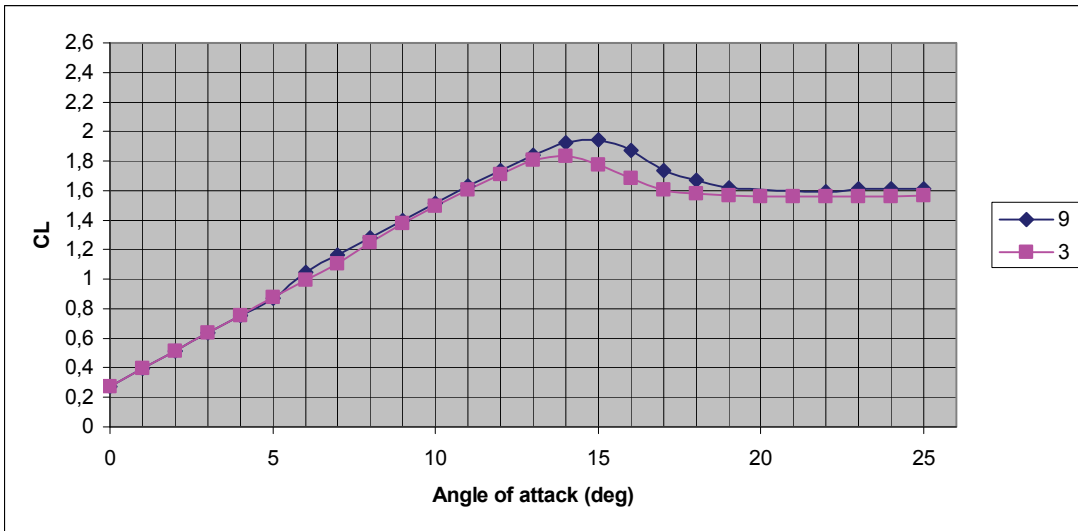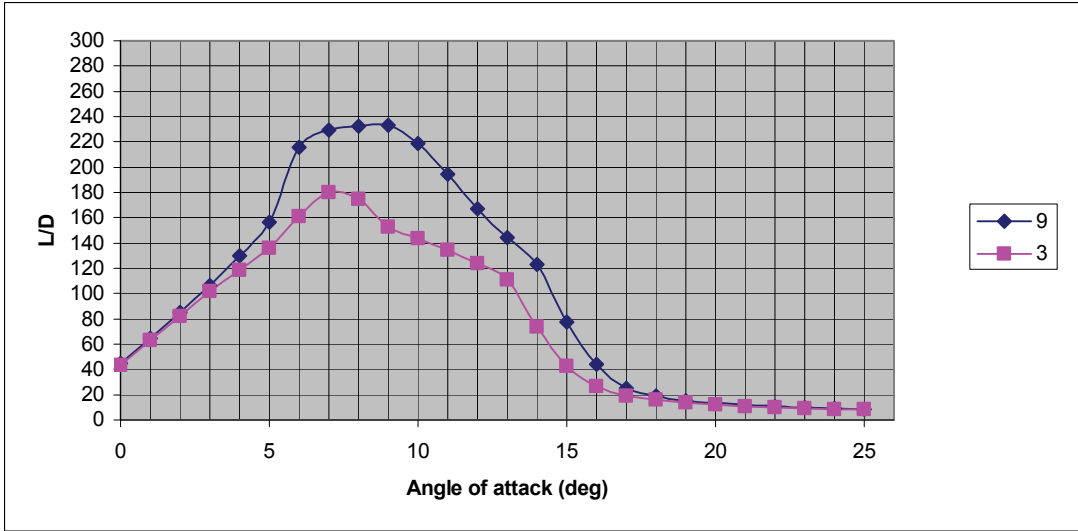
10.5 A3
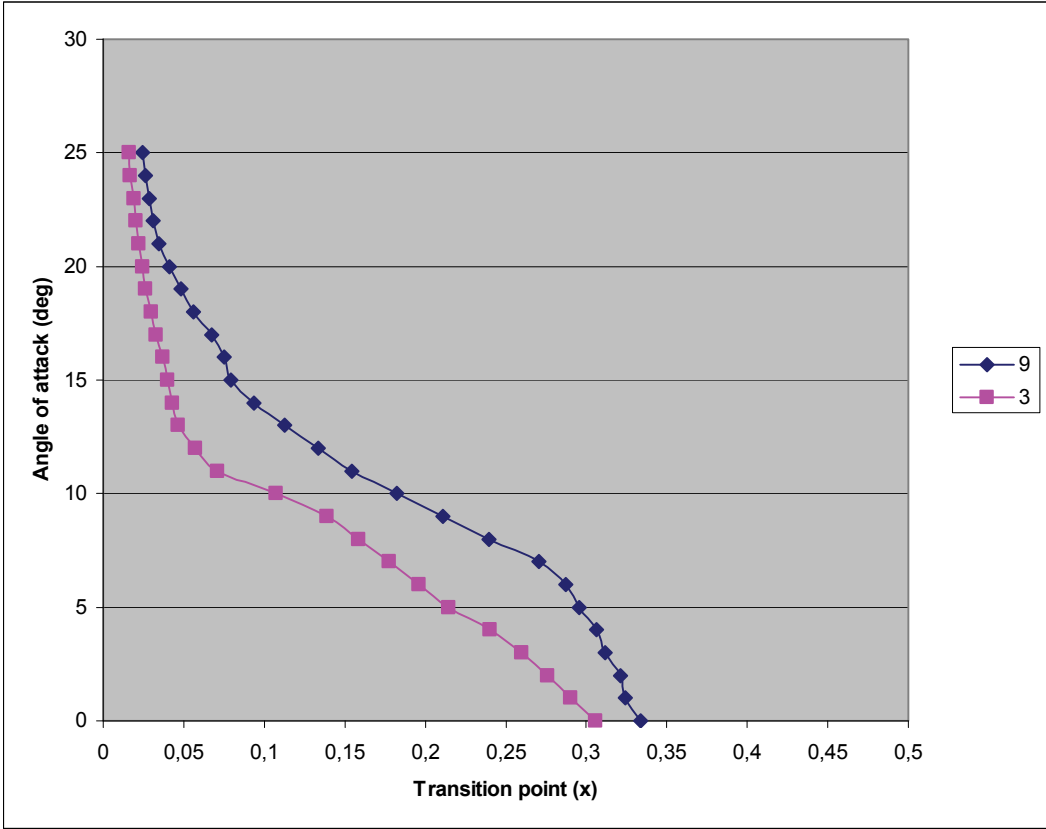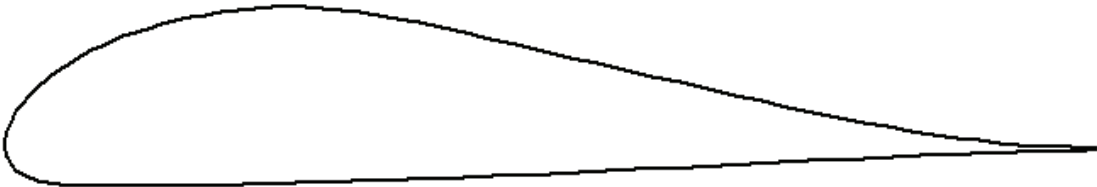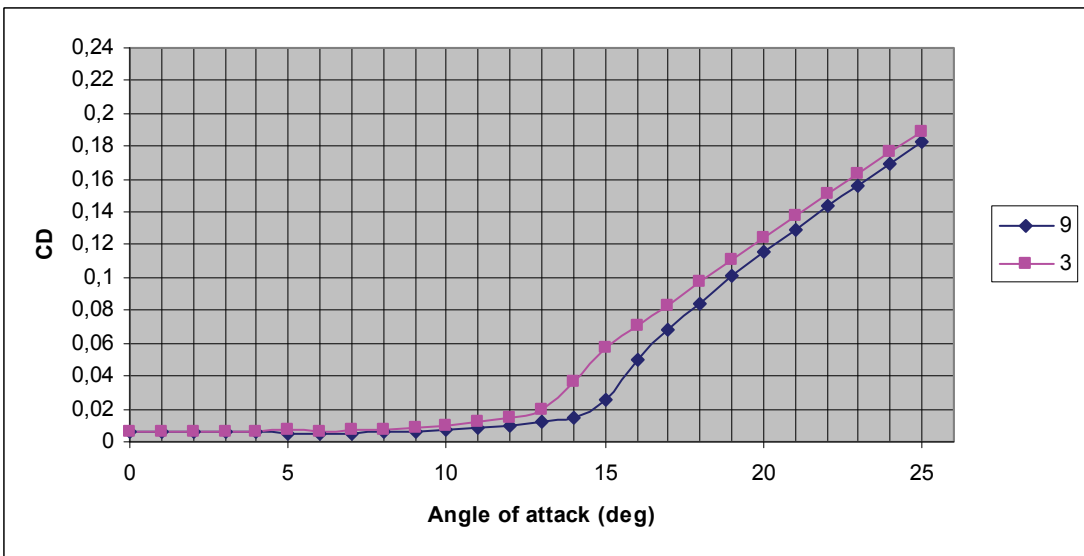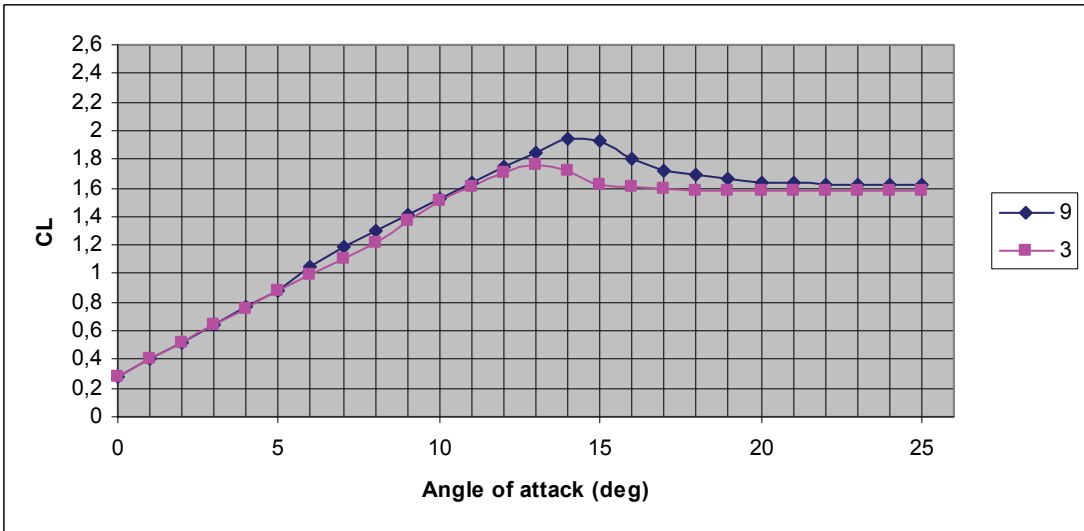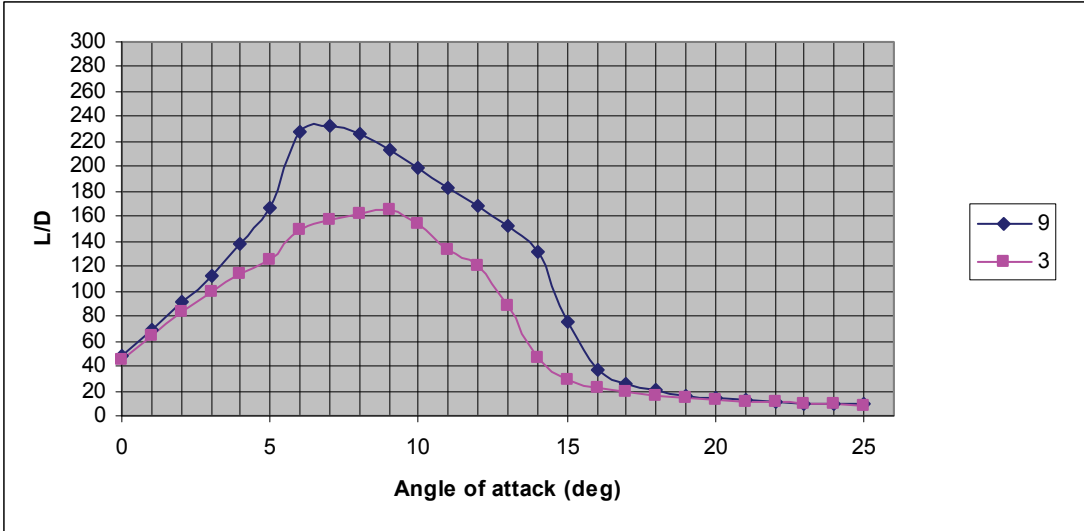
10.6 B1
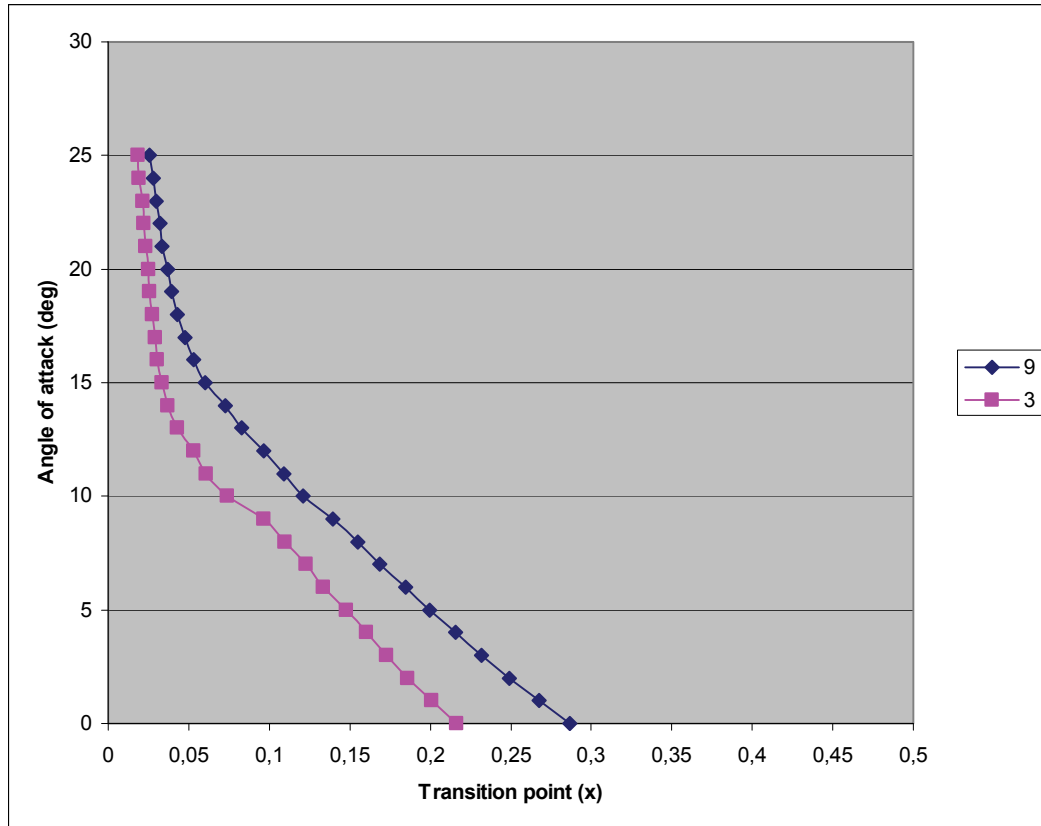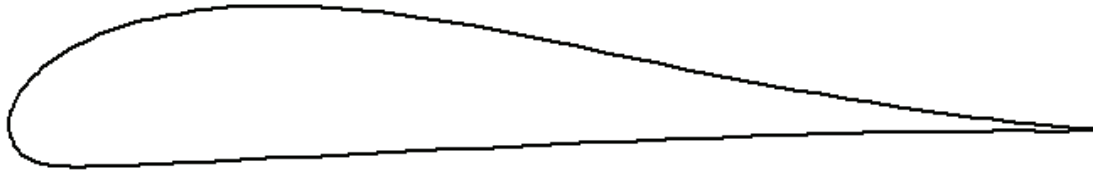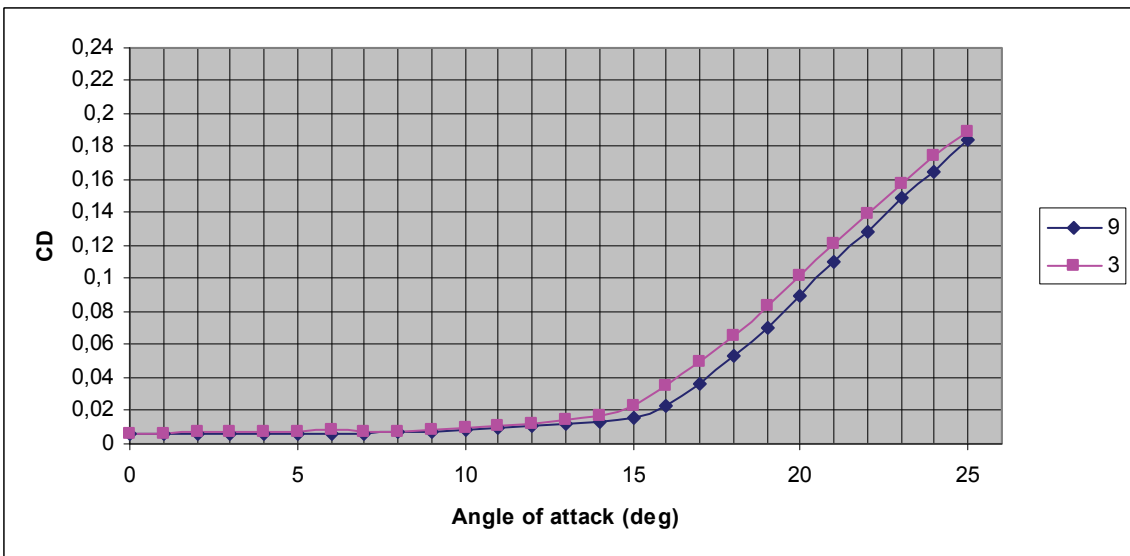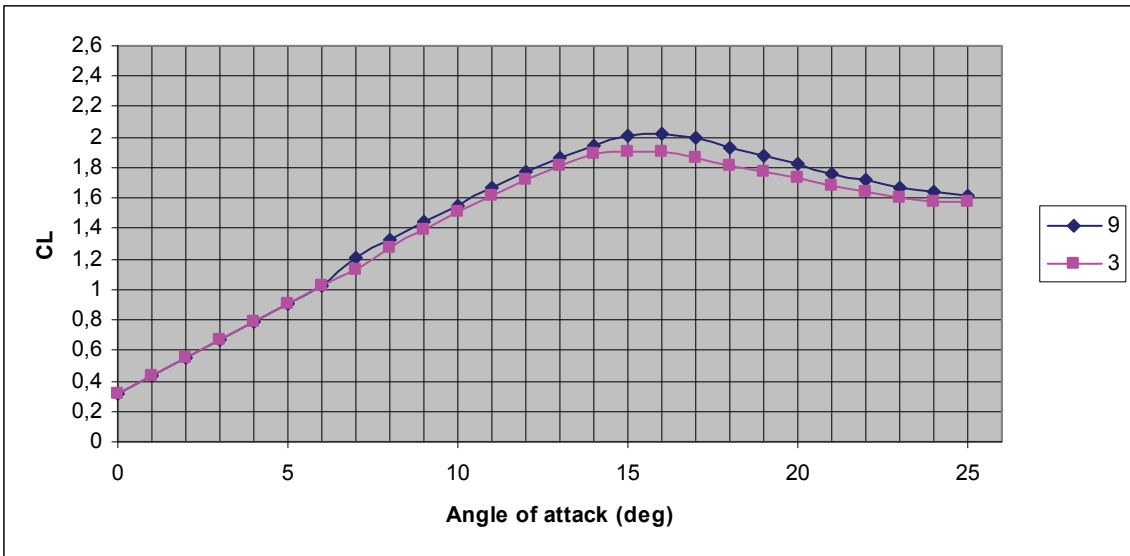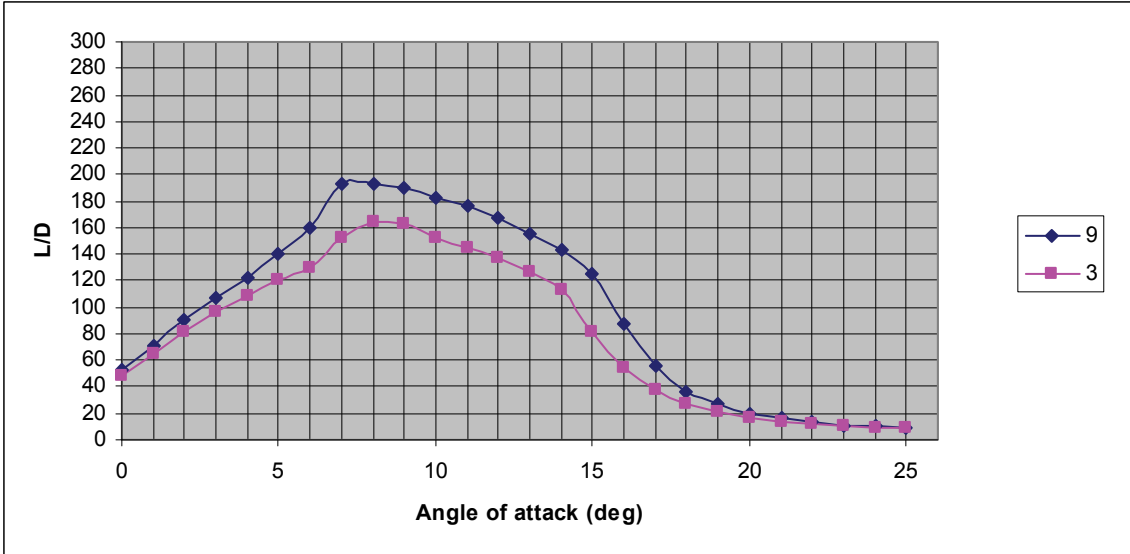
10.7 B2
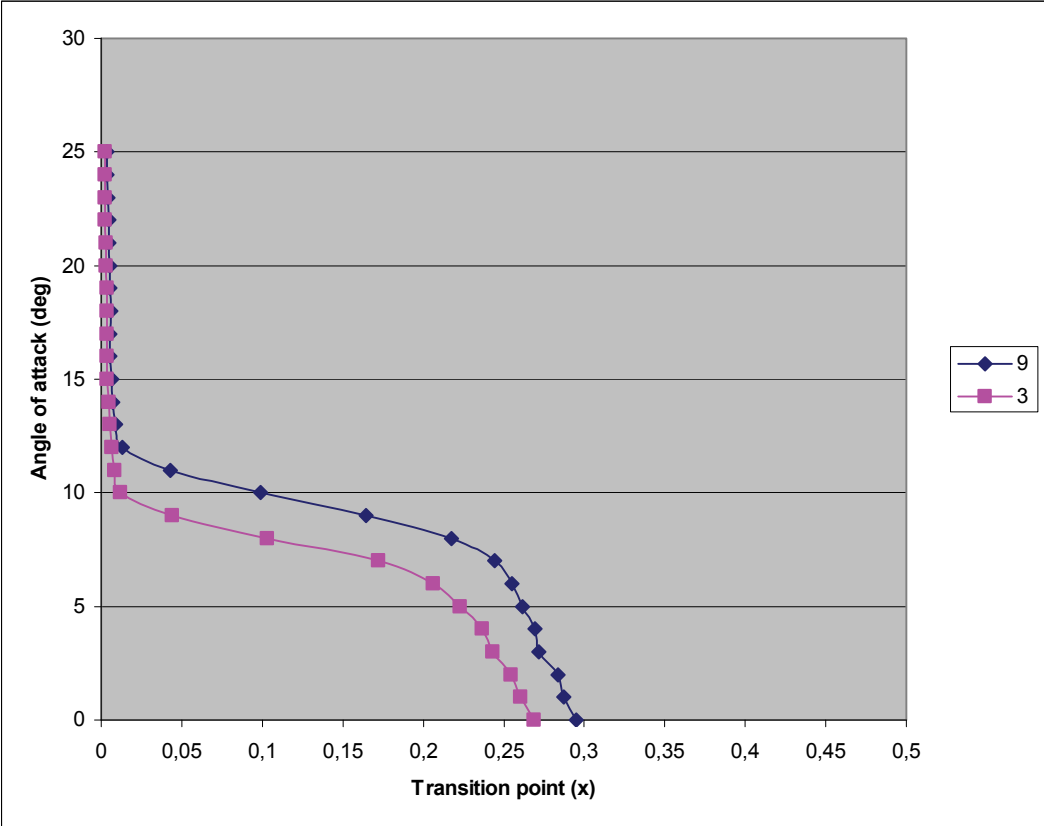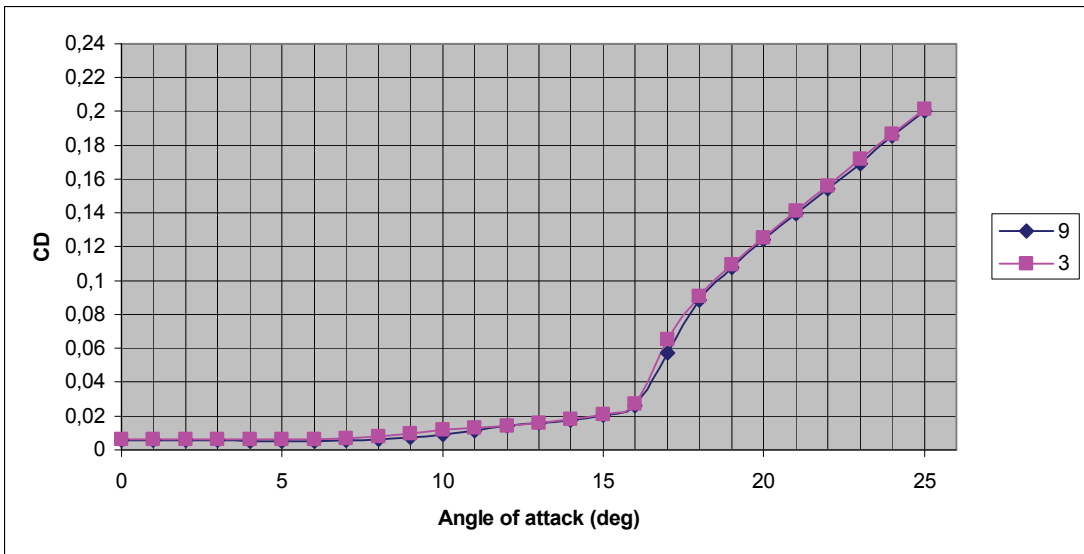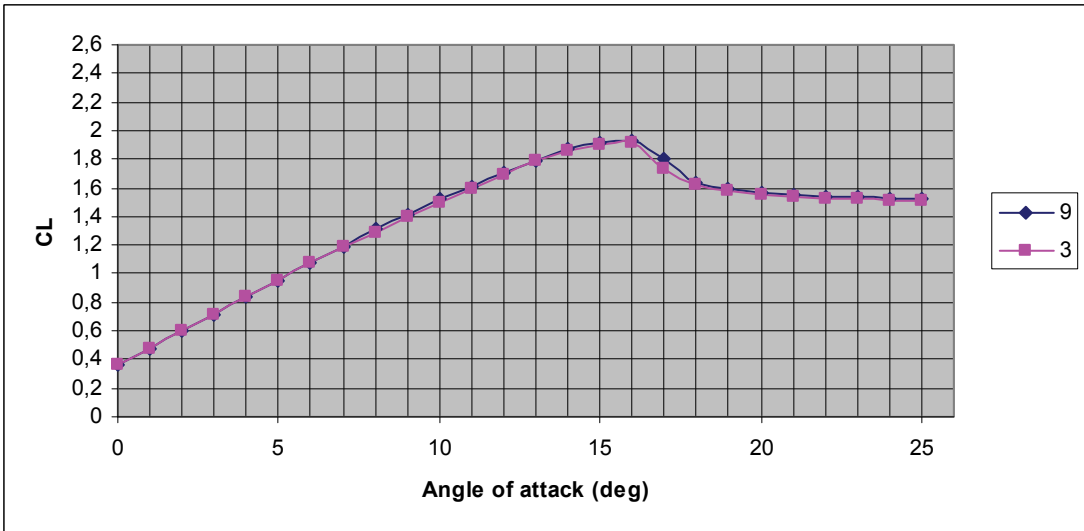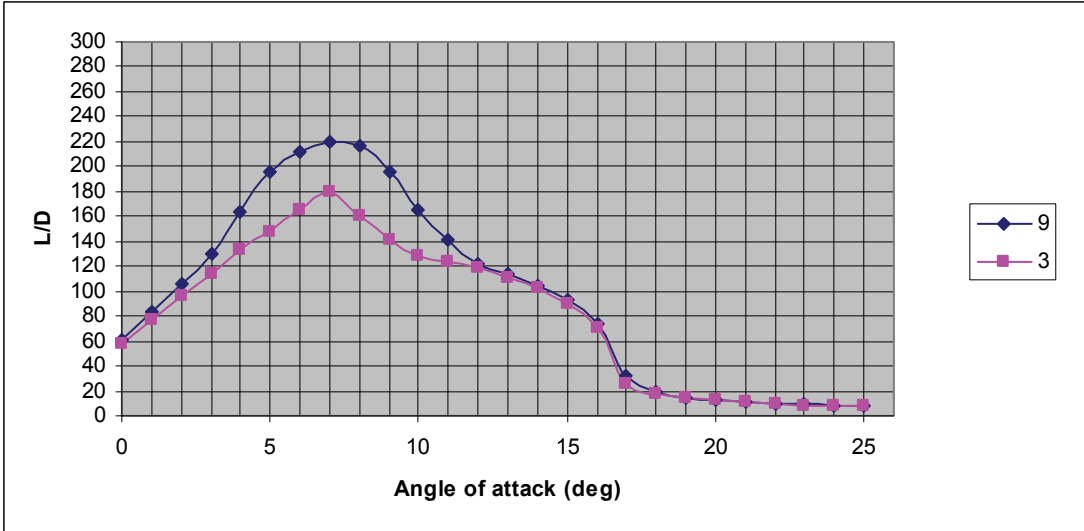
10.8 C-1

10.9 C2

10.10 C3

141

10.11 D1

143
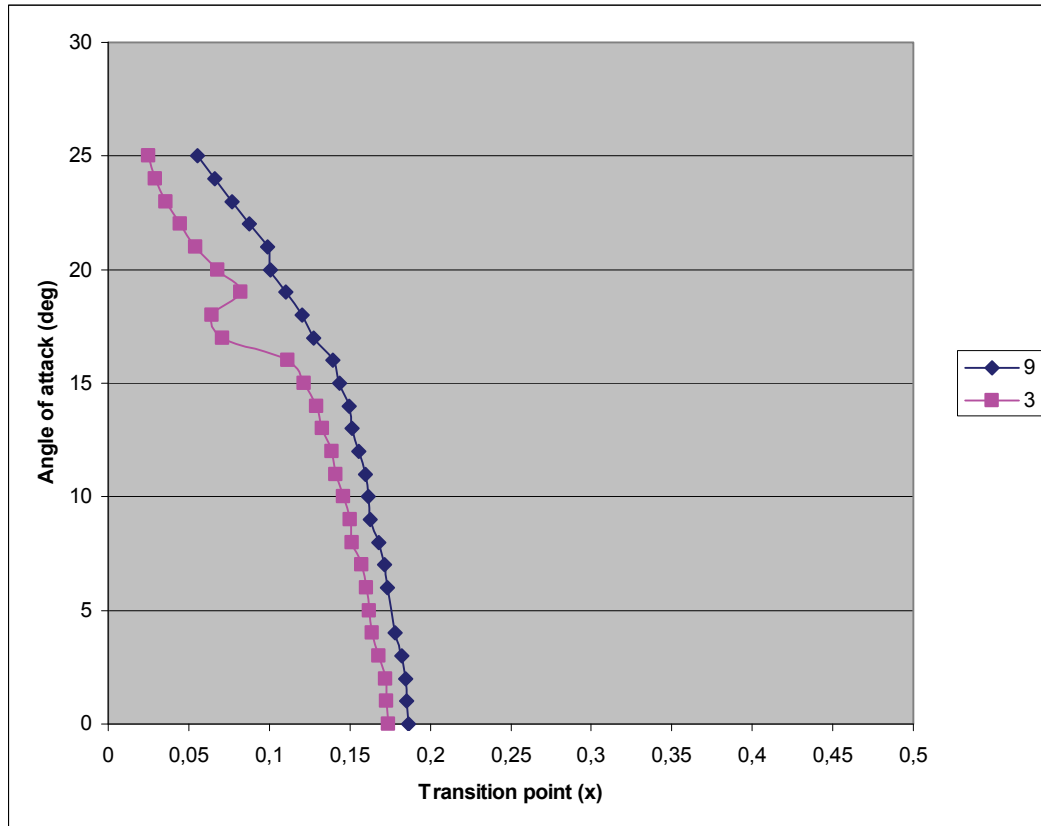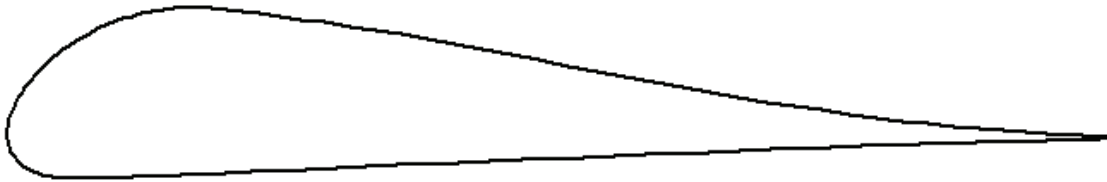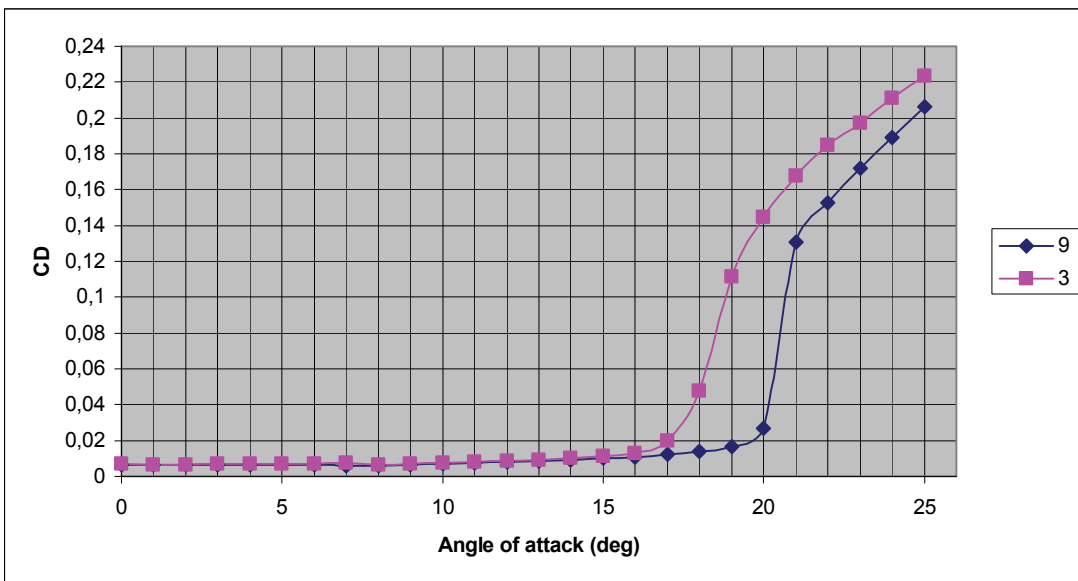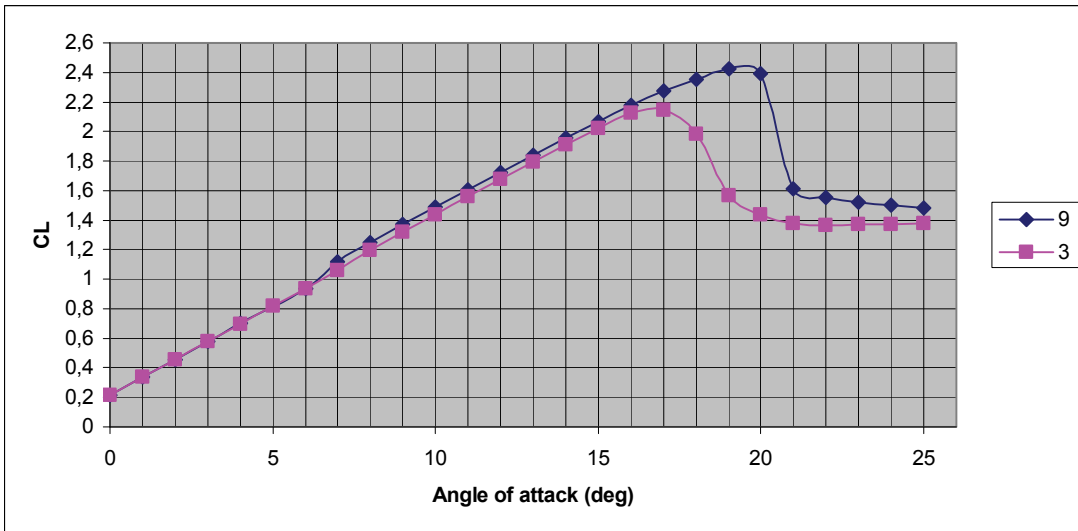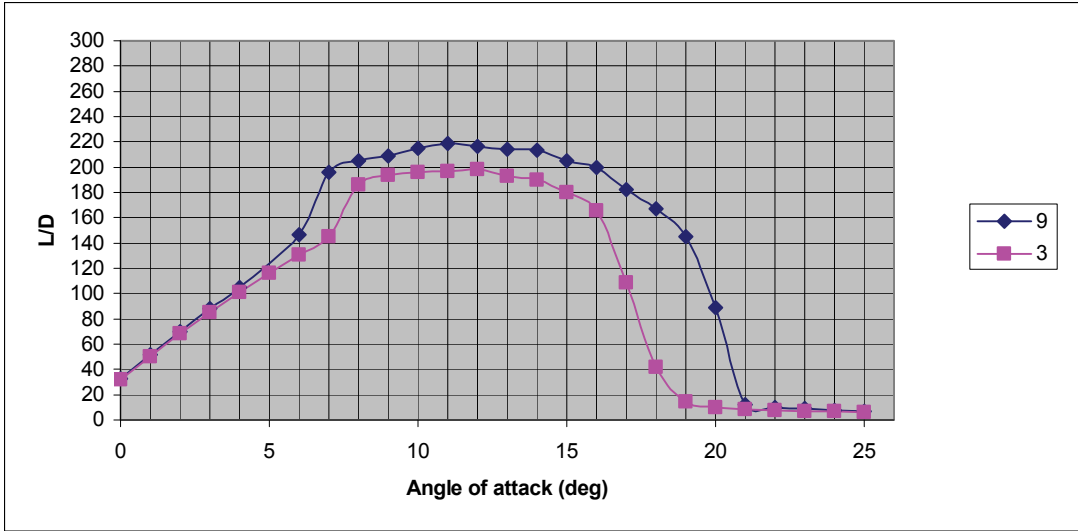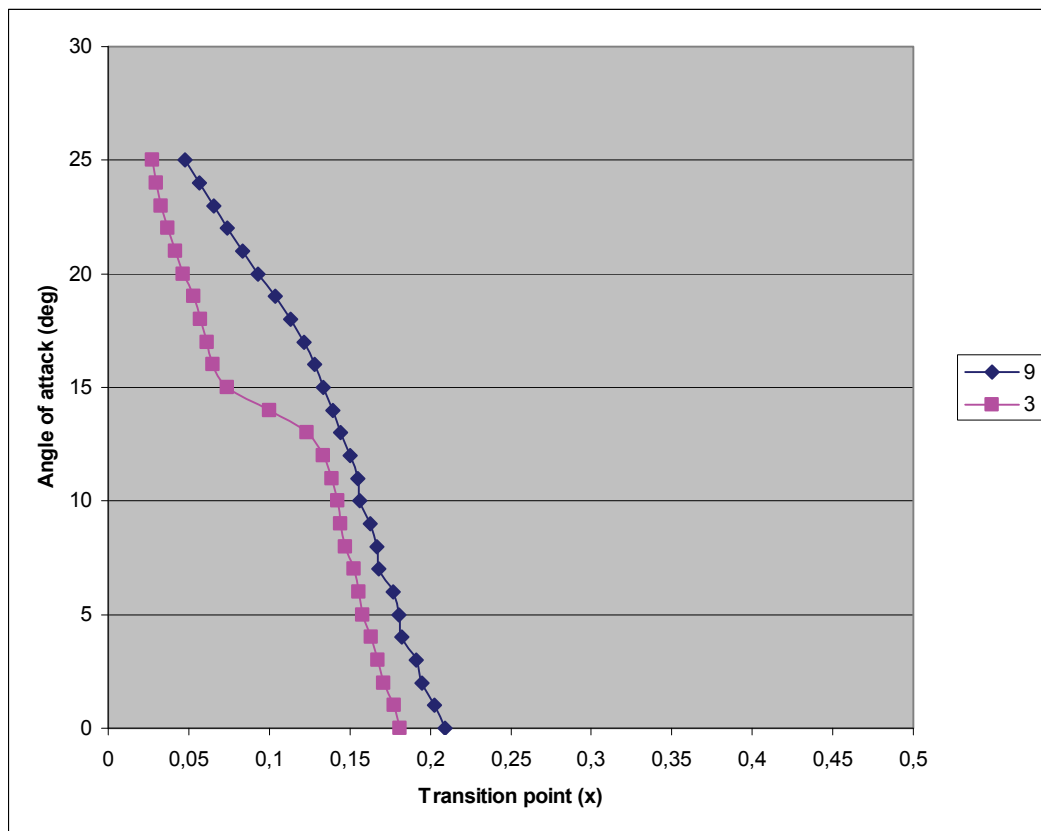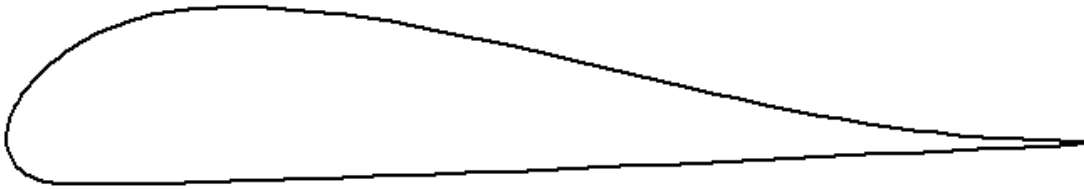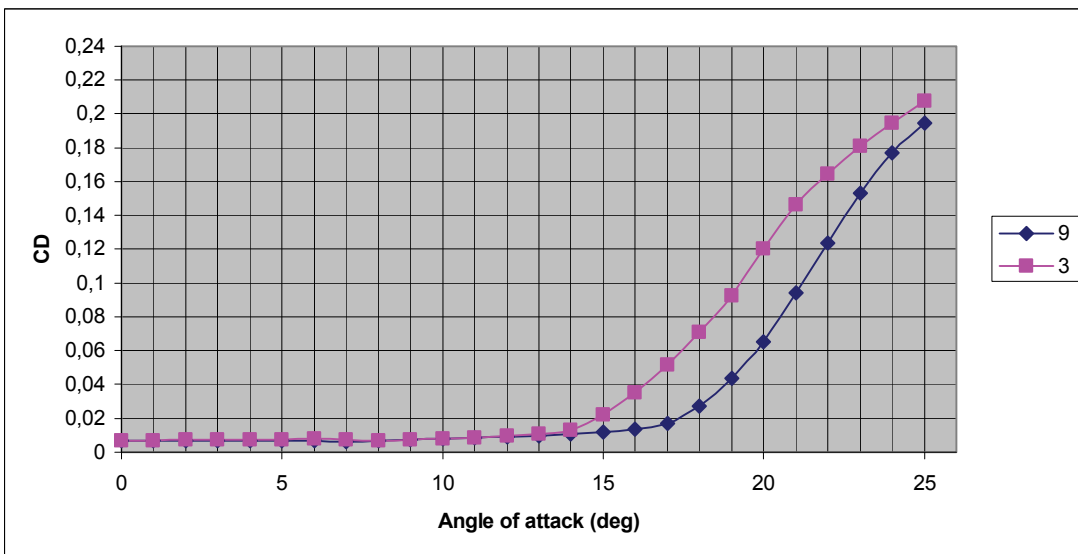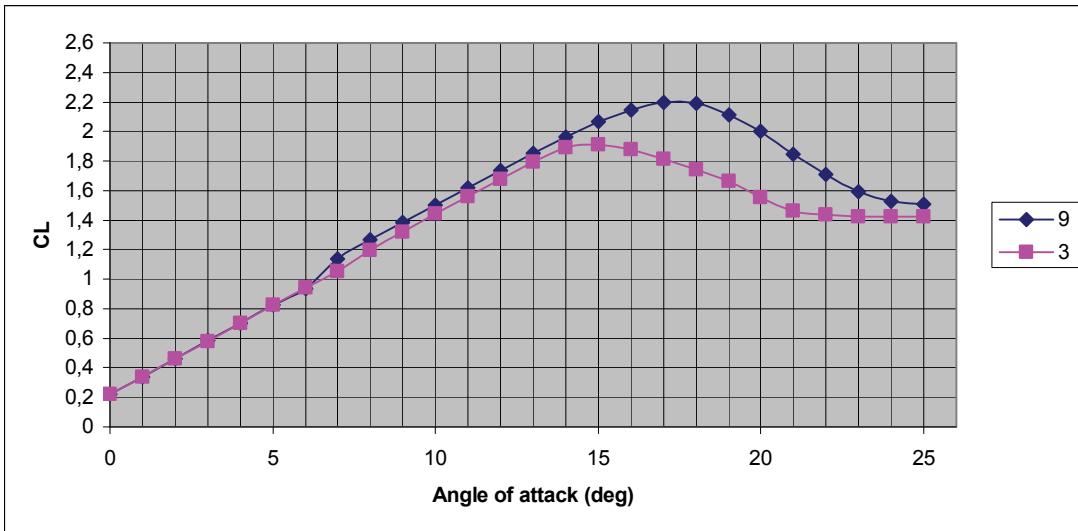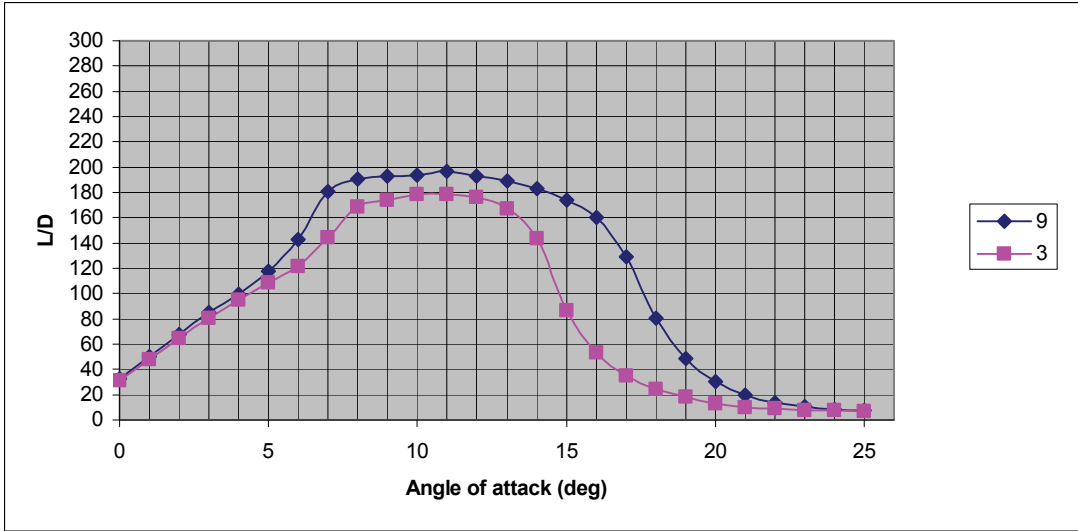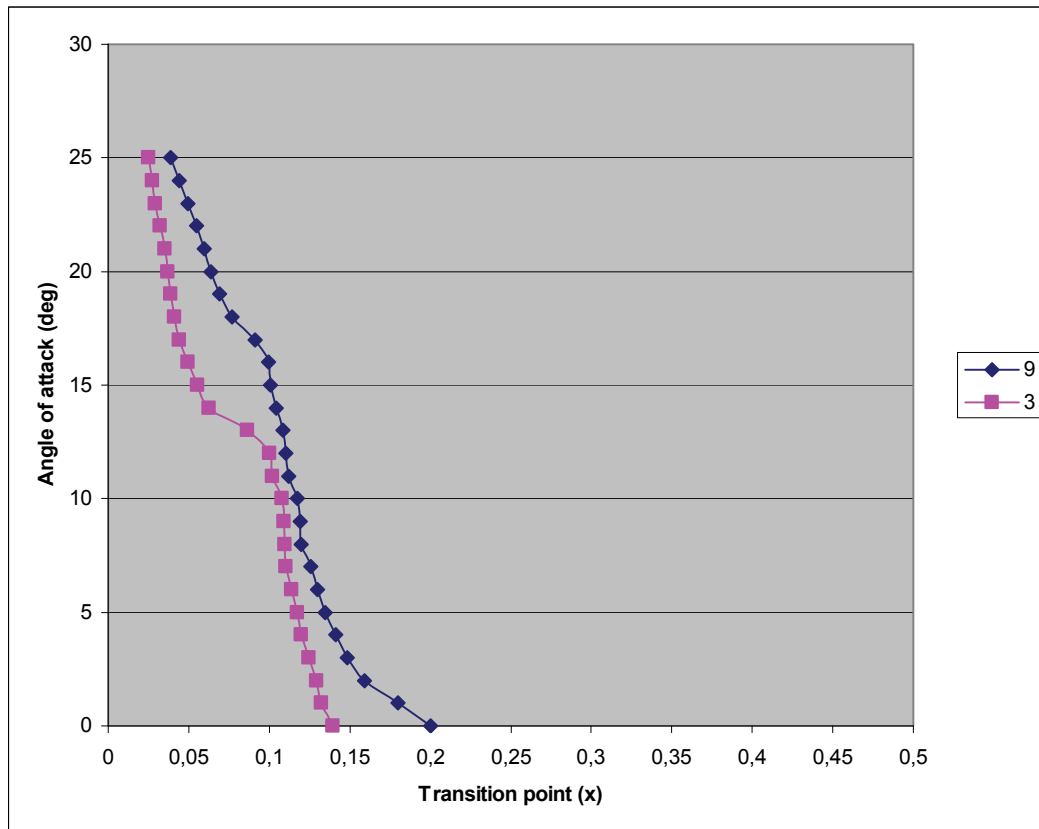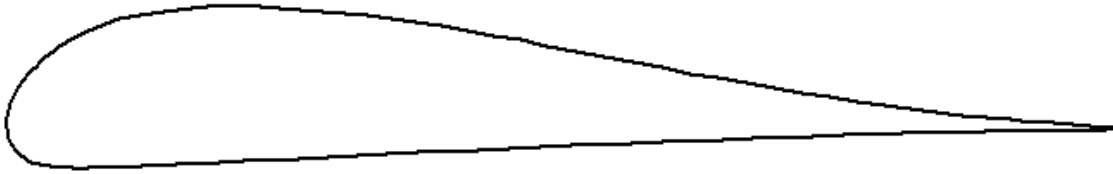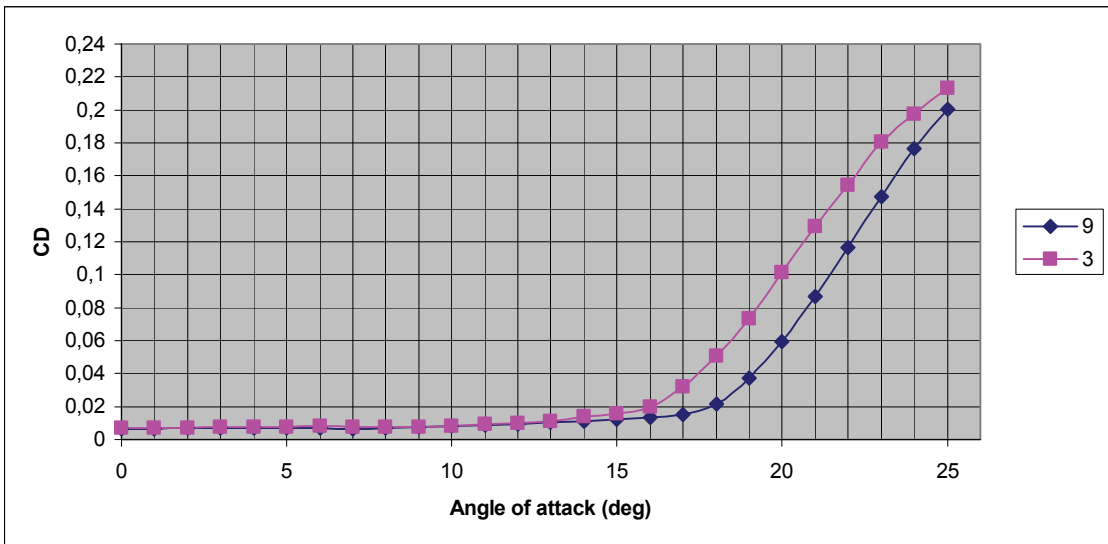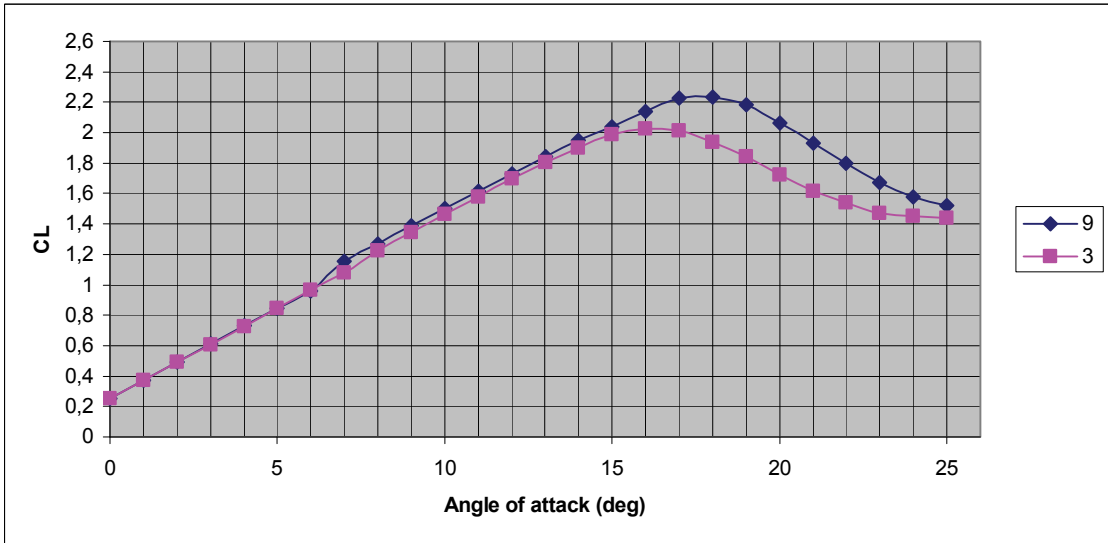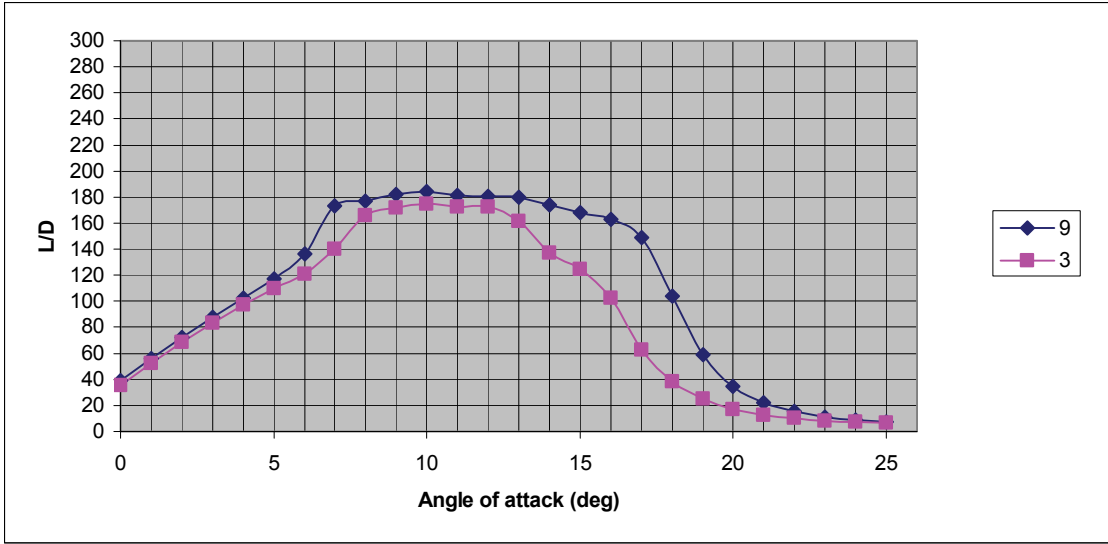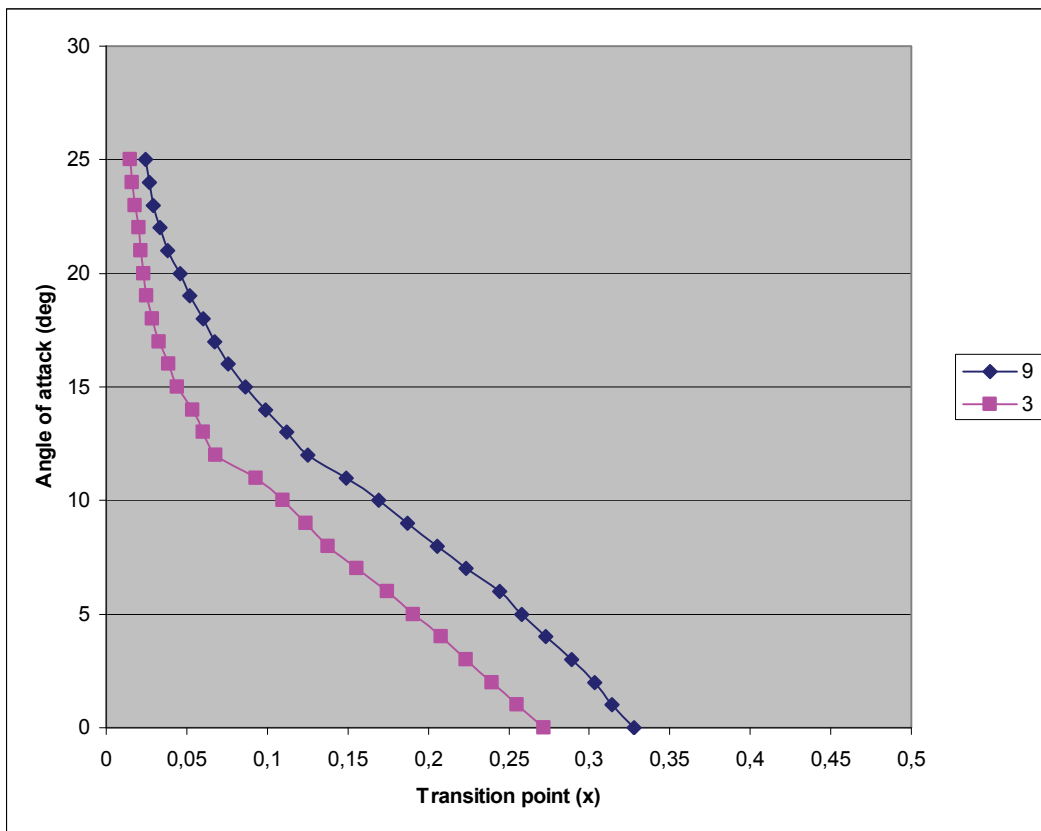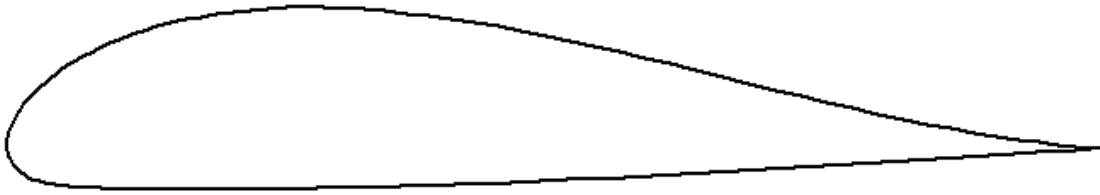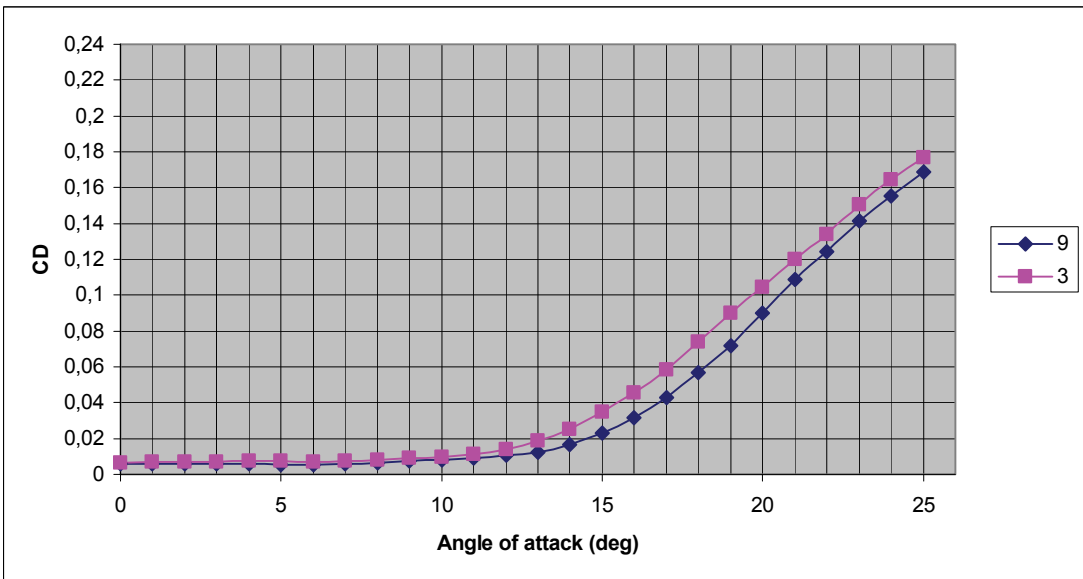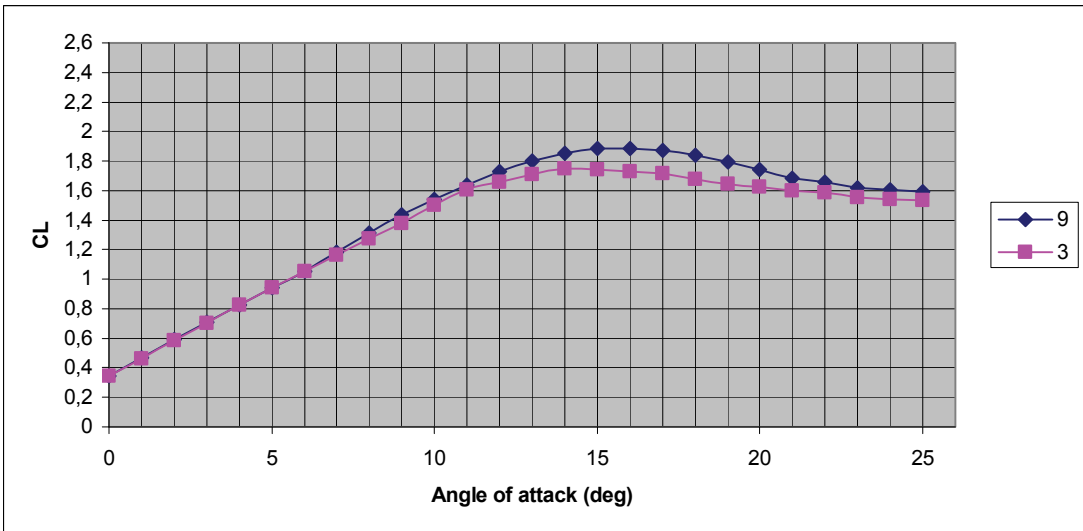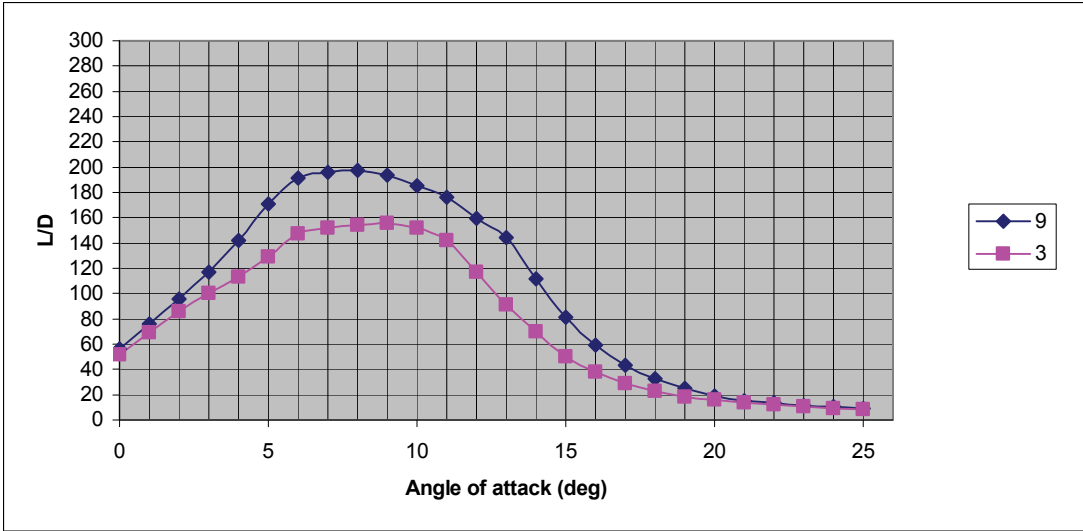
10.12 D2
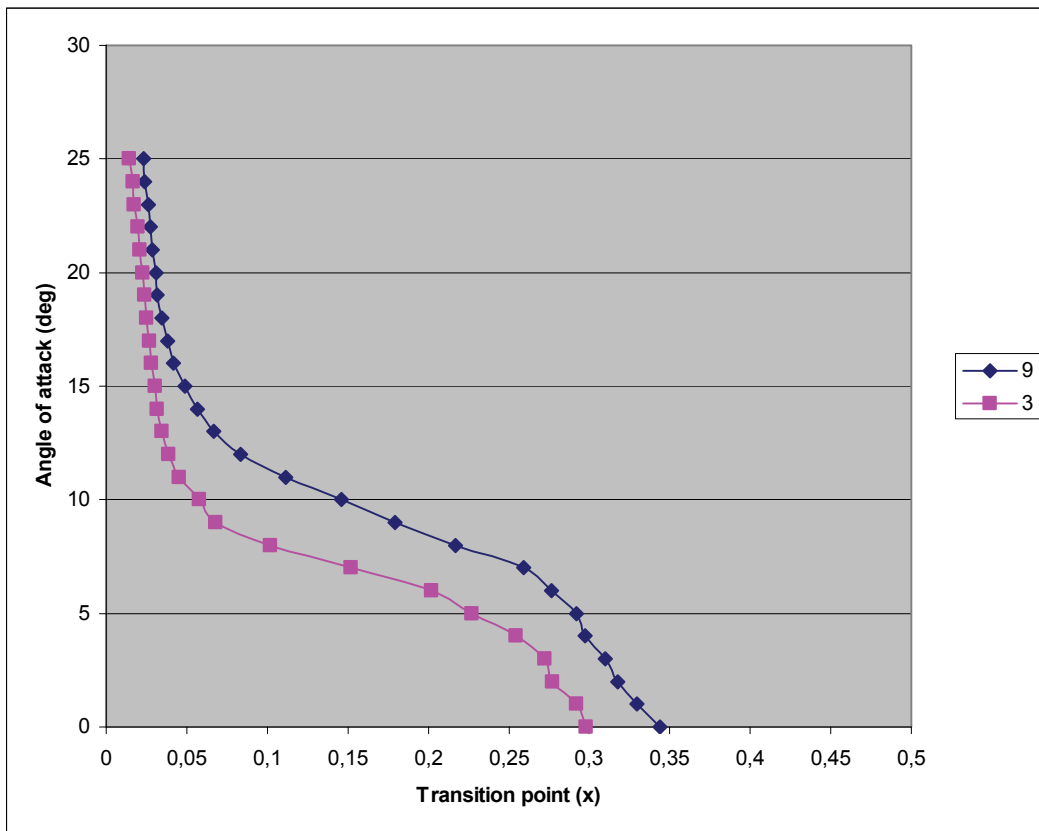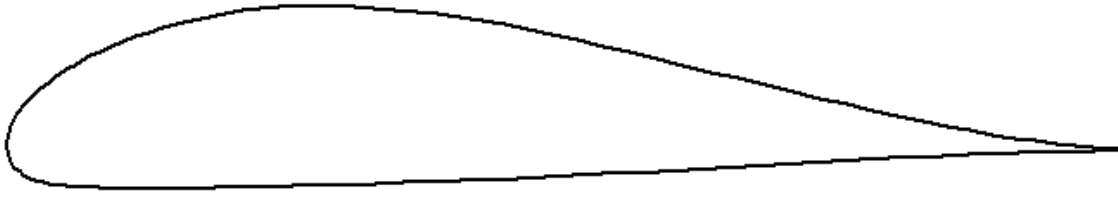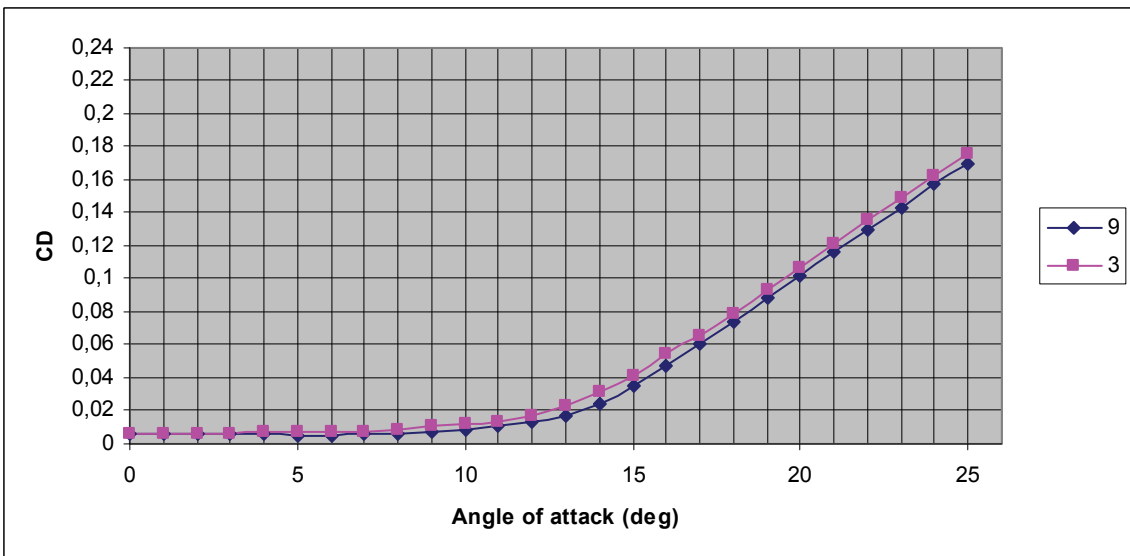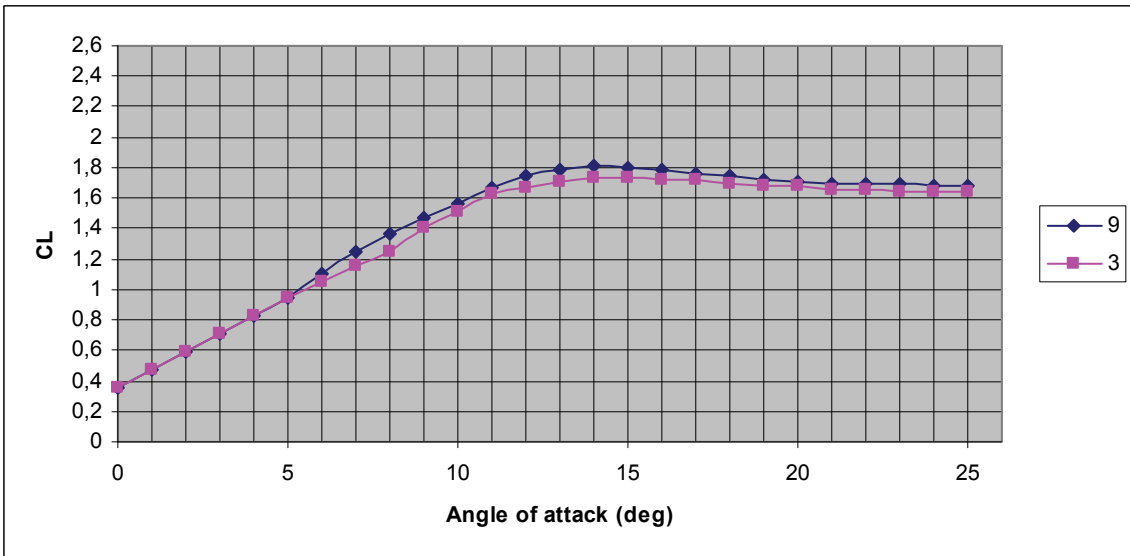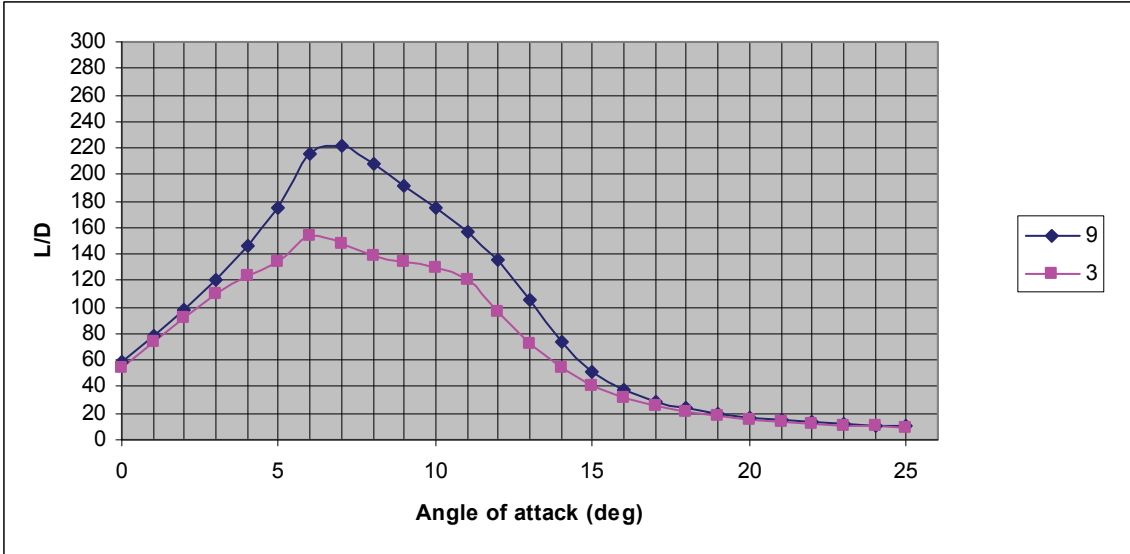
10.13 E1
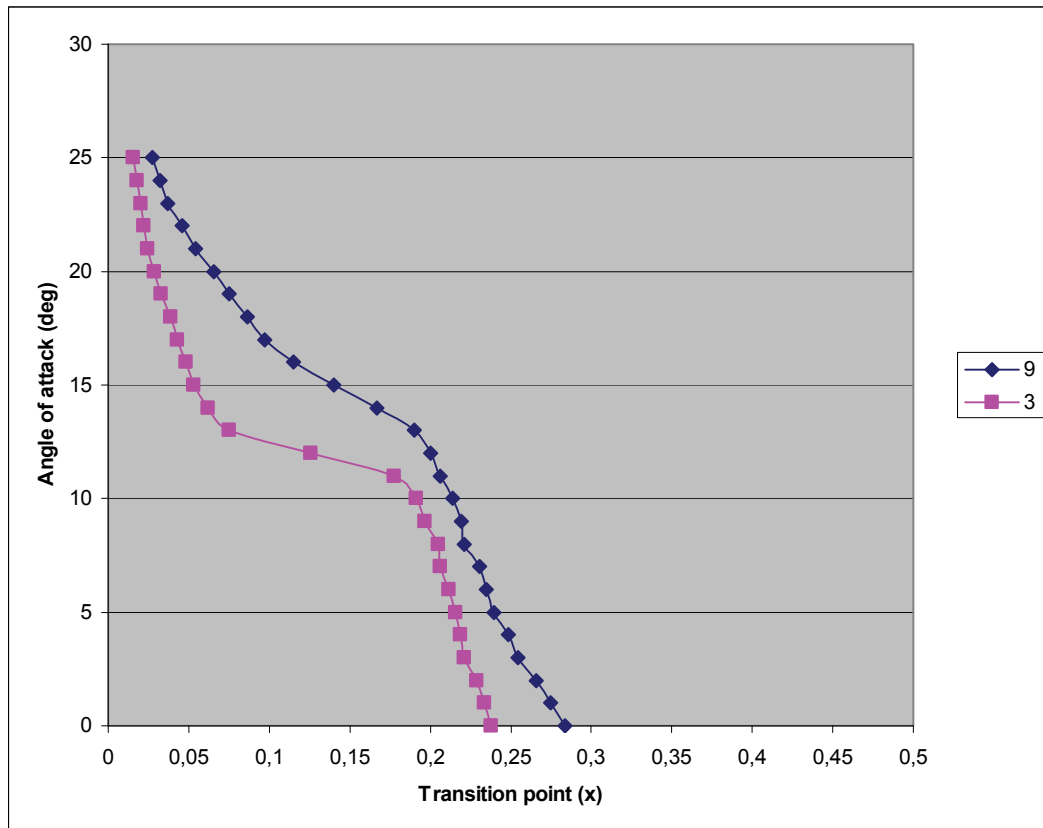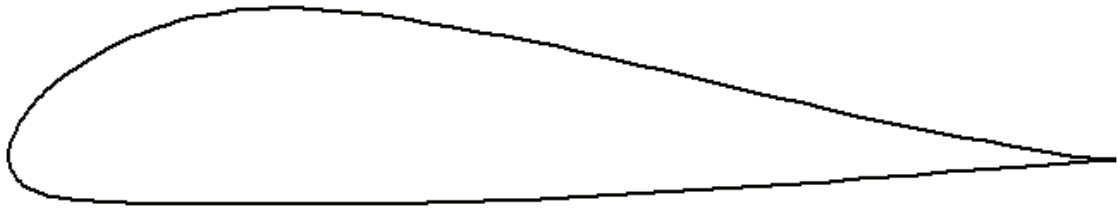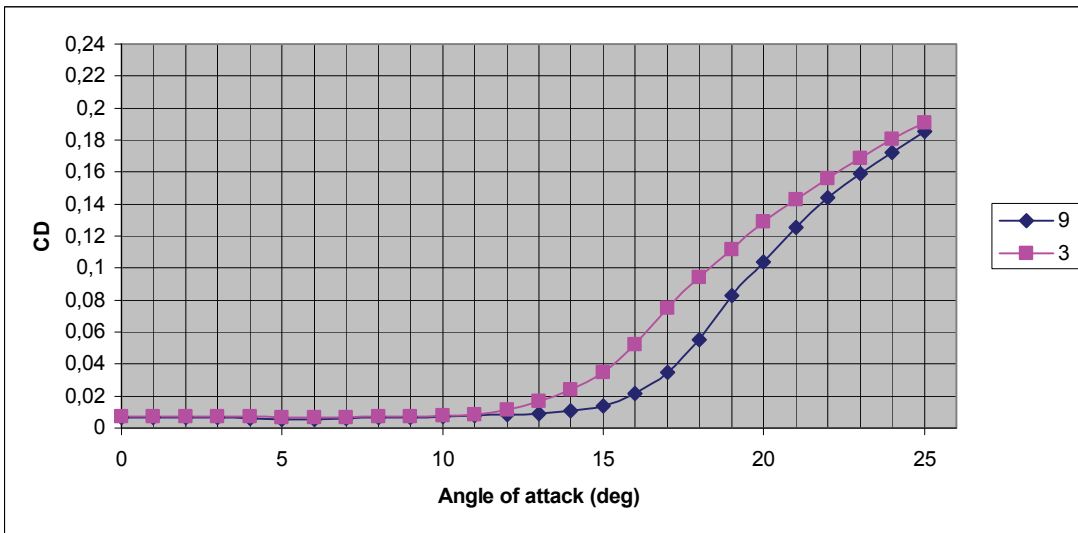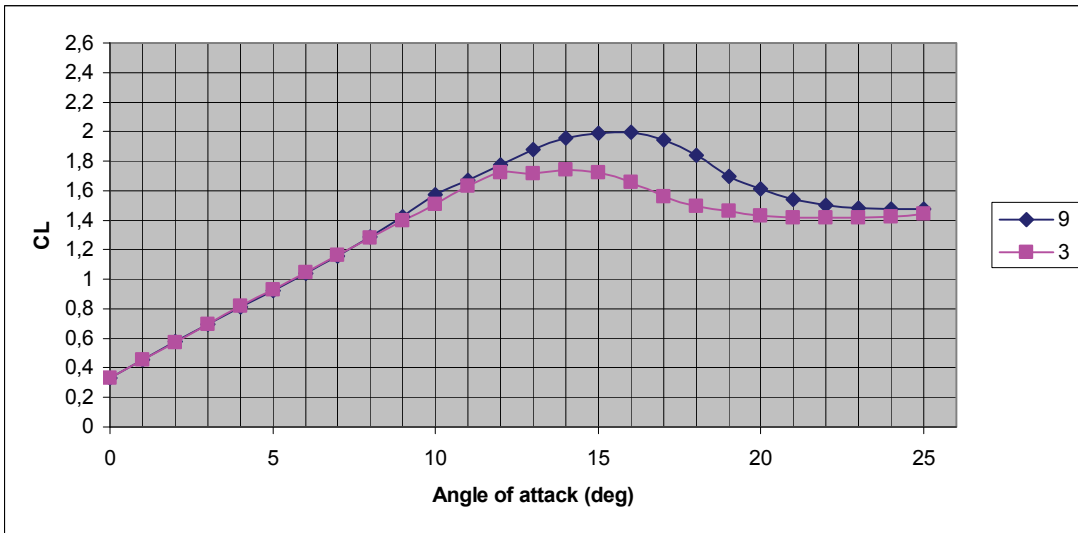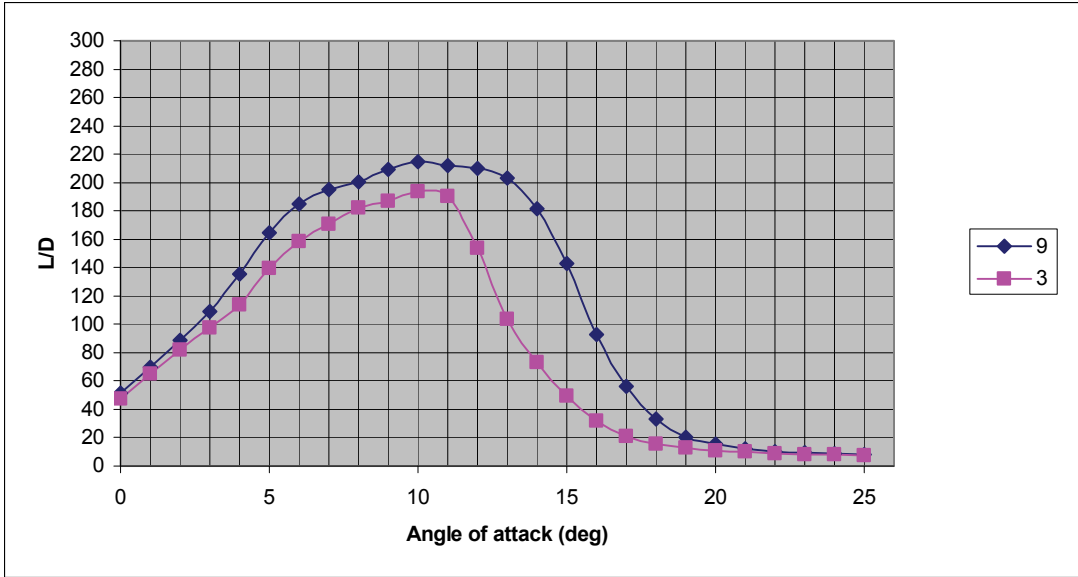
10.14 E2
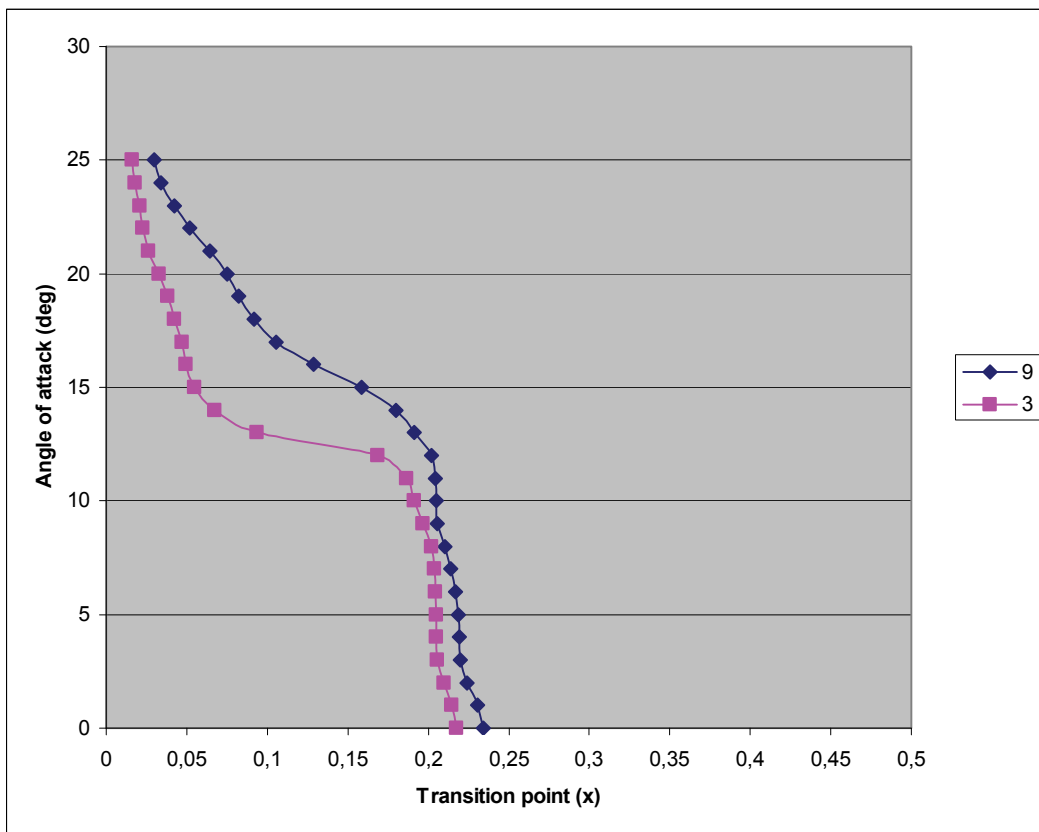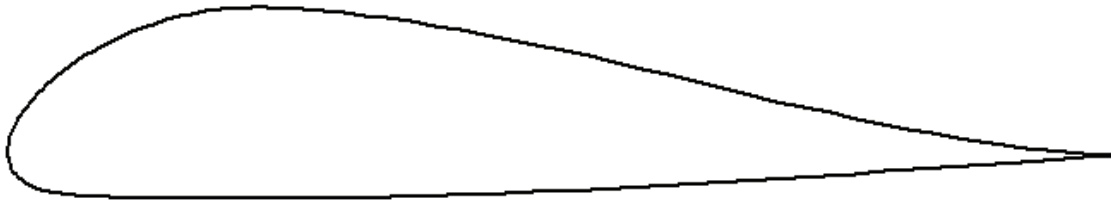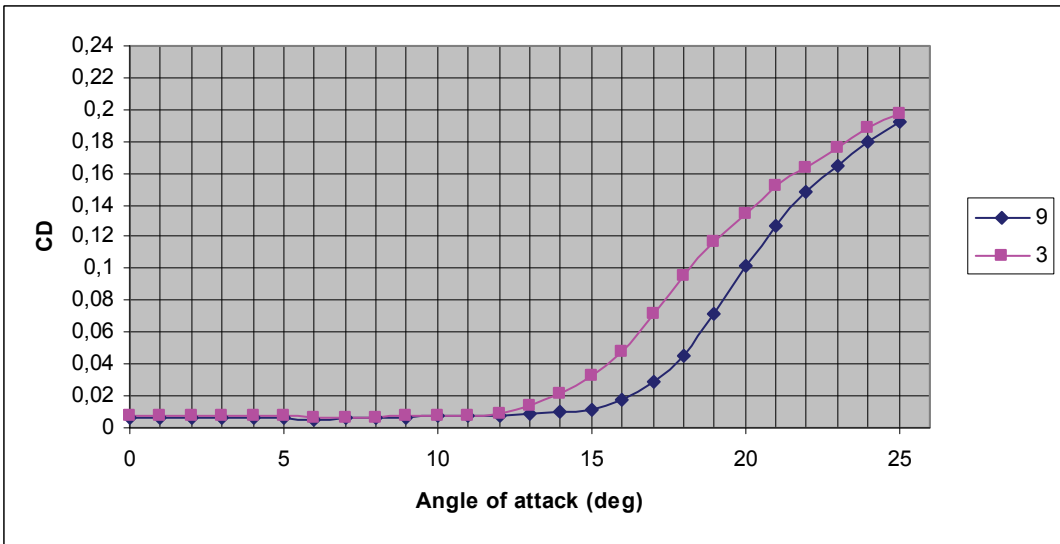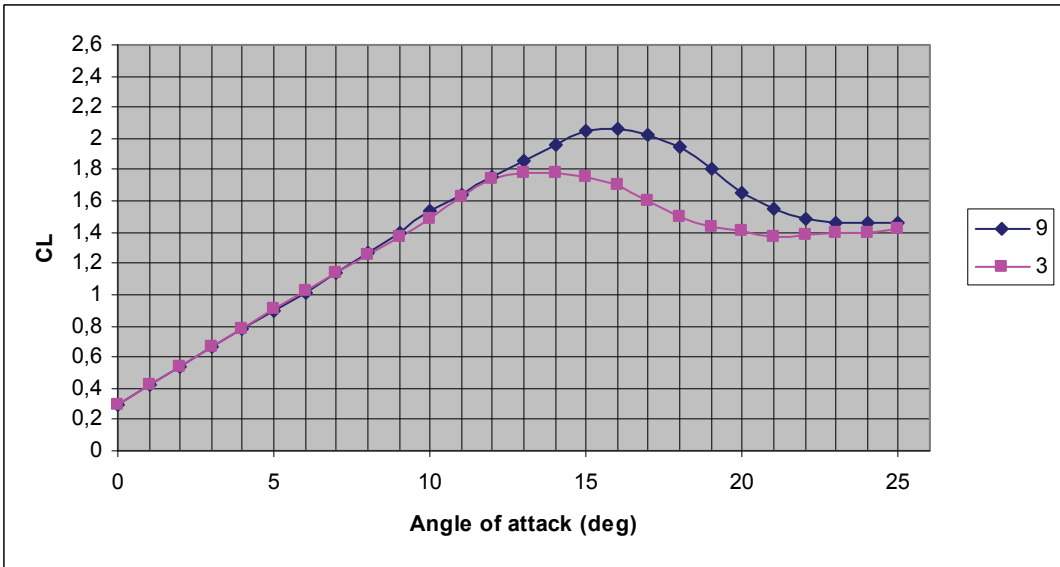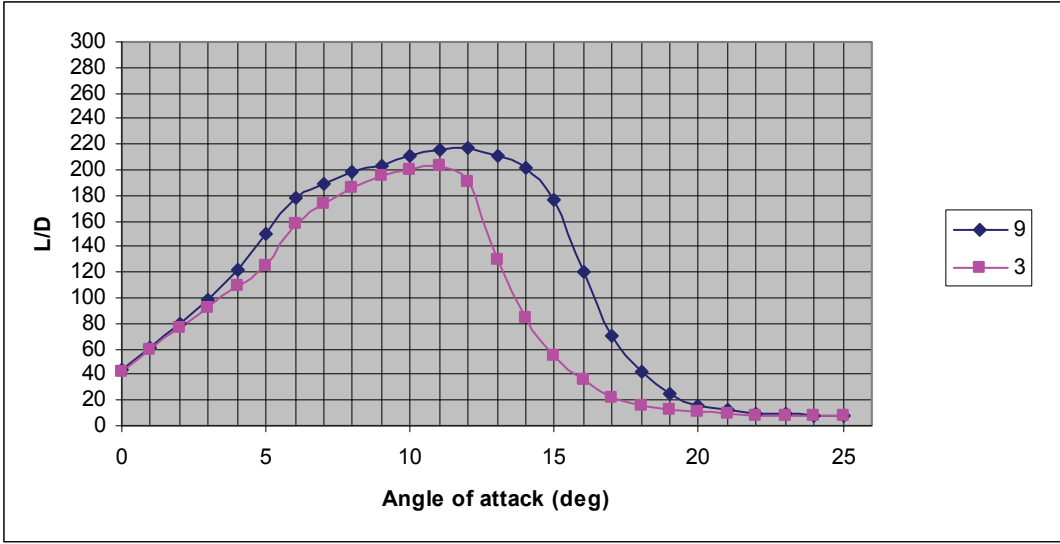
10.15 63_2-415
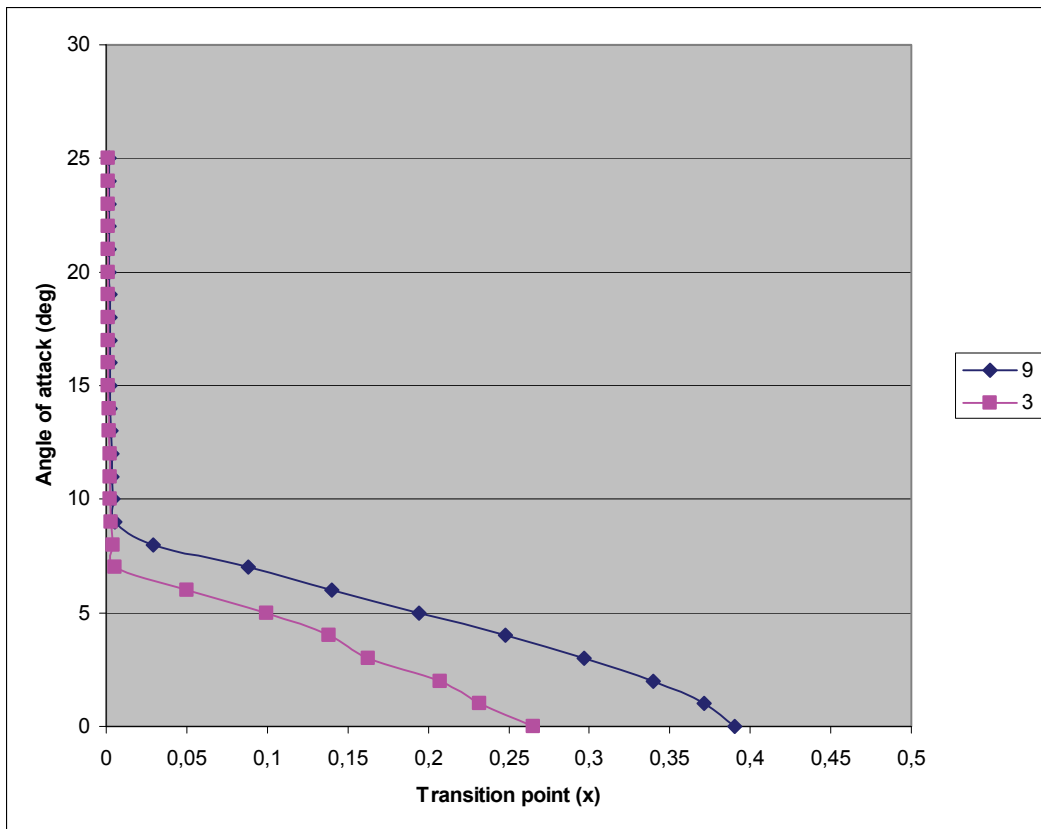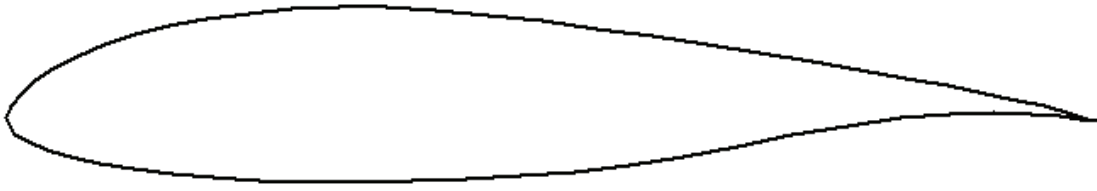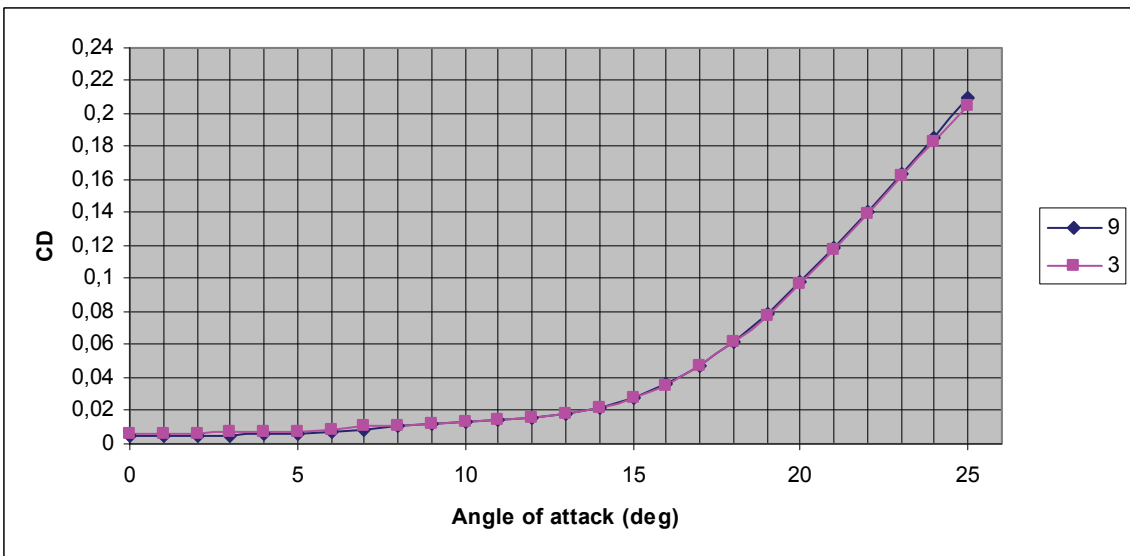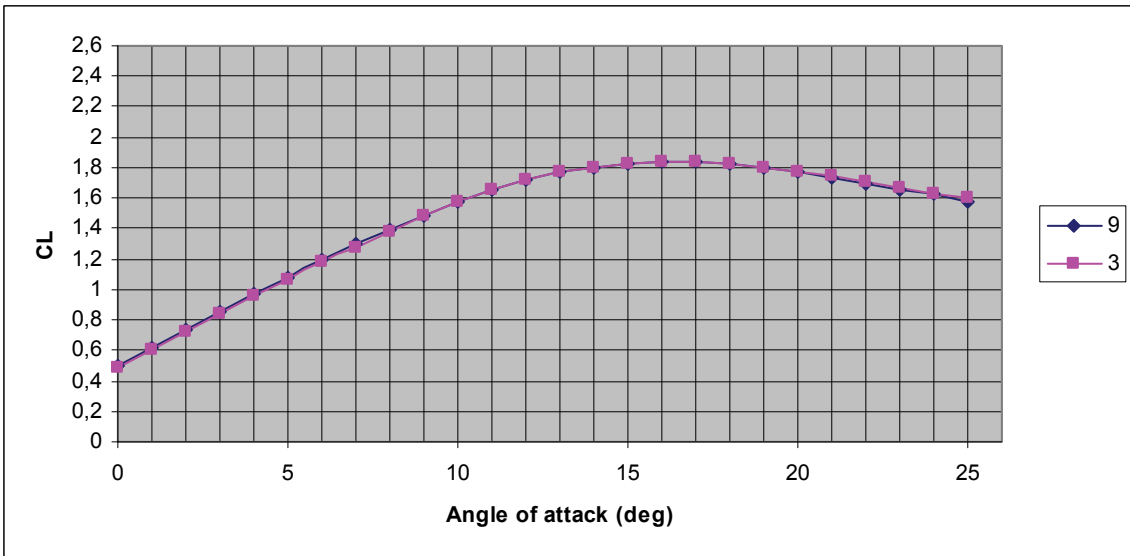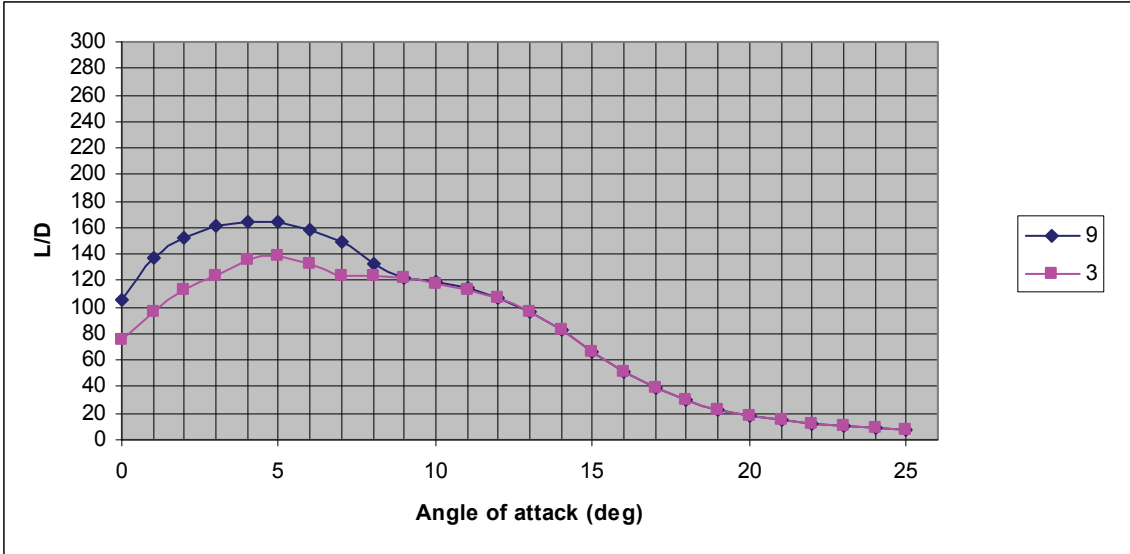
10.16 AR
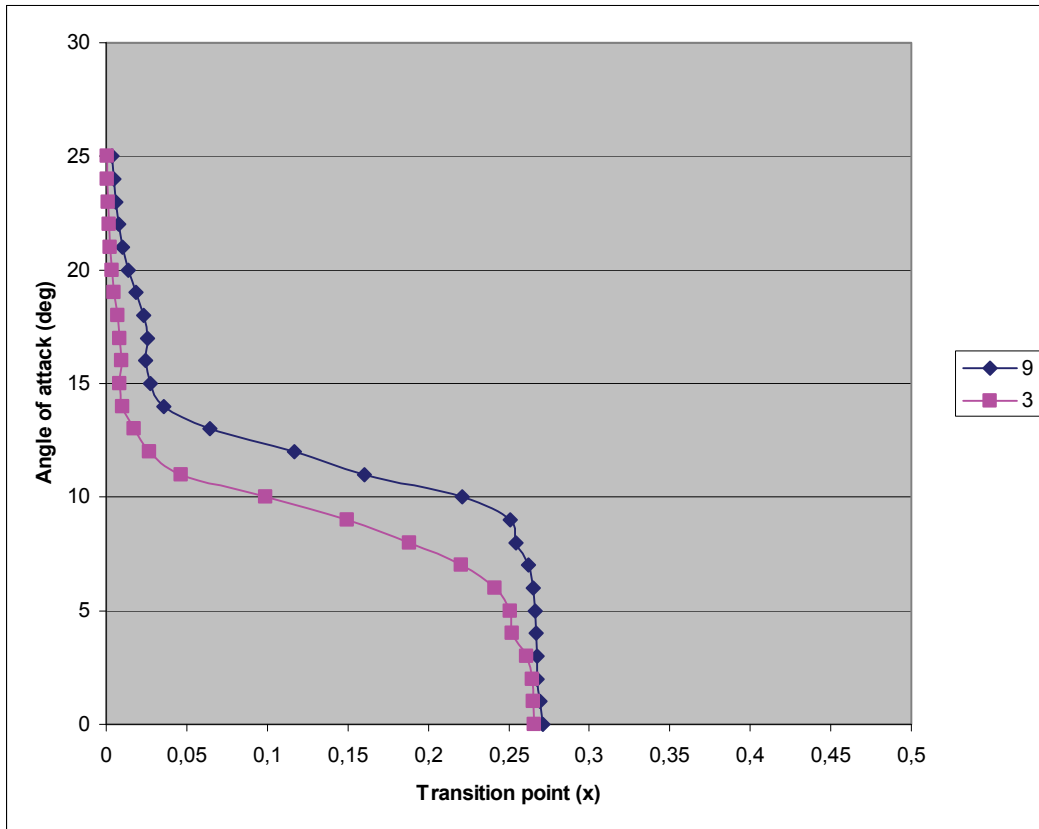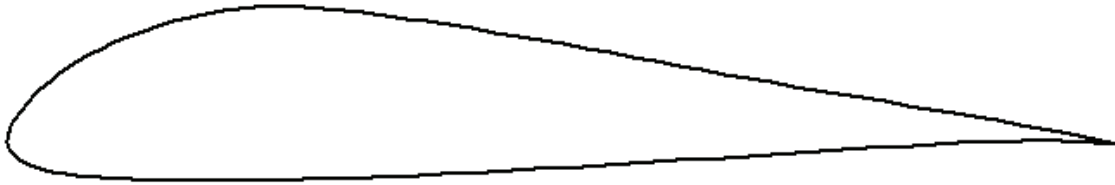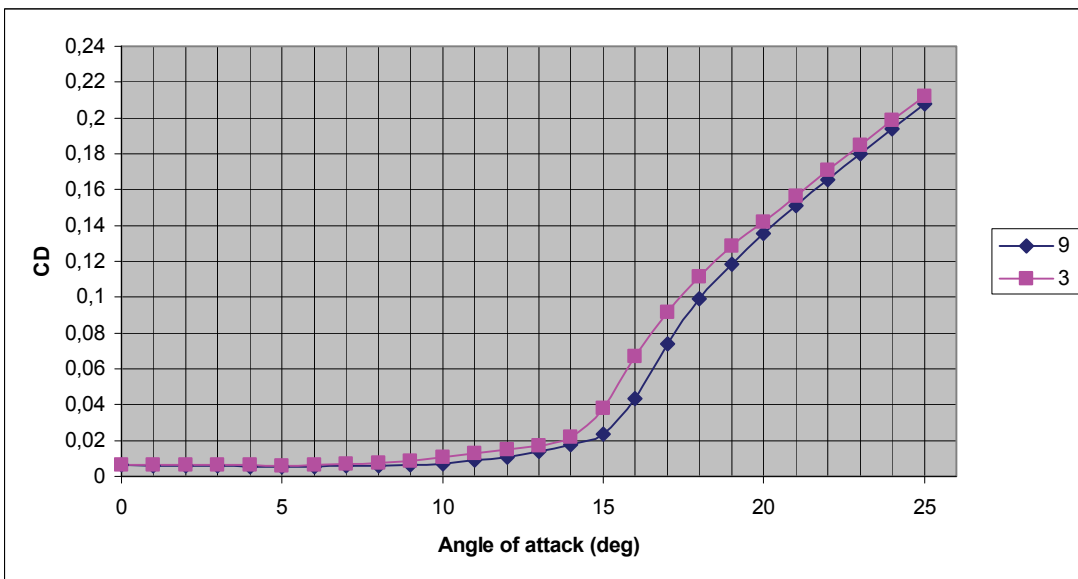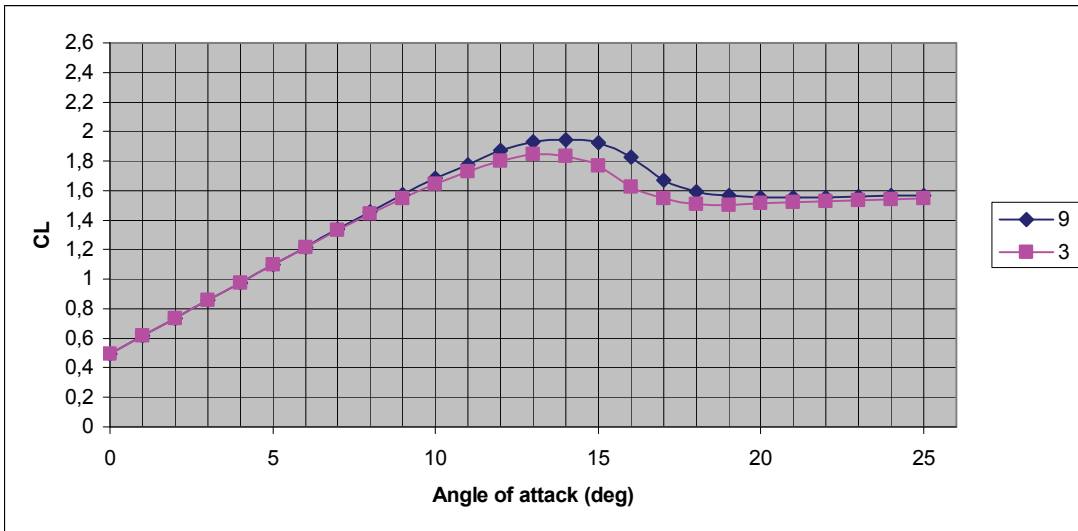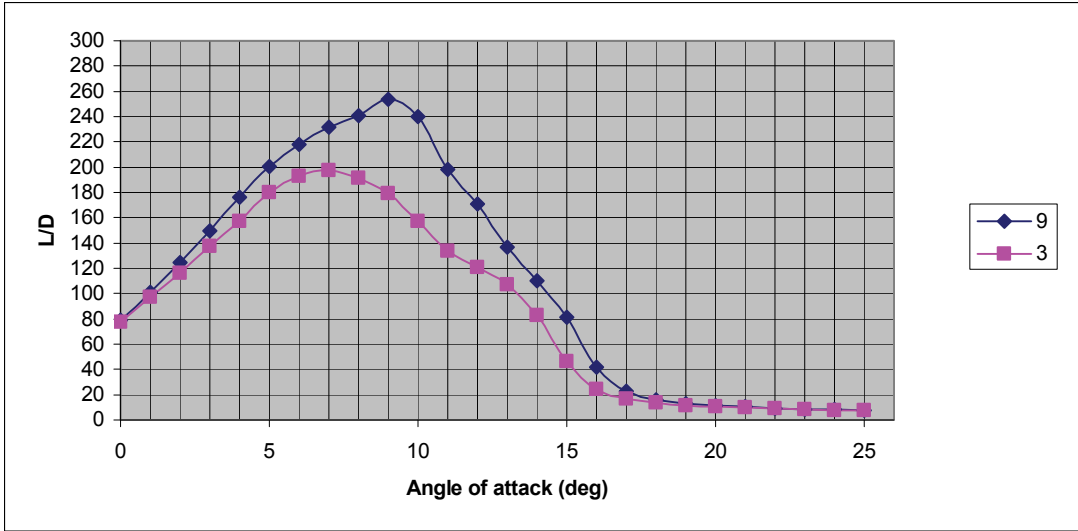
10.17 CR
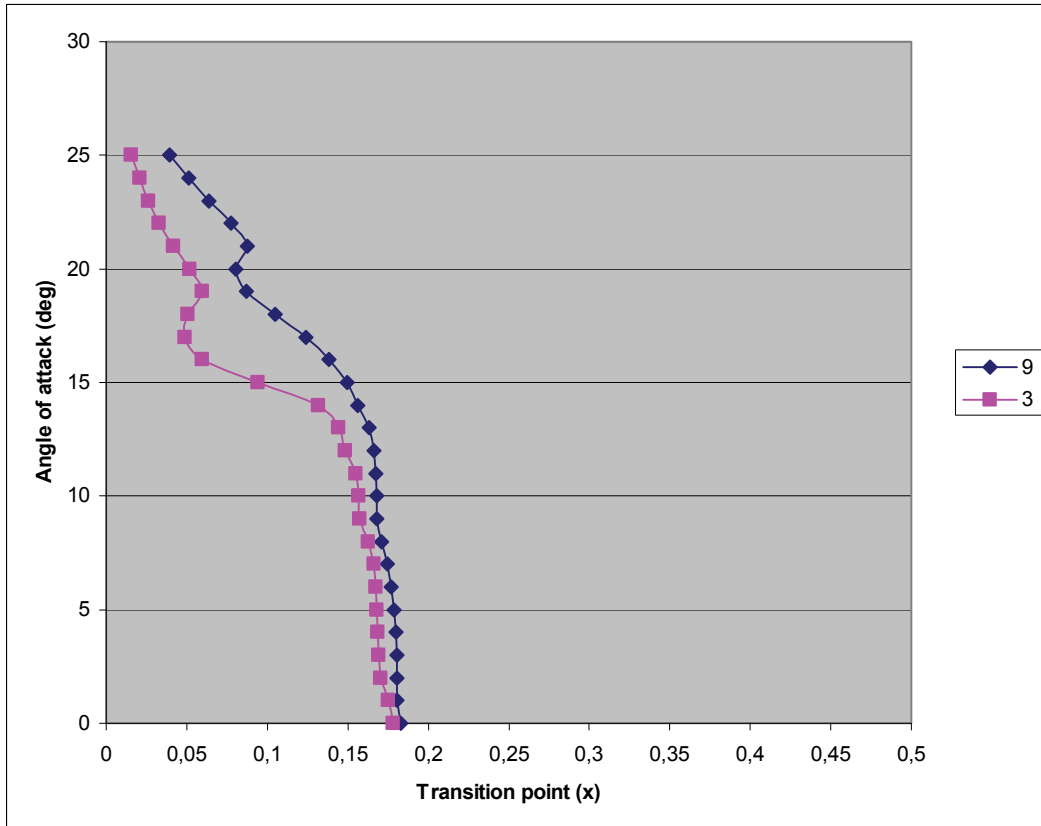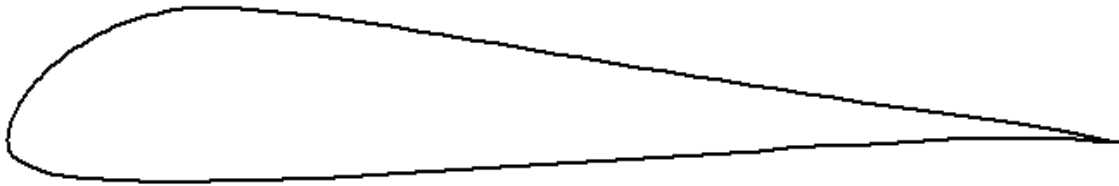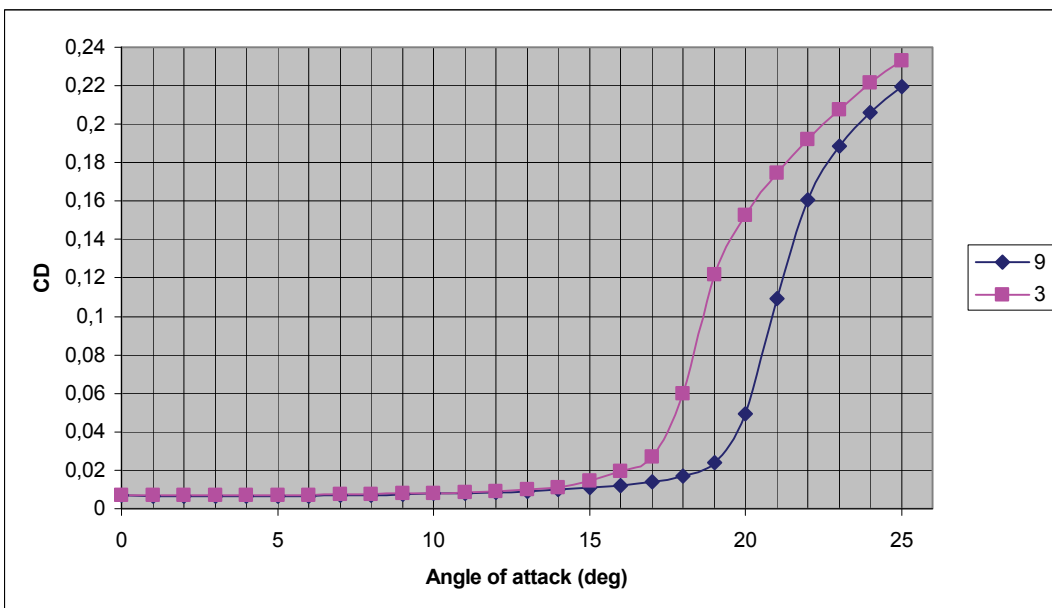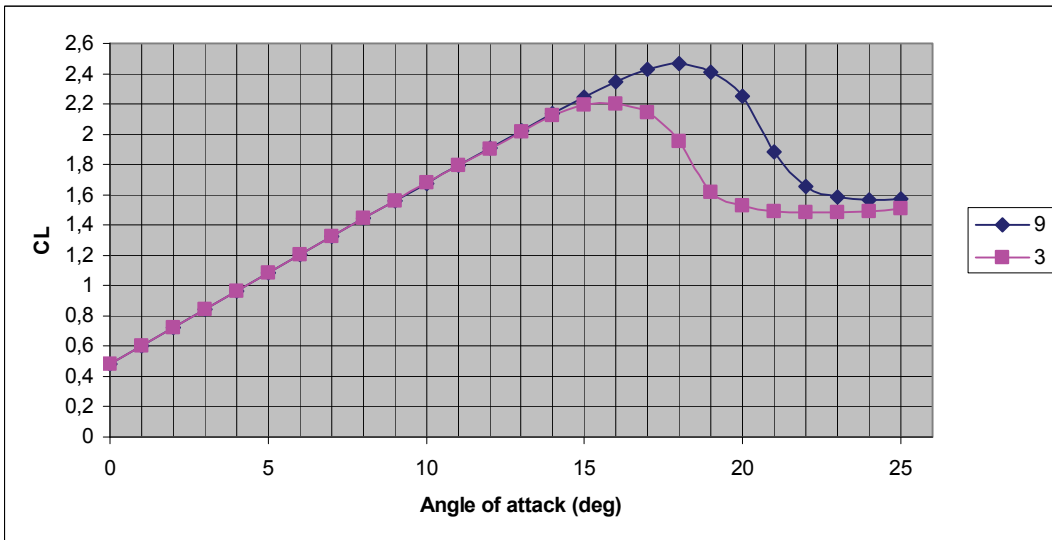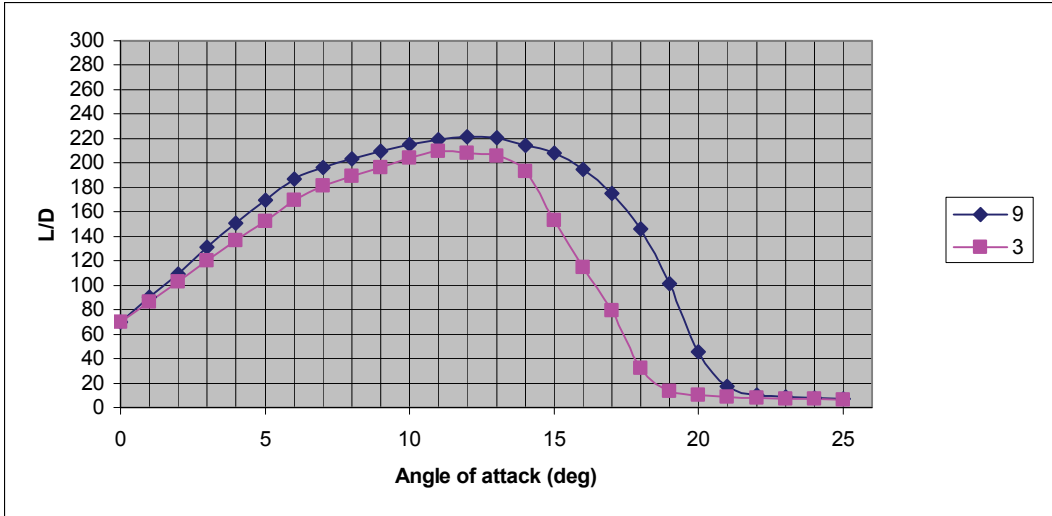
10.18 TR
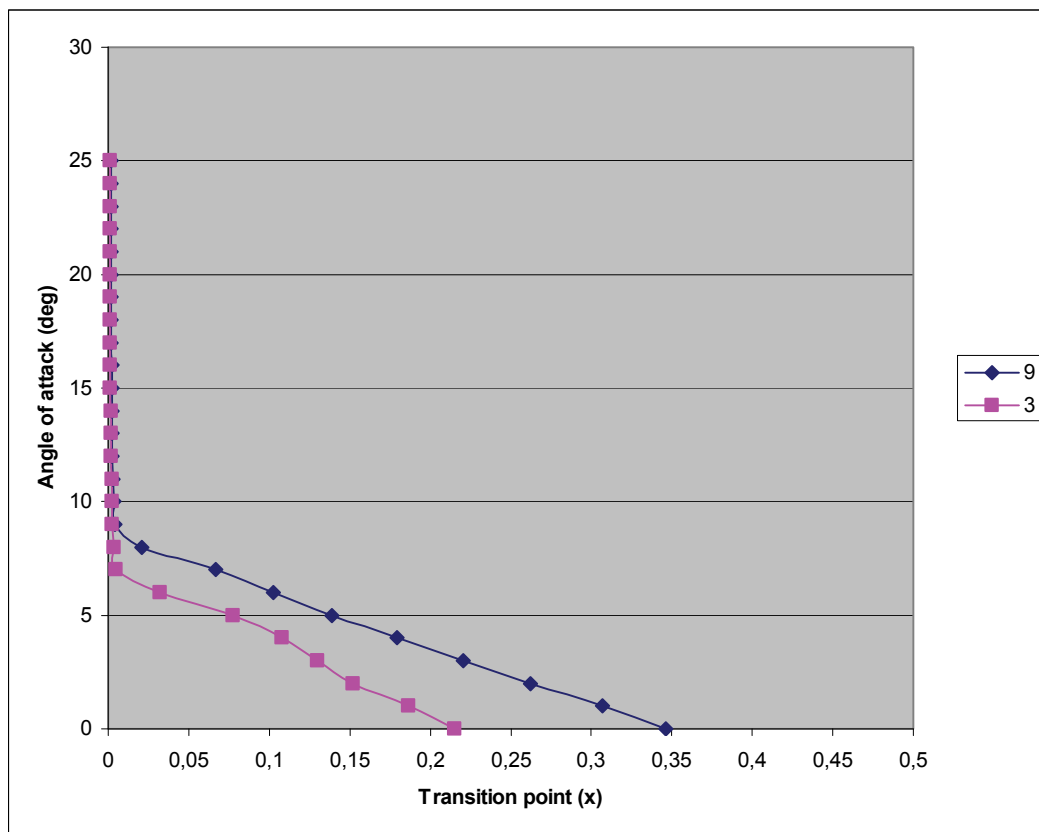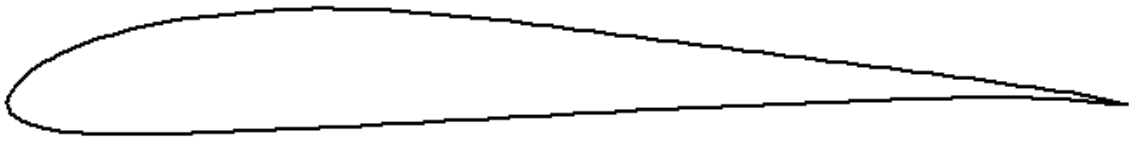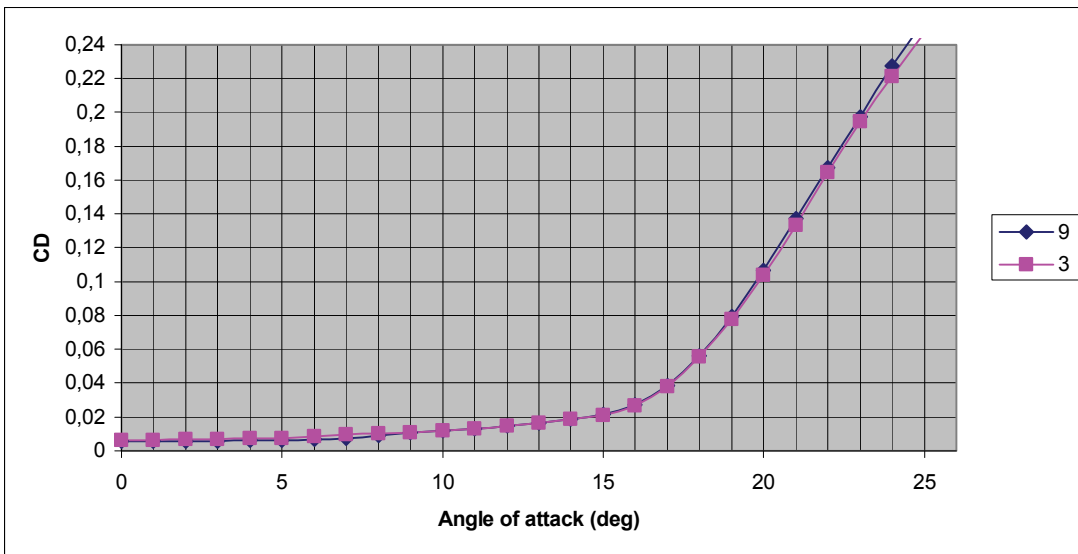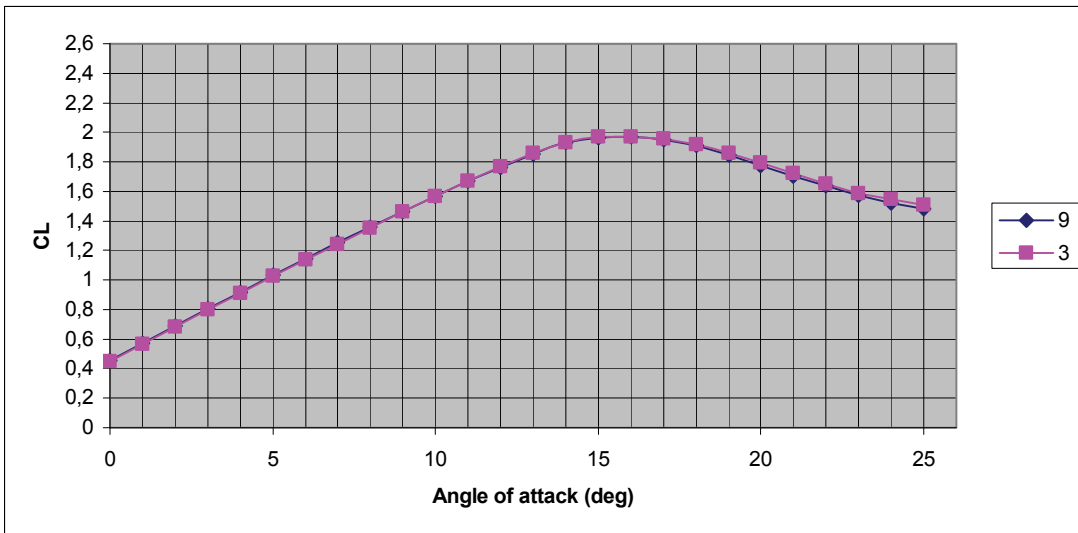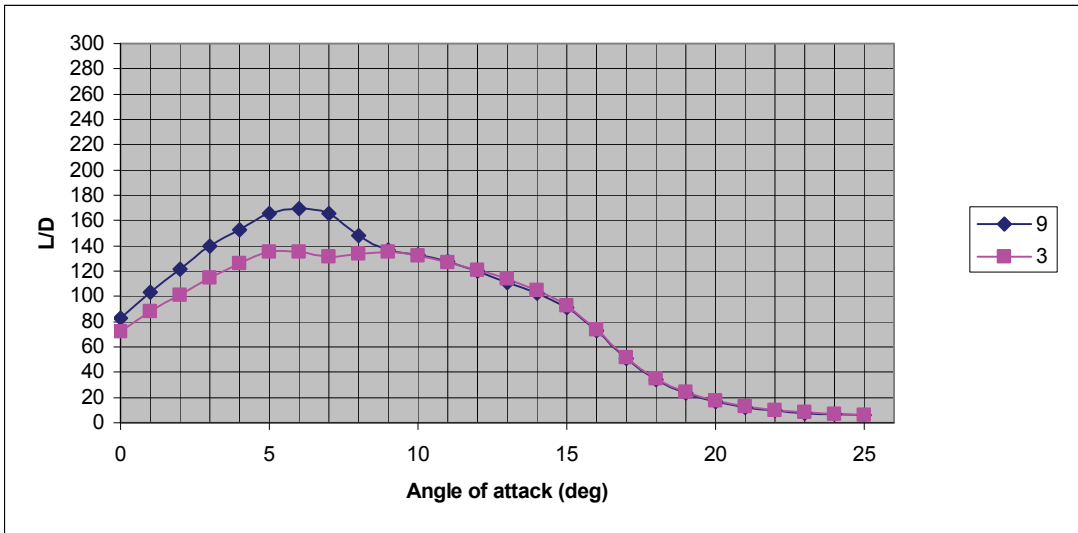
10.19 S1
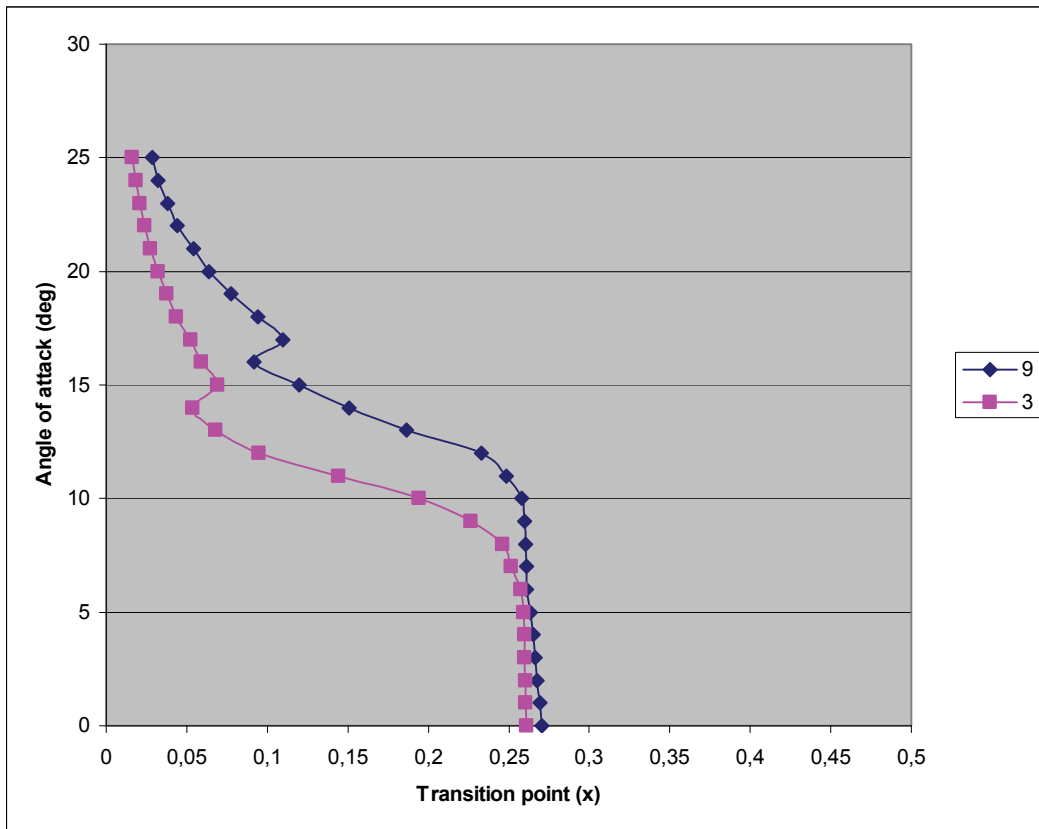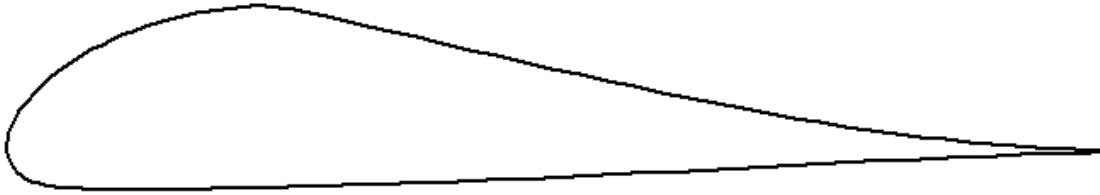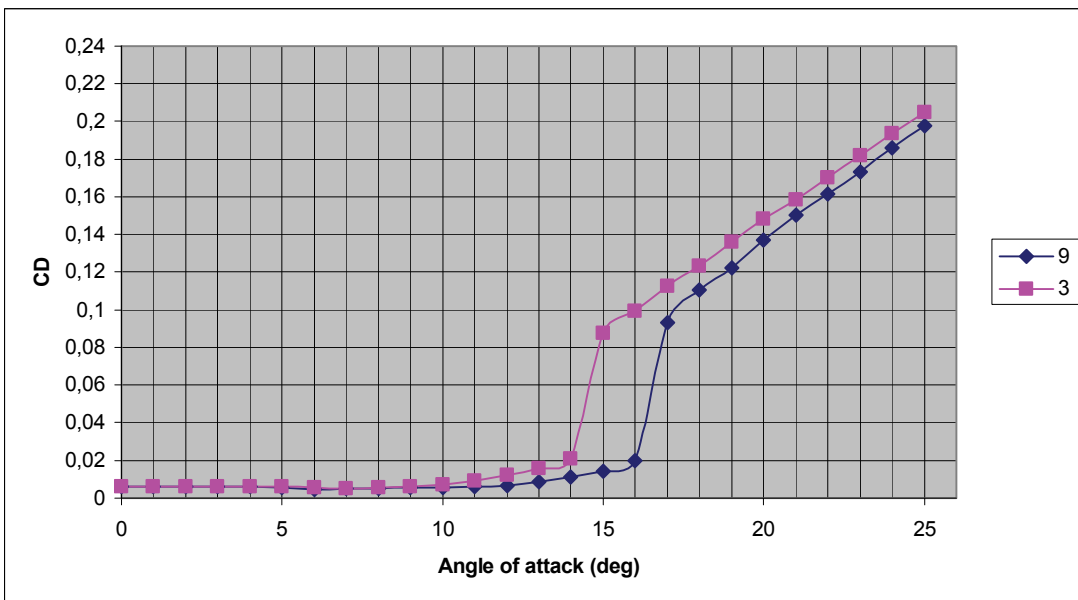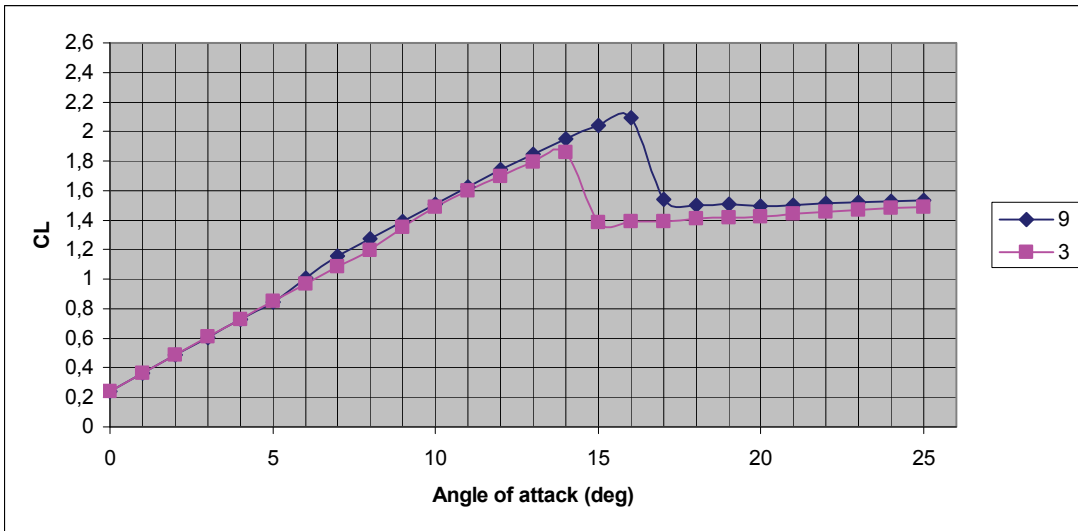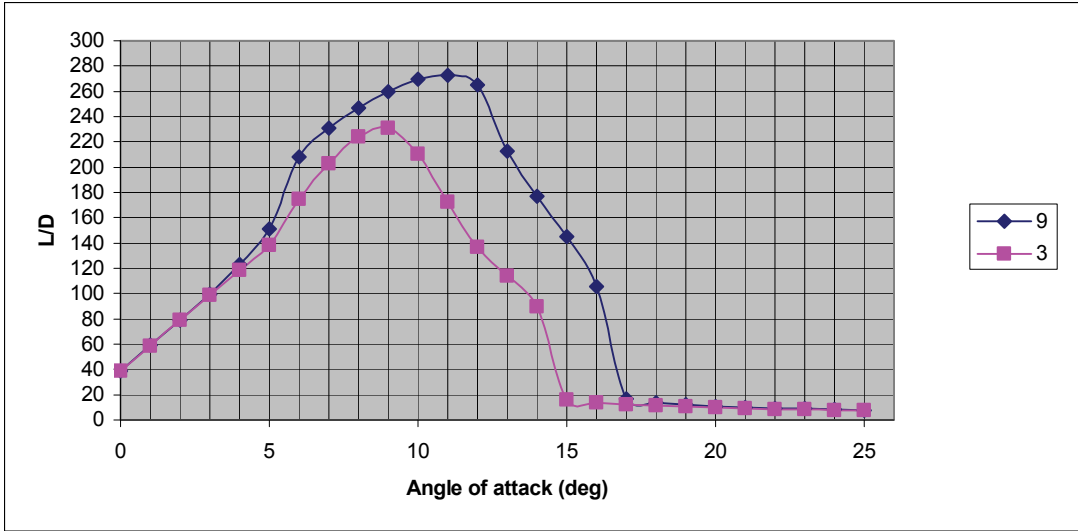
10.20 S2
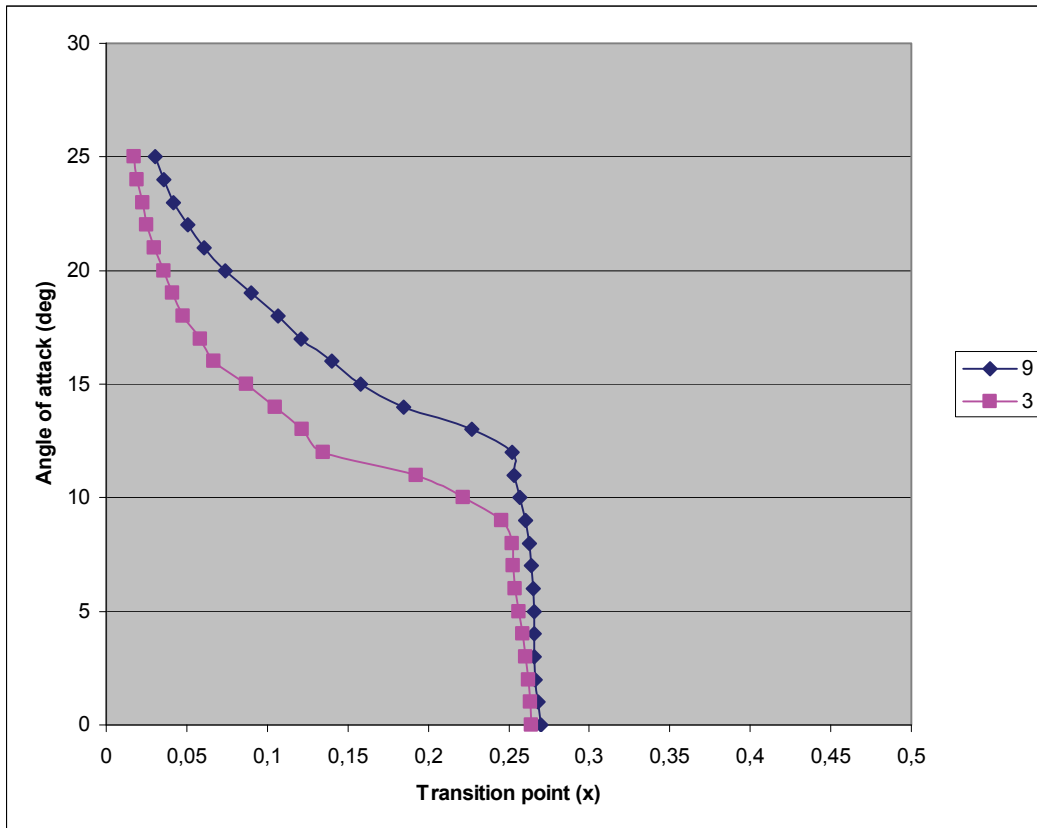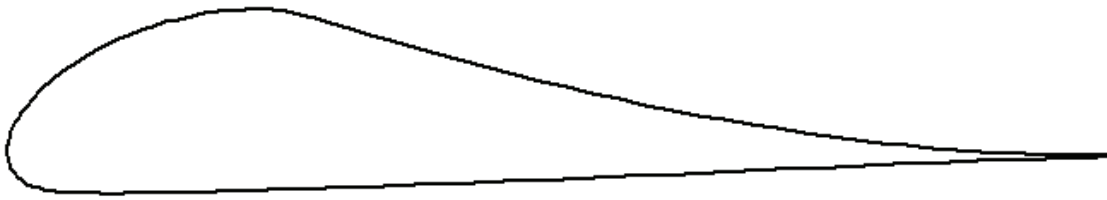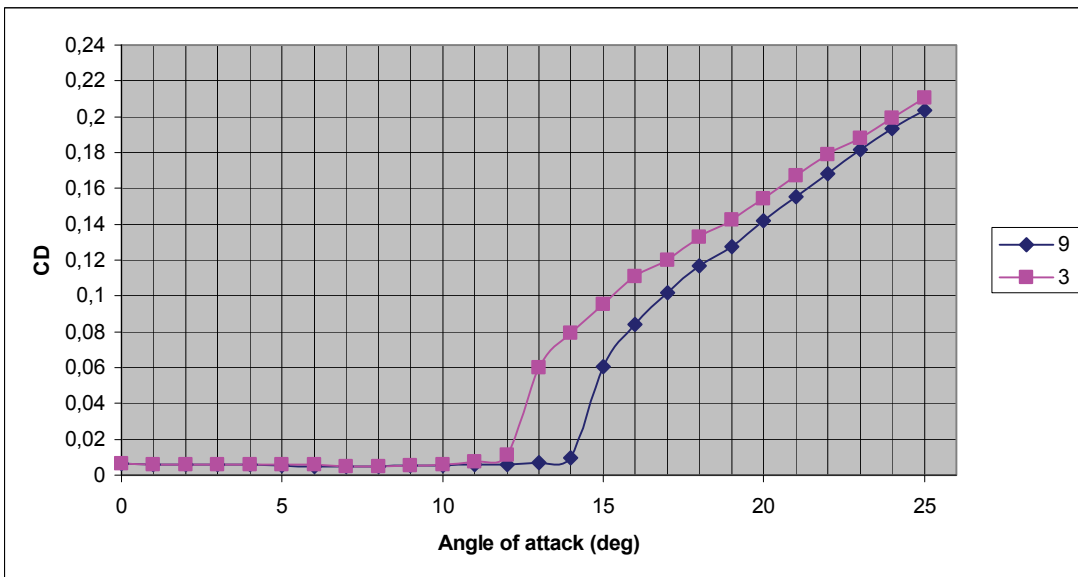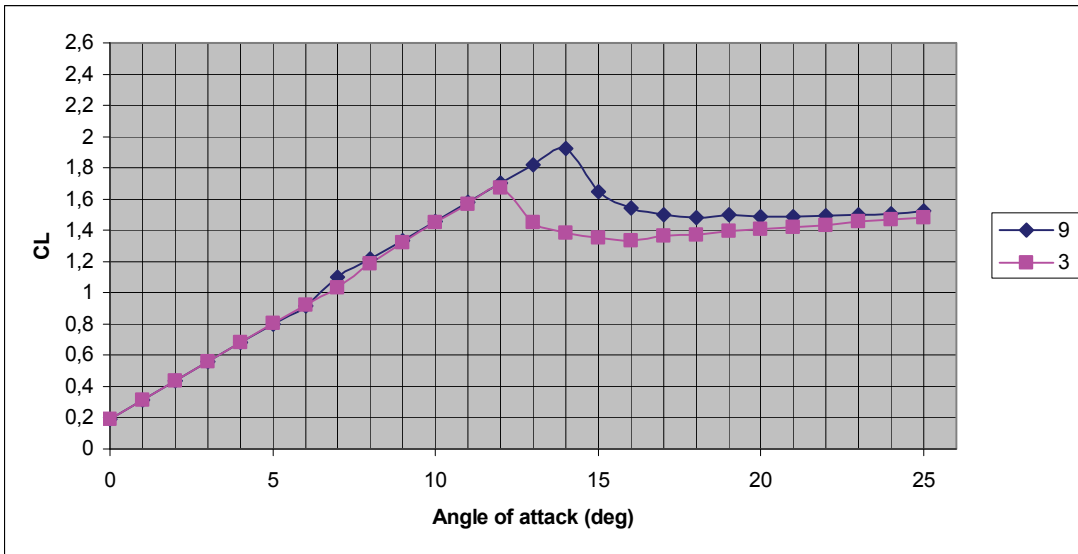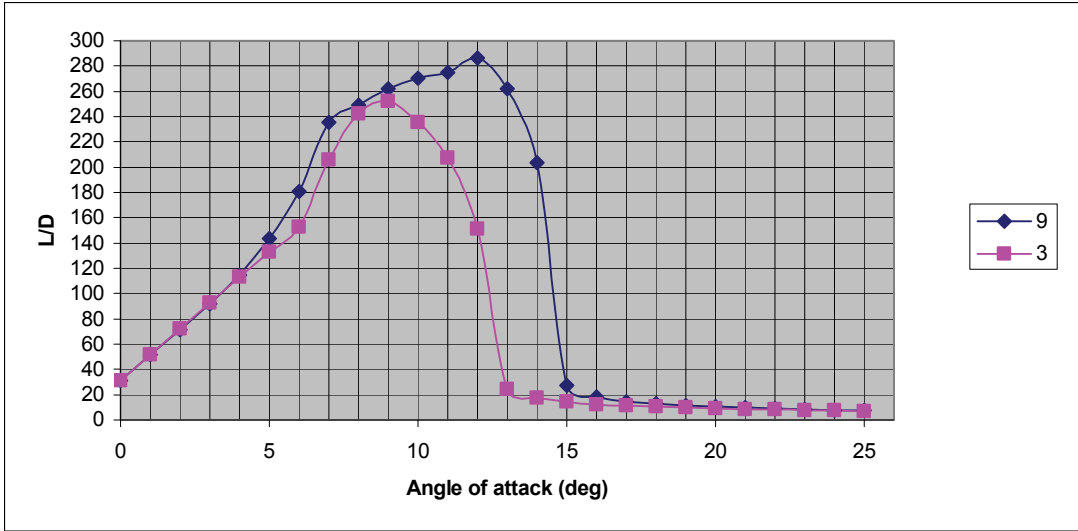
11 Appendix B (coordinates)

NACA 4412	x	y	x	y	4412
	1.000000	0.001260	0.000262	0.002916	
	0.992984	0.003170	0.000019	0.000770	
	0.980512	0.006518	0.000056	-0.001318	
	0.965816	0.010385	0.000399	-0.003449	
	0.949438	0.014597	0.001095	-0.005593	
	0.932047	0.018959	0.002165	-0.007692	
	0.914131	0.023333	0.003613	-0.009713	
	0.895961	0.027648	0.005429	-0.011631	
	0.877663	0.031871	0.007606	-0.013442	
	0.859294	0.035989	0.010147	-0.015152	
	0.840880	0.039994	0.013072	-0.016772	
	0.822434	0.043885	0.016421	-0.018313	
	0.803960	0.047660	0.020254	-0.019788	
	0.785464	0.051318	0.024661	-0.021204	
	0.766946	0.054859	0.029760	-0.022568	
	0.748411	0.058280	0.035709	-0.023879	
	0.729860	0.061583	0.042709	-0.025128	
	0.711295	0.064764	0.051004	-0.026298	
	0.692719	0.067823	0.060837	-0.027354	
	0.674133	0.070759	0.072383	-0.028246	
	0.655540	0.073568	0.085680	-0.028921	
	0.636942	0.076250	0.100567	-0.029338	
	0.618341	0.078802	0.116746	-0.029484	
	0.599740	0.081222	0.133886	-0.029373	
	0.581142	0.083507	0.151714	-0.029036	
	0.562549	0.085654	0.170033	-0.028511	
	0.543964	0.087660	0.188713	-0.027836	
	0.525390	0.089522	0.207668	-0.027044	
	0.506830	0.091236	0.226839	-0.026166	
	0.488290	0.092798	0.246181	-0.025227	
	0.469775	0.094204	0.265652	-0.024252	
	0.451295	0.095448	0.285191	-0.023263	
	0.432869	0.096527	0.304719	-0.022282	
	0.414532	0.097433	0.324192	-0.021324	
	0.396376	0.098160	0.343603	-0.020405	
	0.378468	0.098644	0.362959	-0.019534	
	0.360694	0.098860	0.382280	-0.018720	
	0.343009	0.098808	0.401616	-0.017969	
	0.325400	0.098483	0.421035	-0.017230	
	0.307866	0.097881	0.440551	-0.016463	
	0.290412	0.096995	0.460126	-0.015677	
	0.273046	0.095819	0.479743	-0.014879	
	0.255780	0.094349	0.499385	-0.014077	
	0.238629	0.092578	0.519027	-0.013275	
	0.221608	0.090500	0.538651	-0.012480	
	0.204739	0.088109	0.558253	-0.011696	
	0.188045	0.085400	0.577833	-0.010927	
	0.171559	0.082368	0.597391	-0.010177	
	0.155322	0.079012	0.616931	-0.009448	
	0.139393	0.075332	0.636454	-0.008743	
	0.123851	0.071338	0.655963	-0.008065	
	0.108811	0.067052	0.675460	-0.007415	
	0.094432	0.062517	0.694947	-0.006795	
	0.080917	0.057809	0.714426	-0.006206	
	0.068500	0.053036	0.733899	-0.005649	
	0.057387	0.048327	0.753369	-0.005126	
	0.047691	0.043805	0.772836	-0.004636	
	0.039401	0.039556	0.792302	-0.004180	
	0.032397	0.035616	0.811768	-0.003758	
	0.026506	0.031979	0.831235	-0.003369	
	0.021547	0.028617	0.850700	-0.003013	
	0.017357	0.025491	0.870155	-0.002690	
	0.013806	0.022561	0.889577	-0.002399	
	0.010790	0.019793	0.908908	-0.002139	
	0.008230	0.017154	0.928011	-0.001909	
	0.006070	0.014617	0.946580	-0.001711	
	0.004268	0.012161	0.964043	-0.001545	
	0.002799	0.009769	0.979620	-0.001413	
	0.001646	0.007432	0.992705	-0.001312	
	0.000803	0.005148	1.000000	-0.001260	

A1 - profile	x	y	x	y	A1
	1.000000	0.000000	0.003530	0.021900	
	0.991442	-0.001019	0.004936	0.025104	
	0.977937	-0.001895	0.006576	0.028359	
	0.963151	-0.002016	0.008460	0.031667	
	0.946667	-0.001974	0.010601	0.035024	
	0.928277	-0.002257	0.013019	0.038427	
	0.907868	-0.002639	0.015738	0.041874	
	0.885808	-0.003112	0.018783	0.045363	
	0.862459	-0.003727	0.022169	0.048904	
	0.838148	-0.004444	0.025911	0.052519	
	0.813177	-0.005262	0.030023	0.056226	
	0.787752	-0.006164	0.034536	0.060033	
	0.762006	-0.007136	0.039493	0.063931	
	0.736034	-0.008170	0.044942	0.067917	
	0.709889	-0.009252	0.050923	0.071998	
	0.683606	-0.010376	0.057477	0.076173	
	0.657213	-0.011529	0.064654	0.080423	
	0.630728	-0.012706	0.072501	0.084735	
	0.604179	-0.013897	0.081044	0.089094	
	0.577585	-0.015095	0.090304	0.093462	
	0.550979	-0.016292	0.100295	0.097781	
	0.524390	-0.017483	0.111018	0.101996	
	0.497824	-0.018662	0.122452	0.106058	
	0.471288	-0.019825	0.134555	0.109916	
	0.444780	-0.020971	0.147263	0.113514	
	0.418307	-0.022094	0.160498	0.116792	
	0.391866	-0.023197	0.174185	0.119697	
	0.365475	-0.024274	0.188242	0.122189	
	0.339153	-0.025327	0.202587	0.124233	
	0.312945	-0.026348	0.217157	0.125783	
	0.286921	-0.027338	0.231924	0.126807	
	0.261199	-0.028286	0.246878	0.127289	
	0.235995	-0.029199	0.262017	0.127221	
	0.211666	-0.030069	0.277346	0.126593	
	0.188651	-0.030863	0.292881	0.125392	
	0.167345	-0.031546	0.308654	0.123600	
	0.148066	-0.032108	0.324721	0.121194	
	0.130962	-0.032545	0.341170	0.118140	
	0.115987	-0.032858	0.358137	0.114397	
	0.102944	-0.033055	0.375811	0.109924	
	0.091575	-0.033147	0.394424	0.104706	
	0.081616	-0.033142	0.414141	0.098837	
	0.072831	-0.033051	0.434753	0.092614	
	0.065021	-0.032875	0.455809	0.086464	
	0.058019	-0.032607	0.477298	0.080552	
	0.051688	-0.032241	0.499314	0.074802	
	0.045923	-0.031767	0.521773	0.069175	
	0.040639	-0.031162	0.544563	0.063686	
	0.035772	-0.030403	0.567587	0.058353	
	0.031272	-0.029471	0.590772	0.053194	
	0.027101	-0.028355	0.614065	0.048220	
	0.023232	-0.027055	0.637428	0.043441	
	0.019645	-0.025584	0.660833	0.038866	
	0.016318	-0.023965	0.684265	0.034498	
	0.013250	-0.022194	0.707691	0.030337	
	0.010465	-0.020234	0.731059	0.026394	
	0.008012	-0.018043	0.754317	0.022684	
	0.005926	-0.015622	0.777425	0.019225	
	0.004197	-0.013023	0.800335	0.016029	
	0.002793	-0.010305	0.822980	0.013110	
	0.001682	-0.007512	0.845268	0.010483	
	0.000840	-0.004676	0.867077	0.008162	
	0.000251	-0.001821	0.888225	0.006162	
	-0.000101	0.001034	0.908540	0.004510	
	-0.000227	0.003866	0.927783	0.003147	
	-0.000142	0.006712	0.945598	0.002084	
	0.000156	0.009628	0.962066	0.001572	
	0.000668	0.012609	0.977322	0.001283	
	0.001400	0.015651	0.991300	0.000649	
	0.002352	0.018749	1.000000	0.000000	

A2 - profile	x	y	x	y	A2
	1.000000	0.000000	0.002427	0.018882	
	0.991513	-0.000984	0.003608	0.021983	
	0.978093	-0.001827	0.005016	0.025132	
	0.963386	-0.001952	0.006657	0.028327	
	0.946992	-0.001906	0.008541	0.031569	
	0.928778	-0.002149	0.010677	0.034856	
	0.908636	-0.002522	0.013078	0.038192	
	0.886912	-0.002984	0.015759	0.041577	
	0.863960	-0.003583	0.018738	0.045013	
	0.840083	-0.004289	0.022035	0.048506	
	0.815563	-0.005098	0.025671	0.052059	
	0.790589	-0.005992	0.029674	0.055678	
	0.765296	-0.006959	0.034072	0.059370	
	0.739771	-0.007990	0.038897	0.063142	
	0.714070	-0.009070	0.044186	0.066996	
	0.688227	-0.010195	0.049979	0.070932	
	0.662268	-0.011350	0.056319	0.074945	
	0.636216	-0.012530	0.063249	0.079028	
	0.610092	-0.013726	0.070810	0.083166	
	0.583925	-0.014930	0.079038	0.087337	
	0.557739	-0.016133	0.087958	0.091512	
	0.531566	-0.017332	0.097581	0.095654	
	0.505423	-0.018517	0.107900	0.099714	
	0.479312	-0.019686	0.118895	0.103631	
	0.453235	-0.020835	0.130533	0.107347	
	0.427194	-0.021963	0.142757	0.110812	
	0.401190	-0.023065	0.155497	0.113972	
	0.375231	-0.024141	0.168679	0.116773	
	0.349337	-0.025188	0.182230	0.119169	
	0.323538	-0.026204	0.196086	0.121120	
	0.297891	-0.027184	0.210207	0.122567	
	0.272487	-0.028123	0.224632	0.123438	
	0.247481	-0.029020	0.239464	0.123706	
	0.223152	-0.029875	0.254837	0.123372	
	0.199884	-0.030670	0.270892	0.122444	
	0.178079	-0.031369	0.287780	0.120938	
	0.158082	-0.031955	0.305624	0.118887	
	0.140122	-0.032419	0.324484	0.116328	
	0.124254	-0.032764	0.344360	0.113295	
	0.110362	-0.032993	0.365193	0.109832	
	0.098230	-0.033116	0.386875	0.105987	
	0.087609	-0.033142	0.409259	0.101817	
	0.078258	-0.033082	0.432176	0.097375	
	0.069964	-0.032940	0.455467	0.092704	
	0.062551	-0.032715	0.479008	0.087828	
	0.055873	-0.032402	0.502734	0.082755	
	0.049811	-0.031992	0.526648	0.077482	
	0.044271	-0.031472	0.550788	0.072020	
	0.039180	-0.030820	0.575160	0.066400	
	0.034478	-0.030016	0.599693	0.060685	
	0.030121	-0.029043	0.624182	0.054976	
	0.026079	-0.027893	0.648395	0.049382	
	0.022325	-0.026570	0.672214	0.043983	
	0.018841	-0.025087	0.695606	0.038833	
	0.015613	-0.023454	0.718579	0.033968	
	0.012643	-0.021661	0.741167	0.029413	
	0.009958	-0.019676	0.763407	0.025185	
	0.007598	-0.017470	0.785343	0.021296	
	0.005592	-0.015053	0.807009	0.017753	
	0.003931	-0.012472	0.828425	0.014559	
	0.002587	-0.009779	0.849578	0.011710	
	0.001530	-0.007017	0.870374	0.009191	
	0.000735	-0.004216	0.890655	0.007019	
	0.000187	-0.001400	0.910242	0.005192	
	-0.000130	0.001414	0.928875	0.003665	
	-0.000228	0.004201	0.946255	0.002491	
	-0.000120	0.007010	0.962464	0.001846	
	0.000196	0.009890	0.977542	0.001418	
	0.000724	0.012831	0.991385	0.000692	
	0.001467	0.015830	1.000000	0.000000	

A3 – profile	x	y		x	y	A3
	1.000001	0.000000		0.002616	0.019629	
	0.991398	-0.001091		0.003834	0.022786	
	0.977790	-0.002109		0.005276	0.025995	
	0.962879	-0.002419		0.006947	0.029256	
	0.946274	-0.002581		0.008855	0.032569	
	0.927840	-0.003056		0.011014	0.035933	
	0.907456	-0.003683		0.013440	0.039347	
	0.885449	-0.004415		0.016154	0.042810	
	0.862164	-0.005291		0.019171	0.046327	
	0.837898	-0.006277		0.022506	0.049907	
	0.812947	-0.007361		0.026174	0.053562	
	0.787504	-0.008522		0.030196	0.057300	
	0.761713	-0.009743		0.034601	0.061125	
	0.735677	-0.011012		0.039421	0.065035	
	0.709461	-0.012313		0.044692	0.069029	
	0.683116	-0.013639		0.050452	0.073100	
	0.656696	-0.014972		0.056741	0.077237	
	0.630263	-0.016304		0.063600	0.081428	
	0.603858	-0.017623		0.071067	0.085653	
	0.577500	-0.018923		0.079180	0.089890	
	0.551193	-0.020195		0.087970	0.094108	
	0.524940	-0.021437		0.097462	0.098275	
	0.498738	-0.022641		0.107669	0.102352	
	0.472582	-0.023805		0.118595	0.106296	
	0.446463	-0.024925		0.130232	0.110059	
	0.420386	-0.026001		0.142556	0.113599	
	0.394349	-0.027029		0.155532	0.116869	
	0.368367	-0.028008		0.169112	0.119829	
	0.342461	-0.028937		0.183232	0.122445	
	0.316674	-0.029812		0.197815	0.124682	
	0.291075	-0.030631		0.212772	0.126515	
	0.265779	-0.031388		0.228012	0.127911	
	0.240982	-0.032088		0.243461	0.128828	
	0.217003	-0.032731		0.259096	0.129220	
	0.194239	-0.033298		0.274936	0.129062	
	0.173068	-0.033764		0.291025	0.128339	
	0.153783	-0.034122		0.307431	0.127031	
	0.136542	-0.034373		0.324253	0.125116	
	0.121334	-0.034524		0.341633	0.122565	
	0.108005	-0.034579		0.359765	0.119345	
	0.096329	-0.034548		0.378916	0.115428	
	0.086065	-0.034439		0.399386	0.110853	
	0.076987	-0.034258		0.421288	0.105764	
	0.068901	-0.034008		0.444385	0.100357	
	0.061644	-0.033683		0.468270	0.094817	
	0.055082	-0.033276		0.492707	0.089237	
	0.049107	-0.032777		0.517575	0.083631	
	0.043631	-0.032169		0.542722	0.077983	
	0.038588	-0.031431		0.567968	0.072278	
	0.033923	-0.030541		0.593252	0.066510	
	0.029597	-0.029483		0.618540	0.060703	
	0.025581	-0.028251		0.643709	0.054915	
	0.021850	-0.026847		0.668586	0.049227	
	0.018388	-0.025286		0.693062	0.043708	
	0.015180	-0.023580		0.717087	0.038411	
	0.012233	-0.021715		0.740645	0.033378	
	0.009579	-0.019654		0.763740	0.028643	
	0.007260	-0.017370		0.786383	0.024231	
	0.005301	-0.014880		0.808580	0.020164	
	0.003689	-0.012235		0.830322	0.016457	
	0.002390	-0.009486		0.851568	0.013117	
	0.001376	-0.006675		0.872212	0.010152	
	0.000624	-0.003830		0.892118	0.007581	
	0.000116	-0.000975		0.911140	0.005419	
	-0.000162	0.001875		0.929154	0.003680	
	-0.000224	0.004695		0.946104	0.002432	
	-0.000080	0.007550		0.962137	0.001756	
	0.000273	0.010481		0.977252	0.001328	
	0.000838	0.013474		0.991255	0.000642	
	0.001619	0.016524		0.999999	0.000000	

B1 - profile	x	y	x	y	B1
	1.000000	0.000000	0.001595	0.016740	
	0.991337	-0.000731	0.002574	0.019838	
	0.977604	-0.001725	0.003771	0.022971	
	0.962701	-0.001960	0.005190	0.026138	
	0.946025	-0.001832	0.006837	0.029335	
	0.927415	-0.001812	0.008719	0.032559	
	0.906895	-0.001864	0.010846	0.035805	
	0.884808	-0.001978	0.013228	0.039072	
	0.861507	-0.002211	0.015878	0.042359	
	0.837293	-0.002540	0.018807	0.045664	
	0.812473	-0.002963	0.022030	0.048989	
	0.787223	-0.003498	0.025558	0.052341	
	0.761658	-0.004112	0.029405	0.055724	
	0.735896	-0.004813	0.033590	0.059141	
	0.709962	-0.005596	0.038137	0.062590	
	0.683894	-0.006442	0.043072	0.066067	
	0.657730	-0.007360	0.048424	0.069565	
	0.631455	-0.008330	0.054226	0.073071	
	0.605120	-0.009354	0.060513	0.076575	
	0.578691	-0.010426	0.067320	0.080063	
	0.552218	-0.011535	0.074682	0.083516	
	0.525677	-0.012685	0.082637	0.086917	
	0.499102	-0.013862	0.091220	0.090242	
	0.472486	-0.015073	0.100465	0.093464	
	0.445853	-0.016304	0.110403	0.096554	
	0.419211	-0.017563	0.121061	0.099481	
	0.392578	-0.018839	0.132462	0.102212	
	0.365987	-0.020135	0.144619	0.104713	
	0.339464	-0.021448	0.157543	0.106948	
	0.313091	-0.022770	0.171232	0.108888	
	0.286961	-0.024102	0.185681	0.110501	
	0.261257	-0.025420	0.200871	0.111761	
	0.236218	-0.026734	0.216779	0.112645	
	0.212174	-0.028016	0.233371	0.113137	
	0.189524	-0.029246	0.250606	0.113221	
	0.168679	-0.030369	0.268438	0.112889	
	0.149941	-0.031361	0.286819	0.112129	
	0.133386	-0.032208	0.305714	0.110938	
	0.118908	-0.032916	0.325097	0.109308	
	0.106279	-0.033486	0.344965	0.107240	
	0.095231	-0.033934	0.365323	0.104739	
	0.085511	-0.034268	0.386183	0.101816	
	0.076891	-0.034495	0.407551	0.098484	
	0.069185	-0.034619	0.429449	0.094751	
	0.062239	-0.034640	0.451921	0.090622	
	0.055928	-0.034546	0.475062	0.086100	
	0.050152	-0.034327	0.498971	0.081227	
	0.044832	-0.033965	0.523611	0.076122	
	0.039904	-0.033444	0.548684	0.070917	
	0.035320	-0.032747	0.573889	0.065717	
	0.031045	-0.031863	0.599080	0.060582	
	0.027054	-0.030786	0.624165	0.055559	
	0.023332	-0.029511	0.649136	0.050660	
	0.019870	-0.028035	0.673967	0.045911	
	0.016668	-0.026354	0.698680	0.041309	
	0.013737	-0.024463	0.723236	0.036871	
	0.011088	-0.022361	0.747608	0.032598	
	0.008735	-0.020064	0.771732	0.028530	
	0.006677	-0.017597	0.795586	0.024667	
	0.004911	-0.014992	0.819091	0.021050	
	0.003427	-0.012282	0.842180	0.017676	
	0.002215	-0.009494	0.864706	0.014586	
	0.001261	-0.006653	0.886518	0.011792	
	0.000554	-0.003782	0.907399	0.009313	
	0.000080	-0.000899	0.927099	0.007147	
	-0.000173	0.001977	0.945343	0.005307	
	-0.000222	0.004831	0.962108	0.003897	
	-0.000074	0.007722	0.977383	0.002592	
	0.000276	0.010677	0.991329	0.000957	
	0.000831	0.013685	1.000000	0.000000	

B2 - profile	x	y	x	y	B2
	1.000000	0.001260	0.000614	0.004848	
	0.992574	0.002864	0.000174	0.002548	
	0.979635	0.005585	0.000003	0.000326	
	0.964566	0.008662	0.000098	-0.001856	
	0.947741	0.011994	0.000490	-0.004070	
	0.929709	0.015457	0.001220	-0.006283	
	0.910953	0.018947	0.002313	-0.008449	
	0.891793	0.022405	0.003772	-0.010526	
	0.872407	0.025799	0.005586	-0.012493	
	0.852886	0.029116	0.007742	-0.014341	
	0.833278	0.032352	0.010234	-0.016074	
	0.813604	0.035507	0.013068	-0.017705	
	0.793877	0.038583	0.016267	-0.019245	
	0.774104	0.041583	0.019868	-0.020707	
	0.754289	0.044510	0.023929	-0.022103	
	0.734435	0.047366	0.028526	-0.023440	
	0.714542	0.050154	0.033766	-0.024726	
	0.694613	0.052879	0.039782	-0.025961	
	0.674646	0.055542	0.046745	-0.027143	
	0.654642	0.058149	0.054863	-0.028260	
	0.634598	0.060702	0.064363	-0.029293	
	0.614513	0.063207	0.075458	-0.030211	
	0.594384	0.065667	0.088283	-0.030974	
	0.574206	0.068089	0.102820	-0.031543	
	0.553978	0.070480	0.118885	-0.031891	
	0.533702	0.072846	0.136183	-0.032016	
	0.513395	0.075197	0.154403	-0.031932	
	0.493122	0.077537	0.173288	-0.031669	
	0.472996	0.079873	0.192652	-0.031256	
	0.453122	0.082219	0.212367	-0.030727	
	0.433618	0.084597	0.232348	-0.030109	
	0.414518	0.087099	0.252534	-0.029428	
	0.395550	0.089843	0.272872	-0.028707	
	0.376421	0.092799	0.293311	-0.027968	
	0.357328	0.095797	0.313772	-0.027228	
	0.338824	0.098643	0.334193	-0.026506	
	0.321155	0.101115	0.354562	-0.025814	
	0.304120	0.103102	0.374884	-0.025162	
	0.287531	0.104609	0.395192	-0.024562	
	0.271314	0.105625	0.415544	-0.024003	
	0.255401	0.106141	0.435905	-0.023438	
	0.239782	0.106157	0.456257	-0.022833	
	0.224437	0.105639	0.476636	-0.022190	
	0.209273	0.104558	0.497044	-0.021517	
	0.194210	0.102925	0.517482	-0.020817	
	0.179240	0.100765	0.537950	-0.020095	
	0.164414	0.098102	0.558444	-0.019355	
	0.149815	0.094959	0.578963	-0.018600	
	0.135544	0.091359	0.599501	-0.017834	
	0.121697	0.087320	0.620056	-0.017059	
	0.108361	0.082866	0.640625	-0.016278	
	0.095618	0.078035	0.661204	-0.015491	
	0.083566	0.072893	0.681791	-0.014701	
	0.072319	0.067543	0.702381	-0.013909	
	0.062006	0.062126	0.722972	-0.013114	
	0.052737	0.056797	0.743560	-0.012317	
	0.044564	0.051682	0.764140	-0.011517	
	0.037466	0.046852	0.784709	-0.010713	
	0.031362	0.042311	0.805260	-0.009905	
	0.026135	0.038042	0.825787	-0.009090	
	0.021656	0.034034	0.846275	-0.008266	
	0.017809	0.030279	0.866701	-0.007432	
	0.014493	0.026769	0.887015	-0.006585	
	0.011624	0.023490	0.907120	-0.005726	
	0.009133	0.020424	0.926819	-0.004858	
	0.006977	0.017542	0.945753	-0.003994	
	0.005132	0.014809	0.963368	-0.003157	
	0.003582	0.012192	0.979045	-0.002378	
	0.002316	0.009668	0.992393	-0.001680	
	0.001328	0.007223	1.000000	-0.001260	

C-1 – profile	x	y	x	y	C-1
	1.000000	0.000000	0.002554	0.020787	
	0.990874	-0.001060	0.003722	0.024108	
	0.976471	-0.002459	0.005102	0.027476	
	0.960804	-0.003043	0.006694	0.030892	
	0.943250	-0.003350	0.008503	0.034356	
	0.923631	-0.003793	0.010531	0.037870	
	0.901973	-0.004302	0.012783	0.041435	
	0.878577	-0.004889	0.015264	0.045052	
	0.853776	-0.005584	0.017985	0.048722	
	0.827932	-0.006349	0.020956	0.052442	
	0.801374	-0.007196	0.024190	0.056209	
	0.774295	-0.008113	0.027697	0.060021	
	0.746881	-0.009081	0.031494	0.063870	
	0.719221	-0.010106	0.035593	0.067749	
	0.691382	-0.011168	0.040009	0.071648	
	0.663413	-0.012268	0.044755	0.075554	
	0.635331	-0.013394	0.049846	0.079450	
	0.607175	-0.014544	0.055292	0.083319	
	0.578945	-0.015711	0.061103	0.087138	
	0.550673	-0.016889	0.067290	0.090882	
	0.522365	-0.018076	0.073858	0.094524	
	0.494044	-0.019270	0.080811	0.098032	
	0.465721	-0.020466	0.088152	0.101373	
	0.437420	-0.021665	0.095882	0.104514	
	0.409168	-0.022867	0.104002	0.107417	
	0.381009	-0.024069	0.112514	0.110046	
	0.353001	-0.025274	0.121423	0.112363	
	0.325235	-0.026476	0.130740	0.114327	
	0.297849	-0.027676	0.140488	0.115899	
	0.271056	-0.028858	0.150701	0.117035	
	0.245149	-0.030027	0.161440	0.117686	
	0.220465	-0.031168	0.172798	0.117806	
	0.197389	-0.032261	0.184919	0.117353	
	0.176281	-0.033265	0.198015	0.116300	
	0.157366	-0.034156	0.212375	0.114646	
	0.140662	-0.034927	0.228357	0.112434	
	0.126016	-0.035579	0.246243	0.109823	
	0.113185	-0.036117	0.266036	0.106987	
	0.101904	-0.036549	0.287484	0.103937	
	0.091924	-0.036883	0.310070	0.100659	
	0.083031	-0.037122	0.333363	0.097099	
	0.075044	-0.037269	0.357172	0.093234	
	0.067815	-0.037321	0.381408	0.089070	
	0.061225	-0.037272	0.406041	0.084614	
	0.055176	-0.037107	0.431078	0.079874	
	0.049588	-0.036810	0.456555	0.074869	
	0.044399	-0.036363	0.482457	0.069672	
	0.039559	-0.035748	0.508549	0.064447	
	0.035032	-0.034951	0.534606	0.059317	
	0.030791	-0.033960	0.560546	0.054329	
	0.026818	-0.032769	0.586342	0.049509	
	0.023104	-0.031372	0.612004	0.044873	
	0.019646	-0.029765	0.637542	0.040424	
	0.016451	-0.027941	0.662968	0.036173	
	0.013533	-0.025895	0.688289	0.032117	
	0.010904	-0.023635	0.713490	0.028262	
	0.008575	-0.021179	0.738524	0.024610	
	0.006542	-0.018560	0.763340	0.021186	
	0.004801	-0.015809	0.787884	0.017997	
	0.003340	-0.012956	0.812087	0.015070	
	0.002148	-0.010029	0.835860	0.012404	
	0.001213	-0.007051	0.859066	0.010026	
	0.000522	-0.004044	0.881547	0.007941	
	0.000063	-0.001026	0.903098	0.006155	
	-0.000180	0.001986	0.923491	0.004658	
	-0.000220	0.004990	0.942471	0.003434	
	-0.000065	0.008027	0.959983	0.002584	
	0.000287	0.011131	0.976040	0.001839	
	0.000838	0.014295	0.990789	0.000692	
	0.001593	0.017515	1.000000	0.000000	

C2 - profile	x	y	x	y	C2
	1.000000	0.000000	0.003311	0.023581	
	0.990766	-0.001257	0.004588	0.027030	
	0.976149	-0.002955	0.006058	0.030538	
	0.960190	-0.003902	0.007729	0.034100	
	0.942222	-0.004600	0.009622	0.037708	
	0.922059	-0.005456	0.011759	0.041353	
	0.899725	-0.006420	0.014155	0.045029	
	0.875520	-0.007484	0.016821	0.048736	
	0.849812	-0.008662	0.019763	0.052478	
	0.822992	-0.009909	0.022986	0.056259	
	0.795417	-0.011220	0.026493	0.060087	
	0.767323	-0.012574	0.030296	0.063963	
	0.738904	-0.013952	0.034408	0.067884	
	0.710300	-0.015344	0.038846	0.071840	
	0.681614	-0.016736	0.043631	0.075820	
	0.652912	-0.018117	0.048783	0.079808	
	0.624230	-0.019480	0.054319	0.083789	
	0.595584	-0.020820	0.060255	0.087749	
	0.566978	-0.022128	0.066604	0.091670	
	0.538408	-0.023404	0.073375	0.095534	
	0.509865	-0.024644	0.080575	0.099314	
	0.481349	-0.025848	0.088211	0.102973	
	0.452850	-0.027013	0.096294	0.106469	
	0.424373	-0.028143	0.104839	0.109754	
	0.395931	-0.029237	0.113866	0.112784	
	0.367557	-0.030296	0.123402	0.115522	
	0.339314	-0.031323	0.133483	0.117939	
	0.311313	-0.032313	0.144152	0.120021	
	0.283734	-0.033268	0.155458	0.121750	
	0.256848	-0.034182	0.167466	0.123104	
	0.231057	-0.035061	0.180259	0.124073	
	0.206830	-0.035889	0.193917	0.124665	
	0.184597	-0.036641	0.208498	0.124897	
	0.164617	-0.037296	0.224016	0.124776	
	0.146939	-0.037848	0.240433	0.124288	
	0.131436	-0.038303	0.257679	0.123401	
	0.117874	-0.038662	0.275689	0.122072	
	0.105977	-0.038932	0.294434	0.120262	
	0.095483	-0.039120	0.313918	0.117954	
	0.086163	-0.039227	0.334162	0.115142	
	0.077820	-0.039253	0.355192	0.111832	
	0.070292	-0.039197	0.377021	0.108043	
	0.063447	-0.039049	0.399637	0.103801	
	0.057179	-0.038797	0.423005	0.099138	
	0.051404	-0.038423	0.447073	0.094088	
	0.046052	-0.037911	0.471781	0.088689	
	0.041069	-0.037241	0.497060	0.082984	
	0.036416	-0.036399	0.522833	0.077017	
	0.032062	-0.035371	0.548999	0.070844	
	0.027987	-0.034149	0.575404	0.064539	
	0.024178	-0.032726	0.601779	0.058218	
	0.020630	-0.031098	0.627777	0.052037	
	0.017348	-0.029257	0.653228	0.046123	
	0.014341	-0.027200	0.678141	0.040540	
	0.011624	-0.024929	0.702610	0.035312	
	0.009205	-0.022461	0.726697	0.030411	
	0.007086	-0.019823	0.750297	0.025833	
	0.005261	-0.017045	0.773329	0.021648	
	0.003722	-0.014159	0.795846	0.017910	
	0.002456	-0.011191	0.817991	0.014638	
	0.001451	-0.008166	0.839889	0.011793	
	0.000693	-0.005105	0.861521	0.009320	
	0.000170	-0.002027	0.882748	0.007201	
	-0.000132	0.001050	0.903373	0.005427	
	-0.000229	0.004116	0.923159	0.003979	
	-0.000130	0.007204	0.941858	0.002861	
	0.000162	0.010356	0.959383	0.002130	
	0.000652	0.013575	0.975642	0.001501	
	0.001339	0.016853	0.990645	0.000551	
	0.002227	0.020189	1.000000	0.000000	

C3 - profile

x	y	x	y	C3
1.000000	0.000000	0.001889	0.018366	
0.991099	-0.000900	0.002909	0.021578	
0.977019	-0.002090	0.004130	0.024833	
0.961717	-0.002498	0.005545	0.028132	
0.944592	-0.002589	0.007159	0.031473	
0.925465	-0.002797	0.008983	0.034850	
0.904359	-0.003072	0.011038	0.038251	
0.881590	-0.003416	0.013344	0.041667	
0.857488	-0.003872	0.015908	0.045096	
0.832382	-0.004410	0.018735	0.048539	
0.806592	-0.005037	0.021828	0.052000	
0.780305	-0.005756	0.025192	0.055482	
0.753680	-0.006539	0.028841	0.058981	
0.726821	-0.007399	0.032788	0.062491	
0.699777	-0.008317	0.037049	0.066005	
0.672603	-0.009288	0.041640	0.069516	
0.645312	-0.010311	0.046577	0.073011	
0.617935	-0.011371	0.051878	0.076476	
0.590480	-0.012472	0.057557	0.079900	
0.562962	-0.013599	0.063630	0.083264	
0.535397	-0.014757	0.070112	0.086545	
0.507795	-0.015935	0.077019	0.089713	
0.480174	-0.017136	0.084382	0.092710	
0.452548	-0.018351	0.092258	0.095456	
0.424940	-0.019585	0.100709	0.097923	
0.397373	-0.020832	0.109786	0.100144	
0.369893	-0.022093	0.119542	0.102138	
0.342547	-0.023366	0.130046	0.103891	
0.315434	-0.024646	0.141360	0.105423	
0.288682	-0.025931	0.153517	0.106751	
0.262521	-0.027202	0.166524	0.107839	
0.237232	-0.028464	0.180390	0.108606	
0.213160	-0.029695	0.195178	0.108978	
0.190691	-0.030869	0.210956	0.108972	
0.170186	-0.031940	0.227721	0.108598	
0.151854	-0.032887	0.245467	0.107806	
0.135688	-0.033703	0.264212	0.106591	
0.121527	-0.034392	0.283912	0.105001	
0.109123	-0.034958	0.304384	0.103077	
0.098215	-0.035412	0.325449	0.100783	
0.088561	-0.035762	0.347030	0.098098	
0.079952	-0.036013	0.369106	0.095022	
0.072215	-0.036167	0.391672	0.091568	
0.065208	-0.036222	0.414740	0.087745	
0.058815	-0.036169	0.438343	0.083560	
0.052942	-0.035996	0.462550	0.079021	
0.047513	-0.035685	0.487436	0.074171	
0.042470	-0.035221	0.512917	0.069136	
0.037765	-0.034584	0.538686	0.064067	
0.033364	-0.033763	0.564503	0.059053	
0.029242	-0.032747	0.590247	0.054148	
0.025384	-0.031532	0.615875	0.049384	
0.021782	-0.030111	0.641376	0.044774	
0.018435	-0.028480	0.666747	0.040333	
0.015351	-0.026633	0.691992	0.036065	
0.012545	-0.024568	0.717094	0.031976	
0.010030	-0.022293	0.742007	0.028071	
0.007811	-0.019833	0.766681	0.024379	
0.005886	-0.017219	0.791060	0.020908	
0.004248	-0.014483	0.815081	0.017689	
0.002886	-0.011655	0.838649	0.014723	
0.001788	-0.008760	0.861629	0.012042	
0.000941	-0.005822	0.883858	0.009653	
0.000335	-0.002862	0.905128	0.007568	
-0.000046	0.000104	0.925206	0.005781	
-0.000216	0.003057	0.943841	0.004288	
-0.000188	0.006013	0.960998	0.003184	
0.000034	0.009016	0.976682	0.002183	
0.000453	0.012081	0.991048	0.000818	
0.001071	0.015199	1.000000	0.000000	

D1 – profile	x	y	x	y	D1
	1.000000	0.000000	0.002500	0.019271	
	0.991077	-0.000357	0.003687	0.022394	
	0.976274	-0.001055	0.005093	0.025566	
	0.959605	-0.002036	0.006723	0.028787	
	0.940926	-0.003241	0.008583	0.032058	
	0.920372	-0.004524	0.010681	0.035381	
	0.898137	-0.005791	0.013034	0.038756	
	0.874525	-0.007128	0.015656	0.042181	
	0.849917	-0.008566	0.018563	0.045662	
	0.824650	-0.010070	0.021765	0.049207	
	0.798925	-0.011642	0.025278	0.052825	
	0.772915	-0.013242	0.029120	0.056521	
	0.746774	-0.014867	0.033319	0.060295	
	0.720579	-0.016491	0.037905	0.064142	
	0.694368	-0.018107	0.042911	0.068057	
	0.668185	-0.019700	0.048377	0.072030	
	0.642026	-0.021262	0.054339	0.076053	
	0.615945	-0.022778	0.060838	0.080117	
	0.589921	-0.024246	0.067914	0.084209	
	0.563983	-0.025652	0.075604	0.088316	
	0.538102	-0.026997	0.083944	0.092417	
	0.512297	-0.028270	0.092965	0.096487	
	0.486540	-0.029470	0.102693	0.100492	
	0.460844	-0.030592	0.113144	0.104394	
	0.435187	-0.031634	0.124326	0.108152	
	0.409589	-0.032591	0.136238	0.111722	
	0.384035	-0.033465	0.148870	0.115064	
	0.358561	-0.034251	0.162197	0.118138	
	0.333176	-0.034949	0.176183	0.120911	
	0.307950	-0.035555	0.190783	0.123345	
	0.282946	-0.036067	0.205953	0.125400	
	0.258312	-0.036485	0.221659	0.127042	
	0.234248	-0.036817	0.237881	0.128249	
	0.211092	-0.037070	0.254607	0.129009	
	0.189208	-0.037231	0.271830	0.129311	
	0.168926	-0.037295	0.289548	0.129151	
	0.150487	-0.037264	0.307761	0.128528	
	0.133993	-0.037153	0.326475	0.127443	
	0.119405	-0.036973	0.345691	0.125905	
	0.106565	-0.036728	0.365403	0.123926	
	0.095261	-0.036430	0.385587	0.121524	
	0.085276	-0.036080	0.406202	0.118721	
	0.076404	-0.035683	0.427199	0.115530	
	0.068470	-0.035239	0.448538	0.111962	
	0.061325	-0.034740	0.470197	0.108027	
	0.054847	-0.034176	0.492169	0.103740	
	0.048936	-0.033536	0.514438	0.099122	
	0.043510	-0.032804	0.536970	0.094203	
	0.038507	-0.031957	0.559724	0.088991	
	0.033876	-0.030973	0.582740	0.083457	
	0.029580	-0.029836	0.606157	0.077588	
	0.025590	-0.028535	0.630009	0.071505	
	0.021886	-0.027073	0.654045	0.065429	
	0.018449	-0.025460	0.678132	0.059468	
	0.015264	-0.023711	0.702235	0.053634	
	0.012334	-0.021818	0.726277	0.047934	
	0.009682	-0.019752	0.750136	0.042391	
	0.007352	-0.017481	0.773681	0.037055	
	0.005375	-0.015011	0.796798	0.031977	
	0.003747	-0.012383	0.819443	0.027227	
	0.002439	-0.009649	0.841668	0.022844	
	0.001418	-0.006852	0.863563	0.018828	
	0.000658	-0.004020	0.885061	0.015113	
	0.000141	-0.001179	0.905825	0.011664	
	-0.000150	0.001654	0.925437	0.008556	
	-0.000227	0.004470	0.943728	0.005927	
	-0.000100	0.007308	0.960761	0.003838	
	0.000232	0.010212	0.976605	0.002217	
	0.000775	0.013177	0.991132	0.000835	
	0.001531	0.016198	1.000000	0.000000	

D2 - profile	x	y		x	y	D2
	1.000000	0.000000		0.001905	0.017192	
	0.991534	-0.000956		0.002970	0.020228	
	0.978132	-0.001877		0.004257	0.023310	
	0.963497	-0.002125		0.005769	0.026437	
	0.947267	-0.002181		0.007513	0.029609	
	0.929320	-0.002574		0.009498	0.032826	
	0.909480	-0.003164		0.011736	0.036087	
	0.888052	-0.003866		0.014248	0.039388	
	0.865386	-0.004733		0.017056	0.042726	
	0.841745	-0.005737		0.020184	0.046100	
	0.817403	-0.006856		0.023653	0.049518	
	0.792553	-0.008070		0.027480	0.052998	
	0.767331	-0.009362		0.031681	0.056562	
	0.741835	-0.010713		0.036285	0.060220	
	0.716133	-0.012109		0.041335	0.063969	
	0.690279	-0.013536		0.046879	0.067804	
	0.664324	-0.014979		0.052966	0.071731	
	0.638339	-0.016425		0.059639	0.075753	
	0.612379	-0.017858		0.066953	0.079859	
	0.586474	-0.019271		0.074961	0.084035	
	0.560637	-0.020652		0.083705	0.088271	
	0.534868	-0.021997		0.093211	0.092540	
	0.509169	-0.023297		0.103501	0.096794	
	0.483533	-0.024548		0.114586	0.100976	
	0.457953	-0.025745		0.126459	0.105039	
	0.432427	-0.026885		0.139091	0.108937	
	0.406955	-0.027964		0.152427	0.112621	
	0.381539	-0.028980		0.166397	0.116036	
	0.356193	-0.029929		0.180927	0.119127	
	0.330939	-0.030810		0.195941	0.121854	
	0.305819	-0.031617		0.211361	0.124189	
	0.280903	-0.032347		0.227108	0.126091	
	0.256304	-0.032994		0.243169	0.127495	
	0.232221	-0.033567		0.259606	0.128378	
	0.208972	-0.034063		0.276491	0.128755	
	0.186936	-0.034465		0.293868	0.128653	
	0.166464	-0.034755		0.311736	0.128100	
	0.147833	-0.034933		0.330053	0.127106	
	0.131185	-0.035008		0.348764	0.125679	
	0.116503	-0.034988		0.367819	0.123816	
	0.103632	-0.034883		0.387185	0.121514	
	0.092353	-0.034704		0.406863	0.118761	
	0.082434	-0.034456		0.426905	0.115541	
	0.073658	-0.034146		0.447410	0.111842	
	0.065839	-0.033776		0.468499	0.107671	
	0.058820	-0.033338		0.490281	0.103053	
	0.052473	-0.032823		0.512808	0.098044	
	0.046693	-0.032223		0.536038	0.092720	
	0.041399	-0.031519		0.559850	0.087156	
	0.036524	-0.030686		0.584098	0.081415	
	0.032020	-0.029706		0.608649	0.075544	
	0.027848	-0.028563		0.633394	0.069583	
	0.023981	-0.027253		0.658219	0.063582	
	0.020396	-0.025780		0.682947	0.057614	
	0.017075	-0.024162		0.707439	0.051748	
	0.014004	-0.022412		0.731618	0.046034	
	0.011192	-0.020512		0.755439	0.040514	
	0.008673	-0.018426		0.778865	0.035219	
	0.006493	-0.016128		0.801838	0.030181	
	0.004668	-0.013640		0.824273	0.025438	
	0.003179	-0.011016		0.846064	0.021033	
	0.001994	-0.008304		0.867116	0.017020	
	0.001082	-0.005541		0.887401	0.013467	
	0.000423	-0.002753		0.906989	0.010415	
	-0.000002	0.000037		0.925949	0.007848	
	-0.000205	0.002812		0.944160	0.005647	
	-0.000200	0.005579		0.961267	0.003767	
	0.000009	0.008390		0.977054	0.002238	
	0.000428	0.011269		0.991343	0.000892	
	0.001059	0.014204		1.000000	0.000000	

E1 – profile	x	y	x	y	E1
	1.000000	0.000000	0.002480	0.019564	
	0.990833	-0.000501	0.003661	0.022766	
	0.975706	-0.001470	0.005060	0.026021	
	0.958746	-0.002762	0.006681	0.029332	
	0.939804	-0.004313	0.008528	0.032700	
	0.918979	-0.005973	0.010612	0.036129	
	0.896434	-0.007651	0.012942	0.039620	
	0.872422	-0.009414	0.015532	0.043178	
	0.847332	-0.011279	0.018395	0.046809	
	0.821512	-0.013211	0.021543	0.050520	
	0.795248	-0.015186	0.024994	0.054320	
	0.768748	-0.017167	0.028768	0.058214	
	0.742165	-0.019138	0.032889	0.062205	
	0.715592	-0.021074	0.037384	0.066295	
	0.689077	-0.022963	0.042281	0.070484	
	0.662648	-0.024792	0.047610	0.074768	
	0.636311	-0.026550	0.053404	0.079139	
	0.610068	-0.028229	0.059693	0.083586	
	0.583914	-0.029821	0.066509	0.088089	
	0.557843	-0.031319	0.073877	0.092626	
	0.531847	-0.032719	0.081821	0.097169	
	0.505918	-0.034016	0.090355	0.101684	
	0.480049	-0.035204	0.099483	0.106133	
	0.454233	-0.036283	0.109202	0.110472	
	0.428468	-0.037248	0.119494	0.114656	
	0.402759	-0.038099	0.130331	0.118635	
	0.377116	-0.038833	0.141673	0.122360	
	0.351564	-0.039450	0.153481	0.125772	
	0.326146	-0.039949	0.165726	0.128806	
	0.300936	-0.040329	0.178418	0.131382	
	0.276044	-0.040590	0.191614	0.133454	
	0.251646	-0.040740	0.205371	0.135050	
	0.228007	-0.040791	0.219710	0.136200	
	0.205473	-0.040753	0.234634	0.136898	
	0.184381	-0.040623	0.250145	0.137129	
	0.164997	-0.040407	0.266249	0.136870	
	0.147472	-0.040119	0.282973	0.136094	
	0.131826	-0.039776	0.300376	0.134772	
	0.117960	-0.039387	0.318561	0.132885	
	0.105697	-0.038960	0.337661	0.130436	
	0.094835	-0.038499	0.357801	0.127453	
	0.085173	-0.038005	0.379039	0.124003	
	0.076529	-0.037478	0.401298	0.120174	
	0.068750	-0.036914	0.424358	0.116060	
	0.061704	-0.036306	0.447898	0.111743	
	0.055281	-0.035641	0.471612	0.107240	
	0.049395	-0.034906	0.495395	0.102503	
	0.043971	-0.034084	0.519291	0.097511	
	0.038954	-0.033152	0.543374	0.092255	
	0.034298	-0.032089	0.567718	0.086744	
	0.029970	-0.030879	0.592372	0.080998	
	0.025943	-0.029510	0.617346	0.075055	
	0.022199	-0.027984	0.642573	0.068979	
	0.018720	-0.026310	0.667871	0.062872	
	0.015497	-0.024495	0.693000	0.056846	
	0.012532	-0.022530	0.717833	0.050983	
	0.009849	-0.020392	0.742333	0.045335	
	0.007486	-0.018054	0.766515	0.039935	
	0.005473	-0.015522	0.790418	0.034798	
	0.003814	-0.012832	0.814079	0.029933	
	0.002482	-0.010034	0.837507	0.025334	
	0.001444	-0.007170	0.860620	0.020982	
	0.000674	-0.004272	0.883133	0.016859	
	0.000149	-0.001364	0.904628	0.013016	
	-0.000146	0.001535	0.924747	0.009541	
	-0.000227	0.004416	0.943336	0.006542	
	-0.000104	0.007320	0.960462	0.004101	
	0.000225	0.010290	0.976291	0.002224	
	0.000764	0.013324	0.990922	0.000795	
	0.001515	0.016416	1.000000	0.000000	

E2 - profile	x	y	x	y	E2
	1.000000	0.000000	0.002834	0.020653	
	0.990813	-0.000528	0.004081	0.023887	
	0.975608	-0.001500	0.005547	0.027177	
	0.958535	-0.002772	0.007235	0.030525	
	0.939481	-0.004269	0.009151	0.033934	
	0.918577	-0.005834	0.011306	0.037406	
	0.895946	-0.007387	0.013713	0.040942	
	0.871828	-0.009020	0.016383	0.044548	
	0.846619	-0.010744	0.019329	0.048231	
	0.820686	-0.012522	0.022564	0.052000	
	0.794306	-0.014341	0.026105	0.055860	
	0.767667	-0.016164	0.029975	0.059812	
	0.740930	-0.017981	0.034199	0.063861	
	0.714181	-0.019768	0.038800	0.068007	
	0.687476	-0.021517	0.043808	0.072244	
	0.660838	-0.023212	0.049253	0.076566	
	0.634279	-0.024846	0.055161	0.080963	
	0.607797	-0.026412	0.061562	0.085417	
	0.581396	-0.027902	0.068482	0.089906	
	0.555062	-0.029310	0.075940	0.094403	
	0.528794	-0.030633	0.083953	0.098876	
	0.502581	-0.031865	0.092525	0.103288	
	0.476419	-0.033004	0.101655	0.107597	
	0.450298	-0.034047	0.111327	0.111757	
	0.424224	-0.034992	0.121518	0.115722	
	0.398196	-0.035838	0.132192	0.119441	
	0.372232	-0.036584	0.143312	0.122863	
	0.346360	-0.037230	0.154840	0.125927	
	0.320634	-0.037775	0.166769	0.128555	
	0.295135	-0.038217	0.179139	0.130664	
	0.269997	-0.038557	0.192042	0.132202	
	0.245426	-0.038804	0.205614	0.133177	
	0.221732	-0.038970	0.219976	0.133660	
	0.199290	-0.039055	0.235181	0.133729	
	0.178434	-0.039050	0.251198	0.133400	
	0.159411	-0.038962	0.267983	0.132620	
	0.142327	-0.038802	0.285546	0.131333	
	0.127158	-0.038584	0.303948	0.129520	
	0.113761	-0.038310	0.323259	0.127183	
	0.101934	-0.037991	0.343564	0.124331	
	0.091463	-0.037630	0.364899	0.121039	
	0.082145	-0.037226	0.387084	0.117441	
	0.073800	-0.036782	0.409773	0.113581	
	0.066279	-0.036291	0.432769	0.109430	
	0.059456	-0.035744	0.456001	0.104987	
	0.053227	-0.035130	0.479452	0.100258	
	0.047507	-0.034435	0.503108	0.095263	
	0.042229	-0.033638	0.526936	0.090026	
	0.037341	-0.032715	0.550894	0.084560	
	0.032800	-0.031648	0.575006	0.078834	
	0.028575	-0.030420	0.599380	0.072849	
	0.024644	-0.029026	0.623962	0.066754	
	0.020989	-0.027472	0.648516	0.060764	
	0.017593	-0.025771	0.673007	0.054955	
	0.014448	-0.023928	0.697453	0.049322	
	0.011568	-0.021924	0.721812	0.043859	
	0.008988	-0.019725	0.745981	0.038582	
	0.006750	-0.017313	0.769840	0.033531	
	0.004871	-0.014711	0.793281	0.028752	
	0.003336	-0.011970	0.816253	0.024309	
	0.002111	-0.009138	0.838799	0.020245	
	0.001167	-0.006254	0.860990	0.016559	
	0.000478	-0.003345	0.882768	0.013189	
	0.000029	-0.000431	0.903819	0.010087	
	-0.000195	0.002470	0.923746	0.007306	
	-0.000209	0.005357	0.942370	0.004976	
	-0.000020	0.008286	0.959743	0.003167	
	0.000377	0.011288	0.975942	0.001815	
	0.000984	0.014351	0.990856	0.000686	
	0.001802	0.017474	1.000000	0.000000	

x	y	x	y
1.000000	0.000000	0.000484	0.003974
0.992241	0.001335	0.000874	0.006072
0.979216	0.003252	0.001599	0.008217
0.964763	0.004950	0.002659	0.010464
0.949286	0.006329	0.004059	0.012867
0.933181	0.007302	0.005776	0.015478
0.916668	0.007826	0.007782	0.018308
0.899846	0.007890	0.010112	0.021329
0.882748	0.007498	0.012808	0.024502
0.865390	0.006672	0.015946	0.027816
0.847793	0.005437	0.019655	0.031323
0.829980	0.003820	0.024098	0.035104
0.811972	0.001849	0.029461	0.039237
0.793790	-0.000450	0.035886	0.043721
0.775463	-0.003052	0.043456	0.048477
0.757032	-0.005928	0.052247	0.053434
0.738526	-0.009055	0.062388	0.058546
0.719922	-0.012424	0.073898	0.063725
0.701145	-0.016028	0.086627	0.068821
0.682166	-0.019834	0.100330	0.073692
0.663128	-0.023769	0.114818	0.078232
0.644295	-0.027686	0.130064	0.082405
0.625836	-0.031407	0.146097	0.086254
0.607760	-0.034805	0.162669	0.089799
0.589972	-0.037833	0.179405	0.092949
0.572293	-0.040482	0.196264	0.095653
0.554464	-0.042762	0.213432	0.097954
0.536250	-0.044747	0.230940	0.099904
0.517582	-0.046516	0.248637	0.101507
0.498589	-0.048115	0.266414	0.102755
0.479447	-0.049545	0.284267	0.103654
0.460257	-0.050815	0.302195	0.104209
0.441049	-0.051930	0.320146	0.104423
0.421825	-0.052885	0.338070	0.104290
0.402580	-0.053678	0.356009	0.103796
0.383308	-0.054312	0.374075	0.102946
0.364019	-0.054792	0.392367	0.101767
0.344737	-0.055116	0.410921	0.100292
0.325483	-0.055281	0.429732	0.098556
0.306277	-0.055282	0.448769	0.096605
0.287131	-0.055111	0.467982	0.094476
0.268052	-0.054760	0.487319	0.092196
0.249046	-0.054218	0.506742	0.089788
0.230134	-0.053480	0.526224	0.087268
0.211354	-0.052536	0.545750	0.084644
0.192753	-0.051368	0.565320	0.081926
0.174373	-0.049962	0.584930	0.079121
0.156268	-0.048304	0.604573	0.076239
0.138519	-0.046384	0.624235	0.073288
0.121294	-0.044199	0.643908	0.070271
0.104893	-0.041772	0.663590	0.067192
0.089599	-0.039135	0.683280	0.064054
0.075557	-0.036324	0.702974	0.060861
0.063024	-0.033456	0.722665	0.057616
0.052341	-0.030705	0.742341	0.054319
0.043453	-0.028090	0.761987	0.050973
0.036004	-0.025549	0.781597	0.047573
0.029645	-0.023087	0.801183	0.044115
0.024158	-0.020805	0.820741	0.040599
0.019414	-0.018767	0.840216	0.037034
0.015323	-0.016932	0.859536	0.033417
0.011874	-0.015109	0.878673	0.029734
0.009013	-0.013186	0.897562	0.025986
0.006666	-0.011123	0.915995	0.022198
0.004764	-0.008946	0.933653	0.018381
0.003256	-0.006737	0.950216	0.014504
0.002094	-0.004540	0.965490	0.010491
0.001245	-0.002370	0.979593	0.006282
0.000692	-0.000231	0.992426	0.002228
0.000433	0.001880	1.000000	0.000000

AR - profile	x	y		x	y	AR
	1.000000	0.000000		0.001729	0.010816	
	0.992181	0.000710		0.002584	0.013441	
	0.979110	0.001660		0.003670	0.016175	
	0.964489	0.002412		0.005002	0.019028	
	0.948511	0.002918		0.006600	0.022013	
	0.931425	0.003127		0.008485	0.025147	
	0.913417	0.003031		0.010685	0.028452	
	0.894655	0.002669		0.013244	0.031945	
	0.875317	0.002077		0.016216	0.035646	
	0.855531	0.001285		0.019669	0.039575	
	0.835387	0.000323		0.023677	0.043759	
	0.814941	-0.000778		0.028320	0.048231	
	0.794237	-0.001988		0.033679	0.053017	
	0.773311	-0.003279		0.039844	0.058112	
	0.752201	-0.004623		0.046903	0.063478	
	0.730957	-0.005994		0.054926	0.069058	
	0.709633	-0.007377		0.063948	0.074777	
	0.688280	-0.008758		0.073954	0.080546	
	0.666920	-0.010134		0.084889	0.086256	
	0.645565	-0.011501		0.096663	0.091800	
	0.624216	-0.012856		0.109169	0.097080	
	0.602875	-0.014201		0.122293	0.102016	
	0.581547	-0.015532		0.135934	0.106543	
	0.560233	-0.016847		0.149995	0.110620	
	0.538934	-0.018145		0.164381	0.114218	
	0.517654	-0.019424		0.178976	0.117313	
	0.496397	-0.020681		0.193672	0.119876	
	0.475167	-0.021912		0.208368	0.121882	
	0.453974	-0.023114		0.223012	0.123283	
	0.432826	-0.024280		0.237665	0.124014	
	0.411731	-0.025405		0.252581	0.123982	
	0.390702	-0.026480		0.268224	0.123211	
	0.369747	-0.027496		0.284908	0.121880	
	0.348874	-0.028442		0.302615	0.120137	
	0.328079	-0.029306		0.321113	0.118085	
	0.307355	-0.030078		0.340065	0.115778	
	0.286690	-0.030749		0.359293	0.113203	
	0.266068	-0.031315		0.378786	0.110360	
	0.245484	-0.031774		0.398598	0.107270	
	0.224964	-0.032134		0.418746	0.103988	
	0.204598	-0.032395		0.439178	0.100569	
	0.184544	-0.032556		0.459790	0.097068	
	0.165032	-0.032590		0.480476	0.093506	
	0.146310	-0.032454		0.501177	0.089891	
	0.128608	-0.032098		0.521871	0.086218	
	0.112142	-0.031497		0.542571	0.082483	
	0.097113	-0.030659		0.563292	0.078686	
	0.083679	-0.029647		0.584052	0.074828	
	0.071933	-0.028565		0.604858	0.070923	
	0.061848	-0.027504		0.625663	0.067003	
	0.053261	-0.026468		0.646359	0.063128	
	0.045918	-0.025367		0.666915	0.059342	
	0.039567	-0.024109		0.687370	0.055669	
	0.034006	-0.022660		0.707806	0.052109	
	0.029084	-0.021058		0.728296	0.048645	
	0.024691	-0.019378		0.748893	0.045256	
	0.020741	-0.017689		0.769615	0.041914	
	0.017168	-0.016037		0.790424	0.038594	
	0.013928	-0.014434		0.811171	0.035278	
	0.010997	-0.012849		0.831725	0.031941	
	0.008380	-0.011211		0.852048	0.028548	
	0.006102	-0.009446		0.872157	0.025065	
	0.004189	-0.007518		0.892064	0.021480	
	0.002658	-0.005442		0.911699	0.017827	
	0.001523	-0.003251		0.930723	0.014270	
	0.000798	-0.000987		0.948588	0.010965	
	0.000461	0.001288		0.964820	0.007757	
	0.000437	0.003554		0.979404	0.004537	
	0.000656	0.005874		0.992306	0.001585	
	0.001090	0.008295		1.000000	0.000000	

CR – profile	x	y		x	y	CR
	1.000000	0.000000		0.002437	0.015974	
	0.991351	0.000904		0.003410	0.019091	
	0.977415	0.002097		0.004578	0.022279	
	0.962289	0.003059		0.005950	0.025539	
	0.945967	0.003763		0.007532	0.028871	
	0.928454	0.004165		0.009333	0.032280	
	0.909747	0.004255		0.011362	0.035768	
	0.889885	0.004059		0.013631	0.039337	
	0.868973	0.003597		0.016155	0.042991	
	0.847115	0.002879		0.018946	0.046732	
	0.824424	0.001933		0.022023	0.050563	
	0.800996	0.000789		0.025405	0.054482	
	0.776932	−0.000518		0.029113	0.058487	
	0.752328	−0.001949		0.033169	0.062575	
	0.727298	−0.003466		0.037597	0.066736	
	0.701956	−0.005042		0.042419	0.070957	
	0.676401	−0.006660		0.047658	0.075225	
	0.650704	−0.008309		0.053333	0.079519	
	0.624912	−0.009984		0.059462	0.083812	
	0.599055	−0.011679		0.066054	0.088077	
	0.573149	−0.013393		0.073115	0.092277	
	0.547215	−0.015117		0.080647	0.096370	
	0.521277	−0.016848		0.088642	0.100310	
	0.495364	−0.018574		0.097094	0.104047	
	0.469525	−0.020291		0.105991	0.107534	
	0.443803	−0.021984		0.115319	0.110724	
	0.418239	−0.023643		0.125068	0.113572	
	0.392873	−0.025248		0.135237	0.116029	
	0.367746	−0.026785		0.145849	0.118026	
	0.342897	−0.028228		0.156971	0.119492	
	0.318355	−0.029559		0.168727	0.120367	
	0.294157	−0.030755		0.181311	0.120668	
	0.270363	−0.031804		0.194881	0.120548	
	0.247077	−0.032695		0.209465	0.120041	
	0.224485	−0.033434		0.225162	0.119011	
	0.202871	−0.034024		0.242151	0.117528	
	0.182566	−0.034470		0.260373	0.115683	
	0.163853	−0.034760		0.279733	0.113385	
	0.146879	−0.034879		0.300342	0.110601	
	0.131638	−0.034815		0.322203	0.107502	
	0.118020	−0.034574		0.344907	0.104209	
	0.105869	−0.034175		0.368175	0.100667	
	0.095014	−0.033644		0.391988	0.096881	
	0.085291	−0.033009		0.416330	0.092899	
	0.076554	−0.032307		0.441123	0.088785	
	0.068674	−0.031573		0.466242	0.084591	
	0.061542	−0.030830		0.491535	0.080367	
	0.055063	−0.030084		0.516881	0.076149	
	0.049153	−0.029315		0.542207	0.071957	
	0.043740	−0.028477		0.567477	0.067813	
	0.038761	−0.027517		0.592690	0.063724	
	0.034168	−0.026397		0.617851	0.059700	
	0.029918	−0.025111		0.642973	0.055739	
	0.025974	−0.023684		0.668060	0.051847	
	0.022302	−0.022153		0.693128	0.048024	
	0.018870	−0.020555		0.718185	0.044270	
	0.015652	−0.018922		0.743232	0.040580	
	0.012628	−0.017271		0.768251	0.036955	
	0.009801	−0.015580		0.793175	0.033390	
	0.007214	−0.013771		0.817904	0.029904	
	0.004965	−0.011727		0.842258	0.026505	
	0.003180	−0.009383		0.865946	0.023205	
	0.001913	−0.006796		0.888589	0.020020	
	0.001096	−0.004081		0.909799	0.016988	
	0.000629	−0.001319		0.929293	0.014088	
	0.000431	0.001444		0.947019	0.011223	
	0.000450	0.004215		0.963132	0.008246	
	0.000663	0.007044		0.977897	0.005051	
	0.001066	0.009950		0.991509	0.001847	
	0.001656	0.012927		1.000000	0.000000	

TR - profile	x	y	x	y	TR
	1.000000	0.000000	0.000820	0.005698	
	0.992635	0.000900	0.001563	0.007810	
	0.979867	0.002266	0.002662	0.009970	
	0.965318	0.003526	0.004071	0.012218	
	0.949517	0.004585	0.005763	0.014608	
	0.932915	0.005371	0.007752	0.017183	
	0.915739	0.005886	0.010098	0.019961	
	0.898151	0.006174	0.012900	0.022940	
	0.880278	0.006267	0.016279	0.026122	
	0.862197	0.006186	0.020366	0.029528	
	0.843948	0.005957	0.025310	0.033194	
	0.825558	0.005600	0.031279	0.037147	
	0.807041	0.005138	0.038443	0.041373	
	0.788415	0.004590	0.046950	0.045805	
	0.769692	0.003974	0.056863	0.050345	
	0.750894	0.003308	0.068135	0.054863	
	0.732039	0.002603	0.080608	0.059231	
	0.713151	0.001868	0.094071	0.063333	
	0.694245	0.001106	0.108312	0.067083	
	0.675330	0.000320	0.123230	0.070432	
	0.656415	-0.000490	0.138790	0.073415	
	0.637497	-0.001324	0.154846	0.076089	
	0.618581	-0.002181	0.171143	0.078430	
	0.599665	-0.003063	0.187601	0.080384	
	0.580745	-0.003968	0.204284	0.081963	
	0.561825	-0.004895	0.221217	0.083216	
	0.542901	-0.005846	0.238328	0.084175	
	0.523973	-0.006818	0.255552	0.084842	
	0.505041	-0.007810	0.272854	0.085222	
	0.486099	-0.008823	0.290215	0.085322	
	0.467146	-0.009854	0.307609	0.085150	
	0.448181	-0.010900	0.325004	0.084705	
	0.429197	-0.011960	0.342407	0.083978	
	0.410202	-0.013026	0.359875	0.082963	
	0.391206	-0.014097	0.377488	0.081676	
	0.372229	-0.015162	0.395283	0.080151	
	0.353282	-0.016213	0.413274	0.078418	
	0.334373	-0.017242	0.431468	0.076517	
	0.315497	-0.018241	0.449837	0.074487	
	0.296645	-0.019206	0.468344	0.072359	
	0.277808	-0.020131	0.486952	0.070158	
	0.258963	-0.021016	0.505636	0.067900	
	0.240107	-0.021867	0.524376	0.065602	
	0.221248	-0.022688	0.543155	0.063270	
	0.202432	-0.023482	0.561973	0.060910	
	0.183739	-0.024238	0.580826	0.058534	
	0.165290	-0.024929	0.599705	0.056146	
	0.147197	-0.025496	0.618600	0.053754	
	0.129552	-0.025877	0.637500	0.051363	
	0.112448	-0.026009	0.656392	0.048975	
	0.096043	-0.025850	0.675276	0.046594	
	0.080645	-0.025417	0.694156	0.044221	
	0.066875	-0.024843	0.713033	0.041857	
	0.055299	-0.024207	0.731916	0.039501	
	0.045852	-0.023351	0.750804	0.037151	
	0.038022	-0.022075	0.769698	0.034805	
	0.031390	-0.020460	0.788591	0.032457	
	0.025720	-0.018708	0.807467	0.030107	
	0.020849	-0.016994	0.826313	0.027754	
	0.016654	-0.015412	0.845088	0.025401	
	0.013048	-0.013909	0.863745	0.023033	
	0.009978	-0.012342	0.882246	0.020636	
	0.007416	-0.010601	0.900513	0.018203	
	0.005328	-0.008686	0.918356	0.015740	
	0.003663	-0.006656	0.935491	0.013227	
	0.002369	-0.004572	0.951638	0.010600	
	0.001412	-0.002475	0.966640	0.007756	
	0.000772	-0.000394	0.980452	0.004652	
	0.000453	0.001641	0.992794	0.001641	
	0.000459	0.003646	1.000000	0.000000	

S1 - profile	x	y	x	y	S1
	1.000000	0.000000	0.002742	0.020300	
	0.991250	-0.001148	0.003975	0.023519	
	0.977406	-0.002234	0.005427	0.026796	
	0.962229	-0.002615	0.007104	0.030130	
	0.945335	-0.002886	0.009014	0.033523	
	0.926587	-0.003471	0.011169	0.036976	
	0.905878	-0.004215	0.013583	0.040490	
	0.883514	-0.005069	0.016270	0.044069	
	0.859844	-0.006064	0.019244	0.047717	
	0.835165	-0.007172	0.022522	0.051442	
	0.809756	-0.008373	0.026121	0.055248	
	0.783839	-0.009641	0.030067	0.059139	
	0.757563	-0.010966	0.034384	0.063117	
	0.731037	-0.012326	0.039103	0.067183	
	0.704360	-0.013707	0.044253	0.071335	
	0.677601	-0.015099	0.049868	0.075568	
	0.650811	-0.016484	0.055980	0.079873	
	0.624042	-0.017857	0.062619	0.084236	
	0.597317	-0.019204	0.069815	0.088639	
	0.570648	-0.020522	0.077589	0.093054	
	0.544033	-0.021802	0.085957	0.097448	
	0.517469	-0.023041	0.094926	0.101782	
	0.490953	-0.024234	0.104489	0.106007	
	0.464477	-0.025379	0.114629	0.110078	
	0.438038	-0.026473	0.125313	0.113946	
	0.411635	-0.027516	0.136491	0.117563	
	0.385281	-0.028506	0.148101	0.120880	
	0.358992	-0.029441	0.160070	0.123853	
	0.332806	-0.030321	0.172322	0.126435	
	0.306783	-0.031141	0.184783	0.128587	
	0.281027	-0.031901	0.197387	0.130276	
	0.255704	-0.032597	0.210081	0.131467	
	0.231090	-0.033240	0.222834	0.132116	
	0.207565	-0.033817	0.235673	0.132107	
	0.185528	-0.034308	0.248754	0.131285	
	0.165301	-0.034698	0.262358	0.129573	
	0.147091	-0.034987	0.276870	0.126970	
	0.130935	-0.035177	0.292757	0.123521	
	0.116725	-0.035276	0.310449	0.119356	
	0.104254	-0.035290	0.330091	0.114642	
	0.093287	-0.035226	0.351479	0.109558	
	0.083591	-0.035092	0.374319	0.104198	
	0.074965	-0.034891	0.398218	0.098626	
	0.067233	-0.034621	0.422782	0.092937	
	0.060253	-0.034276	0.447730	0.087220	
	0.053907	-0.033848	0.472903	0.081521	
	0.048100	-0.033324	0.498203	0.075867	
	0.042756	-0.032686	0.523555	0.070271	
	0.037815	-0.031911	0.548890	0.064750	
	0.033231	-0.030978	0.574146	0.059322	
	0.028969	-0.029874	0.599265	0.054011	
	0.025004	-0.028595	0.624188	0.048837	
	0.021316	-0.027148	0.648849	0.043830	
	0.017888	-0.025545	0.673195	0.039026	
	0.014714	-0.023790	0.697199	0.034460	
	0.011806	-0.021862	0.720870	0.030161	
	0.009202	-0.019725	0.744237	0.026153	
	0.006942	-0.017361	0.767352	0.022449	
	0.005042	-0.014800	0.790268	0.019054	
	0.003482	-0.012094	0.813024	0.015962	
	0.002228	-0.009295	0.835613	0.013167	
	0.001254	-0.006438	0.857973	0.010658	
	0.000538	-0.003551	0.879970	0.008435	
	0.000063	-0.000656	0.901402	0.006496	
	-0.000184	0.002228	0.922008	0.004843	
	-0.000217	0.005092	0.941504	0.003474	
	-0.000045	0.008004	0.959628	0.002369	
	0.000335	0.010985	0.976171	0.001482	
	0.000924	0.014031	0.991006	0.000656	
	0.001726	0.017137	1.000000	0.000000	

S2 - profile	x	y	x	y	S2
	1.000000	0.000000	0.004476	0.024915	
	0.991143	-0.001225	0.006026	0.028296	
	0.977183	-0.002339	0.007810	0.031741	
	0.961891	-0.002674	0.009840	0.035250	
	0.944846	-0.002919	0.012128	0.038825	
	0.925789	-0.003504	0.014690	0.042468	
	0.904640	-0.004174	0.017541	0.046183	
	0.881734	-0.004949	0.020694	0.049978	
	0.857407	-0.005860	0.024167	0.053861	
	0.832029	-0.006865	0.027983	0.057832	
	0.805918	-0.007950	0.032170	0.061894	
	0.779301	-0.009101	0.036755	0.066050	
	0.752347	-0.010300	0.041766	0.070296	
	0.725164	-0.011530	0.047240	0.074626	
	0.697832	-0.012788	0.053206	0.079034	
	0.670411	-0.014054	0.059693	0.083504	
	0.642950	-0.015323	0.066732	0.088015	
	0.615482	-0.016585	0.074343	0.092543	
	0.588037	-0.017832	0.082540	0.097050	
	0.560614	-0.019060	0.091330	0.101494	
	0.533229	-0.020260	0.100705	0.105831	
	0.505875	-0.021436	0.110646	0.110003	
	0.478550	-0.022575	0.121117	0.113970	
	0.451249	-0.023686	0.132066	0.117673	
	0.423974	-0.024758	0.143429	0.121069	
	0.396731	-0.025801	0.155127	0.124109	
	0.369532	-0.026805	0.167084	0.126744	
	0.342418	-0.027777	0.179215	0.128944	
	0.315438	-0.028709	0.191451	0.130663	
	0.288706	-0.029602	0.203728	0.131893	
	0.262369	-0.030452	0.215991	0.132587	
	0.236716	-0.031262	0.228236	0.132682	
	0.212150	-0.032031	0.240503	0.132072	
	0.189118	-0.032718	0.252938	0.130622	
	0.167994	-0.033307	0.265760	0.128299	
	0.149022	-0.033782	0.279253	0.124960	
	0.132260	-0.034151	0.293987	0.120562	
	0.117589	-0.034408	0.310458	0.115555	
	0.104776	-0.034568	0.328720	0.110078	
	0.093558	-0.034634	0.348506	0.104142	
	0.083678	-0.034614	0.369588	0.098033	
	0.074917	-0.034518	0.391662	0.091790	
	0.067088	-0.034341	0.414430	0.085576	
	0.060033	-0.034076	0.437683	0.079400	
	0.053627	-0.033718	0.461177	0.073378	
	0.047772	-0.033255	0.484855	0.067520	
	0.042388	-0.032661	0.508608	0.061878	
	0.037413	-0.031914	0.532469	0.056444	
	0.032799	-0.030993	0.556360	0.051227	
	0.028512	-0.029885	0.580316	0.046240	
	0.024527	-0.028587	0.604289	0.041469	
	0.020821	-0.027113	0.628294	0.036941	
	0.017377	-0.025483	0.652311	0.032633	
	0.014192	-0.023697	0.676333	0.028573	
	0.011289	-0.021716	0.700350	0.024733	
	0.008717	-0.019495	0.724297	0.021142	
	0.006517	-0.017032	0.748140	0.017795	
	0.004684	-0.014377	0.771815	0.014723	
	0.003184	-0.011591	0.795288	0.011922	
	0.001984	-0.008723	0.818474	0.009419	
	0.001061	-0.005803	0.841284	0.007211	
	0.000397	-0.002858	0.863589	0.005323	
	-0.000024	0.000092	0.885208	0.003747	
	-0.000214	0.003025	0.905969	0.002518	
	-0.000187	0.005959	0.925653	0.001572	
	0.000051	0.008950	0.943929	0.000878	
	0.000501	0.012015	0.960826	0.000708	
	0.001165	0.015147	0.976516	0.000782	
	0.002048	0.018341	0.990963	0.000475	
	0.003151	0.021597	1.000000	0.000000	